



HAL
open science

The upper atmosphere of the early Earth, a source of prebiotic organic compounds

Benjamin Fleury

► **To cite this version:**

Benjamin Fleury. The upper atmosphere of the early Earth, a source of prebiotic organic compounds. Astrophysics [astro-ph]. Université Paris Saclay (COMUE), 2015. English. NNT : 2015SACLV012 . tel-01328705

HAL Id: tel-01328705

<https://theses.hal.science/tel-01328705>

Submitted on 8 Jun 2016

HAL is a multi-disciplinary open access archive for the deposit and dissemination of scientific research documents, whether they are published or not. The documents may come from teaching and research institutions in France or abroad, or from public or private research centers.

L'archive ouverte pluridisciplinaire **HAL**, est destinée au dépôt et à la diffusion de documents scientifiques de niveau recherche, publiés ou non, émanant des établissements d'enseignement et de recherche français ou étrangers, des laboratoires publics ou privés.

NNT : 2015SACLV012



THESE DE DOCTORAT
DE L'UNIVERSITE PARIS-SACLAY,
préparée à l'Université Versailles Saint-Quentin en Yvelines

ÉCOLE DOCTORALE N° 579
Sciences mécaniques et énergétiques, matériaux et géosciences
Spécialité de doctorat : Structure et évolution de la Terre et des autres planètes

Par

Mr Benjamin Fleury

The upper atmosphere of the early Earth, a source of prebiotic organic compounds

Thèse présentée et soutenue à Guyancourt, le 06 Octobre 2015 :

Composition du Jury :

M. C. Szopa, Professeur, UVSQ, Président du Jury
M. M. Dobrijevic, Maître de Conférences, Université de Bordeaux, Rapporteur
Mme. M. Trainer, Research scientist, GSF/NASA, Rapporteur
Mme I. Couturier-Tamburelli, Maître de Conférences, Université Aix-Marseille,
Examinatrice
Mme N. Carrasco, Professeure, UVSQ, Directrice de thèse
M. M. Gudipati, Research scientist, JPL/CALTECH, Co-directeur de thèse



Remerciements

A la veille de m'envoler pour Pasadena pour mon postdoc, il est temps pour moi d'écrire ces remerciements. Remerciements pour tous ceux que j'ai eu la chance de côtoyer pendant ces 3 années de thèse.

Je tiens particulièrement à remercier ma directrice de thèse Nathalie Carrasco, pour m'avoir fait confiance depuis mon premier stage en 2011 et pour m'avoir permis de faire cette thèse. Merci pour son soutien ainsi que pour sa bonne humeur au quotidien. I also would like to thank Murthy Gudipati, who has accepted to supervise my thesis at JPL and who give me the opportunity to continue as postdoc.

Je tiens également à remercier les membres de mon jury. Merci à Michel Dobrijevic et Melissa Trainer d'avoir accepté d'être rapporteurs et je les remercie pour leurs précieux commentaires. Je remercie également Isabelle Couturier-Tamburelli et Cyril Szopa d'avoir accepté de faire partie de mon jury.

Je souhaite également remercier tous les personnes du LATMOS que j'ai eu l'occasion de côtoyer pendant toutes ces années. Notamment un grand merci à mon équipe pour leurs soutiens ainsi que pour la bonne ambiance qui y a régnée (notamment pendant nos pauses café). En particulier, merci à Ludovic Vettier pour son aide et le temps consacré à régler les problèmes avec la manip. Merci à Guy Cernogora ainsi qu'à Cyril Szopa (encore une fois) pour leurs nombreux conseils. Merci enfin à toutes les personnes avec qui j'ai eu la chance de collaborer dans d'autres laboratoires et qui ont rendu cette thèse possible.

Merci aussi à toute la team des doctorants du LATMOS pour tous les bons moments que j'ai pu partager avec eux au labo, en conférences ou ailleurs. Alors merci à Thomas, Constantino, Loïc, Sophie, Ludivine, Rémi, Christophe, Maëva, Grégoire, Alizée, Anthony, Sabrina, Sarah et tous ceux que je n'ai pas cité. Mais la thèse c'est aussi des rencontres en dehors du labo. Merci notamment à Maïa, Benjamin, Arnaud, Kimo, Tristan, Damien, Imène, Benjamin et tous les autres. Un merci tout particulier pour ceux que j'ai rencontré aux RED, pour tous les bons moments passé ensemble (à Montpellier et Lyon notamment 😊).

Enfin, merci à tous mes amis, notamment Florian (on repart en randonnée quand tu veux), pour leurs soutiens et les bons moments que j'ai passé avec eux loin de la recherche.

Pour finir je voudrais remercier ma famille et tout particulièrement ma mère et mon frère pour leurs soutiens pendant toutes ces années.

Contents

Résumé.....	1
Chapter I The atmosphere of the early Earth and the origin of the organic matter	11
I.1 Context	11
I.2 The origin of the organic matter on the early Earth	13
I.2.1 The exogenous sources	13
I.2.2 The endogenous sources.....	15
I.2.2.a The hydrothermal vents	15
I.2.2.b The atmosphere	16
I.3 The early Earth atmosphere.....	20
I.3.1 Early atmosphere formation and evolution	20
I.3.2 Constraints on the atmospheric composition of the early Earth.....	21
I.3.2.a The context of the young Sun	22
I.3.2.b Nitrogen N ₂	23
I.3.2.c Water H ₂ O	24
I.3.2.d Carbon dioxide CO ₂	24
I.3.2.e Other gaseous compounds.....	26
I.4 Conclusion	28
Chapter II Materials and Methods	31
II.1 The PAMPRE experimental setup.....	31
II.1.1 Context: simulate ionospheric chemistry with a plasma	31
II.1.2 The experimental device	33
II.1.3 Gas phase analysis.....	34
II.1.3.a <i>In situ</i> mass spectrometry	34
II.1.3.b <i>In situ</i> infrared absorption spectroscopy	36
II.1.3.c <i>Ex situ</i> Gas Chromatography coupled to Mass Spectrometry (GC-MS)	37
II.1.4 Solid phase analysis.....	38
II.1.4.a Self-bias voltage of the polarized electrode: <i>in situ</i> detection of tholins formation	38
II.1.4.b Elemental analysis	38
II.1.4.c Infrared analyses of tholins by ATR.....	39
II.2 The Acquabella experiment	39
II.2.1 The experimental device	40
II.2.2 Infrared absorption spectroscopy	43

II.2.3	UV-visible absorption spectroscopy.....	43
Chapter III	CO ₂ : An efficient source of carbon for an atmospheric organic growth	45
III.1	Introduction.....	45
III.2	Experimental methods and protocols	46
III.3	Results	47
III.3.1	Analysis of the gaseous phase composition.....	47
III.3.1.a	Reactive species consumption in the plasma: the first step for the product formation	47
III.3.1.b	<i>Global in situ</i> analysis of the gaseous phase composition by mass spectrometry	50
III.3.1.c	Cryogenic trapping of the gaseous products for an <i>in situ</i> analysis.....	52
III.3.1.d	Cryogenic trapping of the gaseous products for an <i>ex situ</i> analysis by GC-MS	61
III.3.2	Analysis of the solid phase produced in the reactive medium	64
III.3.3	Effect of the CO ₂ initial amount.....	66
III.4	Discussions	68
III.4.1	Impact of high altitudes water vapor formation on the early Earth	68
III.4.1.a	Water content in the early Earth water atmosphere.....	68
III.4.1.b	Formation of high altitudes clouds.....	69
III.4.1.c	Effect of the water atmospheric profile	70
III.4.2	Solid organic aerosols formations	71
III.5	Conclusion	72
Chapter IV	CH ₄ influence on the early Earth atmospheric chemistry	75
IV.1	Introduction.....	75
IV.2	Experimental methods and protocols	76
IV.3	Results	77
IV.3.1	Analysis of the gaseous phase composition.....	77
IV.3.1.a	Reactive species consumption in the plasma.....	77
IV.3.1.b	<i>In situ</i> analysis of the gaseous phase composition by mass spectrometry.....	79
IV.3.1.c	Cryogenic trapping of the gaseous products for an <i>in-situ</i> analysis.....	82
IV.3.1.d	Influence of the CO ₂ initial amount on the gaseous phase	90
IV.3.2	Analysis of the solid phase produced in the reactive medium	92
IV.4	Importance of methane for the formation of organic compounds in the atmosphere of the early Earth	96
IV.5	Conclusion	97
Chapter V	Effect of CO on the Titan's atmospheric reactivity.....	101
V.1	Introduction.....	101

V.2	Experimental method and protocols.....	103
V.2.1	<i>In situ</i> mass spectrometry	103
V.2.2	<i>Ex situ</i> GC-MS analysis: cold trapping principle.....	104
V.3	Results	104
V.3.1	Effect of CO on the kinetics	104
V.3.2	Effects of CO on the steady-state.....	111
V.3.3	Oxygen incorporation.....	116
V.3.3.a	Elemental analysis of tholins	116
V.3.3.b	Analysis of the gaseous phase	117
V.4	Titan's atmospheric reactivity in presence of CO: a natural example of the early Earth atmospheric reactivity?	120
V.5	Conclusion	121
Chapter VI	Chemical evolution of Titan's tholins	123
VI.1	Introduction.....	123
VI.2	Simulation of aging processes in the thermosphere.....	126
VI.2.1	Experimental methods and protocols.....	126
VI.2.2	Results	128
VI.2.2.a	General observations of the infrared signature evolution of Titan's aerosols analogues	128
VI.2.2.b	Wavelength dependence of the irradiation effect on the tholins	131
VI.2.2.c	Expected effect on aerosols in Titan's atmosphere	133
VI.3	Simulation of tropospheric/stratospheric aging processes	137
VI.3.1	Experimental methods and protocols.....	137
VI.3.2	Results	139
VI.3.2.a	C ₂ H ₂ reactivity.....	139
VI.3.2.b	CH ₃ CN reactivity	151
VI.3.3	Importance for the atmosphere of Titan	155
VI.4	Conclusion	155
General conclusion	157
Table of figures and tables	163
References	171

Résumé

Cette thèse est consacrée à l'étude de la formation de matière organique dans l'atmosphère de la Terre primitive. Nos connaissances de l'environnement dans lequel la vie est apparue sur Terre se sont beaucoup améliorées ces 50 dernières années. Toutefois, l'origine de la matière organique sur la Terre primitive reste fortement débattue aujourd'hui. Une des hypothèses proposées est la formation de composés organiques complexes dans l'atmosphère de la Terre primitive. Cette chimie atmosphérique serait initiée par la dissociation et l'ionisation des molécules constituant de l'atmosphère (majoritairement N_2 et CO_2) par le rayonnement solaire. Une des méthodes possibles pour étudier cette question est de reproduire en laboratoire la réactivité supposée de l'atmosphère primitive. Dans cette thèse, j'ai étudié en laboratoire la chimie de l'atmosphère de la Terre primitive ainsi que de son meilleur analogue observable aujourd'hui : Titan.

Le chapitre I présente l'état de l'art de nos connaissances sur l'atmosphère de la Terre primitive durant la période où la vie est supposée être apparue sur Terre, c'est-à-dire durant l'Hadéen et l'Archéen. Ce sont deux éons couvrant une période commençant avec la formation de la Terre il y a 4.56 Ga et se finissant il y a 2.5 Ga. Ces connaissances sont mises en parallèle avec le travail, expérimental notamment, réalisé jusqu'ici sur la formation de composés organiques dans l'atmosphère de la Terre primitive.

Dans le chapitre II, je présente les différents dispositifs expérimentaux utilisés pendant cette thèse ainsi que les protocoles d'analyses employés. J'ai utilisé plusieurs dispositifs expérimentaux pendant cette thèse. Le premier appelé PAMPRE, localisé au Laboratoire Atmosphère Milieux Observations Spatial (LATMOS), est un réacteur permettant de simuler la réactivité ayant lieu dans les hautes atmosphères de la Terre primitive et de Titan à l'aide d'un plasma radiofréquence. Dans le plasma, les constituants de l'atmosphère simulée sont dissociés et ionisés par impact électronique initiant une chimie organique qui peut conduire à la formation de produits en phase gazeuse ainsi qu'à la production d'aérosols organiques solides. Le second dispositif expérimental, appelé Acquabella, localisé au Jet Propulsion Laboratory (JPL) a été employé dans le cadre de la codirection de ma thèse de manière à reproduire en laboratoire le phénomène de vieillissement des aérosols de Titan, qui pourrait avoir lieu durant leur sédimentation à travers l'atmosphère jusqu'à la surface. En effet, les basses températures présentent à la surface et dans les basses couches de l'atmosphère de

Résumé

Titan peuvent conduire à la condensation d'espèces à la surface des aérosols de Titan. L'expérience est constituée d'une chambre sous vide, dans laquelle est placé un film de tholins. Des espèces sont déposées en phase condensée à basse température à la surface des tholins avant d'être irradiées avec un laser UV.

Les chapitres III et IV sont consacrés à l'étude de la réactivité de l'atmosphère de la Terre primitive. Pour cela, j'étudie la réactivité de deux mélanges gazeux, reproduisant deux compositions atmosphériques supposées de la Terre : $N_2/CO_2/H_2$ et $N_2/CO_2/CH_4$. L'analyse de la composition de la phase gazeuse a été réalisée par spectrométrie de masse, par spectroscopie infrarouge et par Chromatographie en phase Gazeuse couplée à la Spectrométrie de Masse (CG-SM). Les expériences réalisées ont montré une formation quantitative de composés organiques dans les deux mélanges gazeux oxydés étudiés. Cela se traduit par la formation en phase gazeuse de produits avec des masses allant jusqu'à 60 uma pour les mélanges contenant H_2 et jusqu'à 65 uma pour les mélanges contenant CH_4 . Un exemple de spectres de masse des produits formés dans des mélanges $N_2-CO_2-H_2$ avec différentes concentrations initiales de CO_2 est présenté en Figure 1.

L'eau est le principal produit gazeux formé. Sa formation est expliquée par la production de radicaux $O(^1D)$ par des voies neutres ou ioniques qui initient la formation de H_2O via l'oxydation de H_2 ou CH_4 . Cette importante production mise en avant dans mes expériences remet en cause nos connaissances de l'atmosphère de la Terre primitive qui est généralement considérée comme sèche au-dessus de la troposphère.

Une importante production d'eau dans les couches supérieures de l'atmosphère de la Terre primitive modifierait le profil de concentration d'eau atmosphérique. Une augmentation de la concentration en eau dans la stratosphère (si elle existait) et la mésosphère pourrait conduire à la formation de nuages de haute altitude similaires aux actuels nuages stratosphériques polaires et aux nuages mésosphériques polaires. La formation de tels nuages pourrait impacter le climat de la Terre primitive en fonction de leurs épaisseurs optiques et pourrait aussi

Résumé

impacter la chimie de l'atmosphère en favorisant des réactions de chimie hétérogène.

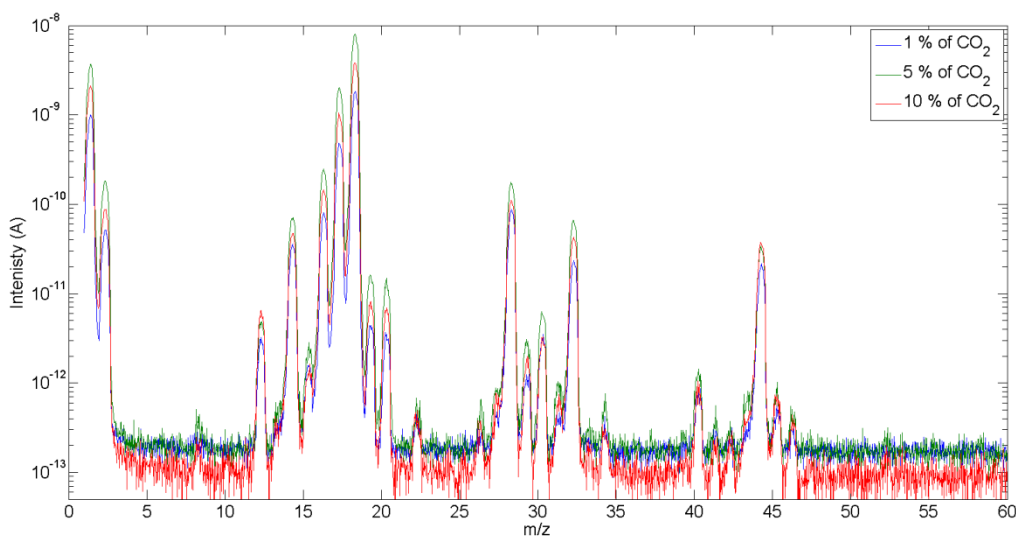


Figure 1: Spectres de masse des produits gazeux formés dans des mélanges N_2 - CO_2 - H_2 pour différentes concentrations initiales de CO_2 : 1 % de CO_2 (courbe bleue), 5 % de CO_2 (courbe verte) et 10 % de CO_2 (courbe rouge).

Le cyanure d'hydrogène et l'ammoniac ont été détectés dans les deux mélanges gazeux étudiés. L'éthanedinitrile et le protoxyde d'azote ont également été identifiés parmi les produits formés dans les mélanges contenant du dihydrogène et le formaldéhyde dans les mélanges contenant du méthane. Ces composés sont des espèces très réactives et sont impliqués dans la formation de composés organiques plus complexes et notamment des aérosols organiques solides.

La composition des différentes molécules détectées implique des atomes de carbone, d'azote, d'hydrogène et d'oxygène. Ce résultat met en avant le couplage entre la chimie de l'azote, du carbone, de l'hydrogène et de l'oxygène dans les expériences réalisées. Ces quatre éléments sont à la base de la formation de composés organiques d'intérêts prébiotiques tels que des bases pyrimidiques ou des acides aminés.

De plus, la formation d'analogues d'aérosols solides, appelés tholins, est observée pour les deux mélanges étudiés. Ces tholins sont formés dans le milieu réactif à partir de précurseurs gazeux. L'analyse élémentaire des tholins formés dans les mélanges contenant du méthane, présentée dans le tableau 1, montre qu'ils sont composés d'atomes de carbone, d'azote, d'hydrogène et d'oxygène. La composition élémentaire de ces tholins évolue en fonction de la concentration initiale de CO_2 . Cela se traduit par une augmentation de la proportion d'oxygène dans les tholins quand la concentration initiale de CO_2 augmente.

Résumé

Table 1: Analyse élémentaire des tholins produits dans des mélanges N_2 - CO_2 - CH_4 pour différentes concentrations initiales de CO_2 .

$[CO_2]_0$ (%)	Azote (%)	Carbone (%)	Hydrogène (%)	Oxygène (%)
1	28.8	32.1	33.6	5.5
	28.9	32	33.8	5.3
5	28.9	28.2	35.6	7.3
	28.6	27.9	36.1	7.4
10	26	28	37.6	8.4

La Figure 2 présente les spectres infrarouges de tholins produits dans des mélanges N_2 - CO_2 - CH_4 pour différentes concentrations initiales de CO_2 . L'analyse de leurs spectres infrarouge montre la présence de fonctions aliphatiques, amines, nitriles et peut-être la présence de fonctions carbonyles et hydroxyles. La présence de ces fonctions est en accord avec la composition de la phase gazeuse dans laquelle croissent les tholins.

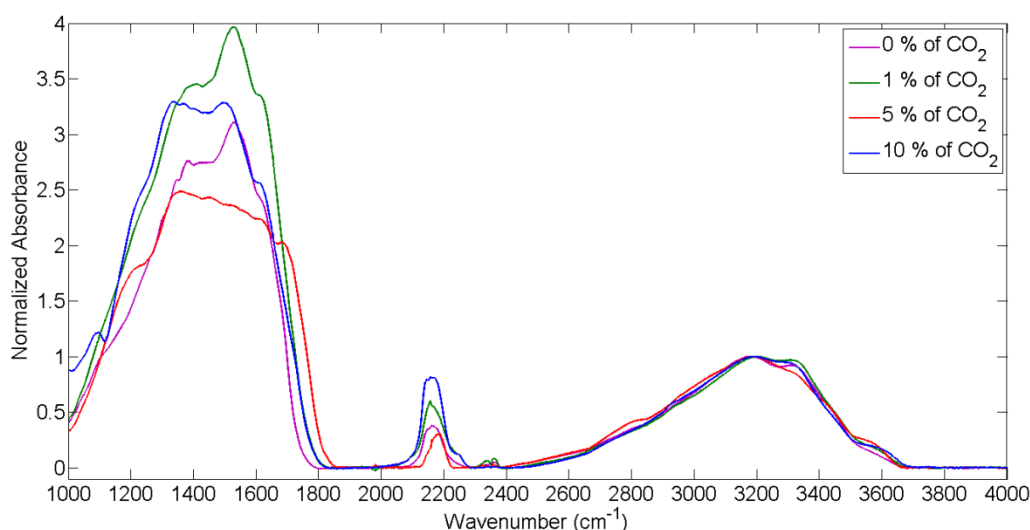


Figure 2: Spectres infrarouge de tholins produits dans des mélanges N_2 - CO_2 - CH_4 pour différentes concentrations initiales de CO_2 .

La comparaison de la réactivité des deux atmosphères simulées fait ressortir quelques différences. Premièrement, les mélanges contenant du méthane produisent des produits organiques gazeux et solides en plus grandes quantités que les mélanges contenant du H_2 . Ce phénomène est particulièrement important pour la formation des tholins. En effet, dans les mélanges contenant du méthane, ils sont produits comme des grains dans le plasma ou comme des films déposés sur un substrat alors qu'ils ne sont produits que comme films déposés sur un substrat pour les mélanges avec du dihydrogène. De plus, l'augmentation de la concentration initiale de CO_2 dans le milieu réactionnel a des effets opposés sur la quantité de

Résumé

produits formés en fonction du mélange gazeux considéré. Le CO₂ est l'unique source de carbone pour la croissance organique dans les mélanges avec H₂. L'augmentation de la concentration initiale de CO₂ induit donc une augmentation de la quantité de produits formés. L'effet inverse est observé pour les mélanges contenant du méthane. Ces tendances sont illustrées dans le tableau 2 qui présente les évolutions de la quantité de tholins collectés et du taux horaire de production de tholins, pour des mélanges contenant du méthane, en fonction de la concentration initiale de CO₂. Ainsi la quantité de tholins produite diminue quand la concentration initiale de CO₂ augmente.

Table 2: Evolution du taux de production des tholins en fonction de [CO₂]₀. a Tholins produits à 0.9 mbar. b Tholins produits à 2.2 mbar.

[CO ₂] ₀ (%)	Masses de tholins collectés (mg)	Taux de production (mg.h ⁻¹)
1	79.5 ^a	9.94 ^a
	120.1 ^a	4.68 ^a
5	36.1 ^b	5.1 ^b
	<0.1 ^a	
10	3 ^a	0.18 ^a
	<0.1 ^a	

Il résulte de l'étude de ces deux mélanges qu'un haut niveau de CO₂ dans l'atmosphère terrestre durant l'Hadéen et l'Archéen serait plus favorable à une production importante de composés organiques si cette atmosphère était composée de N₂, CO₂ et H₂. Toutefois, ce résultat est nuancé par le fait que la croissance organique est plus efficace dans les mélanges contenant du méthane que dans les mélanges contenant du dihydrogène. De plus, si une forte concentration de CO₂ inhibe la formation de tholins, ceux-ci ont une composition chimique différente, incorporant une plus grande quantité d'oxygène. Cette incorporation serait favorable à la formation d'une plus grande variété de molécules organiques et notamment des molécules d'intérêts prébiotiques.

Le chapitre V est consacré à l'étude de l'influence de CO, sur la réactivité de l'atmosphère de Titan. Titan est le plus grand satellite de Saturne et a une atmosphère composée majoritairement de N₂ et CH₄ qui sont à la base d'une chimie organique complexe initiée par les photons VUV solaire et les particules énergétiques de la magnétosphère de Saturne. Bien que plus réduite que l'atmosphère de la Terre primitive, elle contient une faible proportion de

Résumé

composés oxygénés, principalement CO, et l'étude de sa réactivité chimique peut permettre de comprendre la chimie atmosphérique passée de la Terre. Pour cela, j'ai également utilisé l'expérience PAMPRE en utilisant un mélange gazeux composé de N₂, de CH₄ et de CO.

Le principal effet de l'ajout de CO au mélange N₂-CH₄, habituellement utilisé pour simuler l'atmosphère de Titan, consiste en une baisse drastique de la conversion gaz-particule qui est d'autant plus forte que la concentration initiale de CO augmente. Cela se traduit par une augmentation de la quantité de gaz produits et une diminution de la quantité de tholins produits quand la concentration initiale de CO augmente. L'ajout de CO au mélange réactionnel induit également une complexification de la chimie. J'ai observé dans la phase gazeuse la formation de CO₂ et N₂O grâce à une analyse de sa composition par GC-MS. En plus de cette formation de produits gazeux oxygénés, l'analyse élémentaire de tholins formés en présence de CO a mis en évidence une incorporation effective d'oxygène dans les tholins. La présence d'oxygène dans les produits gazeux comme solide met en évidence le couplage entre la chimie de l'oxygène et les chimies du carbone, de l'azote et de l'hydrogène habituellement considérées pour Titan.

La comparaison des expériences réalisées dans un mélange N₂-CO-CH₄ et dans un mélange N₂-CO₂-CH₄ met en évidence certaines similitudes mais aussi des différences. Notamment, l'ajout de CO ou de CO₂ inhibe la croissance organique. Pour CO, cela se traduit par une diminution de la conversion gaz-particule quand pour CO₂ cela se traduit par une diminution conjointe des quantités de gaz et de particules formées. L'ajout des deux molécules entraîne une complexification de la chimie. Cela se traduit par la formation de molécules oxygénées en phase gaz et par l'incorporation d'oxygène dans les tholins mettant en évidence un couplage entre la chimie C, N, H et la chimie de l'oxygène. Toutefois, les molécules observées en phase gazeuse ne sont pas les mêmes. H₂O et H₂CO ont été observés pour les mélanges contenant CO₂ quand N₂O et CO₂ ont été observés dans les mélanges contenant CO. De plus, la présence de CO₂ induit une incorporation d'oxygène dans les tholins plus efficace que CO.

Enfin le Chapitre VI présente une étude expérimentale de l'évolution chimique des aérosols de Titan durant leurs sédimentations à travers l'atmosphère vers la surface. Pour cela, des analogues d'aérosols de Titan, appelés tholins, ont été exposés à un flux de photons VUV pour simuler un processus de vieillissement des aérosols pouvant avoir lieu dans la thermosphère de Titan. D'autre part des tholins recouvert par une espèce en phase condensée ont été exposés un flux de photons UV pour simuler d'autres processus de vieillissement qui

Résumé

pourraient avoir lieu dans la troposphère ou la stratosphère de Titan ainsi qu'à sa surface. Dans l'atmosphère de Titan, la formation des aérosols est initiée dans la thermosphère à environ 1000 km. Après leur formation et durant leur sédimentation notamment entre 1000 et 600 km d'altitude, ils restent exposés au rayonnement VUV solaire. Pour simuler ces effets, des films de tholins ont été exposés au rayonnement VUV d'une ligne du synchrotron SOLEIL. Les effets de l'exposition des tholins à trois longueurs d'ondes différentes ont été étudiés : 95 nm, 121.6 nm et 190 nm. L'évolution chimique des tholins a été mesurée en étudiant l'évolution de leurs signatures par spectroscopie d'absorption infrarouge.

De manière générale, pour toutes les longueurs d'ondes utilisées dans ces expériences, une augmentation des signatures des groupements alkyles est visible dans la région 2700-3000 cm^{-1} . Les spectres infrarouges des échantillons en fonction de la longueur d'onde d'irradiation sont présentés dans la Figure 3. L'effet le plus significatif est observé pour l'échantillon irradié à 95 nm.

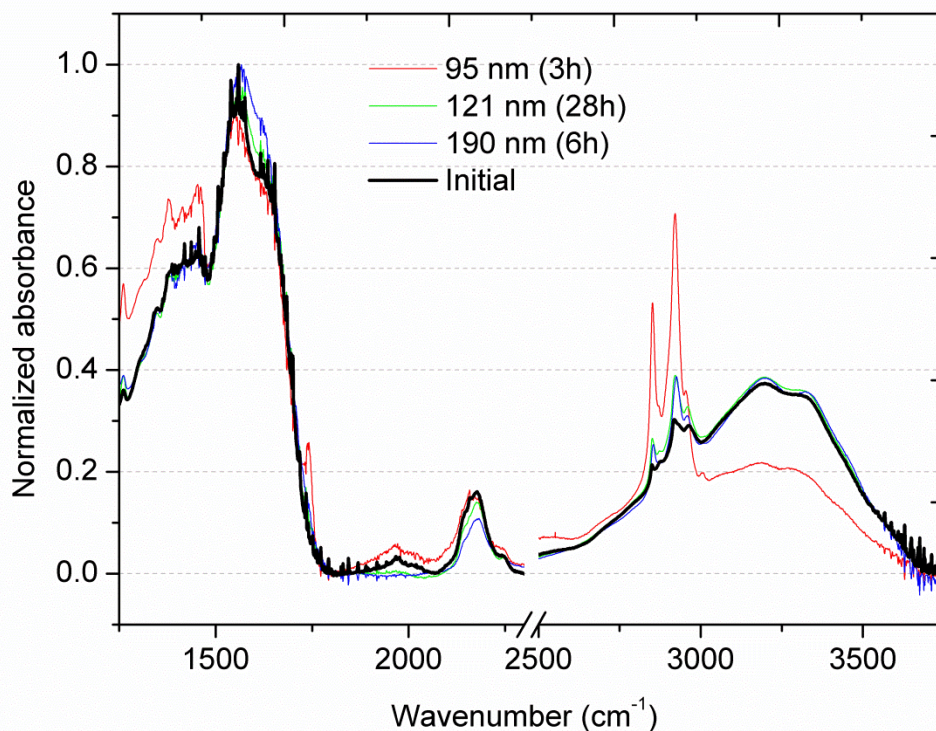


Figure 3: Spectres d'absorption infrarouge enregistrés pour des échantillons irradiés 3 heures à 95 nm, 28 heures à 121.6 nm et 6 heures à 190 nm. La courbe noire épaisse correspond à la moyenne des spectres de tholins non irradiés présenté dans la Figure 49.

En effet, pour l'irradiation à 95 nm, on observe que la signature des fonctions amines présente dans les tholins (NH et NH₂), centrée à 3250 cm^{-1} , diminue de presque 50 % par rapport à l'échantillon de référence. Au contraire, les bandes des groupements alkyles CH₂ et CH₃

Résumé

augmentent drastiquement. Si l'on regarde plus attentivement l'évolution des bandes alkyles dans la région 2700-3000 cm^{-1} , on observe que deux bandes d'absorption deviennent prédominantes à 2850 cm^{-1} et 2920 cm^{-1} . Ces bandes correspondent à des modes d'élongations symétriques et asymétriques de CH_2 mettant en avant que le ratio CH_2/CH_3 augmente dans les échantillons après irradiation. Cette observation est corrélée à l'augmentation des modes de déformations de CH_2 et CH_3 à environ 1400 cm^{-1} . L'irradiation crée donc un transfert de H depuis N vers C entraînant une diminution de la signature des amines et une augmentation de la signature des hydrocarbures saturés. Les fonctions nitriles ($-\text{CN}$) à 2220 cm^{-1} sont moins altérées par l'irradiation. Une forte irradiation VUV avec des longueurs d'ondes inférieures à 100 nm comme dans la thermosphère de Titan, peu sélectivement diminuer les fonctions amines primaires et secondaires en favorisant les fonctions aliphatiques. Cette irradiation préserve les fonctions azotées présentes plus profondément dans la structure des aérosols comme les nitriles, les imines ou les amines tertiaires. Ces résultats peuvent participer à l'interprétation de l'apparente contradiction entre les aérosols riches en azote analysés par l'instrument ACP-GCMS sur l'atterrisseur Huygens et l'absence de fonctions amines observées dans l'infrarouge par l'instrument VIMS sur l'orbiteur Cassini.

La deuxième partie du Chapitre VI qui a été réalisée avec l'expérience Acquabella présente l'étude de la réactivité d'espèces en phase condensée déposées à la surface de tholins lorsqu'elles sont irradiées par un laser dans l'UV. L'étude comparée de la réactivité de l'acétylène seul ou déposé à la surface de tholins et irradié à 355 nm a montré une différence importante de réactivité. En effet, l'acétylène seul réagit peu à cette longueur d'onde. Cela se traduit par une consommation de C_2H_2 inférieure à 10 % après 3 heures d'irradiation. Au contraire, la réactivité de C_2H_2 est promue par la présence des tholins. Cela se traduit par une consommation de C_2H_2 de l'ordre de 45 % après 3 heures d'irradiation. L'utilisation d'acétylène marqué avec du deutérium a montré une modification dans la signature infrarouge des tholins utilisés pour ces expériences après la sublimation du C_2D_2 restant. En effet, de nouvelles bandes d'absorption correspondant à un groupement $-\text{CD}$ ont été observées, mettant en avant l'évolution chimique des tholins lors de ces expériences mettant en avant une réactivité à l'interface tholins/acétylène. Un tel phénomène pourrait avoir lieu dans la basse atmosphère ou la surface de Titan entraînant une évolution chimique des aérosols formés à plus haute altitude.

Résumé

Dans cette thèse, j'ai mis en avant expérimentalement une possible formation quantitative de composés organiques dans deux mélanges gazeux représentatifs de l'atmosphère de la Terre primitive : $N_2/CO_2/H_2$ et $N_2/CO_2/CH_4$. De manière générale, j'observe la formation de composés organiques volatiles ainsi que la formation d'aérosols solides composés d'atomes de carbone, d'hydrogène, d'azote et d'oxygène, mettant en avant un couplage de la chimie de ces quatre éléments dans les expériences réalisées. Des résultats similaires ont été observés dans les expériences que j'ai réalisé avec des mélanges $N_2/CO/CH_4$ représentatifs de l'atmosphère de Titan montrant des similarités entre la réactivité de l'atmosphère de Titan et celle supposée de l'atmosphère de la Terre primitive. De plus, j'ai réalisé des expériences pour étudier l'évolution chimique des aérosols de Titan lors de leur sédimentation à travers l'atmosphère jusqu'à la surface. Ces expériences ont mis en avant une possible évolution des aérosols lorsqu'ils sont exposés à un rayonnement VUV ou lorsqu'ils sont irradiés par un rayonnement UV en interactions avec une espèce en phase condensée. Plusieurs perspectives peuvent être envisagées au travail réalisé durant cette thèse. En premier lieu, la formation d' H_2O pourrait conduire à la formation de nuages de haute altitude dans l'atmosphère de la Terre primitive. Un travail de modélisation serait nécessaire pour mieux comprendre la formation de ces nuages ainsi que leurs impacts sur la chimie atmosphérique et le climat de la Terre primitive. Deuxièmement, l'étude des aérosols formés dans ces expériences a montré une incorporation quantitative d'oxygène dans ces aérosols. Toutefois, la nature des molécules composant les aérosols reste inconnue. Un travail supplémentaire d'analyse de la composition chimique de ces aérosols est nécessaire pour mieux comprendre leur composition et leurs mécanismes de formation.

Chapter I The atmosphere of the early Earth and the origin of the organic matter

I.1 Context

Up to day, the Earth is to our knowledge the only one example of planet where life appeared. Life is supposed to have appeared on Earth before 3.5 Ga during the Archean and maybe before the Late Heavy Bombardment (LHB) during the Hadean (Nisbet and Sleep, 2001). The oldest certain traces of life discovered on Earth are fossils of stromatolite dated back to 2.7 Ga (Brocks, 1999) and the oldest probable traces of life discovered on Earth are fossils of bacteria dated back to 3.5 Ga (Schopf, 2006). Moreover, carbon grains depleted in ^{13}C include in sediment dated back to 3.8 Ga have been proposed as possible traces of life (Mojzsis et al., 1996; Rosing, 1999). However, the dating of the sediments and the biological origin of the ^{13}C depletion measured are contested. Indeed, a new analysis of the crystals where are included the grains of carbon proposed a new dating for their formation 1.75 Ga ago. (Whitehouse et al., 2009). Moreover, other analyses are pointed out that carbon grain presenting a ^{13}C depletion can be formed by non-biological processes and that they can therefore not be used as a biological tracer (Papineau et al., 2011).

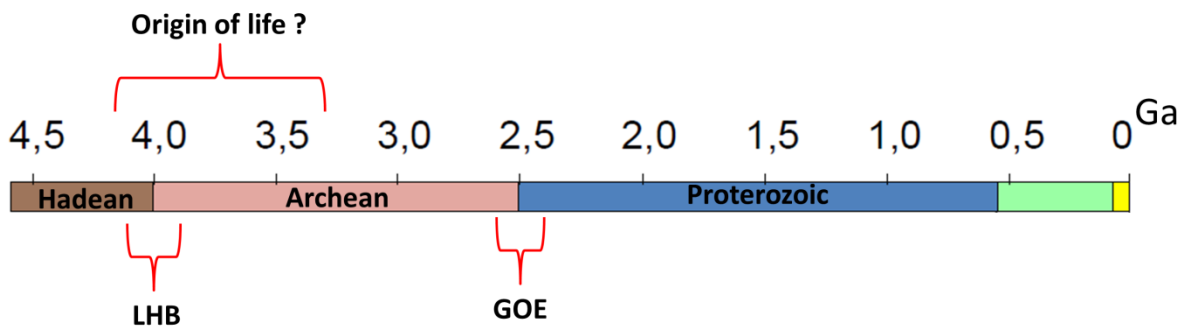


Figure 4: Geological time scale.

The Hadean is a period of the geological time scale (Figure 4), which starts 4.56 Ga ago with the Earth's formation and ends 4 Ga ago with the LHB. The Hadean is followed by the Archean, which starts 4 Ga ago with the end of the LHB and ends 2.5 Ga ago with the Great Oxidation Event (GOE).

The transition from the non-existence to the existence of life remains an enigma for science. The main idea developed is that life could have appeared when physicochemical conditions on the early Earth became compatible with the survival of complex biomolecules (Gargaud et al., 2012b). For this reason, many works are made to understand the environment of the early Earth, where life has appeared. Despite the fact that the Hadean and the Archean represent half of the Earth history, they remain largely unknown notably because the Earth surface has not conserved traces of rocks older than 4.0 Ga and only few minerals as zircons presented in these rocks have been preserved, which provided only indirect information about terrestrial environment as the oxidation state of the magma for example (Bowring and Williams, 1999).

One of these conditions would be the presence of liquid water. Water presents particular properties important for the structuration and the reactivity of biological macromolecules (Bartik et al., 2011). The analysis of oxygen isotopic composition of zircons highlighted the presence of liquid water at the surface 4.3 Ga ago (Mojzsis et al., 2001). This attested the presence of liquid water early in the Earth history, which could be favorable to an early apparition of life during the Hadean. Modeling study showed that the integrated mass of asteroids reaching the Earth during the LHB (Gomes et al., 2005) was too low to evaporate completely the oceans or to warm it up to 100 °C (Abramov and Mojzsis, 2009; Martin et al., 2006; Zahnle and Sleep, 2006). In consequence, if life has appeared during the Hadean, it can have been preserved during the LHB (Abramov and Mojzsis, 2009).

Another important condition will be the presence of organic molecules. Organic molecules implicated in biological processes are mainly composed of carbon, nitrogen, oxygen and hydrogen. Earth accretion has occurred in a Solar System region where temperature was too high for the condensation of these volatile molecules (Albarede et al., 2013; Marty, 2012) implicating an external source later in the Earth history (Owen and Bar-Nun, 1995). These volatile species have been accreted from undifferentiated planetesimals coming from the outer Solar System during an event named Late Veneer (Albarede, 2009). This involves that organic matter has been formed on the Earth after this accretion of volatiles or has been provided by an external source.

I.2 The origin of the organic matter on the early Earth

Three sources are suggested for the organic matter on the early Earth. The first one is an exogenous contribution from meteorites and comets. The two other sources are endogenous: formation of organic matter in hydrothermal vents or in the atmosphere.

I.2.1 The exogenous sources

Today, 40 000 tons of extraterrestrial matters enter in the Earth atmosphere every year (Zook, 2001). The majority of this matter is consumed in the atmosphere but a part reaches the surface. Two types of matter reach the Earth: micrometeorites and meteorites, which are collected at the surface, and Interplanetary Dust Particles (IDP), which are coming from asteroids or comets and are collected in the stratosphere (Brownlee, 1985).

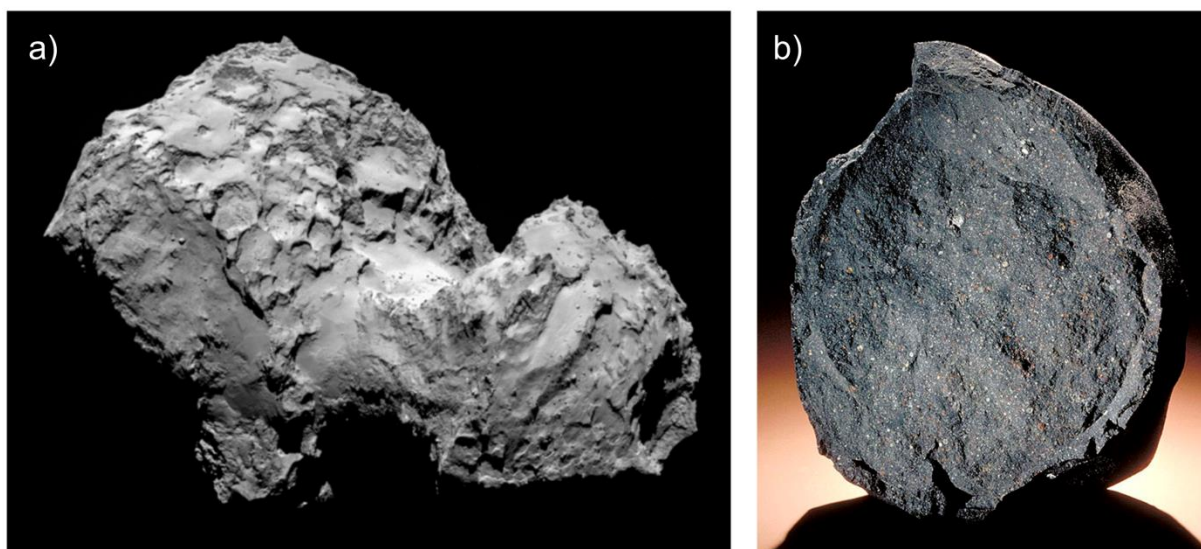


Figure 5: a) Comet 67P/Churyumov-Gerasimenko image recorded by Rosetta's OSIRIS narrow-angle camera from a distance of 285 km. © ESA/Rosetta/MPS for OSIRIS Team MPS/UPD/LAM/IAA/SSO/INTA/UPM/DASP/IDA b) Murchison meteorite © Smithsonian Institution National Museum of Natural History.

Meteorites are classified in different families depending on their composition and their origin from a differentiated or an undifferentiated body. The analysis of the composition of these different types of meteorites has shown that one type of meteorites named carbonaceous chondrites is rich in carbon notably in organic matter, which can represent up to 3.2 % in mass (Kerridge, 1985). This organic matter is composed of two phases: a Soluble Organic Matter (SOM) composed of small molecules and an Insoluble Organic Matter (IOM) composed of macromolecules and, which represent the majority of the organic matter of the chondrites (Pizzarello et al., 2006). SOM is the part of the organic molecules, which is soluble in organic solvent (ethanol for example).

The analysis of the SOM in the Murchison meteorite (panel b) of the Figure 5 has shown the presence of a large variety of chemical functions: carboxylic acid, hydrocarbons, aldehydes, ketones, amines, Polycyclic Aromatic Hydrocarbons (PAH) and amino acids (Botta and Bada, 2002; Kvenvolden et al., 1970; Schmitt-Kopplin et al., 2010). IOM are refractory solid organics made of C, H, N, O and S atoms and containing amines, cyanides and aliphatic groups (Alexander et al., 2007).

IDPs are also rich in organic matter (Brunetto et al., 2011). A part of these IDPs comes from comets. Comets are formed by a silicate nucleus (Greenberg, 1982) surrounded by ices, dusts and refractory organic compounds (Strazzulla et al., 1991). The panel a) of the Figure 5 presents an image of the comet 67P/Churyumov-Gerasimenko realized by the OSIRIS instrument onboard the Rosetta spacecraft.

Comets are presented in two stable reservoirs in the Solar System: the Kuiper belt and the Oort cloud (Morbidelli, 2008). Sometimes, comets can be ejected from their reservoirs because of a gravitational perturbation. Then, they can reach the inner Solar System following elliptic orbits. When they are close to the Sun, ices composing the comet sublime involving an ejection of gases and dusts. An atmosphere named coma is created around the cometary nucleus. Different analysis of the cometary composition have been done with ground based observations or *in-situ* analyzed by space missions. A large variety of volatile organic species (hydrocarbons, nitrile, carboxylic acids, alcohol and aldehydes) have been detected in the coma surrounded comets (Bockelée-Morvan et al., 2004). The *in-situ* analysis of dust from the comet Haley by mass spectrometry has highlighted the presence of organic molecules with a high molecular weight up to 170 u (Kissel and Krueger, 1987). Moreover, organic molecules in cometary dusts have been confirmed by analysis of dust collected by the Stardust comet sample return mission on the 81P/Wild 2 comet (Sandford et al., 2006) despite a possible contamination of the samples by terrestrial organic compounds (Sandford et al., 2010). The analysis of the carbon isotopic ratios of different organic molecules presented in the samples has permitted to establish an extraterrestrial origin for several molecules as for example for the most abundant amino acid presented in the samples: glycine (Elsila et al., 2009).

A possible enrichment of the early Earth in organic matter by comets has been firstly proposed by (Oro, 1961). Indeed, after the Earth accretion, at the start of the Hadean and during the LHB, the Earth was bombarded by meteorites and comets, which could provide the

organic matter on the early Earth (Chyba and Sagan, 1992). Despite the fact that meteorites would be partially burned by their entering in the atmosphere, a part of the organic matter, which contained could be preserved (Chyba et al., 1990). However, it remains difficult to estimate the amount of organic matter provided by meteorite and comets. For this reason, other sources of organic matter are suggested.

I.2.2 The endogenous sources

If meteorites and comets could have contributed to the enrichment of the early Earth in organic molecules, these molecules can be also produced directly on the early Earth in the atmosphere or in hydrothermal vents.

I.2.2.a The hydrothermal vents

The hydrothermal vents were discovered on Earth in 1977. These systems can be found all over the planet at mid-oceans ridges. They are formed by the infiltration of water in the ocean floor, which is heated by the magma present close to the surface. Water dissolves rocks constituents and escapes from the ocean floor trained by hot gases. In contact with cold ocean water, a part of chemical species present in these hydrothermal fluids precipitates forming the vents.

The hydrothermal fluids contain small oxidized or reduced molecules: CO₂, CO, H₂, CH₄ and H₂S. Reactivity of these species leads to the formation of small hydrocarbons (C₁ to C₄) through abiotic Fischer-Tropsch type reactions (Proskurowski, 2008). To resume, Fischer-Tropsch process is a series of reactions, which convert H₂ and CO in hydrocarbons and water. Then a large variety of organic function groups as alcohol, ketones or carboxylic acids can be formed from these small hydrocarbons (Shipp et al., 2013). It has been proposed that this reactivity could contribute to the formation of organic matter during the Hadean (Shock and Schulte, 1998), a period where these systems are supposed to be more than today. Moreover, experimental works have showed the formation of amino acids in hydrothermal conditions (Marshall, 1994). However, this is difficult to extrapolate from these experiments the quantity of amino acids, which have been produced in hydrothermal vents on the early Earth. Furthermore, other experiments point out that hydrothermal conditions are not favorable to the formation of more complex molecules as peptides, which are degraded through hydrolysis reactions (Miller and Bada, 1988; Shock, 1992). It therefore remains difficult to define how the organic chemistry occurring in hydrothermal systems has contributed to enrich

quantitatively the primitive Earth in organic matter, and with what degrees of complexity it can have occurred (Gargaud et al., 2012b).

I.2.2.b The atmosphere

The last important source of organic matter for the early Earth is an abiotic production in the atmosphere from the photochemistry of the atmospheric constituents. This idea was evocated firstly by A. I. Oparin and J. B.S. Haldane, who assumed that the primitive atmosphere of the Earth was reduced and who proposed that organic compounds could be formed in this primitive atmosphere and enriched a primitive ocean, where more complex molecules were formed (Haldane, 1929; Oparin, 1938). They created the idea of the ‘prebiotic soup’.

A new experimental approach

Taking into account this new theory, H. C. Urey proposed a primitive atmosphere made of nitrogen N_2 or ammonia NH_3 , methane CH_4 , hydrogen H_2 and water H_2O (Urey, 1952). The reactivity of this atmosphere was investigated experimentally in Miller, 1953. For that, he designed a new experiment described in Figure 6.

S. Miller used a gaseous mixture made of CH_4 , H_2 and NH_3 as well as water vapor produced by heating liquid water. Chemistry was initiated in the gaseous phase with spark discharges to simulate lightning. Then, water vapor was condensed and its composition analyzed. He highlighted in the collected aqueous phase the presence of different organic compounds as hydrogen cyanide HCN or formaldehyde H_2CO but also the presence of few amino acids: glycine, α -alanine and β -alanine (Miller, 1953).

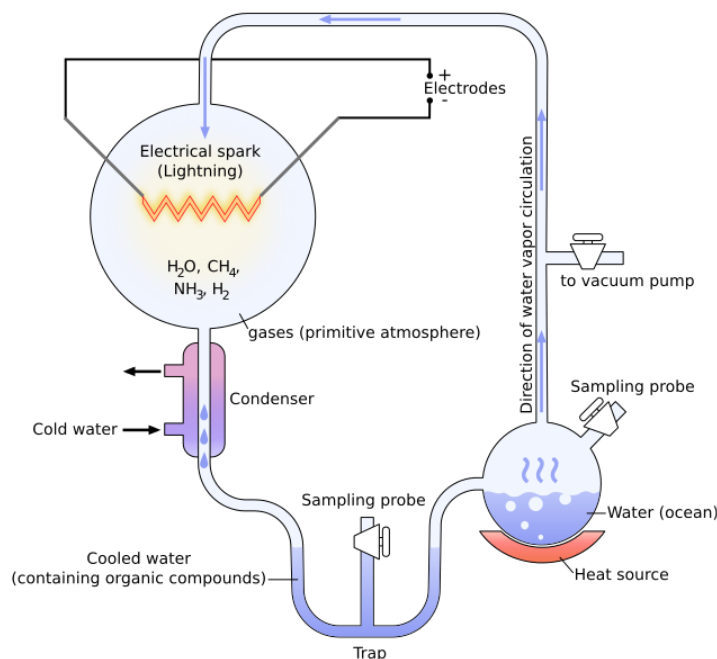


Figure 6: A schematic representation of the Miller-Urey experiment (from (Gargaud et al., 2012c)).

He explained the formation of these amino acids through a mechanism implicating the Strecker synthesis. In this synthesis, HCN and aldehydes, which were formed in the discharge, reacted to form α -aminonitriles. Then, these α -aminonitriles are hydrolyzed to form the corresponding amino acids (Miller, 1957). A later analysis of samples produced in these experiments and in experiments using H_2S to simulate volcanic gases composition (Ring et al., 1972) with new analysis techniques has highlighted the presence of more than the only 5 amino acids detected initially by Miller with the detection of 22 amino acids (Johnson et al., 2008; Parker et al., 2011).

The hypotheses made by Miller and Urey have been questioned since. Firstly, Miller has used spark discharge at room pressure to simulate the lighting on the early Earth troposphere, but this energy source was not the most important for planetary atmospheres. Indeed, chemistry in a planetary atmosphere is principally driven by the UV solar photons flux. Moreover, the more important debate is on the hypothesis of a reduced atmosphere before the apparition of life (Holland, 1962). The question of the composition of the early Earth atmosphere will be discussed in the next section. Nevertheless, different geological constraints on the oxidation state of the magma provided by measurement of isotopic ratio in zircon (Delano, 2001; Trail, 2011) and different modeling studies (Burgisser and Scaillet, 2007; Kasting, 1993) are now in favor of an oxidized early atmosphere mainly composed by N_2 , CO_2 and H_2O . Despite this change about the composition of the primitive atmosphere of the Earth, the Miller's

experiment has inspired lot of other experimental works as well as numerical modeling dedicated to the study of the chemical reactivity of this atmosphere. These studies have explored the reactivity of different atmospheric compositions containing species at different degrees of oxidation. The principal laboratory experiments realized for the primitive atmosphere of the Earth are presented in Table 3. The energy sources used as well as the gaseous mixtures used and the organic products detected in these experiments are indicated.

Table 3: Principal organic synthesis realized with laboratory experiment to simulate the early Earth reactivity. Tholins are solid organic material product in experimental simulations as named by C. Sagan and B. Khare (Sagan and Khare, 1979).

Studies	Energy sources	Gaseous mixtures	Organic products detected
(Johnson et al., 2008; Miller, 1953; Parker et al., 2011)	Electric discharge	H ₂ /NH ₃ /H ₂ O/CH ₄ (+ H ₂ S)	Nitriles/aldehyde Amino acids (after hydrolysis)
(Ferris and Chen, 1975; Ring et al., 1972)	UV (184.9 nm / 253.7 nm) / electric discharge	N ₂ /CH ₄ /H ₂ O	Aldehyde/alcohol/ketone Amino acids (after hydrolysis)
(Bar-Nun and Chang, 1983; Bar-Nun and Hartman, 1978)	UV (184.9 nm/ 253.7 nm)	CO/H ₂ O	hydrocarbon/aldehyde/alcohol/ carboxylic acids Tholins
(Schlesinger and Miller, 1983a; Schlesinger and Miller, 1983b)	Electric discharge	N ₂ /H ₂ /CH ₄ (+NH ₃) N ₂ /H ₂ /CO (+NH ₃) N ₂ /H ₂ /CO ₂ (+NH ₃)	HCN/H ₂ CO/NH ₃ Amino acids (after hydrolysis)
(DeWitt et al., 2009; Hasenkopf et al., 2010; Hasenkopf et al., 2011; Trainer et al., 2004; Trainer et al., 2006)	UV (115-400 nm) / electric discharge	N ₂ /CH ₄ /CO ₂ N ₂ /CH ₄ /CO ₂ /H ₂	Tholins (no diagnosis on the gaseous phase)
(Heinrich et al., 2007)	Electric discharge	N ₂ /H ₂ /CO ₂ /CO N ₂ /H ₂ /CO ₂ /CH ₄	Hydrocarbons/nitriles Tholins

These experiments performed in a large variety of conditions highlighted different points. Organic products could be obtained from the reactivity of a large variety of gaseous mixtures. Volatile products in the gaseous phase but also solid brown refractory organic product are obtained in these experiments. The solid organic product formed in experimental simulations was named tholins by C. Sagan and B. N. Khare (Sagan and Khare, 1979). However, a systematic study of the reactivity of different gaseous mixtures showed that oxidized mixtures are less reactive than reduced mixtures and lead to a lower quantity of organic products (Schlesinger and Miller, 1983a; Schlesinger and Miller, 1983b). Moreover for gaseous mixtures containing CO or CO₂ as oxidized species, the production yields of organic species decrease when the initial amounts of these species increase (Heinrich et al., 2007).

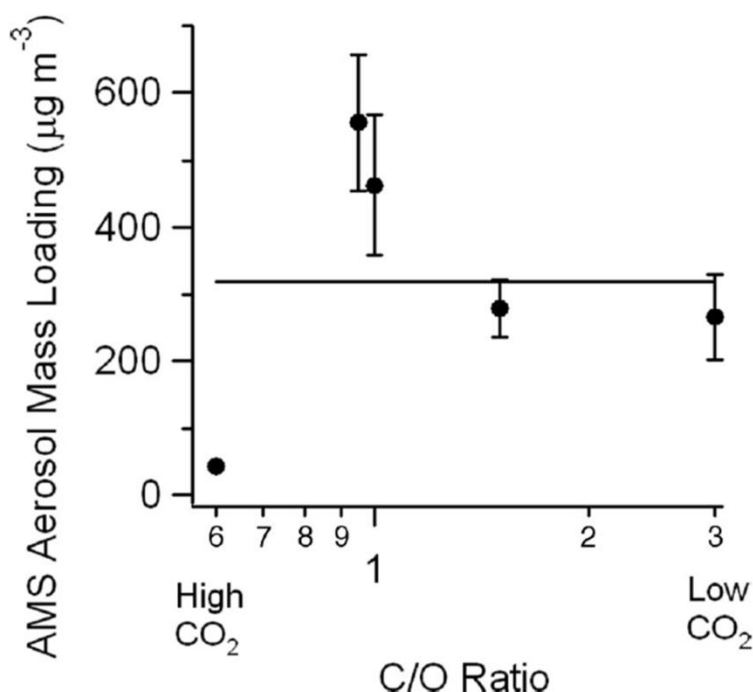


Figure 7: Evolution of the tholins production in experiments of UV irradiation of gaseous mixture made of N₂/CO₂/CH₄ as a function of the C/O ratio. (from (Trainer et al., 2006)).

Nevertheless, a recent experimental study showed that a N₂/CO₂ gaseous mixture, in agreement with the supposed atmospheric composition of the early Earth, was reactive when irradiated by UV photons once a small amount of a reduced species, here 0.1 % of CH₄, was added in the reactive medium (Trainer et al., 2006). Particularly, the formation of tholins is observed for CO₂ concentration as high as 0.5 %. The evolution of the quantity of aerosols detected in this experiment as a function of the C/O ratio is presented in Figure 7. It appears from this study that the atmosphere of the early Earth could be a source of organic matter

even if the major constituents were N_2 and CO_2 . This study highlighted the fact that aerosols could be formed at mixing ratio CH_4/CO_2 as low as 0.2 corresponding to a highly oxidized atmosphere, when previous photochemical modeling indicated that aerosols could be formed only for a ratio CH_4/CO_2 higher than 1 (Pavlov et al., 2001; Zahnle, 1986). Moreover, despite the lower efficiency of the production of organic species, the species produced are more interesting for prebiotic chemistry because they are made of C, N, H and O.

I.3 The early Earth atmosphere

All experimental and modeling studies on the reactivity of the early atmosphere, focused on the formation of organic compounds, are pointed out the importance of the atmospheric composition on the efficiency of this reactivity. Constraining the composition of the atmosphere of the early Earth during the Hadean and the Archean is an important subject of investigation in planetology. If different points are still subject to debate, a scenario has been established for this formation process and constrains the Earth atmospheric composition at this period.

I.3.1 Early atmosphere formation and evolution

Two origins are considered for the formation of early planetary atmospheres: primary and secondary. Primary atmospheres have a Sun-like composition and are mainly made of H_2 and He. This is typically the case of the atmospheres of giant planets in the Solar System. Secondary atmospheres are coming from degassing processes of volatiles from planets interiors (Zahnle et al., 2010). A schematic representation of the early stages of the Earth formation is given in Figure 8 originating from Gargaud et al., 2012a.

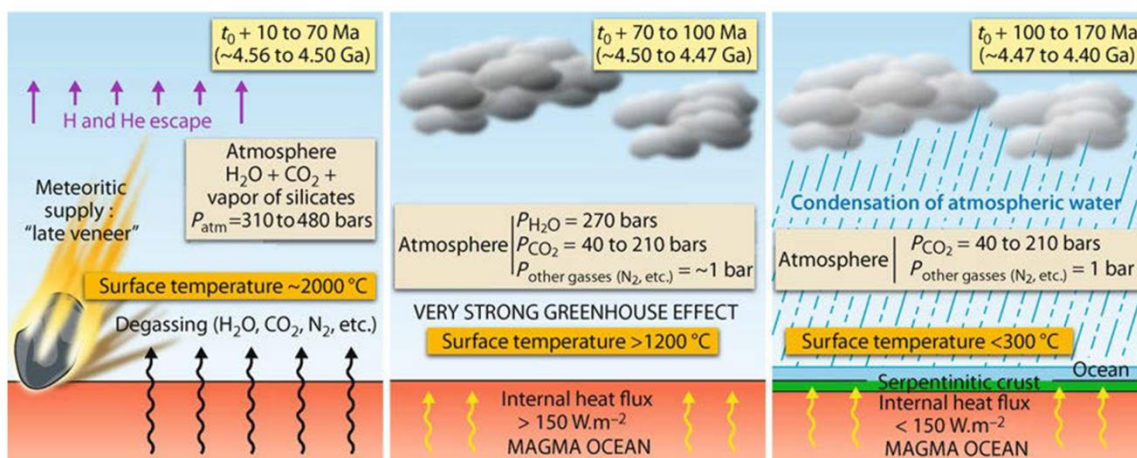


Figure 8: Schematic representation of the various episodes in the evolution of the atmosphere and the hydrosphere before 4.4 Ga (from (Gargaud et al., 2012a))

After the end of the Earth's accretion, the atmosphere was probably originating from the solar nebula and mainly composed of H_2 and He. This primary atmosphere has been lost in space through different mechanisms as hydrodynamic escape and impact erosion during the Late Veneer. The latter event has contributed to enrich the Earth in volatiles (Albarede, 2009; Lammer et al., 2008) and contributed to the C-H-O-N-S Earth's content (Marty, 2012). This primary atmosphere has been replaced by a secondary atmosphere from degassing processes. The composition of the gases emitted is controlled by the oxidation state of the magma (Hirschmann, 2012). Today, the Earth's mantle is oxidized and its oxidation state has not changed since 3.9 Ga (Delano, 2001) and probably 4.4 Ga (Trail, 2011). The resulting atmosphere had a similar composition to actual composition of volcanic emissions, which are mainly made of CO_2 and H_2O and in minor proportion N_2 and SO_2 . Because of the important surface temperature at this time of the Earth history, volatiles emitted and notably H_2O and CO_2 were in gaseous phase in the atmosphere. This involves that the atmosphere contained at least the equivalent of the ocean water content corresponding to a partial pressure of H_2O of 300 bars and contained the CO_2 now trapped as carbonates and corresponding to a minimum partial pressure of 40 bars (Gargaud et al., 2012a). After ~100 Ma, the surface temperature decreased sufficiently to allow the water condensation and the formation of oceans. The measurement of the isotopic composition of Jack Hills zircons dated back to 4.4 Ga has highlighted the presence of a hydrosphere during their formation involving that water was condensed and the oceans formed 4.4 Ga ago. After the condensation of oceans, CO_2 remained the major constituent with at least 40 bars providing an important greenhouse effect resulting in a surface temperature higher than 200 °C. The formation of oceans allowed starting the CO_2 sequestration process. CO_2 dissolved in water could react and precipitate as calcium carbonate $CaCO_3$. Once subduction started on Earth, carbonated could be recycled into the mantle providing a long-term sequestration of CO_2 and permitting a decrease of the greenhouse effect and so of the surface temperature (Nakamura and Kato, 2004).

These different steps of the early formation of the Earth's atmosphere and its evolution have led to the atmospheric composition existing at the end of the Hadean and during the Archean until the GOE.

I.3.2 Constraints on the atmospheric composition of the early Earth

It is now widely accepted that the mechanism of the formation of the Earth atmosphere has led to a primitive atmosphere mainly made of N_2 , CO_2 and H_2O . However, the exact proportions of these species and the proportion of trace gases in the atmosphere as well as

their evolution with time are not clearly determined. This is particularly true for the Hadean, for which no rock has been preserved (Bowring and Williams, 1999). Nevertheless, different constraints are given from geological indices for the Archean (details are given for each species below) and different scenarios are proposed in climate studies. Moreover, these constraints must be replaced in the context of the environment of the Earth 4.5 Ga ago, notably in the context of a young Sun, which have a different spectrum than today as developed in the next section.

I.3.2.a The context of the young Sun

Stars have an important impact on planetary atmospheres, driving different processes such as climate, atmospheric escape and photochemistry. The modeling of the structure of Stars and their evolution during their life time has showed that their luminosity increases with the time, implicating that the Sun has followed the same evolution: it was in the past less luminous than today (Schwarzschild, 1958). The evolution of the solar luminosity over the geological time-scale as described in (Feulner, 2012) is reported on Figure 9.

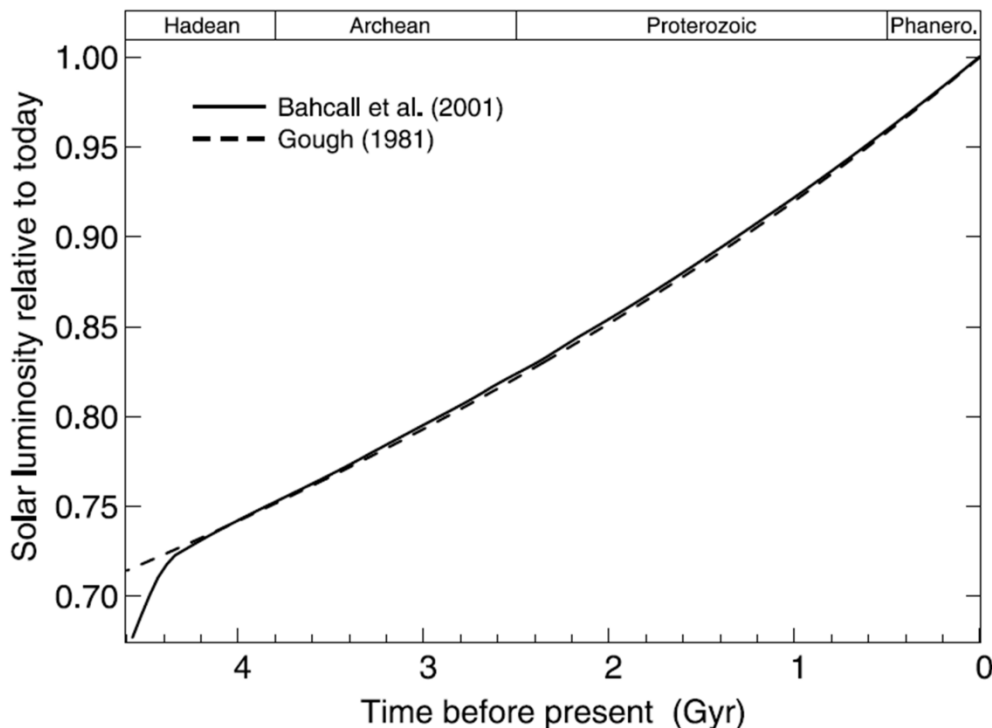


Figure 9: Modeling of the evolution of the solar luminosity over the geological time (from (Feulner, 2012))

Standard models predict that the luminosity of the Sun (i.e. the integrated solar flux) during the Earth's formation was 30 % lower than today (Newman and Rood, 1977). However, modeling studies of the evolution of the solar flux for the different domains of the solar

spectrum have showed that the visible and infrared fluxes increase with the solar life time whereas the UV and X-ray fluxes decrease (Claire et al., 2012; Ribas et al., 2005).

These opposite evolutions have important impacts regarding to our comprehension of the early atmosphere of the Earth. Firstly, higher UV and X-ray fluxes promote the atmospheric escape (Kulikov et al., 2007; Lammer et al., 2008) and modify the photochemistry, increasing the photodissociation rate of molecules (Ribas et al., 2010). The lower visible and infrared fluxes have also an important impact regarding the climate of the early Earth. This gave rise to a paradox named the 'faint young Sun paradox' (Sagan and Mullen, 1972) and, which has been detailed in a recent review (Feulner, 2012). To resume, there is geological evidence of the presence of liquid water on Earth since 4.3 Ga (Mojzsis et al., 2001), which has remained stable during the Hadean and the Archean involving surface temperature higher than 273 K. However, a solar luminosity 30 % lowers than today requires a more efficient greenhouse effect than today to keep the early Earth unfrozen. However, if we consider a N₂-CO₂-H₂O atmosphere, the greenhouse effect provided by the concentrations of these species determined for the Archean (there is no data for the Hadean) would be insufficient to keep the Earth unfrozen. This paradox has led to many studies (Feulner, 2012 and references therein) and many supposition of the early Earth's atmospheric composition, which solved this paradox (Charnay et al., 2013; Kunze et al., 2014; Wolf and Toon, 2014).

I.3.2.b Nitrogen N₂

The analysis of neutral and noble gas isotopes on Earth permit to establish chondritic origins for nitrogen and other volatiles (Marty, 2012). Nitrogen represents today 78 % of the Earth's atmosphere composition corresponding to a partial pressure at the surface of about ~0.79 bar. A recent study has estimated the nitrogen content in the atmosphere by measuring the N₂/³⁶Ar ratio in fluid inclusion of hydrothermal quartz date back 3.0 to 3.5 Ga (Marty, 2013). It comes out from this work that nitrogen is stable in the atmosphere since the Archean. The estimated partial pressure of N₂ for this period is between 0.5 bar and 1.1 bar, close to the present 0.79 bar (Marty, 2013). This concentration is consistent with the surface pressure determined for the end of the Archean from the analysis of the imprints of ancient raindrops dated back to 2.7 Ga (Som et al., 2012). They gave an upper limit for the surface pressure of about 2.1 bars and a probable range between 0.5 bar and 1.1 bars (Som et al., 2012), compatible with the estimation of P_{N₂} (Marty, 2013).

I.3.2.c Water H₂O

In the Earth atmosphere, the water content is principally determined by the surface temperature (Gargaud et al., 2012c). After the condensation of the oceans, the partial pressure of water was probably important because of the important greenhouse effect caused by the CO₂ present in the atmosphere resulting in a 'steam atmosphere'. After the trapping of CO₂ in the carbonates during the Hadean, the partial pressure of H₂O decreased. At the end of the Hadean and the Archean, water mixing ratio is expected to be similar to today with important variations in the time controlled by meteorological phenomenon as precipitations resulting in variations as a function of altitude and latitude (Gargaud et al., 2012c). It must be noticed that atmospheric water is concentrated in the troposphere. Indeed, the decrease of the temperature with a minimum at the tropopause level (if a stratosphere exists) created a cold trap allowing the condensation of water and limiting the transport of water to the high atmosphere, which is considered as dry. Stability of water at the Earth surface over geological time scale has been a key parameter for the apparition of life in opposition with the evolution of Mars and Venus, which have follow different evolution.

I.3.2.d Carbon dioxide CO₂

At a long time-scale, the CO₂ amount in the Earth atmosphere is controlled by the carbonate-silicate cycle (Sleep and Zahnle, 2001). CO₂ atmospheric is trapped by forming CaCO₃, which is recycled in the mantle by subduction process providing a long-time sequestration of CO₂. Then, CO₂ is reemitted in the atmosphere by volcanic emission. CO₂ partial pressure has evolved since a minimum of 40 bars at the Earth formation to the current ~0.4 mbar. The stability of liquid water on the Earth surface was an important parameter to permit this long-time trapping process. Different estimations of the CO₂ partial pressure have been done for the Archean and the Proterozoic from geochemical indicators as paleosols or Banded Iron Formations (BIF). BIF are sedimentary rocks formed in ocean alternating bands of iron oxides whose content could be correlated to the CO₂ atmospheric partial pressure (Rosing et al., 2010). Paleosols are non-marine sedimentary rocks preserved of erosion and whose geochemical composition is used as an indicator of the atmospheric CO₂ partial pressure. A summary of the different values given by Feulner, 2012 is presented in Figure 10.

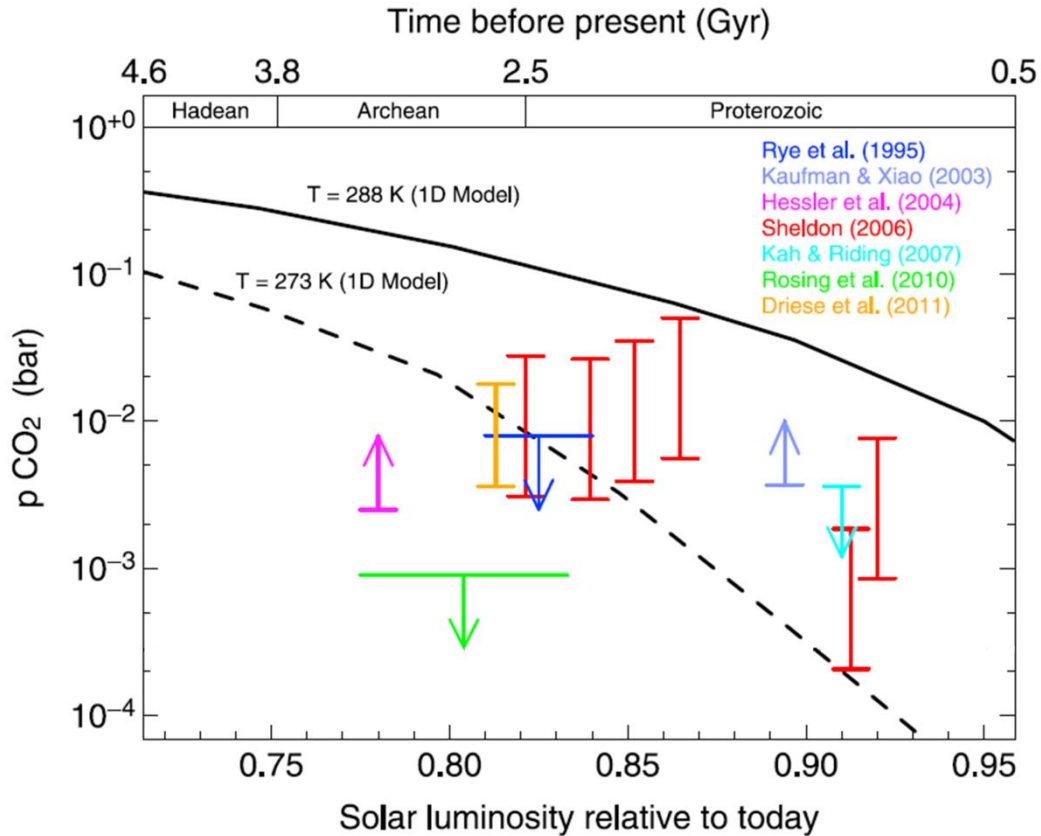


Figure 10: Comparison of the geochemical estimation of the atmospheric CO_2 partial pressure (P_{CO_2}) at different epochs and the calculation in a 1D model of the P_{CO_2} necessary to reach a surface temperature of 273 K and 288 K (from (Feulner, 2012)).

Because of the lack of indicators for the Hadean and the early Archean, the oldest estimation given is dated back to 3.2 Ga with a lower limit for P_{CO_2} of about 2.5 mbar (Hessler et al., 2004).

However, there is some contradiction between the measurements made for the Archean and the quantity necessary to keep the Earth unfrozen as determined by modeling studies. It seems from these data that P_{CO_2} remains lower than 0.01 bar during the Archean corresponding to a content of 1 % according to a total pressure of 1 bar. This is lower than the ~0.03 bar necessary to reach the 273 K and the 0.1 ~bar required to reach a temperature of 288 K for the late Archean (Feulner, 2012; von Paris et al., 2008). For the Hadean, no clear constraint exists. A higher concentration of CO_2 is expected taking into account the mechanism of CO_2 sequestration and the more important greenhouse necessary to keep the Earth unfrozen 3.8 Ga ago than during the late Archean.

I.3.2.e Other gaseous compounds

The model of the Earth's atmosphere formation and different geological indicators have pointed out that the primitive atmosphere of the Earth was oxidized and mainly composed by N_2 , CO_2 and H_2O . However, the presence of trace gases remains possible. Reduced species are suggested to provide a supplementary greenhouse effect to resolve the faint young Sun paradox or as reactive species to provide a source of organic matter before the apparition of life.

Methane CH_4

One of the most studied species is methane, principally as a greenhouse gases (Feulner, 2012). Different modeling studies have studied this possibility. Recently a study using a Global Circulation Model (GCM) showed that a relative small amount of methane about 2 mbar should be sufficient to reach a surface temperature about 285 K in addition of 10 mbar of CO_2 at the end of the Archean and in addition of 0.1 bar of CO_2 at the beginning of the Archean (Charnay et al., 2013). However, such a scenario has two oppositions.

Firstly, the presence of a high level of CH_4 could lead to the formation of organic hazes, which could be responsible for an antigreenhouse effect depending of their form and composition (McKay et al., 1999). Secondly, the presence of methane during the Hadean and the early Archean remains largely debated. Indeed, today 70 % of the methane emissions have biogenic sources and for an important part from ecosystems, which do not exist during the Archean (Denman et al., 2007). Two abiotic sources of CH_4 can be considered for the early Earth atmosphere: delivery by meteoritic and cometary impacts or geological sources (Kasting, 2005). Estimation of the amount of methane, which can be delivered during the LHB correspond to a mixing ratio about ~ 7 ppm_v in the atmosphere, 3.8 Ga ago (Feulner, 2012; Kasting, 2005). The geological source corresponds to mineral alterations ad mid-ocean ridges, named serpentinization process. A mixing ratio of few ppm_v has been estimated from modeling studies when taking into account the methane flux from the only serpentinization process (Emmanuel and Ague, 2007; Guzmán-Marmolejo et al., 2013).

Taking account these abiotic sources, the mixing ratio of CH_4 during the Hadean and the early Archean, prior to the apparition of life, should be lower than 10 ppm_v corresponding to a partial pressure about 10^{-2} mbar for a total pressure of 1 bar, two orders of magnitude lower than the 2 mbar considered in (Charnay et al., 2013). There is no evidence of a significant presence of methane during the Hadean and the early Archean to contribute to the greenhouse

or to contribute to organic chemistry. However, after the apparition of life and particularly the apparition of methanogen bacteria, the methane concentration could increase during the Archean and impact the climate and chemistry of the late Archean. Indeed, a study coupling an atmospheric model with an ecosystem model has given a range between 100 ppm_v and 3.5 % of CH₄ issued of the biogenic activity during the Archean (Kharecha et al., 2005).

Hydrogen H₂

The content of hydrogen in the atmosphere depends on the emission flux from volcanism outgassing and the loss of atomic H in space through Jeans escape (Martin et al., 2006). Assuming that the loss of hydrogen to space was limited by diffusion, a mixing ratio of 10⁻³ has been established for the early Earth's atmosphere by Kasting, 1993. However, these assumptions have been reconsidered by Tian, 2005, which proposed that Jeans escape in the past was less efficient than today. This hypothesis is explained by the dependence of the Jeans escape on the exobase temperature. The important temperature of the present exobase at ~1000 K results in the efficient UV absorption by atomic oxygen O. However, the early atmosphere was anoxic and rich in CO₂, which absorbs UV but also efficiently radiates energy back in space resulting in a colder exobase (Martin et al., 2006; Tian et al., 2005). It results in the fact that the hydrogen mixing ratio could be 100 times higher than proposed by (Kasting, 1993), representing 10 % of the atmospheric content and up to 30 % (Tian et al., 2005). However this new calculation have been debated in (Catling, 2006; Tian et al., 2006). Principally, (Catling, 2006) argued that the exobase temperature could not be as low as proposed by Tian, 2005 because of the limited amount of CO₂ to cool it and because of a possible effective heating by other molecules than oxygen. A more recent study has tried to reconsider this hypothesis of a high level of hydrogen. Calculation realized by a model, considered as more realistic than the one used by Tian, 2005, proposed that hydrogen escape remains efficient during the Hadean and Archean resulting in a hydrogen mixing ratio about 1 % at the homopause (Kuramoto et al., 2013). It results that the exact concentration of hydrogen remains difficult to determine and dependent on the hypothesis used. Depending on the study considered, the mixing ratio varied from 10⁻³ to few percents. A high level of hydrogen would have an important impact for the early Earth, favoring the formation of organic compounds in this oxidized atmosphere or providing an additional greenhouse effect by H₂-N₂ collision-induced absorption depending of the amount of the both gases (Wordsworth and Pierrehumbert, 2013). For these reasons, H₂ could be an important

component of the primitive atmosphere and its influence of the atmospheric reactivity must be studied.

I.4 Conclusion

The origin and the nature of the organic matter present on the early Earth before the apparition of life remain largely unknown today. A possible formation of organic molecules on the reduced primitive atmosphere has been proposed by Oparin and Haldane and investigated experimentally by Miller and Urey (Miller, 1953). But, the atmosphere of the early Earth was probably neutral or oxidized, dominated by N_2 and CO_2 , which are less reactive (Kasting, 1993). More recently, the irradiation at Lyman- α of a $N_2/CO_2/CH_4$ gaseous mixture has highlighted a potential CH_4 -based organic growth (Trainer et al., 2006). This wavelength prevents the direct coupling with the molecular nitrogen chemistry by the N_2 dissociation, necessary to form complex molecules including C, N, H and O important for the prebiotic chemistry. However, nitrogen chemistry activation is possible at these wavelengths at high pressure through trimolecular reactions (Trainer et al., 2012; Yoon et al., 2014).

Based on these previous experiments, this thesis is dedicated to the study of a possible organic chemistry, in an experiment representative of the upper atmosphere of the early Earth and involving molecular nitrogen chemistry. The aim of this thesis is to characterize the nature of the organic molecules formed in the simulated atmospheres as well as the influence of the atmospheric composition on the chemistry: qualitatively and quantitatively.

After a description of the experimental methods employed for this thesis in the Chapter II, the Chapters III and IV are dedicated to the study of two gaseous mixtures corresponding to two potentials primitive atmospheric compositions: $N_2/CO_2/H_2$ and $N_2/CO_2/CH_4$ respectively. A systematic approach is used with an analysis of the gaseous phase principally by mass spectrometry and also by infrared spectroscopy and GC-MS. The characterization of solid organic, which could be formed in the gaseous phase, is realized using infrared spectroscopy and elemental analysis.

A similar approach has been employed in the Chapter V, which is dedicated to the study of the influence of CO, which is present as a trace species in the atmosphere of Titan, the largest satellite of Saturn. Titan has a dense atmosphere principally made of N_2 and CH_4 at the origin of a complex atmospheric chemistry drive by VUV solar photons. If the Titan's atmosphere is more reduced than one expected for the early Earth atmosphere, the processes taking place in

Chapter I The atmosphere of the early Earth and the origin of the organic matter

the atmosphere of Titan provide a natural case to help the understanding of the phenomena, which have occurred in the early Earth atmosphere.

Our knowledge of the Titan's atmospheric reactivity is more important than one concerning the early Earth reactivity. The aerosols formation is known to be initiated in the thermosphere from, which they sediment to the surface. The Chapter VI presents an experimental study of a two possible mechanism of chemical evolution of the aerosols of Titan during their sedimentation to the surface.

Chapter II Materials and Methods

In this chapter, I present the two experimental setups used in this thesis and the different analytical techniques associated. The first experiment named PAMPRE, located in the Laboratoire Atmosphere Milieux Observations Spatial (LATMOS), is used in this thesis to simulate the chemistry occurring in the upper atmosphere of the early Earth and Titan. This experiment is also used to synthesize analogues of aerosols formed in these atmospheres. The second experimental setup is the Acquabella cryogenic device of the Titan's Organic Aerosol Spectroscopy and chemistry (TOAST) laboratory, located in the Jet Propulsion Laboratory (JPL) of the California Institute of Technology (CALTECH). Acquabella is used to simulate the chemical evolution of aerosols during their sedimentation through the atmosphere and particularly processes occurring in the lower atmosphere.

II.1 The PAMPRE experimental setup

II.1.1 Context: simulate ionospheric chemistry with a plasma

In the solar system, chemistry occurring in planetary atmosphere is principally driven by dissociation and ionization by solar photons of atmospheric constituents. In particular, the activation of molecular nitrogen, which is the main constituent of the early Earth and Titan's atmospheres, need VUV photons with wavelengths below 100 nm (Peng et al., 2013). Such a process, which could occur in the ionosphere of the early Earth, is difficult to reproduce in the laboratory. Indeed, VUV radiations below 100 nm are difficult to produce and need specific facility as synchrotron. Deuterium lamp used as source of photons in experimental simulations presents emissions bands in the VUV with maxima at 121.6 nm (Lyman- α) and 160 nm (Trainer et al., 2006). Typical windows used in photochemical experiments are made of LiF or MgF₂ which absorb radiation below ~110 nm.

In this thesis, I used an experimental device, named PAMPRE, which is described in detail below, to reproduce complex organic chemistry initiated by VUV solar photons in the upper atmospheres of the early Earth and Titan. This experiment uses an electrical discharge as energy source. The modeling of the used plasma has been done in pure N₂ (Alves et al., 2012). The Electrons Energy Distribution Function (EEDF) presents a maximum at 2 eV and a relatively populated tail for electron energy above 4 eV and up to 14 eV. However, to facilitate comparison between the EEDF and the young Sun spectrum, the energy of the electrons has been converted in the corresponding wavelength. Figure 11 presents a

comparison between the calculated young Sun spectrum (panel a)) and the converted EEDF in the 89 nm (14 eV) to 250 nm (5 eV) (panel b)).

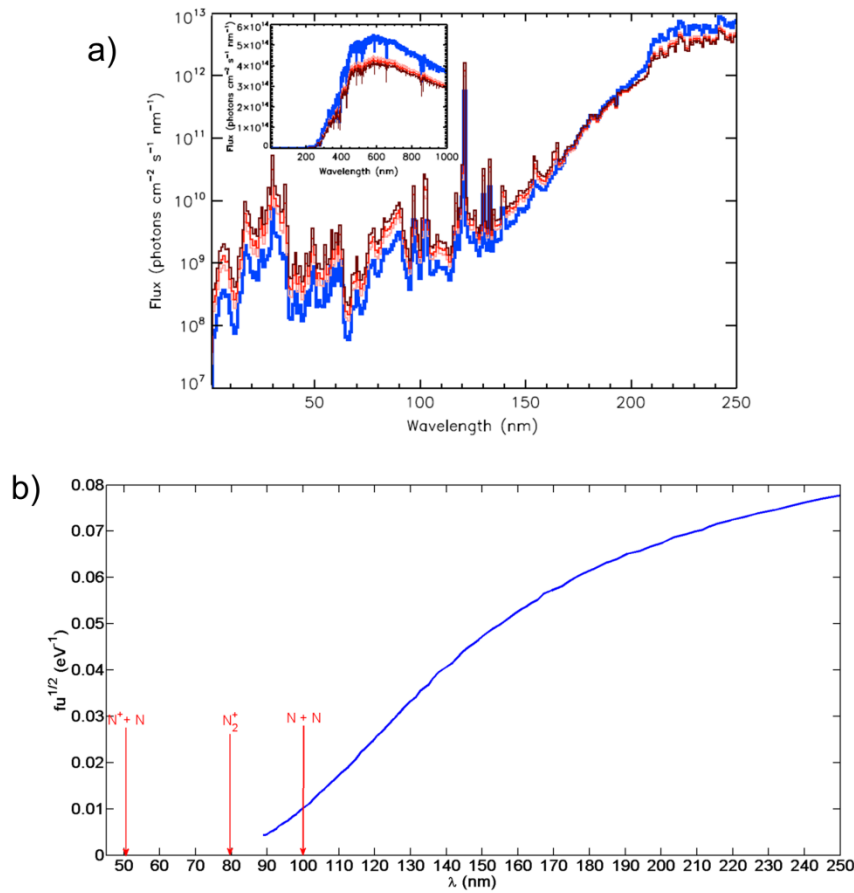


Figure 11: Comparison of the calculated young Sun spectrum in the 10-250 nm range (from (Hébrard and Marty, 2014)) and the calculated EEDF in a pure N₂ plasma for the PAMPRE experiment (adapted from (Alves et al., 2012)).

This Figure shows that the plasma produced electrons with enough energy to dissociate and to ionize the different gases constituting the simulated atmosphere. For example, in the case of N₂, the energy distribution of the electrons allows its dissociation which needs an energy higher than 12.4 eV (100 nm) and its ionization which needs an energy higher than 15.6 eV (79.5 nm) (Thissen et al., 2009). The limitation of the EEDF calculation at energy of 14 eV is not sufficient to conclude about the dissociative ionization of N₂ in the plasma which needs energy higher than 24.3 eV (51 nm) (Thissen et al., 2009). However, N⁺ ion has been observed by ionic mass spectrometry in a N₂ radiofrequency plasma (Mutsukura, 2001). This is indirect evidence that dissociative ionization mechanism is presented in the type of plasma used in PAMPRE experiment. Despite the non-modeling of the EEDF for these energies, electrons with enough energy for these reactions (i.e. ~24 eV) are present in the plasma.

This PAMPRE device can therefore be used to reproduce the chemistry occurring in the early Earth atmosphere induced by the VUV solar photons at a time where this flux emitted by the young Sun was higher than today (Claire et al., 2012).

II.1.2 The experimental device

The PAMPRE (French acronym for Production d'Aérosols en Microgravité par Plasma REactif - Aerosols Production in Microgravity by REactive Plasma) experiment is a radiofrequency (13.56 MHz) capacitively coupled plasma (RF CCP) developed in the LATMOS laboratory (Alcouffe et al., 2010; Szopa et al., 2006).

A scheme of the PAMPRE setup is given in Figure 12. The reactor is a stainless-steel cylinder of 30 cm diameter and 40 cm height. Optical windows are displaced around the reactor to allow infrared absorption spectroscopy diagnosis. A quadrupole mass spectrometer is connected at the bottom of the reactor by a capillary tube.

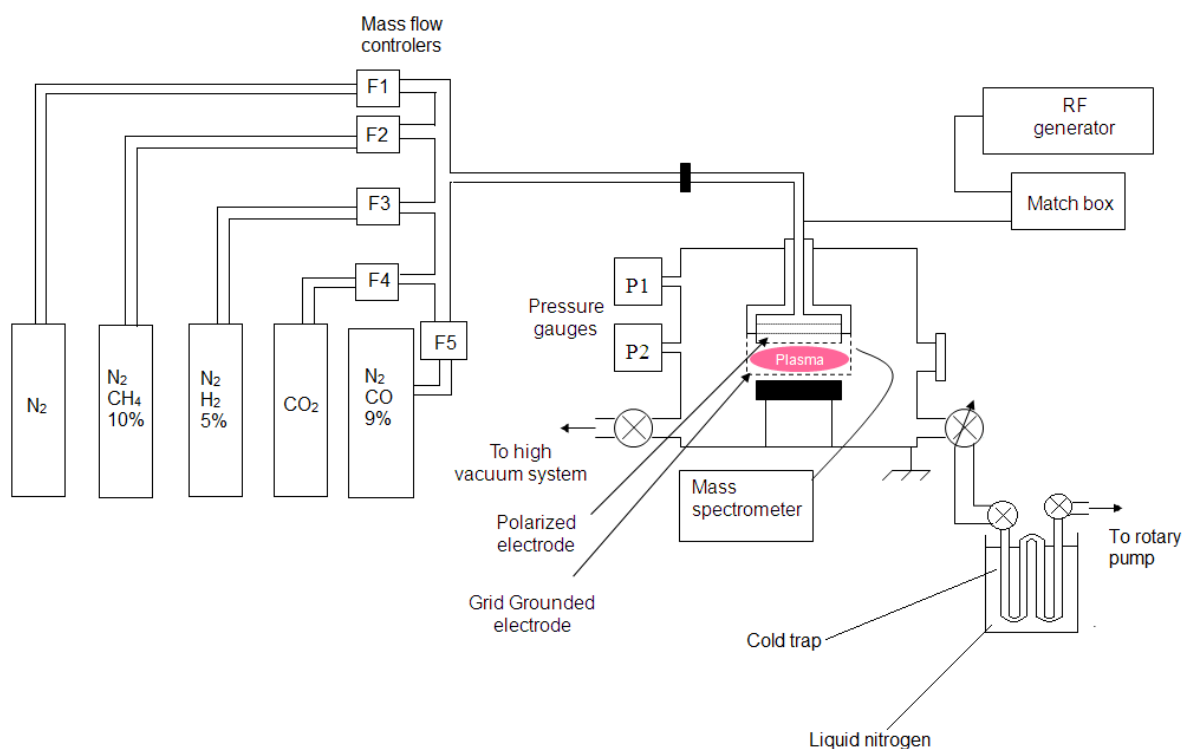


Figure 12: The PAMPRE experimental setup.

The discharge is generated between a polarized electrode and a grid grounded electrode, with 13.7 cm in diameter and with 5 cm in height, confining the plasma. In all the experiments presented in this thesis the generator RF power is set to 30 W. Five gas bottles can be used to generate the reactive gaseous mixture: one with high purity of N_2 ($> 99.999\%$), one

containing a N₂-CH₄ mixture with 10 % of CH₄, one containing a N₂-CO mixture with 9 % of CO, one with CO₂ (> 99.995 %) and one containing a N₂-H₂ mixture with 5 % of H₂. The detail of the gaseous mixture employed is given in each chapter. The gaseous mixture is continuously introduced through the polarized electrode in the reactor using a mass flow controller (MKS 1179) with a total gas flow of 55 standard cubic centimeter per minute (sccm). Then, the gas is pumped with a rotary vane vacuum pump. It results a pressure about 0.9 ± 0.05 mbar measured with a baratron pressure gauge (MKS 127). Before each experiment, the reactor is heated and a turbo molecular pump (Alcatel ATP 80) is used to pump the reactor down 2.10^{-6} mbar for cleaning purposes. The ultimate vacuum is checked with a Penning gauge (Alcatel CF2P).

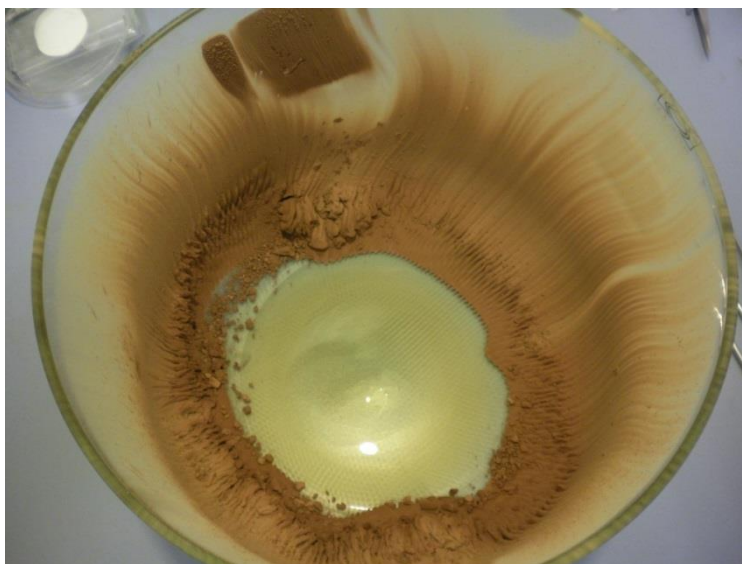


Figure 13: Glass vessel recovered by tholins produced in the PAMPRE experiment.

The cylindrical grid is surrounded by a glass vessel in order to collect the solid organic aerosols, named tholins, ejected from the plasma (Figure 13).

II.1.3 Gas phase analysis

II.1.3.a *In situ* mass spectrometry

The first diagnosis available on the PAMPRE reactor to study the gaseous phase composition is mass spectrometry. *In situ* monitoring of the gaseous phase were achieved with a Pfeiffer QME 200 quadrupole mass spectrometer (QMS). The mass spectrometer covers a mass range between 1 and 100 u with a resolution of 100 at m/z 100. Gases are transferred in the spectrometer through a capillary tube (0.8 mm internal diameter) which is long enough to keep the pressure below 10^{-5} mbar in the spectrometer when the pressure inside the reactor is

0.9 mbar. Only neutral stable species can be detected with this technique. In the spectrometer, neutral species are ionized by electron impact at 70 eV. In this thesis two acquisition methods have been used with the QMS.

First one named ‘scan analog’ provides a mass spectrum for a selected mass range, *i.e.* the intensity of the peak in function of the m/z ratio of this peak. This method has been used for the detection and the identification of species in the reactive gaseous mixture. This diagnosis is useful because of the sensitivity of the mass spectrometer as well as important dynamic, which allow detecting an important number of species formed in the reactor.

A blank spectrum of the isolated mass spectrometer is presented in Figure 14. The signature of residual air is visible on this figure. The residual air signature corresponds to the vacuum limit of the MS pumping, at $3 \cdot 10^{-8}$ mbar. Nitrogen has contribution at m/z 14 (N^+), 15 ($^{15}N^+$), 28 (N_2^+), 29 ($^{15}N^{14}N^+$), 30 ($^{15}N_2$). Oxygen has contribution at m/z 16 (O^+) and 32 (O_2^+). Carbon dioxide has contribution at 12 (C^+), 16 (O^+), 28 (CO^+) and 44 (CO_2^+). Finally, water has contribution at m/z 1 (H^+), 16 (O^+), 17 (OH^+), 18 (H_2O^+), 19 (HDO^+), 20 (D_2O^+).

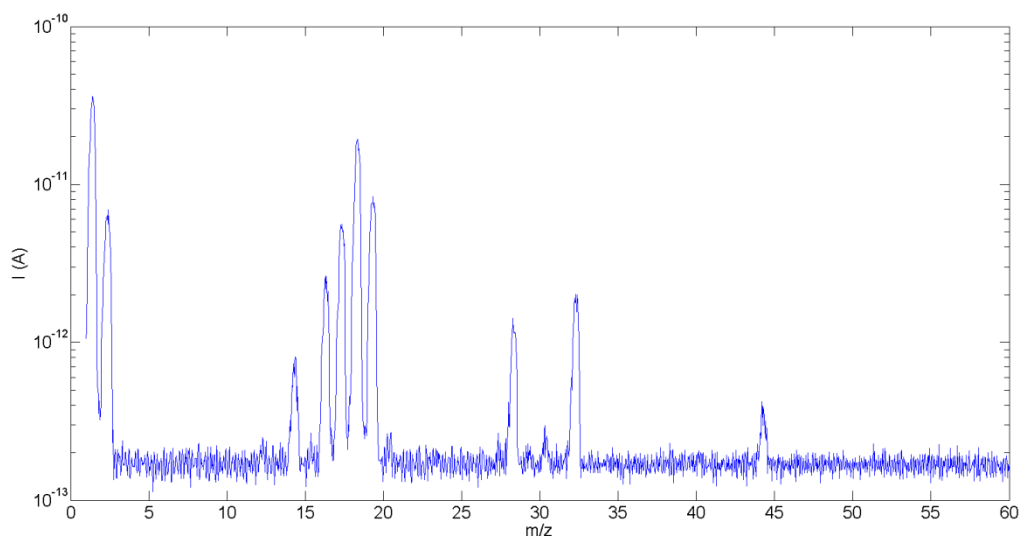


Figure 14: Blank mass spectrum of the isolated mass spectrometer.

Each species presents multiple peaks. This is characteristic of the ionization by electronic impact at 70 eV, which involves an important fragmentation of the species. This limits the identification of the species composing a complex gaseous mixture. Indeed, different species can contribute to a mass peak as for m/z 28 with N_2^+ and CO^+ .

The second method, Multiple Ion Detection (MID), provides the temporal evolution of one (or several) selected ion signal with a time resolution of 2 s. This method has been used for the kinetic monitoring of species of interest.

II.1.3.b *In situ* infrared absorption spectroscopy

In complement to the *in situ* mass spectrometry, I used the *in situ* infrared spectroscopy. The sensitivity of the IR spectrometer is lower than the sensitivity of the QMS because of the low path length of the IR beam in the reactor and only the major products are detected. However, these products can be detected without ambiguity because they have specific absorption bands in the infrared. Since the detected species has absorption bands without overlapping other species, it is possible to estimate their concentration using the Beer-Lambert law where the absorbance $A(\lambda)$ at a given wavelength is defined by:

$$A(\lambda) = \varepsilon(\lambda) \times l \times [C] \quad (1)$$

Where $\varepsilon(\lambda)$ is the absorption cross section of the molecule at a given wavelength, l is the path length of the beam through the gas cell and $[C]$ is the concentration of absorbing molecules in the reactor.

$$[C] = \frac{A(\lambda)}{\varepsilon(\lambda) \times l} \quad (2)$$

However, contrary to mass spectrometry, the long acquisition time (~10 min depending the acquisition parameters) of one spectrum with the IR spectrometer does not allow to realize kinetic monitoring of the gaseous species in the reactor.

I used a Thermo Scientific Nicolet 6700 Fourier Transform Infrared Spectrometer (FTIR). A schema of the FTIR setup on the PAMPRE reactor is presented in Figure 15.

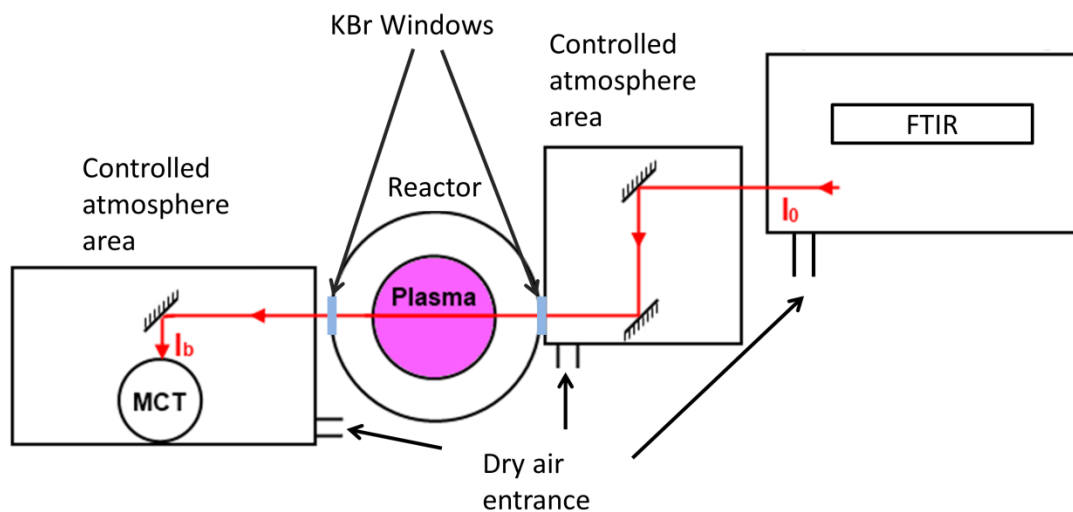


Figure 15: Schematic of the FTIR setup on the PAMPRE reactor.

The infrared beam is emitted by the FTIR and passes through the reactor via two KBr windows. Then, the beam is collected by a Mercury Cadmium Telluride (MCT) detector cooled by liquid nitrogen to avoid thermal noise. The spectrometer covers a range from 650 cm^{-1} up to 4500 cm^{-1} with a resolution used of 1 cm^{-1} . With only one passage of the beam through the reactor, the corresponding path length through the gas volume is $50.8 \pm 0.2\text{ cm}$.

II.1.3.c *Ex situ* Gas Chromatography coupled to Mass Spectrometry (GC-MS)

In complement of mass spectrometry and infrared spectroscopy, a third diagnosis used to analyze the gaseous phase is the *ex situ* Gas Chromatography coupled to Mass Spectrometry (GC-MS). GC-MS is an analytical technique that allows separating and identifying chemical species. Firstly, the species are separated depending of their elution time on the chromatographic column. The column outlet is connected to a mass spectrometer, which allows the identification of each separated species. As for IR spectroscopy, GC-MS permits a better identification than mass spectrometry and with a better sensitivity than IR spectroscopy. However, the configuration used for GC-MS analysis in our experiments does not permit to realize an absolute quantification of the gas trapped.

An external or an internal cryogenic trapping is used to accumulate volatile products in order to analyze the gaseous phase composition by GC-MS. The two cases are described in the corresponding chapters.

Gases trapped are directly injected through a six port gas valve. The GC-MS used is a Thermo Scientific trace GC-ultra with a Thermo Scientific ITQ 900 mass spectrometer. The MS is composed of an ion trap using a 70 eV ionization system. For the gas separation, the column is a MXT-QPLOT (Restek, 30 m long, 0.25 mm internal diameter and 10 μm stationary phase thickness). The column temperature is set with an isothermal initial plate at 30 $^{\circ}\text{C}$ during 5 min, then the temperature is increased with a gradient of 5 $^{\circ}\text{C}/\text{min}$ up to 190 $^{\circ}\text{C}$ and kept at this final temperature for 5 min. Helium is used as the carrier gas (>99.9995 purity) at a constant 1mL/min flow rate. A blank is done before each sample analysis.

II.1.4 Solid phase analysis

II.1.4.a Self-bias voltage of the polarized electrode: *in situ* detection of tholins formation

This diagnosis is used to detect appearance of dust in the plasma discharge. A self-bias voltage (V_{dc}) appears at the driven electrode of a RF CCP discharge if both electrodes differ in size when a blocking capacitor is inserted between the RF generator and the electrode (Bogaerts et al., 2002). In our discharge configuration, the polarized electrode is disk-shaped, when the grounded electrode one is the cylindrical confining grid. As a matchbox containing a tunable capacitor is placed between the RF generator and the electrodes, and the surfaces or the electrodes are different, a V_{dc} exists in the used discharge configuration. The self-bias voltage V_{dc} is negative in our case. The variation is related to changes in the electrons density and temperature. It has already been shown that the appearance of dust in the discharge induces V_{dc} perturbations (Praburam and Goree, 1996; Samsonov and Goree, 1999). These perturbations are explained by the fact that, during their growth, the solid particles attach some electrons present in the plasma. It results in a decrease of the electrons density and a sharp variation of V_{dc} (Alcouffe et al., 2010; Cavarroc et al., 2006; Mikikian and Boufendi, 2004). V_{dc} is measured using a 4-channels numerical oscilloscope (Tektronix TDS2004B).

II.1.4.b Elemental analysis

An elemental composition analysis of the tholins samples produced in PAMPRE is achieved to determine the C, N, H and O molar percentages of these tholins. This technique gives quantitative information about the constitution of tholins in these four elements. The analysis is achieved using a Thermo Scientific Flash 2000 Series CHNS/Oxygen Automatic Elemental Analyzer. In our organic materials, carbon, nitrogen and hydrogen were measured by flash combustion under a helium flow. The sample (1-2 mg) is weighted in Tin capsules (a capsule

of silver for O analysis) and placed in the Thermo Scientific MAS200R auto sampler at a preset time, and then dropped into an oxidation or reduction reactor kept at a temperature of 900-1000 °C. The gases released, *i.e.* CO₂, H₂O and N₂, are separated on a chromatographic column and detected by a highly sensitive thermal conductivity detector (TCD). Oxygen determination is achieved through the same protocol but with a specific oxygen pyrolysis reactor. CO is then measured using a TCD. Elemental analysis for C, N, H and O are realized on a same PAMPRE sample divided in two subsamples: one for C, N and H analysis and one for O analysis.

II.1.4.c Infrared analyses of tholins by ATR

An infrared analyses of solid samples produced with PAMPRE is achieved by Attenuated Total reflectance (ATR). This technique is used to determine the absorbance spectrum of solid material and to identify its main absorption bands. However, this technique does not give a quantitative analysis because of the dependence of the spectrum to the amount of solid deposited on the crystal surface and to the pressure applied on the solid.

A sample is disposed on the surface of a prism with a high reflection index (ATR crystal). The infrared beam entering in the prism is totally reflected inside it and an evanescent wave can escape the crystal through the upper face and passed then through the sample. The wave is then attenuated in the absorbance area of the sample depending on the chemical functions present in the sample. The resulting signal is measured by a Deuterium TriGlycine Sulfate (DTGS) detector in the 1200-4500 cm⁻¹ range. Each spectrum is a co-addition of 500 spectra recorded with a resolution of 4 cm⁻¹.

II.2 The Acquabella experiment

The Acquabella experimental setup is used in this thesis to study the chemical evolution of tholins produced in the upper atmosphere of Titan during their sedimentation through this atmosphere. Particularly, this setup is used to simulate processes, which could occur in the lower atmosphere where the conditions of pressure and temperature could allow a condensation of species on the surface of aerosols. The aerosols coated with condensed species can then evolve when exposed to the solar photons flux.

II.2.1 The experimental device

The Acquabella experimental setup has been developed at JPL in order to study the photo-reactivity of condensate species relevant of the lower atmosphere of Titan (Couturier-Tamburelli et al., 2014; Gudipati et al., 2013). Indeed, the drop of temperature in the lower atmosphere measured by the HASI instrument onboard the Huygens probe (Fulchignoni et al., 2005) lets consider a condensation of some species in the stratosphere and the troposphere of Titan.

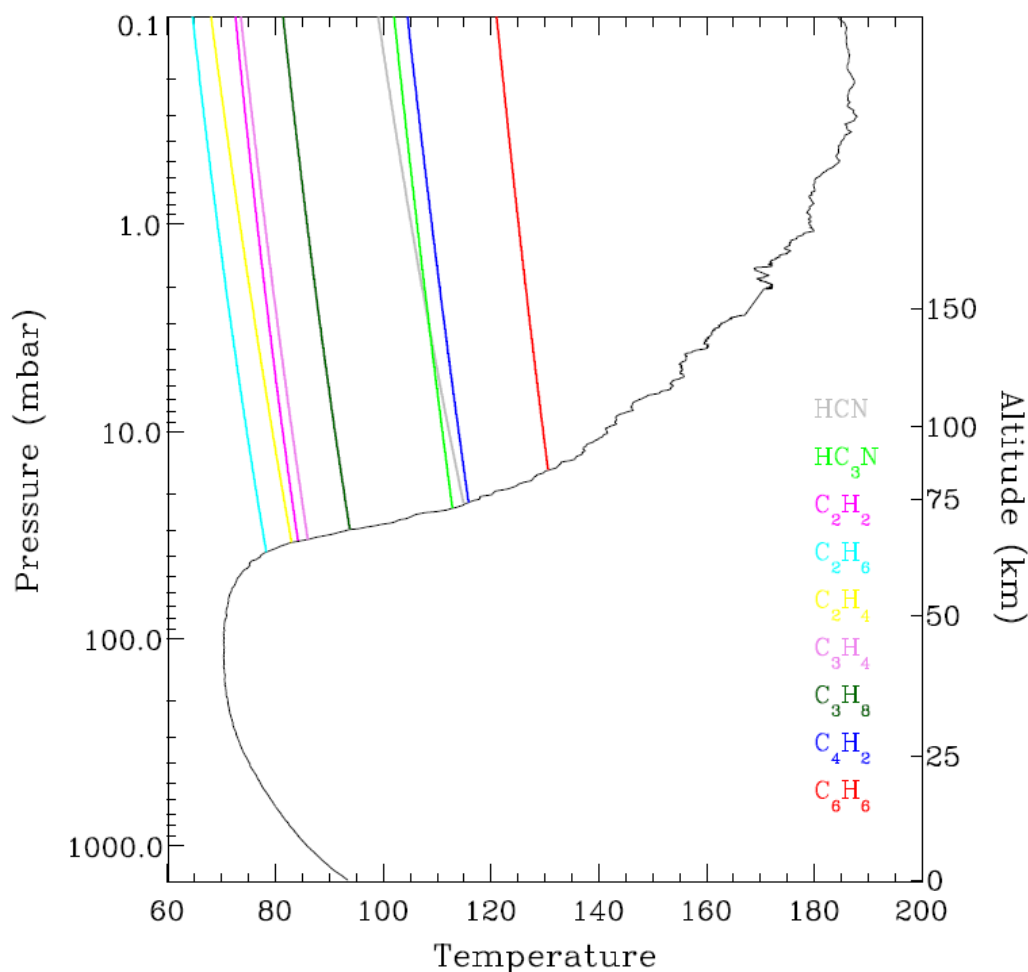


Figure 16: Vertical temperature profile retrieval by HASI (black line) and saturation temperature profiles (color lines) for different gas species (from (Lavvas et al., 2011a)).

This is illustrated in Figure 16 which presents the profile of temperature and the saturation profile for different species in the atmosphere of Titan. This figure shows that several hydrocarbons and nitrogen species can condense for an altitude lower than 100 km. This condensation could occur on the aerosols surfaces. These aerosols coated by condensed species could continue to evolve chemically when exposed to the solar flux reaching the

lower layers of the Titan's atmosphere. I used the Acquabella device to simulate such phenomenon.

The schema of the experimental setup is presented in Figure 17. The reactor is composed by a vacuum chamber link to a turbo molecular pump (Pfeiffer) assuring a high vacuum about 10^{-7} mbar at room temperature. The pressure is measured with a penning gauge. The chamber is connected to an Advanced Research System close-cycle helium cryostat assuring a cooling of the sample down to 10 K.

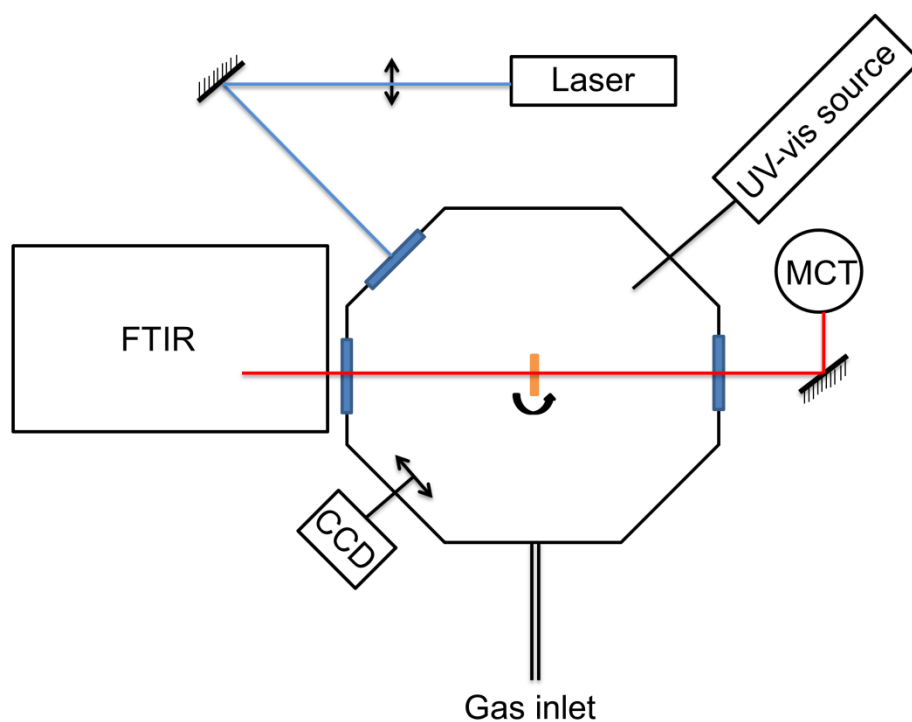


Figure 17: Schema of the Acquabella experimental setup.

Optical windows are displaced around the chamber to allow UV-visible absorption spectroscopy and infrared absorption spectroscopy diagnosis. A tholins sample (Figure 18), produced in PAMPRE, and deposited on a sapphire window (25 mm diameter, 2 mm thickness), is placed in the cryostat.

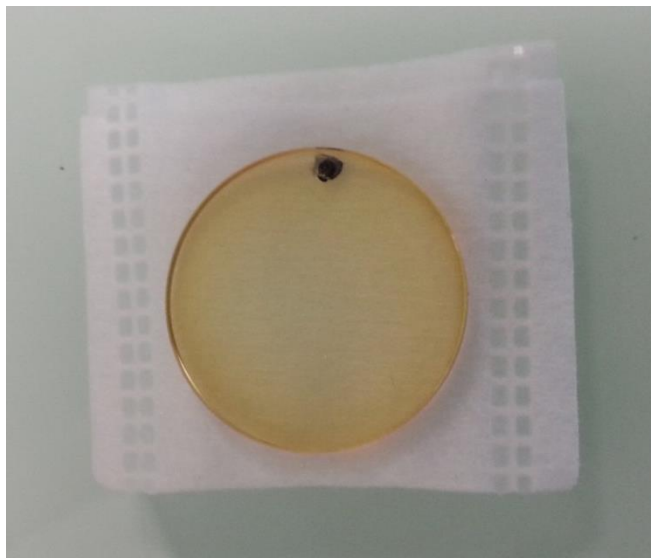


Figure 18: Tholins thin film deposited on a sapphire window produced with the PAMPRE experiment.

A laser is used to irradiate the sample at different wavelength characteristic of the solar flux reaching the lower atmosphere of Titan. The sample can be oriented for spectroscopy, laser irradiation or species deposition. Two lasers have been used to produce the four wavelength used in this thesis. Firstly, a tunable Opotek OPO laser was used for 355 nm, 410 nm and 450 nm generation. For 355 nm, laser beam was defocused with a lens to avoid multi-photons processes. Thus, the beam diameter is decreased from ~ 3 mm at the laser outlet to ~ 25 mm on the sample. In reason of the lower flux emitted at 410 nm and 450 nm by the laser, the lens was removed for these two wavelengths. The corresponding photons fluxes irradiating the sample are given in Table 4. Secondly, a Continuum Nd-Yag laser with a quadrupling frequency crystal is used for 266 nm generation. As for 410 nm and 450 nm, no lens is used in order to compensate the low photon flux emitted by the laser. The corresponding flux is given in Table 4.

Table 4: Photons flux reaches the sample in function of the laser wavelength.

Laser wavelength (nm)	266	355	410	450
Photons flux (photons.cm ⁻² .s ⁻¹)	1×10^{17}	9.5×10^{16}	1.8×10^{17}	1.9×10^{17}

II.2.2 Infrared absorption spectroscopy

I used infrared absorption spectroscopy to monitor the chemical evolution of the samples. Indeed, PAMPRE tholins samples and condensed species coated in these samples present important absorption band in the mid-IR (Gautier et al., 2012). It is thus possible to monitored qualitative and quantitative evolution of the samples during the experiments. Moreover, the condensed species used in this thesis present important absorption bands in the IR range which can be used to control the chemistry of the species and particularly their consumption during the irradiation experiments. I used a Thermo Scientific Nicolet 6700 Fourier transform Infrared Spectrometer (FTIR). The measurement is realized in transmission. As shown on the Figure 17, the infrared beam is emitted by the FTIR and enters in the reactor through a ZnSe window where it can be absorbed by the sample. Then, the beam goes out from the reactor through a second ZnSe window and the signal is collected by a MCT detector cooled by liquid nitrogen. Infrared spectra are recorded in the 1600cm^{-1} (sapphire window cut off) 4500cm^{-1} range with a resolution of 1cm^{-1} after a co-addition of 200 spectra.

II.2.3 UV-visible absorption spectroscopy

In complement of the Infrared spectroscopy, I used UV-visible absorption spectroscopy in transmission with an Ocean Optics USB4000 spectrograph. UV-visible spectroscopy is used to measure the absorption of the tholins samples and condensed species at the wavelengths used to irradiate the samples. The beam is emitted by a deuterium-halogen lamp and enters in the reactor through an optical fiber. Then, the flux is absorbed by the sample. The transmitted light is focused by a lens on the entry of a second optical fiber and finally measured by a Charged Couple Detector (CCD). Spectra are recorded in the 220-850 nm range. Each spectrum is a co-addition of 500 scans recorded with an integration time of 10 ms.

Chapter III CO₂: An efficient source of carbon for an atmospheric organic growth

III.1 Introduction

The question of the organic chemistry, which could have occurred in the ionosphere of the early Earth, with a possible formation of complex organic compounds, is connected to the question of the composition of the early Earth atmosphere. As developed in the Chapter 1, the exact composition is still unknown. A primitive atmosphere mainly composed by N₂ and CO₂ is widely accepted today. Different proposition have been done for the other constituent of this atmosphere. In this chapter I focused my work on a case where the primitive atmosphere of the Earth is composed by H₂ in addition of N₂ and CO₂. Different works have tried to determine the hydrogen content at this time. A study has proposed that during the Hadean and Archean, the atmosphere of the Earth could be made up to 30 % of H₂ because of a lower temperature of the thermosphere (Tian et al., 2005). However, this result remains contested (Catling, 2006; Tian et al., 2006) as developed in Chapter I. Another work modeling study has estimated that H₂ was present in a much lower amount with an upper limit about 1 % (Kuramoto et al., 2013) in agreement with an older study about the atmospheric composition of the early Earth (Kasting, 1993).

The aim of this chapter is to study the chemistry simulated with the PAMPRE experiment in an initial gaseous mixture composed by nitrogen, carbon dioxide and hydrogen. This study takes into account two aspects of this chemistry: the formation of gaseous products, which is initiated by the dissociation and the ionization of the three initial gases, and the possible formation of a solid phase, which would grow in the gaseous reactive medium.

The first part of this chapter is dedicated to the analysis of the gaseous products formed in the reactor. A second part presents the characterization of the solid phase growing in the reactive medium. As the carbon dioxide concentration is not precisely known for the Hadean and the early Archean, the effect of the initial amount of CO₂ on the organic chemistry simulated in PAMPRE is discussed.

III.2 Experimental methods and protocols

In the experiments presented here, three gas bottles are used to generate the reactive gaseous mixture: one with high-purity of N₂ (99,999 %), one containing a N₂-H₂ mixture with 5 % of H₂ and one with CO₂ (99,995 %). The generator RF power is set to 30 W and the total gas flow rate to 55 sccm resulting in a 0.9 mbar pressure in the reactor.

The initial Hydrogen mixing ratio is kept constant at 4 % for all experiments. This concentration is chosen in agreement with recent modeling of H₂ mixing ratio giving an upper limit about 1 % for the Archean atmosphere (Kuramoto et al., 2013). The gas flow is adjusted among N₂ and CO₂ gas bottles from an experiment to another to introduce carbon dioxide at various mixing ratios ranging from 1 to 10 %. Compositions of the different gaseous mixtures studied here are given in Table 5.

Table 5: Initial composition of the studied gaseous mixtures.

Mixture number	[N ₂] ₀ (%)	[CO ₂] ₀ (%)	[H ₂] ₀ (%)
1	95	1	4
2	91	5	4
3	86	10	4

Firstly, a series of experiments is done at room temperature to monitor the CO₂ consumption in the plasma by *in situ* mass spectrometry. Secondly, in order to detect and identify gaseous species product in low quantity, a new series of experiment is realized using a cold trapping of these species on the plasma box. For that, we used a continuous injection of liquid nitrogen (L_{N2}) inside the stainless-steel block supporting the grounded electrode. The plasma box is cooled by thermal conduction. The temperature is fixed at 173 K to prevent N₂, H₂ and CO₂ condensations. The temperature measurement is realized on the polarized electrode. Products are accumulated during 4 or 8 hours of plasma duration. After plasma is turned off, the reactor is pumped to eliminate reactive species. The reactor is isolated and the plasma box is warmed up to room temperature to release the gases trapped. Then, the gaseous phase is analyzed *in situ* by mass spectrometry and infrared spectroscopy or *ex situ* by GC-MS.

Moreover, CaF₂ substrates are placed on the grounded electrode for thin films deposition. These films are produced at room temperature during 30 hours of plasma duration. Then, they are analyzed by infrared spectroscopy.

III.3 Results

III.3.1 Analysis of the gaseous phase composition

III.3.1.a Reactive species consumption in the plasma: the first step for the product formation

The first aspect concerning the reactivity of the gaseous phase is the reactivity of the three initial species: N₂, CO₂ and H₂. The consumption of these species is monitored using *in situ* mass spectrometry. The carbon dioxide consumption is measured using a time-tracking of CO₂⁺ at m/z 44 and the hydrogen consumption using a time-tracking of H₂⁺ at m/z 2.

The low dissociation rate of N₂ in the plasma does not allow to determine its consumption efficiently by this technique. However, the modeling of a N₂ plasma in our device has shown a dissociation about 4 % (Alves et al., 2012).

Figure 19 shows the evolution of the CO₂ mixing ratio when the plasma is switched on for three different mixing ratios: 1 %, 5 % and 10 %. The initial concentration of CO₂ is known and it is possible to calibrate the m/z 44 signal intensity in order to obtain the evolution of the *in-situ* CO₂ concentration. The concentration obtained has been multiplied for 1 % and 5 % of CO₂ by a factor 10 and a factor 2 respectively. The CO₂ mixing ratio decreases when the plasma is switched on and reaches a steady-state after a transient regime.

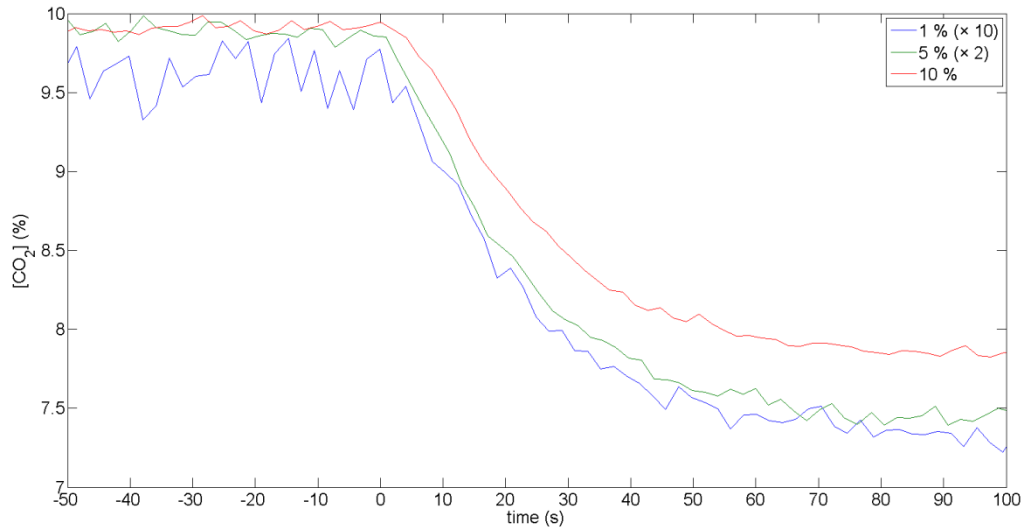


Figure 19: Evolution of the CO₂ mixing ratio in the gaseous reactive medium with the plasma duration. Origin of the time is set as the moment when the plasma is turned on. CO₂ mixing ratio has been multiplied by a factor 10 and a factor 2 for an initial amount of 1 % and 5 % respectively.

We define the carbon dioxide consumption efficient e_{CO_2} which can be deduced from Figure 19 with the following equation (3):

$$e_{\text{CO}_2} = \frac{\Delta_{\text{CO}_2}}{[\text{CO}_2]_0} = \frac{[\text{CO}_2]_0 - [\text{CO}_2]_{\text{ss}}}{[\text{CO}_2]_0} \quad (3)$$

Where $[\text{CO}_2]_0$ and $[\text{CO}_2]_{\text{ss}}$ represent the initial and steady-state percentages of carbon dioxide respectively and where Δ_{CO_2} represents the absolute consumption of CO₂. Results are presented in Table 6. The CO₂ consumption efficient has the same order of magnitude for the three initial amounts of CO₂ studied in spite of a decrease of the consumption efficient from 24 % to 20 % for an initial amount of 10 % of CO₂ comparatively to 1 % and 5 %.

Table 6: Evolution of the absolute consumption Δ_{CO_2} and the consumption efficient e_{CO_2} of carbon dioxide in the plasma as a function of the initial amount of CO₂. Evolution of the absolute consumption Δ_{H_2} and the consumption efficient e_{H_2} of hydrogen in the plasma as a function of the initial amount of CO₂. Evolution of the C/H and C/O ratios in the fraction of gases consumed as a function of the initial amount of CO₂. The uncertainties are given as 2 σ (standard deviation) and are calculated from the standard fluctuations of the mass spectrometry measurements.

$[\text{CO}_2]_0$ (%)	Δ_{CO_2}	Δ_{H_2}	e_{CO_2} (%)	e_{H_2} (%)	“C/H” consumption	“O/H” consumption
1	0.24	0.72	24 ± 2	18 ± 0.5	0.2	0.3
5	1.2	1.3	24 ± 0.6	32 ± 1	0.5	0.9
10	2	1.4	20 ± 0.4	36 ± 1	0.7	1.4

This similar e_{CO_2} for each CO₂ initial amount results in an absolute consumption of CO₂ Δ_{CO_2} , which increases linearly when the initial amount of CO₂ increases because the same percentage of a more important quantity of CO₂ is consumed.

The same study is realized on hydrogen. Figure 20 presents the evolution of the H₂ mixing ratio when the plasma is switched on for the three initial amounts of CO₂: 1 %, 5 % and 10 %. The initial concentration of H₂ is known and it is possible to calibrate the m/z 2 signal intensity in order to obtain the evolution of the *in-situ* H₂ concentration. The H₂ concentration decreases when the plasma is switched on and reached a steady-state after a transient regime. We defined the hydrogen consumption efficient e_{H_2} which can be deduced from the Figure 20 with the following equation (4):

$$e_{\text{H}_2} = \frac{\Delta_{\text{H}_2}}{[\text{H}_2]_0} = \frac{[\text{H}_2]_0 - [\text{H}_2]_{\text{ss}}}{[\text{H}_2]_0} \quad (4)$$

Where $[\text{H}_2]_0$ and $[\text{H}_2]_{\text{ss}}$ represent the initial and steady-state percentages of hydrogen respectively and where Δ_{H_2} represents the absolute consumption of H₂. Results are presented in Table 6.

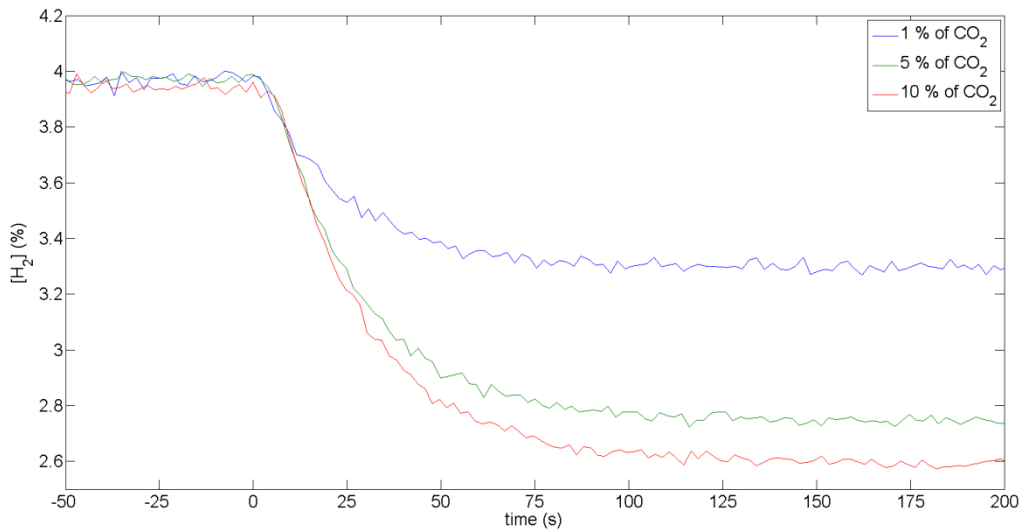


Figure 20: Evolution of the H₂ mixing ratio in the gaseous reactive medium with the plasma duration for the different CO₂ initial amounts. Origin of the time is set as the moment when the plasma is turn on.

Contrary to the consumption efficient of CO₂ which does not present a significant evolution, the modification of the CO₂ initial amount drastically increase the consumption efficient of H₂. Indeed, e_{H_2} increases from 18 % to 36 % when the initial amount of CO₂ increases from 1 % to 10 %. This increase is not linear. Indeed, e_{H_2} increases from 18 % to 32 % when $[\text{CO}_2]_0$

increases from 1 % to 5 % but e_{H_2} increases only from 32 % to 36 % when $[\text{CO}_2]_0$ increases from 5 % to 10 %. Perhaps, it can be noted that despite this important increase of e_{H_2} , the absolute consumption of H₂ Δ_{H_2} increases less than Δ_{CO_2} with the increase of the initial amount of CO₂ because the amount of H₂ does not change.

Two types of parameters can influence the consumption of the species. First one is a modification of the plasma parameters. Indeed, the consumption of the initial gaseous species is initiated in the plasma by electron impact. This phenomenon is controlled by the electron density and the electrons temperature of the plasma. However, if the modification of the CO₂ initial amounts involves a change in these two quantities, the evolution of e_{H_2} and e_{CO_2} should be the same. However, when e_{H_2} increases with the increase of the CO₂ initial amount, e_{CO_2} is not altered and decreases a little for the higher $[\text{CO}_2]_0$. The other one possibility is a modification of the chemistry in the plasma involved by the increase of CO₂ initial amount.

To better emphasize this change of the chemistry, we will now study the resulting products of this chemistry in a gaseous mixture composed by N₂, CO₂ and H₂.

III.3.1.b Global *in situ* analysis of the gaseous phase composition by mass spectrometry

Firstly the composition of the gaseous phase has been studied at room temperature by *in situ* mass spectrometry. The composition of the gaseous phase at the stationary-state before and after the initiation of the plasma is studied for m/z 1 to 60 u. The resulting spectra are presented in the Figure 21 for an initial gaseous mixture made of N₂:CO₂:H₂ 91:5:4 %.

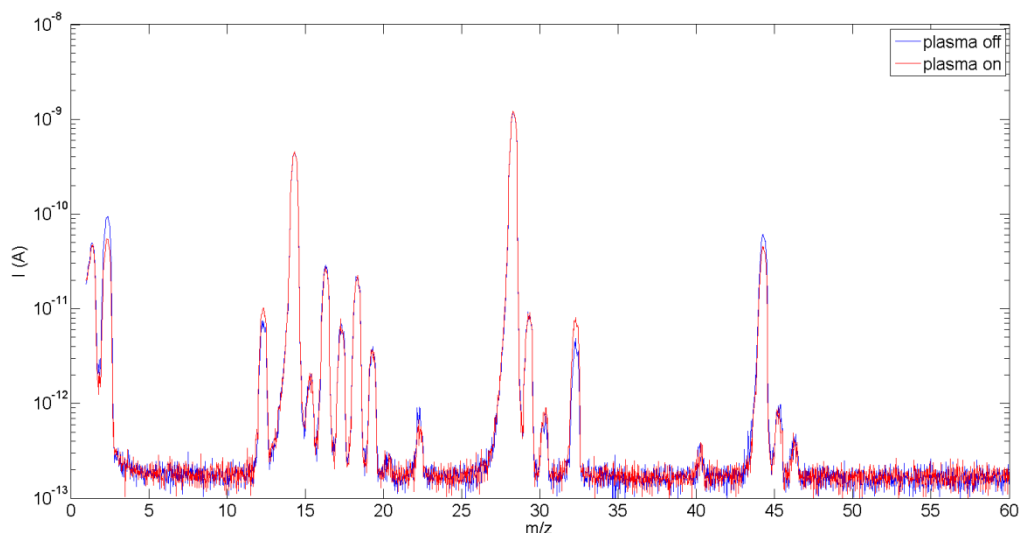


Figure 21: Mass spectra obtained for a N₂:CO₂:H₂ 91:5:4 % gas mixture plasma off (blue) and plasma on (red) at room temperature.

Firstly, the mass spectrum recorded before the initiation of the plasma presents the typical mass signature corresponding to the used gaseous mixture in addition of the mass signatures corresponding to the residual air in the mass spectrometer see in (Figure 14). Molecular nitrogen involves fragments at m/z 14 (N⁺), 15 (¹⁵N⁺), 28 (N₂⁺), 29 (¹⁵N¹⁴N⁺) and 30 (¹⁵N¹⁵N⁺). Carbon dioxide involves fragments at m/z 12 (C⁺), 22 (CO₂²⁺), 28 (CO⁺), 29 (¹³CO⁺), 30 (C¹⁸O⁺), 44 (CO₂⁺), 45 (¹³CO₂⁺) and 46 (CO¹⁸O⁺). Hydrogen presents fragments at m/z 1 (H⁺) and 2 (H₂⁺). Signatures of Ar (not visible on the blank spectrum) are also visible in this spectrum at m/z 20 (Ar²⁺) and 40 (Ar⁺).

For the spectrum recorded with the plasma on, a change is observed on the signatures of the initial gas species H₂ and CO₂. Indeed the signature of these species decreases in agreement with the results presented in the previous section. However, no new mass peak corresponding to a new gas species is observed on the spectrum recorded plasma on comparatively to the spectrum recorded plasma off. This result is in apparent contradiction with the gaseous products expected from the consumption of CO₂ and H₂ in the plasma.

If we supposed that the consumption of the initial species in the plasma leads to the formation of volatiles products, their non-detection by *in situ* mass spectrometry supposed that their abundances in the gaseous medium is under the detection limit of the spectrometer. A previous study realized with PAMPRE in a N₂/CH₄ gaseous mixture has shown the limit of this technique for the detection of the minor species and also shown the interest of the

cryogenic trapping technique in order to concentrate and then to detect the minor species (Gautier et al., 2011).

III.3.1.c Cryogenic trapping of the gaseous products for an *in situ* analysis

In order to concentrate the gas species product in PAMPRE during the experiment, I used an internal cryogenic trapping following a method described in section III.2. After 4 hours of trapping at 173 K, the plasma is switched off; the reactor is pumped and then isolated. The plasma box is warmed up to room temperature. The pressure in the reactor is measured for different temperature during this warm up. The evolution of the pressure in the reactor is presented in Figure 22. During the increase of the plasma box temperature, there is an increase of the pressure in the reactor. The pressure increases slowly in a first time to reach 0.1 mbar at 230 K and then the pressure increases more importantly to reach finally 2 mbar at 294 K after 12 hours of warming and, which corresponds to the room temperature.

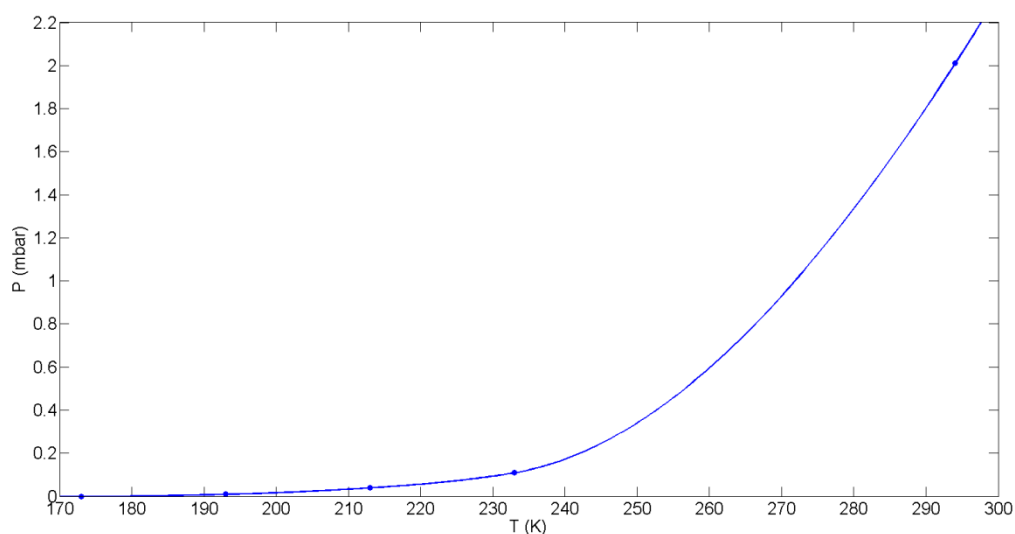


Figure 22: Evolution of the pressure in the reactor during the warm up of the plasma box to room temperature.

This increase of the pressure can be attributed to the release of the species trapped during the experiment and which sublimate when the temperature increases.

The composition of the gas released is then analyzed by *in situ* mass spectrometry. Figure 23 presents two mass spectra recorded after a trapping of gaseous products with 4 hours of plasma duration and an initial CO₂ amount of 5 %. The first spectrum is recorded at a

temperature of 173 K. The second spectrum is recorded after the warm up the plasma box to room temperature.

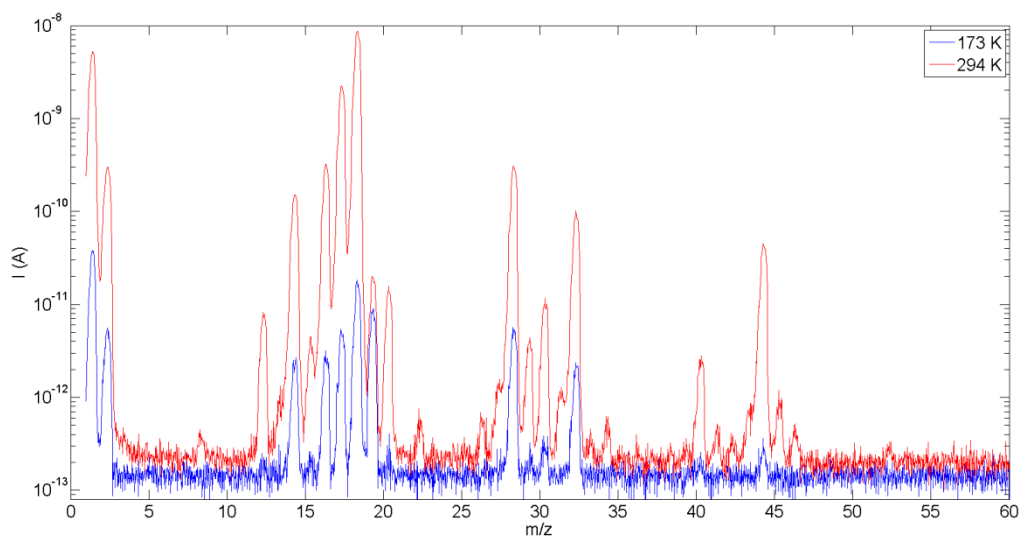


Figure 23: Mass spectra recorded at 173 K (blue) and 294 K (red) after 4 hours of gaseous products trapping in N₂-CO₂-H₂ (91/5/4) plasma.

The signature of residual air in the mass spectrometer can be identified in the mass spectrum recorded at 173 K in agreement with the blank spectrum presented in Figure 14. The apparition of new peaks is visible on the spectrum recorded at room temperature. These signatures can be attributed to the gaseous products formed during this experiment and which were trapped. We observed peaks with masses up to 60 u. This reflects a chemical growth in the gaseous phase during the experiment and an efficient organic chemistry. Because of the necessary time to warm up the plasma box to room temperature, the two spectra have been recorded during two consecutive days. For this reason, a drift of the response of the mass spectrometer is observed, resulting in a small increase of the base line level of the spectrum recorded at room temperature comparatively to the spectrum recorded at 173 K.

The complexity of the gaseous mixture can lead to the formation of molecules composed by C, N, H and O atoms. The low resolution of the QMS does not allow differentiating molecules with closed masses; several molecules can be attributed to one observed mass peak on the spectrum. However, few peaks can be attributed unambiguously.

The case of water: H₂O

The major peak on the spectrum recorded at room temperature in Figure 23 is for m/z 18. This peak is attributed to water. This attribution to H₂O is in agreement with the high level of the peak at m/z 17 (OH⁺) which is a major fragment of H₂O.

This result is confirmed by the analysis of the gaseous phase by *in situ* infrared spectroscopy. Figure 24 presents two infrared spectra recorded at 173 K and 294 K, at the same time as the mass spectra of the Figure 23.

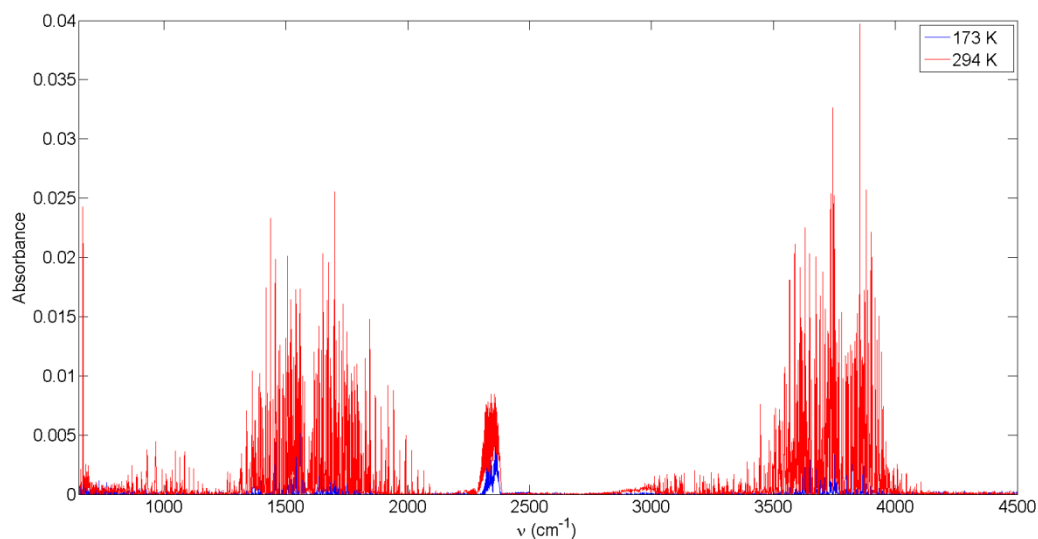
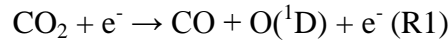


Figure 24: Infrared spectra recorded at 173 K (blue) and 294 K (red) after the trapping of the gaseous product during 4 hours of plasma duration in an initial gaseous mixture made of N₂/CO₂/H₂ (91/5/4).

A low water vapor signature with an absorbance lower than 0.005 is observed on the spectrum recorded at 173 K corresponding to the remaining water vapor presents in the reactor and in the boxes displayed on the path of the infrared beam. After the warm up of the plasma box to room temperature, an important increase of the water vapor absorption band is observed in the 1300-2000 cm⁻¹ range and in the 3400-4000 cm⁻¹ range. The correlation of this important increase of the infrared signature of H₂O with the high signal detected with the mass spectrometry at m/z 18 enables to attribute this detection to an important water formation in the plasma during the experiment.

Chapter III CO₂: An efficient source of carbon for an atmospheric organic growth

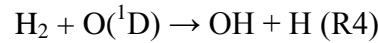
The water formation can be explained by the production of oxygen radical O(¹D) by the dissociation of CO₂ in the plasma:



Oxygen radicals can be also produced by the dissociative recombination of CO₂⁺ (Geppert and Larsson, 2008; Skrzypkowski et al., 1998):



Then O(¹D) can react with molecular hydrogen to form OH radical:



Finally OH induced the formation of H₂O by the following reactions:



Since H₂O has absorption bands without overlapping other species, it is possible to estimate their concentration using the Beer-Lambert law, following the equation (1) and (2).

To calculate the concentration of H₂O, we used the absorption cross section from the HITRAN 2008 database (Rothman et al., 2009). In order to overcome the difference of resolution between the database and laboratory data, we calculate the concentration on the area of the bands. For H₂O, integration is performed both in the 1300-1600 cm⁻¹ range and in the 3400-4000 cm⁻¹ range. Knowing the volume of the reactor, we calculate the number of molecules of water N_{H₂O} trapped in 4 hours.

Table 7: Evolution as a function of the CO₂ initial amount of the mean of H₂O molecules formed in a 4 hours of plasma duration N_{H₂O} and the number of NH₃ molecules formed in 4 hours of plasma duration. The uncertainties are given as 2σ (standard deviation) and are calculated from the standard fluctuations of the infrared spectroscopy measurements

[CO ₂] ₀ (%)	Mean N _{H₂O} (molecules)	N _{NH₃} (molecules) 920-940 cm ⁻¹	N _{NH₃} (molecules) 950-970 cm ⁻¹
1	$(2.1 \pm 0.1) \times 10^{20}$	$(5.4 \pm 0.4) \times 10^{18}$	$(6.2 \pm 0.5) \times 10^{18}$
5	$(3.1 \pm 0.1) \times 10^{20}$	$(6.3 \pm 0.4) \times 10^{18}$	$(6.2 \pm 0.5) \times 10^{18}$
10	$(3.9 \pm 0.1) \times 10^{20}$	-	$(4.8 \pm 0.2) \times 10^{17}$

The consistent values of N_{H₂O} obtained for the 2 ranges are averaged and reported in Table 7 for each CO₂ initial amount study: 1 %, 5 % and 10 %.

The number of water molecules trapped has the same order of magnitude for the three amounts of CO₂ studied. A low increase of the number of H₂O molecules trapped is observed when the initial CO₂ percentage increases. This increase can be explained by an increase of the number of O(¹D) radical produced when the CO₂ initial amount increases. Indeed, despite a little decrease for an initial amount of CO₂ of 10 %, the consumption efficient of CO₂ in the plasma has the same value for the three initial amounts studied. We can so expected an increase of the number of CO₂ molecules dissociated and ionized in the plasma resulting in an increase of the number of O(¹D) radicals produced and then the number of H₂O molecules formed.

The case of ammonia: NH₃ and hydrogen cyanide: HCN

Ammonia is of great interest for prebiotic chemistry. The signature of ammonia in mass spectrometry is principally at $m/z = 17$ with the ion NH₃⁺. This is one of the principal peaks of the mass spectrum at room temperature in Figure 24. However, water has also a contribution at this mass due to OH⁺ fragment. Here, I used the infrared spectroscopy to remove this ambiguity.

Figure 25 presents an infrared spectrum recorded at 300 K. This is a spectra center on the 700-1200 cm⁻¹ range where species with a strong absorption is visible. This species is identified as NH₃ according to the NIST database and the Hitran database. The presence of a doublet at 930 cm⁻¹ and 967 cm⁻¹ is characteristic of NH₃ and allows identification unambiguously. This is possible to quantify the concentration of ammonia in the reactor using equation (2).

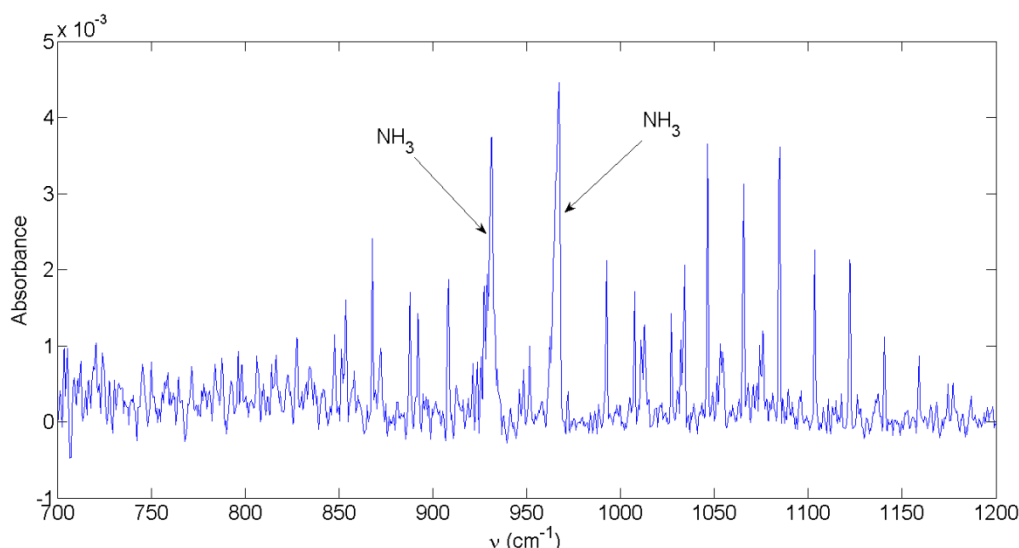
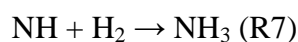


Figure 25: Infrared spectra in the 700-1200 cm⁻¹ range recorded at 300 K after 4 hours of gaseous products trapping in a N₂-CO₂-H₂ (91/5/4) plasma.

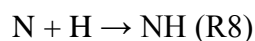
To calculate the concentration of NH₃, we used the absorption cross section from the Hitran 2008 database (Rothman et al., 2009). In order to overcome the difference of resolution between the database and laboratory data, we calculate the concentration on the area of the bands. For NH₃, integration is performed both in the 920-940 cm⁻¹ range and in the 950-970 cm⁻¹ range. Knowing the volume of the reactor we calculate the number ammonia molecules N_{NH3} trapped in 4 hours. The number of ammonia molecules N_{NH3} for the 2 ranges is reported in Table 7 for each CO₂ initial amounts.

For an initial amount of 1 % and 5 % of CO₂, Table 7 shows a good agreement for N_{NH3} between the bands. Moreover the number of ammonia molecules trapped is similar for these two [CO₂]₀. However, the quantity of ammonia decreases by one order of magnitude for an initial amount of CO₂ of 10 %. The question of the ammonia formation in a N₂-CH₄ plasma was discussed previously in (Carrasco et al., 2012). The formation of NH₃ requires the formation of NH radical which can then react with molecular hydrogen to form ammonia.

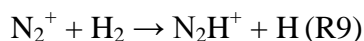


For our gaseous mixture, three pathways can be proposed from the literature to explain the formation of NH radical.

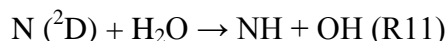
The first one involves radical chemistry (Carrasco et al., 2012; Mutsukura, 2001):



The second one involves ion chemistry (Green and Caledonia, 1982):



The last one involves radical chemistry and has been described in (Dobrijevic et al., 2014):



In addition to these mechanisms, another pathway has been proposed by (Yelle et al., 2010) through the dissociative recombination of the protonated methanimine CH₂=NH₂⁺.

Methanimine CH₂=NH has a mass spectrum with a main fragment at *m/z* 29. A peak is visible on the mass spectrum recorded at room temperature at *m/z* 29. However, this detection is not sufficient to conclude about the presence or not of methanimine in our gaseous products. Indeed, a contribution at *m/z* 29 is expected from the propane fragmentation 44 (50 %) 29 (100 %) pattern or from the formaldehyde fragmentation 30 (60 %), 29 (100 %) pattern (from NIST database). The influence of the carbon dioxide initial amount on the ammonia production is difficult to interpret taking into account the different chemical pathways proposed. The important decrease of the ammonia production for an initial amount of 10 % of CO₂ comparatively to the productions for 1 % and 5 % can be potentially caused by competitive reaction involving oxygen radicals from the dissociation of CO₂.

The production of ammonia is interesting by the formation of highly reactive nitrogen-containing species which can participate to the formation of more complex molecules. Another precursor for the formation of complex organic molecules is hydrogen cyanide HCN.

The signature of HCN in mass spectrometry is principally at *m/z* 27 with a relative contribution at *m/z* 26 (20 %). This signature is visible on the mass spectrum of the release species presented in Figure 23. However, HCN has not been clearly identified by infrared spectroscopy. Indeed, HCN presents an absorption band at 713 cm⁻¹ which is not visible on the IR spectrum in Figure 25. According to the low signal of the mass peak at *m/z* 27, the concentration of HCN in the gaseous phase is low. As explained in the Chapter II, the sensitivity of the FTIR is quite low comparatively to the QMS and HCN concentration in the gas trapped is probably under the detection limit of the FTIR.

The formation of HCN in a N₂/CO₂/H₂ gaseous mixture cannot be explained by the pathways proposed habitually to explain its formation from the chemistry of N₂ and CH₄. Indeed, these classical pathways used the CH₃ radical (Hébrard et al., 2012; Krasnopolsky, 2009; Krasnopolsky, 2012; Loison et al., 2015; Wilson and Atreya, 2004) which is issued from the methane photodissociation. However, this radical is not expected to be produced in a gaseous mixture without methane.

Identification of other organic species

Apart H₂O, NH₃ and HCN which have been clearly identified by their specific mass spectra signature or by the cross comparison between the mass spectrum and the infrared spectrum, the attribution of the other peaks of the mass spectrum in Figure 23 is more difficult because of the important number of molecules and fragment of molecules corresponding to a mass peak.

Table 8: List of the peaks detected in the mass spectrum of the gases released and their possible attribution to molecules (black) or their major fragments (red).

<i>m/z</i>	Possible attribution
17	NH ₃ ⁺ , OH ⁺
18	H ₂ O ⁺
26	C ₂ H ₂ ⁺ , CN ⁺
27	HCN ⁺ , C ₂ H ₃ ⁺
28	C ₂ H ₄ ⁺ , CO ⁺ , N ₂ ⁺ , CH ₂ N ⁺
29	CH ₂ NH ⁺ , HCO ⁺ , N ₂ H ⁺ , C ₂ H ₅ ⁺
30	H ₂ CO ⁺ , C ₂ H ₆ ⁺ , N ₂ H ₂ ⁺ , CH ₄ N ⁺ , NO ⁺
31	CH ₅ N ⁺ , CH ₃ O ⁺ , N ₂ H ₃ ⁺
32	O ₂ ⁺ , CH ₃ OH ⁺ , N ₂ H ₄ ⁺
40	C ₃ H ₄ ⁺ , Ar ⁺ , CH ₂ CN ⁺
41	CH ₃ CN ⁺ , C ₃ H ₅ ⁺
42	C ₂ H ₂ O ⁺ , CH ₂ N ₂ ⁺ , C ₃ H ₆ ⁺ , C ₂ H ₄ N ⁺
43	HCNO ⁺ , C ₂ H ₅ N ⁺ , C ₂ H ₃ O ⁺
44	CO ₂ ⁺ , C ₂ H ₄ O ⁺ , C ₃ H ₈ ⁺ , N ₂ O ⁺
45	CH ₃ NO ⁺ , C ₂ H ₇ N ⁺ , ¹³ CO ₂ ⁺ , CH ₅ N ₂ ⁺
46	C ₂ H ₆ O ⁺ , CH ₆ N ₂ ⁺ , C ¹⁸ OO ⁺
52	C ₂ N ₂ ⁺ , C ₄ H ₄ ⁺

A list of the different peak detected in the mass spectrum (Figure 23) of the gases released after the cold trapping and their possible attribution is given in Table 8. For each m/z the possible molecules and their major fragment are given.

The mass spectrum can be divided in different block called C_x where x is a number of “heavy” atoms other than hydrogen. In the case of this thesis, x is C, N and O. Taking into account the possible attribution proposed in this table, the identification of several peaks is possible.

First block named C₁ has two major peaks at m/z 17 and 18. Firstly, the presence of NH₃ and H₂O at m/z 17 and 18 respectively has been confirmed by a comparison with the infrared spectroscopy analysis.

For the C₂ block, different peaks are observed on the mass spectrum at m/z 26, 27, 28, 29, 30, 31 and 32. The production of HCN is expected at m/z 27 with the presence of CN⁺ fragment at m/z 26. However, the ratio between the peak at 27 and 26 is larger than the ratio expected from the NIST database for HCN. This more important intensity of the m/z 26 peak can be explained by the contribution of all abundant nitriles with their CN⁺ fragments. Another explanation could be the presence of acetylene C₂H₂. However, acetylene is not expected to condense in these conditions of pressure and temperature. The peak at m/z 29 is possibly attributed to methanimine CH₂=NH. However, different fragments of molecules can also contribute: HCO⁺ (formaldehyde fragment) and C₂H₅⁺ (propane fragment). The peak at m/z 30 is another important peak of the mass spectrum of the products. There are two species at this mass: formaldehyde H₂CO and ethane C₂H₆. However, ethane does not condense in these conditions of temperature and pressure as acetylene. Moreover, another contribution is possible at this peak with NO⁺. If NO does not condense in these conditions, this is an important fragment of NO₂ or N₂O. The last major peak of this group is at m/z 32 with two possible species: methanol CH₃OH and N₂H₄ which have both a contribution at m/z 31. For m/z 31, another possibility in addition of the two species at m/z 32 is CH₅N⁺. Finally at m/z 32, O₂⁺ fragment can possibly contribute for this peak.

Different peaks are observed for the C₃ block for m/z 40, 41, 44. The first important peak is at m/z 40. Three species are possible: propyne C₃H₄, CH₂CN, a fragment of acetonitrile and argon Ar. The low intensity at m/z 39 relatively to m/z 40 is not in agreement with the spectrum provided by the NIST database for C₃H₄.

At m/z 41, one species is possible, acetonitrile CH₃CN. This is in agreement with the formation of HCN which is more abundant. A contribution of C₃H₅⁺, a fragment of propene C₃H₆ is also possible. At m/z 44 the major contribution can be attributed to CO₂⁺. The presence of CO₂ in the gases released is confirmed by the increase of the CO₂ IR absorbance in Figure 24. Moreover the ratio between the peak at m/z 44 and the two peaks at m/z 45 and 46 is in agreement with the ratio between the CO₂ and its isotope at these masses in gas used in the initial gaseous mixture as visible in Figure 21. Other species can also contribute at these masses: acetaldehyde C₂H₄O⁺, propane C₃H₈ and nitrous oxide N₂O.

A last peak is observed at m/z 52. It can be classified in the C₄ block even if only one peak is observed for this block. Two species can contribute to this peak: ethanedinitrile C₂N₂ and vinylacetylene C₄H₄.

The attribution of species to the observed mass peaks has been done only for a limited number of masses. Indeed, despite a relatively low number of peaks observed on the mass chromatogram of the release species, the complexity of the species composition, which can be composed with 4 atoms: C, N, O and H, limited the number of peaks which can be attributed unambiguously to one compound.

III.3.1.d Cryogenic trapping of the gaseous products for an *ex situ* analysis by GC-MS

The previous section has shown that cryogenic trapping technique is useful to detect volatile trace species product in the plasma during the experiment. However their detection and identification *in situ* by mass spectrometry and infrared spectroscopy is limited. Indeed the resolution of the QMS is too limited to distinguish products with close mass and the detection limit of the FTIR permits to detect only major products.

For these reasons, I couple the cryogenic trapping to another analysis technique: the GC-MS. Such analysis has been realized previously for other gaseous mixtures used with the PAMPRE experiment (Fleury et al., 2014; Gautier et al., 2011). For these analyses, the gases are condensing in a cold trap immersed in liquid nitrogen (LN₂) and placed at the gas outlet of the reactor. In this thesis, I used gaseous mixtures containing carbon dioxide which condense at the temperature of LN₂. In order to prevent this effect, I choose to trap internally the gases in the reactor as for the *in situ* analysis and then to transfer the gases trapped in the cold trap for the GC-MS analysis. The external cold trap is a cylindrical glass coil immersed in liquid nitrogen and connected to the reactor. Before transferring gases, the cold trap is

pumped down to 5.10^{-5} mbar with a turbo molecular pump. Then, the trap is isolated from the turbo molecular pump and the valve isolating the trap from the reactor is opened and the gaseous species are thus transferred into the cold trap.

The gases have been trapped during 8 hours of plasma duration at 173 K. After the warming up of the plasma box and the release of the species trapped, the pressure in the reactor was about 4.1 mbar. Then the gases have been transferred in the cold trap and the pressure in the trapped has been measured before the injection in the GC-MS. A pressure about 50 mbar has been measured. The chromatogram of the gases trapped for an initial gaseous mixture containing 5 % of CO₂ is presented in Figure 26. All the peaks have been identifier using their elution order and their mass spectra. The list of the peaks their retention time and their attribution are given in Table 9.

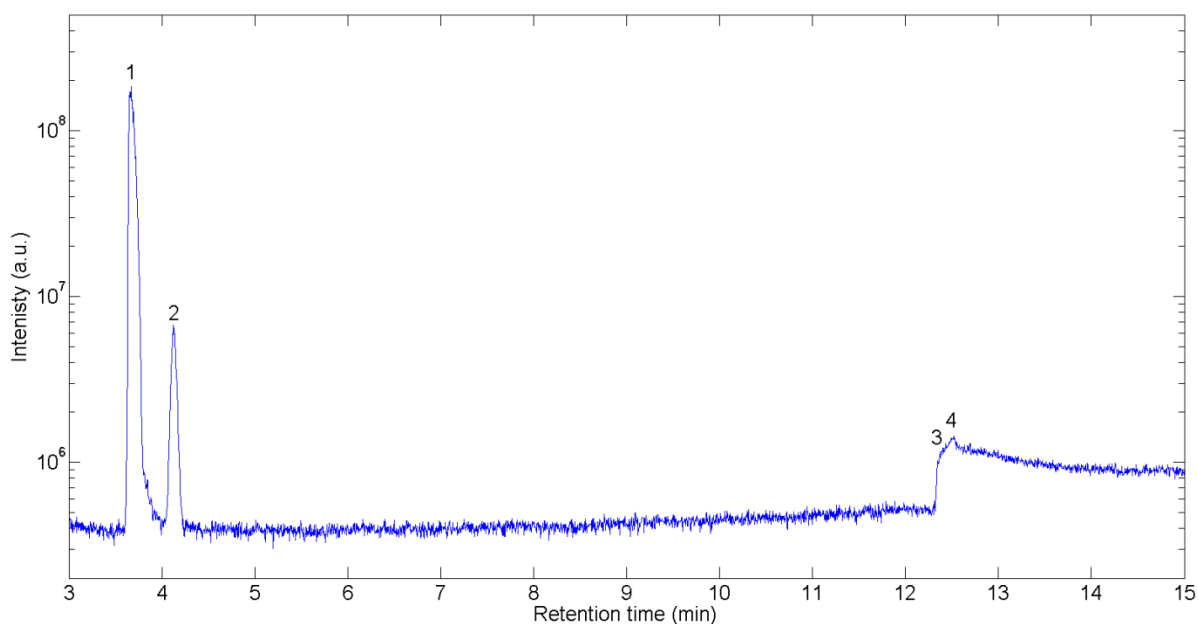


Figure 26: Chromatograms of gas trapped during an experiment with 5 % of CO₂.

Four species have been detected in the chromatogram. First one corresponds to carbon dioxide. This is the major peak in our chromatogram. This detection is in agreement with the important signal at m/z 44 in the *in situ* mass spectrum in Figure 23 and with the important absorption of the CO₂ band in the *in situ* infrared spectrum in Figure 24.

The confirmation of the CO₂ trapping by GC-MS in addition of the analysis of the gaseous phase composition by *in situ* mass spectrometry and *in situ* infrared spectroscopy must be take into account for the analysis of the gaseous phase composition. Indeed, if CO₂ was not

expected to condense in the condition of pressure and temperature used in these experiments, different explanation can be proposed. Firstly, the technique used to cool the plasma box is based on a circulation of LN₂ in a copper tube in contact with the polarized electrode, which is cooled by conduction. This circulation is commanded by a valve, which is open when the temperature of the electrode is higher than the chosen temperature and, which is closed when the temperature drops below this temperature. This mode of operation involves a variation of few Kelvins around the chosen value. This can explain the condensation of CO₂ and potentially other gas products, which were not expected to condense as hydrocarbons with 2 carbons. Secondly, as explained before LN₂ flows through a copper pipe which is a good thermal conductor. This pipe can be at a lowest temperature than the electrode and can permit the condensation of a part of the gases presents in the reactor on its surface. Finally, the most likely explanation is the important formation of water ice observed during the experiment. Indeed, it has been observed experimentally that water ice and particularly amorphous water ice can trap small molecules depending of the temperature (Bar-nun et al., 1985; Notesco and Bar-Nun, 1997). This phenomenon can explain the CO₂ trapping observed and the potential signature of argon at m/z 40 on the mass spectrum in Figure 23.

Table 9: List of gaseous compounds detected in our experiment.

Peak identification in chromatogram	Retention time (min)	Formula	Name
1	3.7	CO ₂	Carbon dioxide
2	4.1	N ₂ O	Nitrous oxide
3	-	H ₂ O	Water
4	12.5	C ₂ N ₂	Ethanedinitrile

The second species detected is nitrous oxide N₂O. In mass spectrometry, N₂O has a principal fragment at m/z 44 which is mixed with the CO₂ signature. The second fragment is m/z 30 and represents 31 % of m/z 44 intensity. This pattern is compatible with the mass spectrum presented above. N₂O was detected in the gaseous products in a simulation realized with the PAMPRE reactor and using an initial gaseous mixture made of N₂, CO and CH₄ (Fleury et al., 2014).

The third species detected is water. The exact retention time cannot be determined because of the saturation of the chromatographic column by water. This is in agreement with the important water signature observed by *in situ* mass spectrometry and IR spectroscopy.

The last detected species is co-eluted with water. This is ethanedinitrile (C₂N₂). The presence of C₂N₂ is in good agreement with the signature at m/z 52 on the mass spectrum in Figure 23.

GC-MS allowed highlighting the formation of two other products in the gaseous phase. They have been identified as N₂O and C₂N₂. With NH₃, detected before, this results point out the importance of the nitrogen chemistry, which composed the majority of the products detected. Moreover, the nature of these products highlighted a coupling between this nitrogen chemistry and the chemistry of CO₂ and H₂.

III.3.2 Analysis of the solid phase produced in the reactive medium

The first part of the results presented in this chapter was dedicated on the study of the formation of volatile species in the gaseous phase. This study has shown the possibility of an active chemistry initiated in a gaseous mixture made of N₂, CO₂ and H₂. Another important question about the reactivity of such gaseous mixture is to know if the reactivity can lead to the formation of solid organic aerosols. The formation of such aerosols from the gas phase reactivity has been observed in the atmosphere of Titan (Waite et al., 2007). The formation of analogues of aerosols has been also observed in experimental simulation of the early Earth atmospheric reactivity in gaseous mixture containing N₂, CO₂, and CH₄ (Hasenkopf et al., 2010; Hasenkopf et al., 2011; Heinrich et al., 2007; Trainer et al., 2004; Trainer et al., 2006). However, all these studies only take account the formation of aerosols in gaseous mixture with methane.

In the PAMPRE experiment tholins are deposited in the glass vessel surrounded the plasma. Thin films deposition can be also achieved on substrates placed on the grounded electrode. In the experiment presented in this chapter and which have been realized in a gaseous mixture made of nitrogen, carbon dioxide and hydrogen, there is no observation of the deposition of tholins in the glass vessel. However during these experiments, CaF₂ substrates were disposed on the grounded electrode. The analyzed of the substrates by IR spectroscopy (ATR technique) has shown the formation of a solid thin film on the substrate. Figure 27 presents the absorption spectrum of the films deposited on the two substrates disposed in the plasma box during the same experiment. The films were produced during 40 hours of plasma duration in gaseous mixture containing 10 % of CO₂.

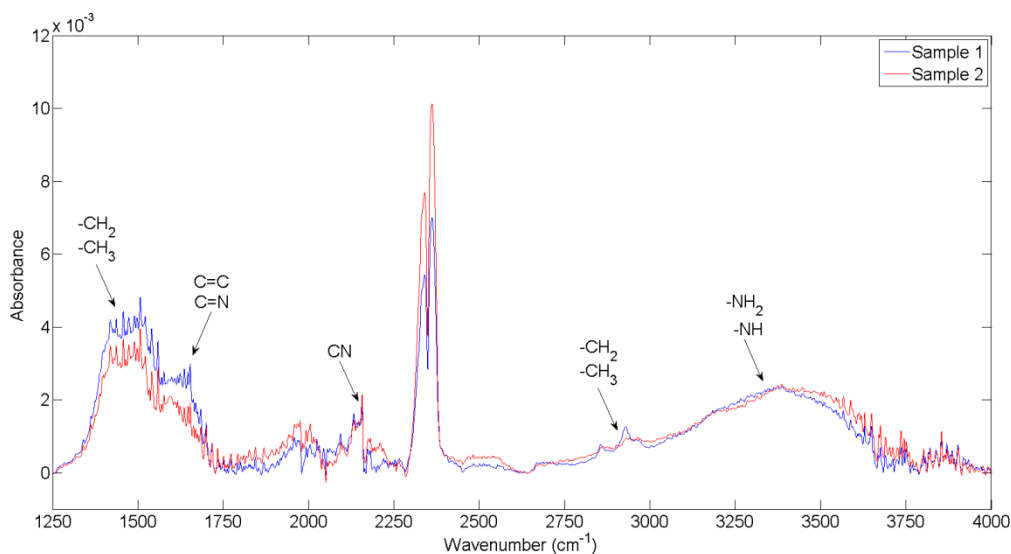


Figure 27: ATR spectra of tholins samples produced in a gaseous mixture made of N₂/CO₂/H₂ (86/10/4).

A residual atmospheric absorption is visible with the CO₂ absorption band at 2349 cm⁻¹ and the water vapor absorption bands in the 1300-2000 cm⁻¹ range and in the 3400-4000 cm⁻¹ range. In addition of these atmospheric signatures, different absorption band characteristic of solid organics are observed on the spectrum.

Firstly a broad band is observed at 3380 cm⁻¹. This band could be due to primary -NH and secondary amine -NH₂ or could be due to hydroxyl -OH. The 2860 cm⁻¹ band is attributed to -CH₃ symmetric stretching mode. The 2930 cm⁻¹ and 2960 cm⁻¹ bands are attributed to -CH₂ asymmetric stretching mode and -CH₃ asymmetric stretching mode.

Secondly the band observed at 2140 cm⁻¹ can be attributed to nitriles -C≡N or isocyanides -N≡C.

Finally at lower wavenumber, two broad bands are observed at 1465 cm⁻¹ and 1630 cm⁻¹. As suggested in study dedicated to Titan's aerosols and their analogues, the 1465 cm⁻¹ band can be a contribution of asymmetric bending mode of -CH₃ and scissor in plane bending mode of -CH₂ (Gautier et al., 2012; Vinatier et al., 2012). The band at 1465 cm⁻¹ cannot be attributed to one chemical function in particular. Indeed, this band can correspond to several functional groups as C=N and C=C double bonds, aliphatic and aromatic -NH₂ or aromatics and heteroaromatics functions.

This result shown a production of a solid organic film in an oxidized gaseous mixture, without methane, and deposited on a substrate. This formation seems to be promoting on the substrate as no formation of aerosols have been observed in the volume of the plasma.

III.3.3 Effect of the CO₂ initial amount

If different estimations have been done for the Archean CO₂ mixing ratio, this one is not precisely known for the Archean atmosphere and mostly for the Hadean atmosphere (Feulner, 2012). For this reason, I investigate the effect of the CO₂ initial amount, in the gaseous mixture mimicking the primitive atmosphere of the Earth, on the reactivity of this simulated atmosphere.

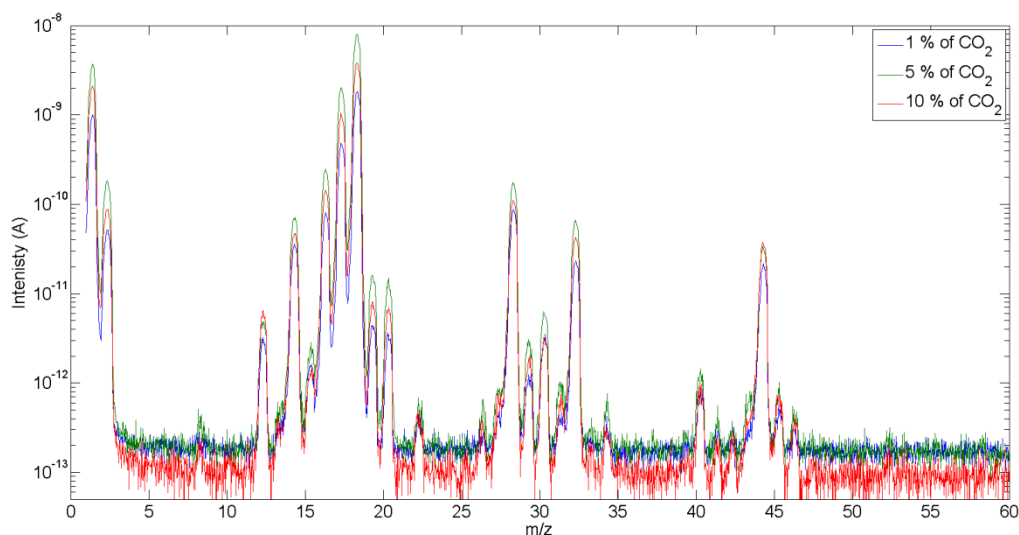


Figure 28: Mass spectra of the gases trapped realized at room temperature for different initial CO₂ amounts: 1 % of CO₂ (blue), 5 % of CO₂ (green) and 10 % of CO₂ (red).

Firstly I am interested at the effect of the CO₂ initial amount on the composition of the gaseous phase. A first effect observed is the modification of the consumption efficient of H₂ in function of the initial amount of CO₂. Indeed, if e_{CO_2} does not evolve significantly with the increase of the CO₂ percentage, e_{H_2} increase by a factor 2 when [CO₂] increase from 1 % to 10 %. As explained in section III.3.1.a, this modification can be linked to a modification of the chemistry in the plasma and so in a modification of composition of the gaseous phase composition qualitatively or/and quantitatively.

Figure 28 presents three mass spectra of the gaseous compounds recorded at room temperature and corresponding to the analysis of the gases released after an experiment of cold trapping for three different CO₂ initial amounts 1 %, 5 % and 10 %. If the identification

of all peaks of these mass spectra is not achieved, the modification of the CO₂ initial amount does not seem to modify qualitatively the composition of the gaseous phase. The same peaks are visible on the three mass spectra. Quantitatively a first comparison can be done of the total quantity of gases released. This can be measured with the pressure in the reactor after the release of the gases trapped. The final pressure measured at room temperature is given for the different CO₂ initial amounts in the Table 10.

Table 10: Pressure in PAMPRE after the release of the gases trapped during 4 hours of plasma duration at 173 K for different CO₂ initial amounts: 1 %, 5 % and 10 %.

[CO ₂] ₀ (%)	Pressure in the reactor (mbar)
1	1.44 ± 0.05
5	2.01 ± 0.05
10	2.15 ± 0.05

This measurement shows that the quantity of gas trapped is less important for an initial amount of 1 % of CO₂ than for the two higher initial amounts i.e. 5 % and 10 %. This is in good agreement with the lower consumption of H₂ for a CO₂ initial amount of 1 %. These two results highlight the fact that a higher CO₂ initial amount increases the global production of volatile species.

The number of H₂O molecules N_{H₂O} and the number of NH₃ molecules N_{NH₃} released is measured by infrared spectroscopy. Table 7 presents the evolution N_{NH₃} and N_{H₂O} as a function of the CO₂ initial amount. Contrary to the evolution of the pressure in the reactor, which informs us on the evolution of the total quantity of gas product, the evolution of N_{NH₃} and N_{H₂O} give information about quantitative evolution of two particular species. For H₂O, the quantity forms increases when the CO₂ initial amounts increases. N_{H₂O} increases by a factor 2 when [CO₂]₀ increases from 1 % to 10 %. Contrariwise N_{NH₃} decreases when the CO₂ initial amount increases. N_{NH₃} decreases of one order of magnitude when [CO₂]₀ increases from 1 % to 10 %.

For the other compounds detected a direct quantitative comparison between the different amounts of CO₂ used is not possible. Indeed, for compounds detected by GC-MS, the absolute intensities of the peak differed from a chromatogram to another even for two experiments realized in the same conditions. A quantitative analysis in gas chromatography requires the addition of an internal or an external standard in the gaseous mixture analyzed, which is not possible in this experimental configuration. For the mass spectrometry results,

this is the absolute intensity of the peaks, which are not faithfully reproducible from one day to another one. As the three experiments and the records of the corresponding mass spectra have been realized in different days, we cannot realize any quantitative comparison.

Finally the formation of a solid phase in the reactive medium is directly influence by the CO₂ initial amount. Indeed, a solid thin film has been observed only in experiments realized with 10 % of CO₂.

These different results have highlighted the importance of the CO₂ concentration on the reactivity of the gaseous mixture simulated. Indeed, if the CO₂ initial amount does not seem to modify qualitatively the composition of the gaseous phase, it involves different quantitative modification. A higher CO₂ initial amount seems to be favorable to a quantitative production of organic compounds both in the gaseous and in the solid phase. However, this evolution differs from a product species to another one as for H₂O, whose the production is promoted by a higher CO₂ amount when the NH₃ production is inhibited with this same higher CO₂ initial amount.

Knowing the absolute quantity of H₂ and CO₂ consumed in the plasma as function of the initial amount of CO₂, I am able to calculate the evolution of the C/H and O/H ratios in the fraction of gases consumed in the reactive medium. These results are presented in Table 6. As explained before, Δ_{CO_2} and Δ_{H_2} increase when the initial amount of CO₂ increases. It results that the C/H and O/H ratio in the fraction of gases consumed increase with the initial amount of CO₂. As the products are formed from the fraction of gases consumed, their composition must follow the same ratios. A decrease of the hydrogenation of the products formed is so expected.

III.4 Discussions

III.4.1 Impact of high altitudes water vapor formation on the early Earth

III.4.1.a Water content in the early Earth water atmosphere

Experimentally we have highlighted a source of water located in higher atmospheric layers of the early Earth where CO₂ is photodissociated. We provide here a first order estimation of the water concentration in the atmosphere considering this new mechanism. The present stratopause level is chosen as a benchmark for the calculation.

Water concentration is driven by the competition between the production rate ($\text{Prod}_{\text{H}_2\text{O}}$) and the destruction rate ($\text{Loss}_{\text{H}_2\text{O}}$).

$$\text{Prod}_{\text{H}_2\text{O}} = \text{Loss}_{\text{H}_2\text{O}} \quad (5)$$

Above the stratopause, we roughly assess that the production of H₂O is limited by the CO₂ photodissociation rate, which provides the reactive oxygen atoms. Nowadays, J_{CO_2} is equal to about 10^{-10} s^{-1} . A model study has shown that during the Archean, J_{CO_2} was equal to twice the actual value with a constant value from the stratopause to the atmospheric layers above (Claire et al., 2012). At the stratopause, following the study of (Kasting, 1993), the partial pressure of CO₂ is about 0.1 mbar, corresponding to a concentration of $10^{15} \text{ molecules.cm}^{-3}$. We can deduce the production rate of H₂O at the stratopause:

$$\text{Prod}_{\text{H}_2\text{O}} = J_{\text{CO}_2} \times [\text{CO}_2] \quad (6)$$

The resulting production rate of H₂O is about $10^5 \text{ molecules.cm}^{-3}.\text{s}^{-1}$.

The destruction of H₂O is equal to the product between the water concentration and the photochemical rate constant which is the inverse of the lifetime of water ($\tau_{\text{H}_2\text{O}}$):

$$\text{Loss}_{\text{H}_2\text{O}} = [\text{H}_2\text{O}] \times (1/\tau_{\text{H}_2\text{O}}) \quad (7)$$

The water concentration is deduced by combining the equations (5), (6) and (7):

$$[\text{H}_2\text{O}] = \text{Prod}_{\text{H}_2\text{O}} \times \tau_{\text{H}_2\text{O}} \quad (8)$$

For a water lifetime of about 1 day (Kasting, priv. comm.), a concentration about $10^{10} \text{ molecules.cm}^{-3}$ is obtained, corresponding to a partial pressure of water $\sim 10^{-6}$ mbar. This rough calculation informs us on the efficiency of the process with a water value as important at the stratopause (~ 50 km) as the ones predicted at the tropopause (~ 10 km) in (Kasting, 1993) without this source. Moreover, the water value calculated here is comparable with the few ppm_v of water vapor measured today in the mesosphere (Körner and Sonnemann, 2001) of the Earth and which is for a part issue of the methane oxidation in these layers (Thomas et al., 1989).

III.4.1.b Formation of high altitudes clouds

In a CO₂-rich atmosphere the average temperature at the stratopause level is expected to be close to the planetary skin temperature, around 200 K (Kasting, 1988), or even below. These low temperature and pressure conditions should result in the solid condensation of any

produced water vapor, were the temperature fall below ~170 K. This would lead to the formation of high altitude water ice clouds, analogous to the present day Polar Mesospheric Clouds (PMC) (DeLand et al., 2006; Määttänen et al., 2013; Pérot et al., 2010) whose formation is known to be favored by local water emission, e.g. from rockets engines (Siskind et al., 2013) and by local water production from the methane oxidation (Thomas et al., 1989) or analogous to the present day Polar Stratospheric Clouds (PSC) (Lowe and MacKenzie, 2008) if the water production takes place at relatively low altitudes.

These clouds are usually optically thin, but could nevertheless alter Earth's radiation budget in both visible (raising the albedo) and thermal IR radiation (through backscattering of thermal IR radiation), making predictions of their exact influence on early Earth's climate hard to assess without proper microphysical and radiative modeling, which is beyond the scope of this thesis.

These clouds can influence the atmospheric chemistry of the early Earth. Indeed, they are known to play an important role in planetary atmospheres. In the Martian atmosphere, water ice clouds have been found to directly influence the ozone concentration: in the absence of clouds, OH radicals titrate ozone, whereas heterogeneous chemistry of those radicals on water ice clouds enable ozone transient productions (Lefevre et al., 2008) Similarly in the present Earth atmosphere, the PSC are involves in the stratospheric O₃ destruction (Lowe and MacKenzie, 2008).

III.4.1.c Effect of the water atmospheric profile

The local extra greenhouse effect of this produced water vapor at stratopause level is almost certainly negligible due to the very low thermal IR opacity of the atmosphere at such low pressures. However, if the produced water could reach the denser and optically thicker layers at the tropopause level (whether by direct mixing of H₂O, or sedimentation and sublimation of the aforementioned PMC), possible radiative impacts could be: (1) a local cooling of the stratosphere since the extra water vapor is a very effective thermal IR radiator – that is, assuming that a positive temperature anomaly would exist in the first place in an already CO₂-rich atmosphere; and (2) a slight increase of the greenhouse (~0.1 K assuming a vertically uniform H₂O mixing ratio above the tropopause), effectively moving the tropopause slightly upwards.

If a water production in the ionosphere has a negligible effect on climate, it however impacts the whole atmosphere through chemistry and transport processes. This has been learned with

the case of Titan, the largest satellite of Saturn. This object is being observed by the Cassini-Huygens mission, which has highlighted the importance of ionospheric chemistry for the production of organic aerosols, impacting the entire atmosphere (Waite et al., 2007). In the early Earth, the presence of water at high altitudes can sensibly modify the concentration of all the other traces species, as H₂O is known to be a very reactive species at these altitudes. For example, H₂O can be a source of NH radicals through its reaction with N(²D), produced by photodissociation of N₂ at these altitudes (Dobrijevic et al., 2014). Consequences on ammonia NH₃ concentration in the upper atmosphere of the early Earth can therefore be expected.

III.4.2 Solid organic aerosols formations

The possible formation of organic aerosols in the atmosphere of the early Earth is of the prime interest for the comprehension of the environment of the Earth during the Hadean and the Archean. First of all, the formation of fractal organic hazes can provided an ultraviolet shield for the early Earth (Wolf and Toon, 2010) against the high UV flux of the young Sun (Claire et al., 2012). This shield can affect the composition of the atmosphere protecting certain constituents of the atmosphere such as ammonia from photochemical destruction (Sagan and Chyba, 1997). Furthermore, the formation of hazes can affect the climate of the early Earth providing an antigreenhouse effect (Haqq-Misra et al., 2008; Hasenkopf et al., 2011; McKay et al., 1999).

If the formation of aerosols have been observed in previous experimental studies of the early Earth atmospheric reactivity and, which used gaseous mixture made of N₂, CO₂ and CH₄ (Hasenkopf et al., 2010; Hasenkopf et al., 2011; Trainer et al., 2004; Trainer et al., 2006), this is not the case for gaseous mixture without methane as in this chapter. In the experiments described in this chapter, I observed the formation of an organic thin film which has growth on a substrate placed on the grounded electrode of the plasma device. In contrary, the formation of spherical shaped individual grains is not observed. The mechanism of formation of these two types of solid in the plasma is not completely known. Both grow from reactive species present in the plasma. For the formation of grains in the plasma, the process starts with the formation of nanometer-size monomers, which aggregates to form larger particles with a negative charge when the density of the monomers in the plasma reaches a critical value. Then the particles growth by deposition of species present in the gaseous phase (Wattiaux et al., 2015). The hypothesis, which can be done to explain the absence of these grains in gaseous mixture without CH₄ is that the less reactivity of these mixture does not

permitted to reach the critical value of monomers in the plasma necessary to started the growth in larger particles. The growth of the film is also driven by another process, which may be the bombardment of the grounded electrode by negative ions and which may be explained the formation of a film when the formation of grains is not observed.

In our gaseous mixture, solid organic products are only observed as deposited on a substrate. In such mechanism, the water formation observed in this gaseous mixture can play a role for the formation of solid organic in the atmosphere of the early Earth. Indeed, as discussed before, water formed above the troposphere could conduct to the formation of high altitude clouds analogues to the present PSC and PMC. These clouds are composed of water ice, which can play the role on nucleus cores, promoting a heterogeneous nucleation of organic at the surface of ice grains. This formation of solid organics in interaction with water ice can also be important to consider in the perspective of a potential chemical evolution of aerosols formed in the atmosphere of the early Earth during their sedimentation to the surface. Indeed, during their sedimentation to the surface, aerosols are continuously irradiated by UV solar photons flux, which can drive an evolution of the aerosols.

III.5 Conclusion

In this chapter I have presented the first study of the reactivity of the early Earth atmosphere realized with the PAMPRE reactor in a gaseous mixture made of N₂, CO₂ and H₂.

The study of the formation gaseous and solid products has shown the potential of such oxide mixture to form quantitatively organic compounds. Indeed, the reactivity of this gaseous mixture leads to the formation of gaseous compounds with mass up to 60 u and leads to the formation of a solid organic thin film.

The analysis of the composition of the gaseous phase is realized by *in situ* mass spectrometry and infrared spectroscopy with the help of a cryogenic trapping of the gaseous species. This analysis points out the formation of water vapor which is quantified as the major product in the gaseous phase, which represents ~10 % of the gases trapped.

This important formation of H₂O in the ionosphere of the early Earth from the oxidation of H₂ can play an important role for the chemistry of the early Earth atmosphere above the troposphere. Indeed, H₂O is a very reactive species, which can notably contribute to the formation of NH radicals by its reaction with N(²D). Moreover, this water forms in the thermosphere could condense in the mesosphere and involves the formation of high altitudes

clouds comparable to actual PMC. The formation of such clouds can also impact the chemistry through heterogeneous processes.

In addition of this important water formation different gaseous species have been identified with these techniques or *ex situ* by GC-MS. Different small reactive organic species have been identified: HCN, NH₃ and C₂N₂. N₂O has been also identified. The identification of these species highlights the reactivity of this gaseous mixture with an effective coupling between the chemistry of C, N, H and O. Moreover, in addition of these gaseous species, the formation of a solid organic thin film has been observed highlighting the important complexity that can be reached by this gaseous mixture reactivity and so the early Earth atmosphere.

Finally, the CO₂ mixing ratio in the initial gaseous mixture mimicking the early Earth atmosphere has been found as an important parameter for the observed chemistry. Indeed, the increase of the CO₂ initial mixing ratio is favorable for this chemistry from a quantitative point of view. Indeed, the global quantity of gaseous compounds increases when the CO₂ initial amount increases from 1 % to 10 % even if this evolution differs from one species to another one. Moreover, the formation of a solid organic thin film has been observed only in the experiment using the higher initial amounts used for this chapter.

Chapter IV CH₄ influence on the early Earth atmospheric chemistry

IV.1 Introduction

As developed in the Chapter I, the composition of the early Earth atmosphere prior to the apparition of life is subject to debate. A primitive atmosphere mainly composed by N₂ and CO₂ is widely accepted today. Different proposition have been done for the other constituents of this atmosphere. One of the most currently proposed species in addition of N₂ and CO₂ is methane CH₄. The presence of methane in the early Earth atmosphere is mainly used as additional greenhouse gases, in addition of CO₂ to resolve the faint young Sun paradox (Feulner, 2012).

The presence of methane is also interesting from the perspective of organic chemistry. Several photochemical studies of the reactivity of an early atmosphere made of N₂, CO₂ and CH₄ have highlighted the formation of organic volatile species and the formation of organic solid aerosols (haze) in such an atmosphere (Kasting et al., 1983; Pavlov et al., 2001; Tian et al., 2011; Zahnle, 1986). The formation of these hazes can influence the composition of the atmosphere providing a UV shield for different species as NH₃ (Pavlov et al., 2001; Wolf and Toon, 2010) or impact the climate providing an anti-greenhouse effect (McKay et al., 1999).

The formation of hazes has been explored previously by exposing a gaseous mixture mimicking the atmosphere (i.e. made of N₂, CO₂ and CH₄) to the photon flux of a UV lamp (Hasenkopf et al., 2010; Hasenkopf et al., 2011; Trainer et al., 2006) or using an electric discharge as energy source (Trainer et al., 2004). Studies using a UV lamp have irradiated their gaseous mixture to Lyman- α (121.6 nm) radiations. They showed a potential CH₄ based organic growth. However, this wavelength prevents the photodissociation of molecular nitrogen, which involve a direct coupling with nitrogen chemistry. However, a coupling with nitrogen chemistry is possible with a such energy source for experiments realized at higher pressure involving trimolecular reactions (Trainer et al., 2012).

Based on these previous experimental works, I study in this chapter a possible organic growth, in gaseous mixtures made of N₂, CH₄ and CO₂, involving a nitrogen abundance representative of the upper atmosphere of the early Earth. The first part is dedicated to the formation of volatile species in the gaseous phase. The second part is focused on the

formation of a solid phase in the reactive medium. Due to the lack of constraints about the CO₂ mixing ratio in the early atmosphere of the Earth, the effect of the CO₂ initial amount on the composition of the gaseous phase and the solid phase as well as the quantity of product formed will be discussed.

IV.2 Experimental methods and protocols

In the experiments presented here, three gas bottles are used to generate the reactive gaseous mixtures: one with high-purity of N₂ (99,999 %), one containing a N₂-CH₄ (99,999 %) mixture with 10 % of CH₄ and one with CO₂ (99,995 %). The generator RF power is set to 30 W and the total gas flow rate to 55 sccm resulting in a 0.9 mbar pressure in the reactor. The initial methane mixing ratio is kept constant at 1 % for all experiments. This value has been chosen as an upper limit, in the range of methane mixing ratio expected in the Archean atmosphere after the apparition of methanogen bacteria (Kharecha et al., 2005) and compatible with the mixing ratio possible with our experimental setup. The gas flow is adjusted from an experiment to another to introduce carbon dioxide at various mixing ratios ranging from 1 to 10 %. Compositions of the different gaseous mixtures studied here are given in Table 11.

Table 11: Initial compositions of the studied gaseous mixtures.

Mixture number	[N ₂] ₀ (%)	[CO ₂] ₀ (%)	[CH ₄] ₀
1	98	1	1
2	94	5	1
3	89	10	1

Firstly, a series of experiments is done at room temperature to monitor the CO₂ and the CH₄ consumption in the plasma by *in situ* mass spectrometry. Secondly, in order to detect and identify gaseous species product in low quantity, a new series of experiment is realized using a cold trapping of these species on the walls of the plasma box. For that, we use a continuous injection of liquid nitrogen (L_{N2}) inside the stainless-steel block supporting the grounded electrode. The plasma box is cooled by thermal conduction. The temperature is fixed at 173 K to prevent N₂, CH₄ and CO₂ condensations. Products are accumulated during 4 hours of plasma duration. After plasma is turned off, the reactor is pumped to eliminate reactive species. The reactor is isolated and the plasma box is warmed up to room temperature to release the gases trapped. Then, the gaseous phase is analyzed *in situ* by mass spectrometry and infrared spectroscopy.

Moreover, the tholins produced in the different conditions studied are collected to determine their IR absorption properties and their elemental composition.

IV.3 Results

IV.3.1 Analysis of the gaseous phase composition

IV.3.1.a Reactive species consumption in the plasma

The consumption of CO₂ and CH₄ is monitored using *in situ* mass spectrometry. The carbon dioxide consumption is measured using a time-tracking of CO₂⁺ at *m/z* 44. In order to prevent any overlapping of CH₄ ion signal with O⁺ signal at *m/z* 16; the methane consumption is measured using a time tracking of CH₃⁺ (*m/z* 15) after a correction of the contribution of ¹⁵N⁺ based on laboratory calibration.

Figure 29 presents the evolution of the CO₂ mixing ratio when the plasma is switched on for three different mixing ratios: 1 %, 5 % and 10 %. The initial concentration of CO₂ is known and it is possible to calibrate the *m/z* 44 signal intensity in order to obtain the evolution of the *in situ* CO₂ concentration. The concentration obtained has been multiply for 1 % and 5 % of CO₂ by a factor 10 and a factor 2 respectively. The CO₂ mixing ratio decreases when the plasma is switched on and reaches a steady-state after a few minutes of transient regime.

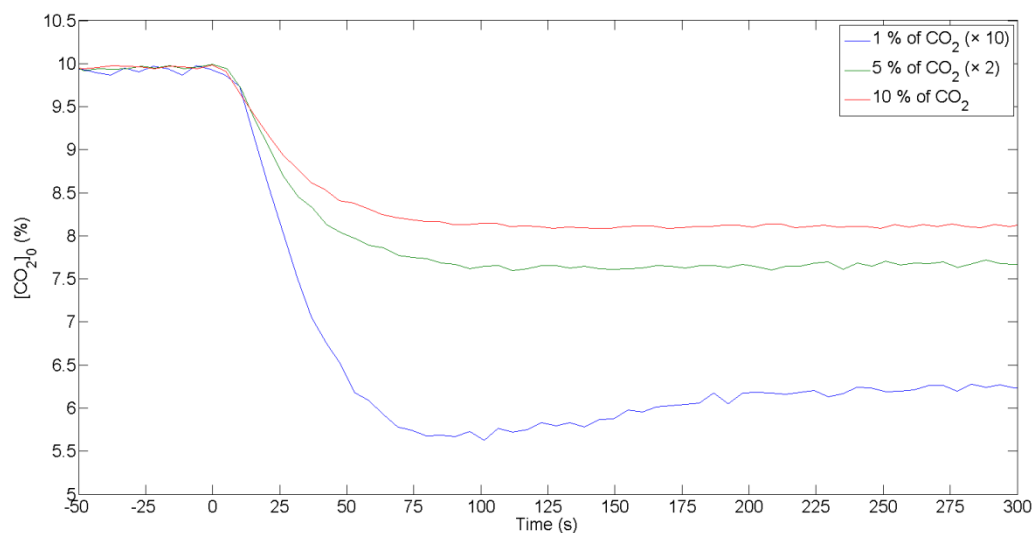


Figure 29: Evolution of the CO₂ mixing ratio in the gaseous reactive medium with the plasma duration. Origin of the time is set as the moment when the plasma is turn on. CO₂ mixing ratio has been multiply by a factor 10 and a factor 2 for an initial amount of 1 %

We defined the carbon dioxide consumption efficient e_{CO_2} which can be deduced from Figure 29 with the equation (3) defined in the Chapter III:

$$e_{\text{CO}_2} = \frac{[\text{CO}_2]_0 - [\text{CO}_2]_{\text{ss}}}{[\text{CO}_2]_0} \quad (3)$$

Where $[\text{CO}_2]_0$ and $[\text{CO}_2]_{\text{ss}}$ represent the initial and steady-state percentages of carbon dioxide respectively. Results are presented in Table 12. The consumption efficient of CO₂ decreases from 38 % to 19 % when the initial amounts of CO₂ increases from 1 % to 10 %.

Table 12: Evolution of the consumption efficiencies of carbon dioxide e_{CO_2} and methane e_{CH_4} in the plasma as a function of the initial amount of CO₂. The uncertainties are given as 2σ (standard deviation) and are calculated from the standard fluctuations of the mass spectrometry measurements.

$[\text{CO}_2]_0$ (%)	e_{CO_2} (%)	e_{CH_4} (%)
1	38 ± 1	66 ± 2
5	23.9 ± 0.5	58 ± 3
10	19.2 ± 0.2	54 ± 2

The same study is realized on methane. Figure 30 presents the evolution of the CH₄ mixing ratio when the plasma is switched on for the three initial amounts of CO₂: 1 %, 5 % and 10 %. The initial concentration of CH₄ is known and it is possible to calibrate the m/z . 15 signal intensity in order to obtain the evolution of the *in situ* CH₄ concentration. The CH₄ concentration decreases when the plasma is switched on and reached a steady-state after a transient regime.

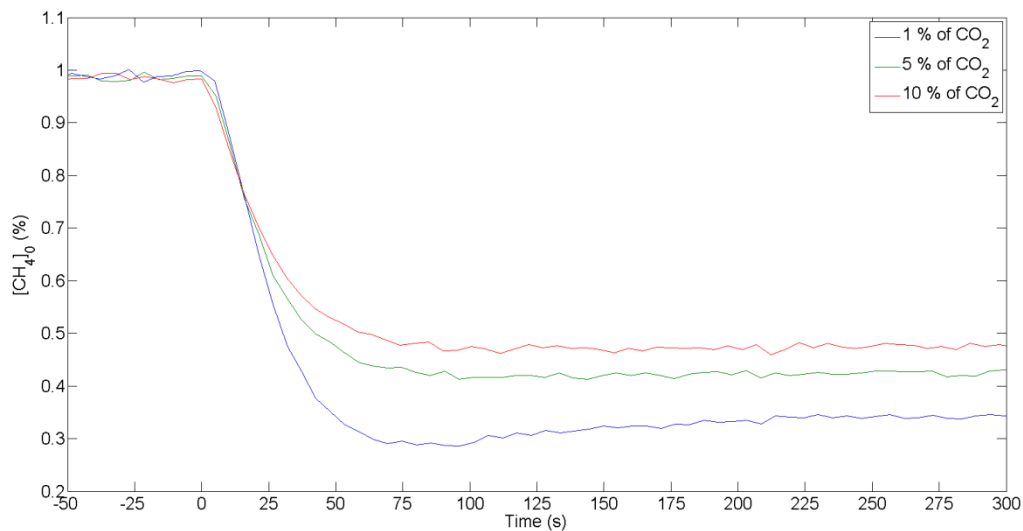


Figure 30: Evolution of the CH₄ mixing ratio in the gaseous reactive medium with the plasma duration for the different CO₂ initial amounts. Origin of the time is set as the moment when the plasma is turn on.

We defined the methane consumption efficient e_{CH_4} which can be deduced from the Figure 30 with the following equation (9):

$$e_{\text{CH}_4} = \frac{[\text{CH}_4]_0 - [\text{CH}_4]_{\text{ss}}}{[\text{CH}_4]_0} \quad (9)$$

Where $[\text{CH}_4]_0$ and $[\text{CH}_4]_{\text{ss}}$ represent the initial and steady-state percentages of methane respectively. Results are presented in Table 12. The CH₄ consumption efficient decreases from 66 % to 54 % when the initial amount of CO₂ increases from 1 to 10 %. Moreover, CO₂ involves a decrease of e_{CH_4} as soon as it is added in the gaseous mixture. Indeed, the consumption efficient of CH₄ in a gaseous mixture without CO₂ has been previously studied and a consumption efficient of methane about 81.9 % has been found for a gaseous mixture made of N₂ and CH₄ with 1 % of CH₄ (Sciamma-O'Brien et al., 2010). CO₂ inhibits the consumption of CH₄ in the plasma and this effect increases when the CO₂ initial amount increases.

IV.3.1.b *In situ* analysis of the gaseous phase composition by mass spectrometry

Firstly the composition of the gaseous phase has been studied at room temperature by *in-situ* mass spectrometry. The composition of the gaseous phase at the stationary-state before and after the initiation of the plasma is studied for m/z 1 to 60 u. The resulting spectra are presented in Figure 31 for an initial gaseous mixture made of N₂:CO₂:CH₄ 94:5:1 %.

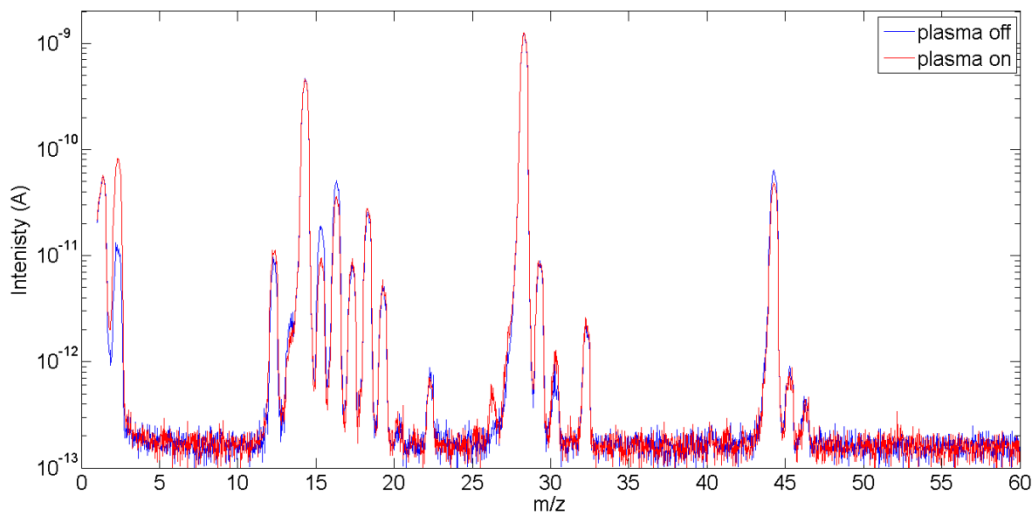


Figure 31: Mass spectra obtained for a N₂:CO₂:CH₄ 94:5:1 % gas mixture plasma off (blue) and plasma on (red) at room temperature.

Firstly, the mass spectrum recorded before the initiation of the plasma presents the typical mass signature corresponding to the used gaseous mixture in addition of the mass signatures corresponding to the residual air in the mass spectrometer see in Figure 14. Molecular nitrogen involves fragments at m/z 14 (N^+), 15 ($^{15}N^+$), 28 (N_2^+), 29 ($^{15}N^{14}N^+$) and 30 ($^{15}N^{15}N^+$). Carbon dioxide involves fragments at m/z 12 (C^+), 22 (CO_2^{2+}), 44 (CO_2^+), 45 ($^{13}CO_2^+$) and 46 ($CO^{18}O^+$). Methane presents fragments at m/z 12 (C^+), 13 (CH^+), 14 (CH_2^+), 15 (CH_3^+) and 16 (CH_4^+).

The mass spectrum recorded when the plasma is on shows several differences with the mass spectrum recorded when the plasma is off (Figure 31). Firstly, the comparison between the two mass spectra shows a decrease of the intensity of three mass peaks at m/z 15, 16 and 44. This corresponds to the consumption of CH₄ and CO₂ in the plasma. An increase of the intensity is observed at m/z 2, which corresponds to the formation of H₂ from the dissociation of methane. An increase of two other peaks is also observed at m/z 26 and 27. The signature at m/z 27 can be attributed to HCN, which have also a contribution at m/z 26 with the fragment CN⁺.

To better represent this signal evolution for different mass peaks, I have monitored the evolution of two abundant species in N₂-CH₄ mixtures without CO₂, i.e. HCN (at m/z 27) and CH₃CN (at m/z 41) (Gautier et al., 2011). Figure 32 presents the evolution of the m/z 27 signal (panel a) and the evolution of the m/z 41 signal (panel b) as a function of time for different CO₂ initial amounts: 1 %, 5 % and 10 %.

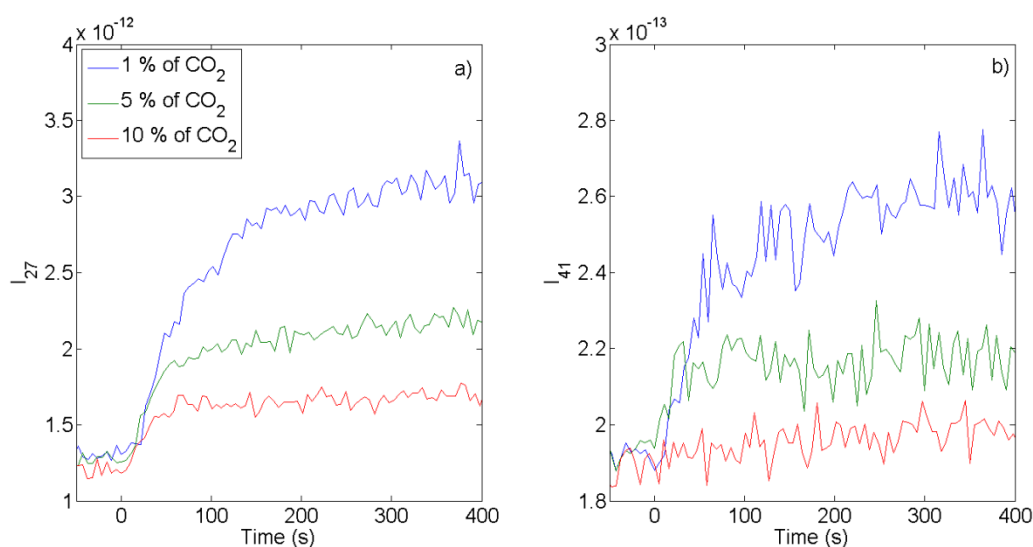
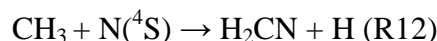


Figure 32: Evolution of the m/z 27 signal (panel a) and m/z 41 signal (panel b) in the gaseous reactive medium with the plasma duration. The origin of time is set as the moment when the plasma is turned on.

When the plasma is turned on, we observe an increase of the signal for HCN and CH₃CN. The concentration of these species increases and reaches a steady-state after about 100 s with 1 % of CO₂. For every CO₂ amounts, CH₃CN signal is found to be one order of magnitude lower than HCN, in agreement with a previous quantification by GC-MS analysis in gaseous mixture without CO₂ (Gautier et al., 2011). This involves a lower signal to noise ratio in the case of CH₃CN. For the two species we observe an important decrease of the intensity of the steady-state signal when the initial CO₂ amount increases. This reflects a decrease of the production yield of HCN and CH₃CN. For CH₃CN, we do not observe any variation of the *m/z* 41 signal for 10 % of CO₂ initial amount. CH₃CN is produced in lower quantity than HCN and in the case with 10 % of HCN, the signal to noise ratio is too low to detect the formation of CH₃CN. The increase of CO₂ concentration inhibits the formation of these two products. This is in good agreement with the decrease of the CH₄ consumption in the plasma when the CO₂ initial amount increases. The formation of HCN in the early atmosphere has been modeled previously (Tian et al., 2011; Zahnle, 1986). These studies have shown that HCN is efficiently formed through the following reactions:



Moreover, CN radicals from the photodissociation of HCN in the upper atmosphere of the early Earth can be efficiently recycled to reform HCN through reactions with hydrocarbons (Tian et al., 2011);



The different mechanisms of the HCN formation show the importance of CH₃ and H radicals as well as hydrocarbons. These species come from the CH₄ dissociation and chemistry. The decrease of CH₄ consumption shown in Table 12 in the presence of CO₂, involves a decrease in the formation of these species and explains the decrease of the HCN production yield observed in Figure 32 (panel a). The formation of heavier nitrile molecules has been proposed to be a polymerization process, where CH₃ radical reacts with a C_{*x*-1}H_{2*x*-1}CN nitrile to form a C_{*x*}H_{2*x*+1}CN nitrile (Dobrijevic and Dutour, 2006; Gautier et al., 2011). The decrease of the CH₃CN production yield, when the CO₂ initial amount increases, is in agreement with this mechanism where CH₃CN comes from HCN.

IV.3.1.c Cryogenic trapping of the gaseous products for an *in-situ* analysis

In order to concentrate the gas species produced in PAMPRE during the experiment, I used an internal cryogenic trapping following a method described in section IV.2. After 4 hours of trapping at 173 K, the plasma is switched off; the reactor is pumped and then isolated. The plasma box is warmed up to room temperature. The composition of the gas released is then analyzed by *in-situ* mass spectrometry. Figure 33 presents two mass spectra recorded after a trapping of gaseous products with 4 hours of plasma duration and an initial CO₂ amount of 5 %. The first spectrum is recorded at a temperature of 173 K. The second spectrum is recorded after the warming of the plasma box up to room temperature.

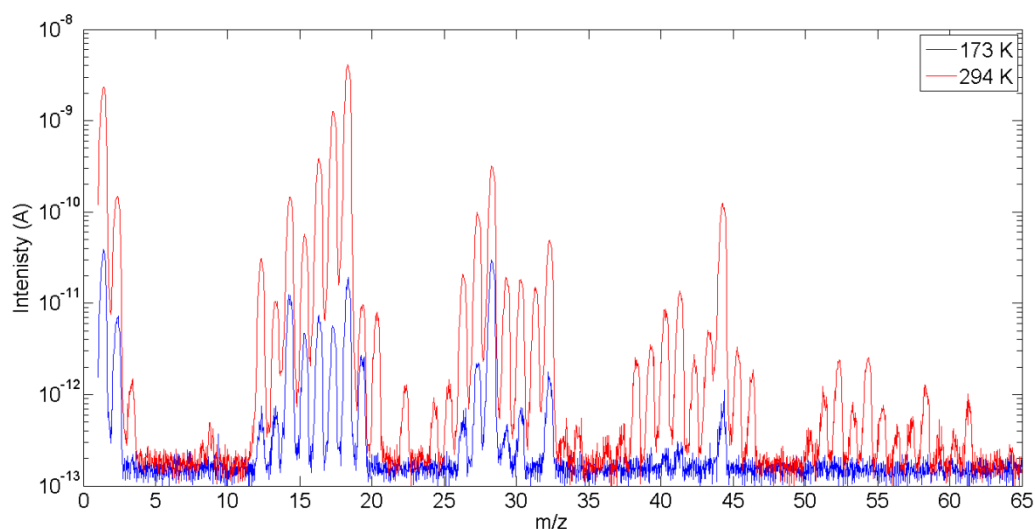


Figure 33; Mass spectra recorded at 173 K (blue) and 294 K (red) after 4 hours of gaseous products trapping in N₂-CO₂-H₂ (94/5/1) plasma.

The signature of the residual air in the mass spectrometer can be identified in the mass spectrum recorded at 173 K in agreement with the blank spectrum presented in Figure 14. The apparition of new peaks is visible on the spectrum recorded at room temperature. These signatures can be attributed to the gaseous products formed during this experiment and which have been trapped. We observe peaks with masses up to 65 u. This reflects a chemical growth in the gaseous phase during the experiment and an efficient organic chemistry. Because of the necessary duration of the warming of the plasma box up to room temperature, the two spectra have been recorded during two consecutive days. The complexity of the gaseous mixture can lead to the formation of numerous molecules composed by C, N, H and O atoms. The low resolution of the QMS does not allow differentiating molecules with same mass units; several

molecules can be attributed to one mass peak in the spectrum. However, few peaks can be attributed unambiguously.

The case of water: H₂O

The major peak on the spectrum recorded at room temperature in Figure 33 is for m/z 18. This peak is attributed to water. This attribution to H₂O is in agreement with the high level of the peak at m/z 17 (OH⁺) which is a major fragment of H₂O.

This result is confirmed by the analysis of the gaseous phase by *in situ* infrared spectroscopy. Figure 34 presents two infrared spectra recorded at 173 K and 294 K, at the same time as the mass spectra of Figure 33.

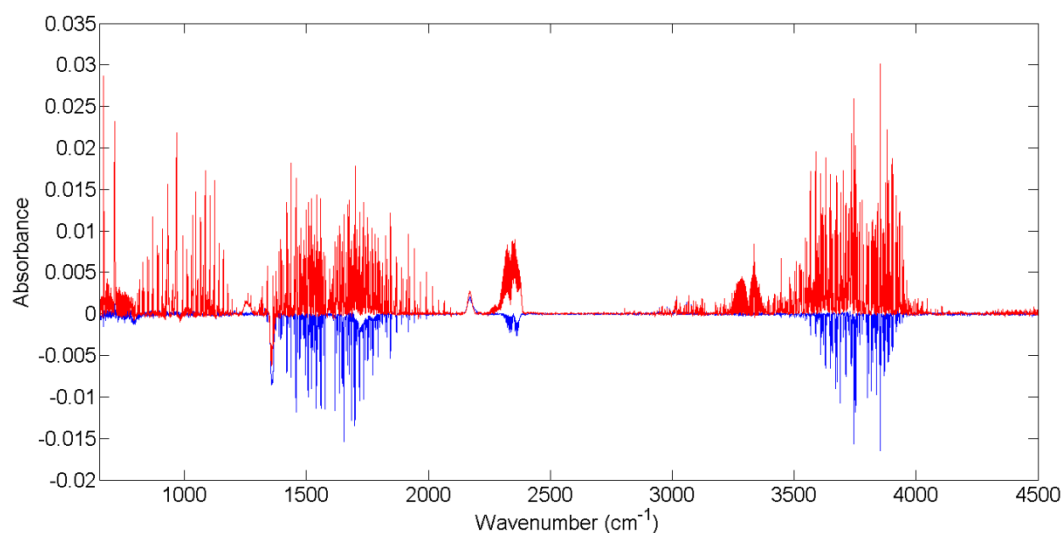


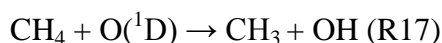
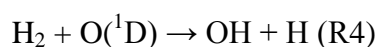
Figure 34: Infrared spectra recorded at 173 K (blue) and 294 K (red) after the trapping of the gaseous product during 4 hours of plasma duration in an initial gaseous mixture made of N₂/CO₂/CH₄ (94/5/1).

For the two spectra, absorbance is calculated using the same reference spectrum taken in the reactor under vacuum at room temperature. For the first spectrum recorded at 173 K, we observe a negative signature for H₂O as well as CO₂. This is due to a decrease of the air signature in the box where the detector is located (Figure 14). After the warm up of the plasma box to room temperature, an important increase of the water vapor absorption band is observed in the 1300-2000 cm⁻¹ range and in the 3400-4000 cm⁻¹ range despite the decrease of the water signature in the box of the detector comparatively to the signature of the reference spectrum. The correlation of this important increase of the infrared signature of H₂O with the high signal detected with the mass spectrometry at m/z 18 enables to attribute this detection to

an important water formation in the plasma during the experiment. However this variation in the water signature does not allowed realizing water quantification as for the chapter III.

Similarly to mechanism proposed in the chapter III to explain the water formation in simulation containing H₂, in the present case water formation can be explained by the formation of oxygen radicals O(¹D) through reactions R1 to R3:

Then O(¹D) can react with H₂ coming from the methane dissociation or directly with methane to form OH radicals:



Finally OH induced the formation of H₂O by the following reactions:



The importance of this quantitative water formation above the troposphere of the early Earth has been discussed in the Chapter III. Principally water formed at high altitude could condense in the mesosphere and the stratosphere of the early Earth resulting in the formation of high altitude clouds similar to actual Polar Stratospheric Clouds (PSC) and Polar Mesospheric Clouds (PMC). These clouds could impact the photochemistry occurring in the atmosphere and the climate depending on their optical thickness.

The case of ammonia: NH₃ and hydrogen cyanide: HCN

Ammonia and hydrogen cyanide are of great interest for prebiotic chemistry. The signature of ammonia in mass spectrometry is principally at $m/z = 17$ with the ion NH₃⁺. This is one of the principal peaks of the mass spectrum at room temperature in Figure 33. However, water has also a contribution at this mass due to OH⁺ fragment. Here, I used the infrared spectroscopy to remove this ambiguity. Figure 35 presents an infrared spectrum recorded at 300 K. This is a spectra center on the 700-1200 cm⁻¹ range.

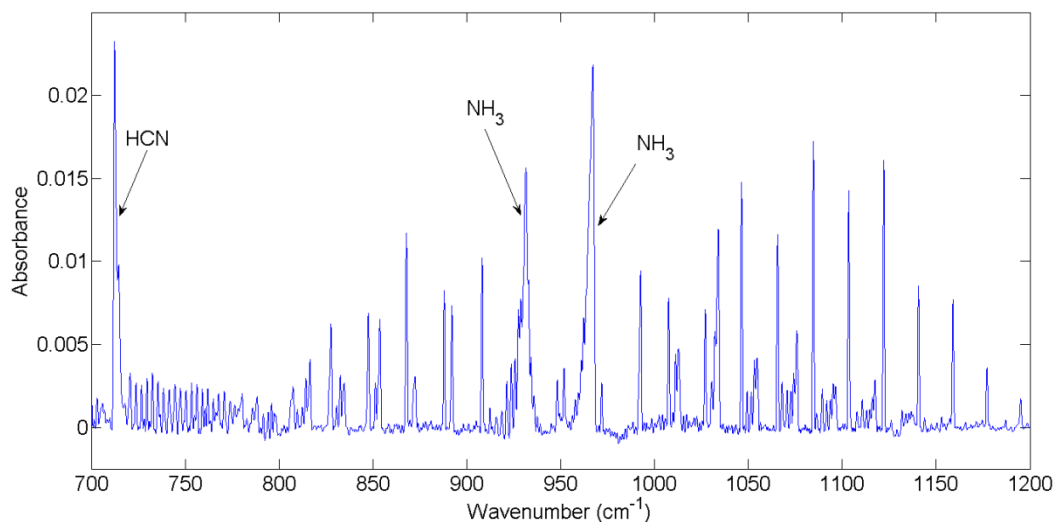


Figure 35: Infrared spectra in the 700-1200 cm⁻¹ range recorded at 300 K after 4 hours of gaseous products trapping in a N₂-CO₂-CH₄ (94/5/1) plasma.

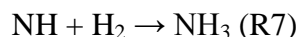
Two species presenting a strong absorption are visible in this spectrum. The first one is identified as NH₃ according to the NIST database and the Hitran database (Rothman et al., 2009). The presence of a doublet at 930 cm⁻¹ and 967 cm⁻¹ is characteristic of NH₃ and allows identification unambiguously. The second species is identified as HCN according to the NIST database and the Hitran database (Rothman et al., 2009). In this range of wavenumber, HCN presents a strong absorption band at 713 cm⁻¹. This is possible to quantify HCN and NH₃ with the beer-lambert law, following the equation (1) and (2). To calculate the concentration of NH₃ and HCN, we used the absorption cross sections from the Hitran 2008 database (Rothman et al., 2009). In order to overcome the difference of resolution between the database and laboratory data, we calculate the concentrations on the area of the bands. For NH₃, integration is performed both in the 920-940 cm⁻¹ range and in the 950-970 cm⁻¹ range. For HCN, integration is performed in the 710-720 cm⁻¹ range. Knowing the volume of the reactor we calculate the number of ammonia molecules N_{NH_3} and the number of HCN molecules N_{HCN} trapped in 4 hours. The number of ammonia molecules N_{NH_3} for the 2 ranges and the number of HCN molecules N_{HCN} are reported in Table 13.

The values of the number of molecules trapped have the same order of magnitude for HCN and NH₃ even if N_{NH_3} is two times greater than N_{HCN} .

Table 13: Number of NH₃ molecules N_{NH3} and number of HCN molecules N_{HCN} formed during for hours of plasma duration in a gaseous mixture made of N₂/CO₂/CH₄ (94/5/1).

N _{HCN} (molecules)	N _{NH3} (molecules) 920 - 940 cm ⁻¹	N _{NH3} (molecules) 950 - 970 cm ⁻¹
$(4.9 \pm 0.2) \times 10^{19}$	$(8.0 \pm 0.2) \times 10^{19}$	$(9.8 \pm 0.2) \times 10^{19}$

Formation processes of NH₃ have been discussed in the Chapter III for gaseous mixture made of N₂, CO₂ and H₂. In any case, NH₃ is formed through the following reaction:



The different mechanisms discussed in the previous chapter are about the formation processes of NH radicals through reactions (R7) to (R11). In addition to these mechanisms, another ionic pathway has been proposed for the formation of NH radicals in plasma containing methane (Carrasco et al., 2012):



Moreover, NH₃ formation from the dissociative recombination of protonated amines, as the protonated methanimine CH₂=NH₂⁺, has been evocated (Yelle et al., 2010). Methanimine CH₂NH has been previously detected by *in-situ* mass spectrometry in experiment realized without CO₂ (Carrasco et al., 2012). An important peak is observed in Figure 33 at *m/z* 29, for which methanimine can contribute. However, this one detection is not sufficient to conclude about the presence or not of methanimine in our gaseous products. Indeed, a contribution at *m/z* 29 is expected from the propane fragmentation 44 (50 %) 29 (100 %) pattern or from the formaldehyde fragmentation 30 (60 %), 29 (100 %) pattern (from NIST database).

Identification of another gaseous products by IR spectroscopy

Other infrared absorption bands are visible on the spectrum recorded at room temperature on Figure 34. Figure 36 presents a spectrum recorded at room temperature of the gases released and center on the 2750-3400 cm⁻¹ range.

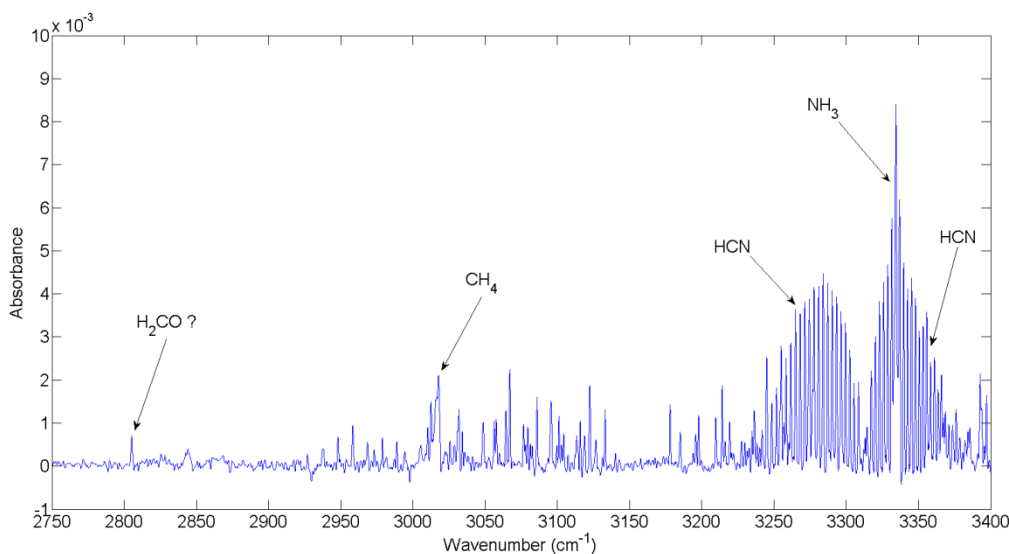


Figure 36: Infrared spectra in the 2750-3400 cm⁻¹ range recorded at 300 K after 4 hours of gaseous products trapping in a N₂-CO₂-CH₄ (94/5/1) plasma.

Firstly this spectrum presents absorption bands, which can be attributed to HCN from 3250 to 3400 cm⁻¹ according to HITRAN database (Rothman et al., 2009). Another absorption band, which is convoluted with HCN absorption band, is visible at 3335 cm⁻¹ and can be attributed to NH₃ according to HITRAN database (Rothman et al., 2009).

Another absorption band is visible at 3018 cm⁻¹ on Figure 36. This band can be attributed unambiguously to methane according to the GEISA database (Jacquinet-Husson et al., 2011). The trapping of methane, which is one of the species composing the initial gaseous mixture, was unexpected. Indeed methane does not condense at the temperature used during this experiment, i.e. 173 K. Explanations have been proposed in the chapter III to explain a similar trapping of CO₂. These hypotheses suggest that small variations of the plasma box temperature or a colder temperature of the copper pipe transporting liquid nitrogen can explain the trapping of species, which are not supposed to condense. However, these hypotheses cannot explain the condensation of methane in the present case, which does not condense at temperature as low as the temperature of LN₂. Another phenomenon can be at the origin of the present methane trapping. Indeed different studies have showed that volatile gases such as CH₄ can be efficient trapped in amorphous or crystalline water ice (Notesco and Bar-Nun, 1997). This study showed that a gaseous species can be trapped in the pores of the water ice during its condensation depending of the temperature. In our experiment, the plasma box is cooled at 173 K with a variation of few Kelvin and a potential cooler point with the

copper transporting LN₂. This phenomenon can explain the observed trapping of CH₄ and potentially the trapping of other species.

A last absorption band is visible on Figure 36 at 3805 cm⁻¹. This band can correspond to a C-H stretching mode of an aldehyde. Two molecules are particularly susceptible to absorb at this wavelength: formaldehyde H₂CO and propanal C₃H₆O, which presents both absorption bands at ~2800 cm⁻¹ corresponding to a C-H stretching mode (Köroğlu et al., 2015; Rothman et al., 2009; Sharpe et al., 2004). These molecules present also an absorption band at ~1750 cm⁻¹. Corresponding to a C=O stretching mode. However, Figure 34 shows in the spectrum recorded at room temperature after the release of the gases that this range of the IR spectrum is dominated by H₂O absorption and if a C=O stretching mode absorption band of one of these molecules is presented, it is hidden by the water band. In addition to the band at ~2800 cm⁻¹, propanal presents also a strong absorption band at ~2990 cm⁻¹ corresponding to a -CH₃ stretching mode (Köroğlu et al., 2015). This band is not present on Figure 36. The non-detection of this second absorption band of C₃H₆O is in disagreement with the presence of this molecule. In the absence of another absorption band observable in another range of the spectrum, H₂CO seems to be the better candidate for the attribution of the absorption band observed at 2805 cm⁻¹.

Other gaseous compounds

H₂O, NH₃ and HCN and possibly H₂CO have been identified by their specific mass spectra signature or by the cross comparison between the mass spectrum and the infrared spectrum. However, the mass spectra of these compounds do not explain all the peaks visible on the mass spectrum of the gaseous products trapped. The mass spectrum at room temperature in Figure 33 can be divided in different blocks called C_x where x is a number of “heavy” atoms other than hydrogen. In the case of this thesis, x is C, N and O. Figure 33 shows mass peaks for masses up to 61 u. This reflects an important organic growth with species detected in block C₁ to C₅. The identification of the different peaks remains complicated. Indeed, the relatively low resolution of the spectrometer and the important fragmentation of the molecules involve potentially a contribution of multiple species and fragments for one peak. This difficulty is emphasized by the relative complexity of the initial gaseous mixture leading to the formation of products, which can be made of 4 different atoms: C, H, N and O.

A list of the different peaks detected in the mass spectrum (Figure 33) of the gases released after the cold trapping and their possible attribution is given in Table 14.

Table 14: List of the peaks detected in the mass spectrum of the gases released and their possible attribution to molecules (black) or their major fragments (red).

<i>m/z</i>	Possible attribution	<i>m/z</i>	Possible attribution
17	NH ₃ ⁺ , OH ⁺	43	HCNO ⁺ , C ₂ H ₅ N ⁺ , C ₂ H ₃ O ⁺ , CN ₂ H ₃ ⁺ , C ₃ H ₇ ⁺
18	H ₂ O ⁺	44	CO ₂ ⁺ , C ₂ H ₄ O ⁺ , C ₃ H ₈ ⁺ , N ₂ O ⁺ , CONH ₂ ⁺
22	CO ₂ ²⁺	45	CH ₃ NO ⁺ , C ₂ H ₇ N ⁺ , ¹³ CO ₂ ⁺ , CH ₅ N ₂ ⁺
24	C ₂ ⁺	46	C ₂ H ₆ O ⁺ , CH ₆ N ₂ ⁺ , C ¹⁸ OO ⁺ , NO ₂ ⁺ , CO ₂ H ⁺
25	C ₂ H ⁺	50	C ₄ H ₂ ⁺
26	C ₂ H ₂ ⁺ , CN ⁺	51	C ₄ H ₃ ⁺
27	HCN ⁺ , C ₂ H ₃ ⁺	52	C ₂ N ₂ ⁺ , C ₄ H ₄ ⁺
28	C ₂ H ₄ ⁺ , CO ⁺ , N ₂ ⁺ , CH ₂ N ⁺	53	C ₃ H ₃ N ⁺ , C ₄ H ₃ ⁺ , C ₃ HO ⁺
29	CH ₂ NH ⁺ , HCO ⁺ , N ₂ H ⁺ , C ₂ H ₅ ⁺	54	C ₃ H ₂ O ⁺ , C ₄ H ₆ ⁺
30	NO ⁺ , H ₂ CO ⁺ , C ₂ H ₆ ⁺ , N ₂ H ₂ ⁺ , CH ₄ N ⁺	55	C ₃ H ₅ N ⁺ , C ₂ H ₃ N ₂ ⁺ , C ₃ H ₃ O ⁺
31	CH ₅ N ⁺ , CH ₃ O ⁺ , N ₂ H ₃ ⁺	56	C ₃ H ₄ O ⁺ , C ₂ H ₄ N ₂ ⁺ , C ₄ H ₈ ⁺ , C ₃ H ₆ N ⁺
32	O ₂ ⁺ , CH ₃ OH ⁺ , N ₂ H ₄ ⁺	57	C ₂ H ₃ NO ⁺ , C ₃ H ₇ N ⁺
39	C ₃ H ₃ ⁺	58	C ₃ H ₆ O ⁺ , C ₄ H ₁₀ ⁺
40	C ₃ H ₄ ⁺	59	C ₂ H ₅ NO ⁺ , CH ₅ N ₃ ⁺ , C ₃ H ₉ N ⁺
41	CH ₃ CN ⁺ , C ₃ H ₅ ⁺	60	C ₂ H ₄ O ₂ ⁺ , CH ₄ N ₂ O ⁺ , C ₃ H ₈ O ⁺ , C ₂ H ₈ N ₂ ⁺
42	C ₂ H ₂ O ⁺ , CH ₂ N ₂ ⁺ , C ₃ H ₆ ⁺ , C ₂ H ₄ N ⁺	61	CH ₃ NO ₂ ⁺

For each *m/z* the possible molecules and their major fragment are given.

The analysis of the gaseous phase composition in N₂-CH₄ plasma has been realized previously *in situ* by mass spectrometry (Carrasco et al., 2012) and *ex situ* by GC-MS (Gautier et al., 2011). They have highlighted the formation of a variety of chemical species: hydrocarbons, nitriles and imines. In addition to these species, the presence of CO₂ leads to a potential complexity of the gaseous phase composition with the formation of oxygenated species. The discussion of the attribution of the principal peaks observed has been done in the Chapter III for gaseous mixtures made of N₂, CO₂ and H₂. The exact attribution of the species contributing at the different mass peaks remains impossible because of the limited resolution of the QMS and the fact that the limited sensitivity of the IR spectroscopy has allowed identifying only four species. Another analysis of the gaseous phase composition by *ex situ* GC-MS for the experiments using N₂, CO₂ and CH₄ would be necessary to better identify the species produced in the gaseous phase

IV.3.1.d Influence of the CO₂ initial amount on the gaseous phase

The exact CO₂ concentration in the Hadean and the Archean remaining largely unknown and having evolved over geological times (Feulner, 2012), I investigate the effect of the CO₂ initial amount on the production of volatile products. For this a new series of internal trapping experiment has been realized with an accumulation of the volatile products during 2 hours of plasma duration. Then the gases releases have been analyzed by *in situ* mass spectrometry.

Table 15 presents the evolution of the final pressure in the reactor after the warm up at room temperature of the plasma box and the release of the gases trapped as a function of the CO₂ initial amount.

Table 15: Pressure in PAMPRE after the release of the gases trapped during 2 hours of plasma duration at 173 K for different CO₂ initial amounts: 1 %, 5 % and 10 %.

[CO ₂] ₀	Pressure in the reactor (mbar)
1	0.43 ± 0.05
5	0.36 ± 0.05
10	0.26 ± 0.05

We observe a decrease of the pressure of the gases released when the CO₂ initial amounts increases. This reflects a decrease of the organic growth in the gaseous phase and an inhibition effect of CO₂ on the formation of gaseous products. This is in agreement with the decrease of the HCN and CH₃CN production yield observed *in situ* by mass spectrometry with the increase of the carbon dioxide initial amount.

Figure 37 presents three mass spectra of the gaseous compounds recorded at room temperature and corresponding to the analysis of the gases released after an experiment of cold trapping for three different CO₂ initial amounts 1 %, 5 % and 10 %.

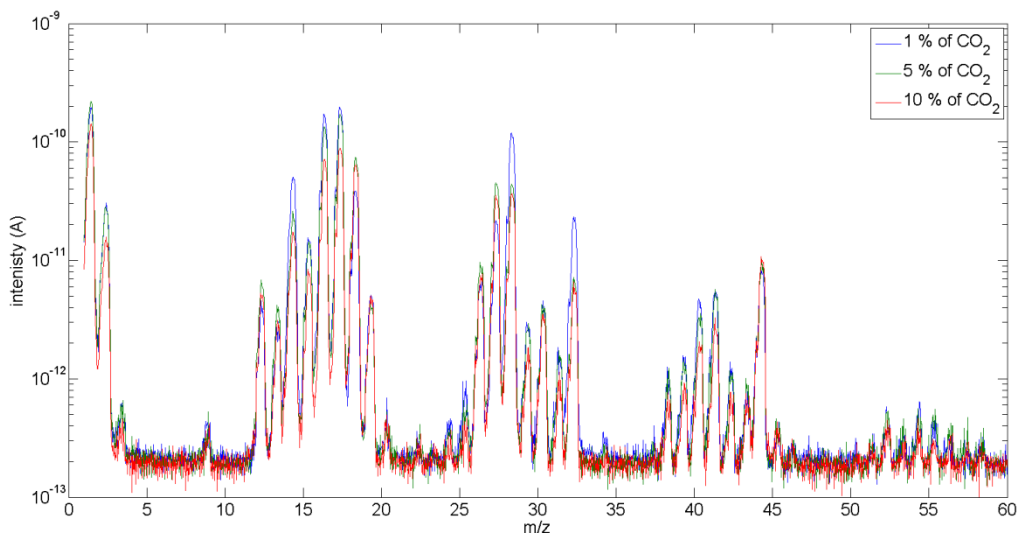


Figure 37: Mass spectra of the gases trapped realized at room temperature for different initial CO₂ amounts: 1 % of CO₂ (blue), 5 % of CO₂ (green) and 10 % of CO₂ (red).

The comparison of these three spectra does not highlight any qualitative change. Indeed, in the 1 to 60 u range we observe the same mass peaks for the three CO₂ initial amounts. However, as multiple species can contribute to one mass peak, this analysis by mass spectrometry is not sufficient to study each species separately. As no calibration can be done, a direct quantitative comparison of the intensity of the peaks between the three spectra cannot be achieved because of a possible drift of the spectrometer from one day to another. However, a global trend can be observed for the evolution of the intensities of the mass peaks when the initial amount of CO₂ increases from 1 % to 10 %. Indeed, for the majority of the masses, a decrease of the intensity of the peaks is observed with the increase of the carbon dioxide initial amount. This effect is in agreement with the observed decrease of the total pressure in the reactor corresponding to a decrease of the organic growth when the CO₂ initial amount increases.

This inhibition effect of CO₂ of the organic growth has been observed in previous experimental studies where they had observed a decrease of the aerosols productions rate when the concentration of CO₂ increases for a same concentration of CH₄ resulting in a decrease of the C/O ratio in the gaseous phase (Trainer et al., 2004; Trainer et al., 2006). Trainer et al. (2006) have explained the decrease of the organic growth for gaseous mixture

with higher CO₂ concentration by an increase of O atoms, coming from the CO₂ dissociation in the reactive medium, which terminate the hydrocarbon molecules and inhibit the growth of long-chains.

IV.3.2 Analysis of the solid phase produced in the reactive medium

In the first part of the results presented in this chapter, I have highlighted that the addition of CO₂ in a N₂-CH₄ gaseous mixture inhibits the organic growth but modifies the chemical composition of this gaseous phase, initiating a coupling between the oxygen chemistry and the C, N, H chemistry.

This second part is dedicated to the formation of tholins in N₂-CH₄-CO₂ gaseous mixtures. Different productions of tholins have been realized in the different gaseous mixtures presented in Table 11. Tholins have been produced during few hours of plasma duration at room temperature. Firstly the evolution of the tholins mass production rate with the amount of CO₂ is determined following the protocol described in (Sciamma-O'Brien et al., 2010). Tholins collected are weighted with a 0.1 mg precision scale. As a part of the tholins produced is dragged by the gas flow outside the glass vessel, the production rates given here are lower limits. Results are presented in Table 16. Results presented here concern tholins produced for a pressure of 0.9 mbar with one exception for a tholins sample produced in a gaseous mixture with 5 % of CO₂ at a pressure of 2.2 mbar. This tholins sample has been produced during an experiment using the cold trap at the outlet of the reactor. The study realized in gaseous mixtures made of N₂ and CH₄ has shown that an increase of the pressure in PAMPRE can lead to an increase of the tholins production rate for a same gas composition but the pressure has a limited effect on the tholins composition (Sciamma-O'Brien et al., 2010).

We observe an important decrease of the tholins production rate with the addition of CO₂. The injection of a few percent of CO₂ leads to a strong inhibition of tholins formation with a production rate of ~6 mg.h⁻¹ for an initial amount of 1 % of CO₂ comparatively to the 18.2 mg.h⁻¹ observed in (Sciamma-O'Brien et al., 2010) for a gaseous mixture without CO₂.

Table 16: Tholins production rate as a function of [CO₂]₀. ^a Tholins produced at 0.9 mbar. ^b Tholins produced at 2.2 mbar.

[CO ₂] ₀ (%)	Tholins mass collected (mg)	Production rate (mg.h ⁻¹)
1	79.5 ^a	9.94 ^a
	120.1 ^a	4.68 ^a
5	36.1 ^b	5.1 ^b
	<0.1 ^a	
10	3 ^a	0.18 ^a
	<0.1 ^a	

The tholins production rate reaches values lower than 0.2 mg.h⁻¹ for a CO₂ initial amount of 10 % of CO₂. This decrease is in agreement with the observed decrease of the methane and carbon dioxide consumption and the decrease of the volatiles production when the CO₂ initial amount increases. This decrease of the production rate is in agreement with the effect observed on the gaseous phase and with previous studies (Trainer et al., 2004; Trainer et al., 2006).

In addition, CO₂ modified also the gaseous phase composition, which can impact the tholins composition. Particularly, potential oxygen incorporation can be expected. The quantification of the content of the tholins in N, C, H and O is realized by the present elemental analysis. Previous elemental studies realized for tholins produced in N₂-CH₄ gaseous mixture have shown a small contamination of the sample by oxygen with ~3 % of the total elementary composition (Fleury et al., 2014). This oxygen contamination has been discussed previously in (Sciamma-O'Brien et al., 2010): plasma polymers are very quickly oxidized when exposed to air for collection. The protection of the tholins samples from the oxygen contamination is difficult, however the oxygen contamination remains constant at a level of ~3 %, which will be considered as a reference for comparison with sample produced with CO₂.

The elemental analysis for tholins produced with different CO₂ amounts is presented in Table 17. Table 17 shows a quantitative increase of the oxygen content in the tholins with the increase of the CO₂ initial amount. For an initial amount of 1 % of CO₂, the oxygen content reaches 5.5 %, which correspond to an increase of 2.5 % comparatively to the oxygen contamination level.

Table 17: Elemental composition of tholins for different [CO₂]₀. ^a Tholins produced at 0.9 mbar. ^b Tholins produced at 2.2 mbar.

[CO ₂] ₀ (%)	Nitrogen (%)	Carbon (%)	Hydrogen (%)	Oxygen (%)
1 ^a	28.8	32.1	33.6	5.5
	28.9	32	33.8	5.3
5 ^b	28.9	28.2	35.6	7.3
	28.6	27.9	36.1	7.4
10 ^a	26	28	37.6	8.4

These 2.5 % can be attributed to an incorporation of the oxygen from CO₂ in the tholins formed in the plasma. The total oxygen content increases up to 8.5 % for an initial amount of 10 % of CO₂ resulting to an incorporation of 5.5 % in tholins. This increase of the oxygen incorporation in the tholins with the increase of the CO₂ amount is associated to an increase of hydrogen and a decrease of carbon.

These modifications of the tholins composition are important for the formation of complex molecules composed by C, N, H and O in the early Earth atmosphere. Moreover, these modifications can impact their optical properties. IR spectroscopy is achieved in order to study the evolution of the IR signature of the tholins as a function of [CO₂]₀.

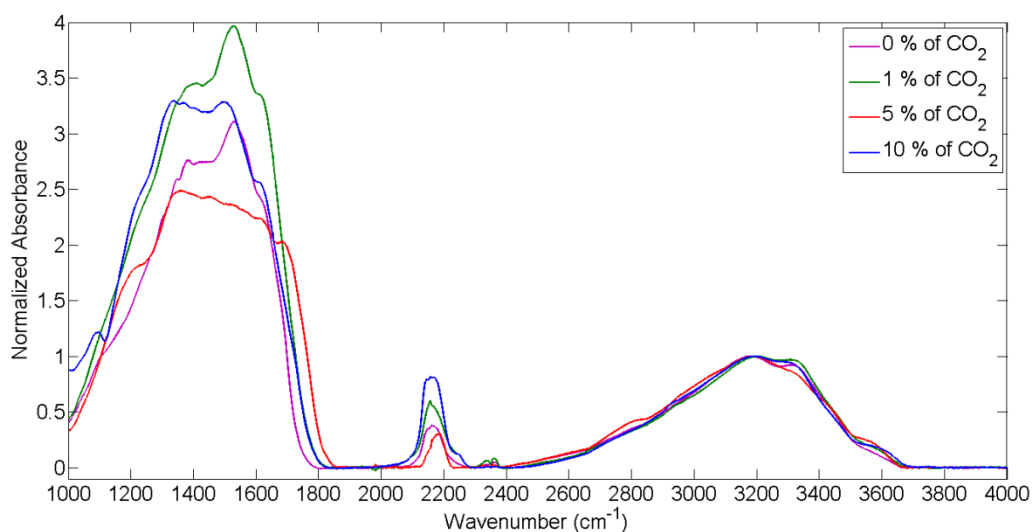


Figure 38: Comparative IR spectra of tholins produced in PAMPRE in gaseous mixture containing 1 % of CH₄ and different amounts of CO₂: 0 %, 1 %, 5 % and 10 %. The spectra were normalized on the amine band at 3200 cm⁻¹.

Since ATR does not give a quantitative measurement, all the spectra have been normalized and the amine band at 3200 cm⁻¹ for comparative purposes. The identification of the absorption bands of the sample produced in the N₂-CH₄ mixture without CO₂ has been realized previously (Gautier et al., 2012).

Firstly two broad bands are observed at 3200 cm⁻¹ and 3320 cm⁻¹. This band is due to primary -NH and secondary amines -NH₂. The band observed at 2160 cm⁻¹ can be attributed to nitriles -C≡N or isocyanides -N≡C.

Finally at lower wavenumber, the large intense pattern observed around 1500 cm⁻¹, with principally two strong bands at 1380 cm⁻¹ and 1530 cm⁻¹, can correspond to several functional groups present in the tholins as C=N and C=C double bonds with also a contribution of aliphatic and aromatic -NH₂ or aromatics and heteroaromatics functions.

Other spectra of tholins produced in gaseous mixture containing CO₂ are very similar to this one recorded for tholins produced without CO₂. Firstly, the range where are present the amines functions are not modify. This is in disagreement with the formation of -OH bond in the tholins, which absorbed also in this range of the IR spectrum. The nitrile band at 2160 cm⁻¹ is not modified.

For the important pattern around 1500 cm⁻¹, few changes can be observed. Firstly, for CO₂ initial amounts higher than 1 %, the ratio between the two important bands compositing the pattern is changed. The intensity of the band at 1530 cm⁻¹ decreases comparatively to the other one. These bands are not clearly identified and the interpretation of this change remains unclear. The change in the bands, corresponding to functions made of C, N and H, is linked to the modification of the tholins composition with an increase of the H content and a decrease of the C content. Finally, a last change is observed for this large pattern. For the three samples produced with CO₂, the band is shifted to the higher wavenumber. This is particularly marked for the spectrum of the sample produced with 5 % of CO₂. This band could correspond to C=O bond. Quantitative oxygen incorporation has been observed in the aerosols produced with CO₂. This incorporation is expected to form new bonds in the tholins and so modify its infrared signature. Figure 38 emphases a potential presence of C=O bond implicating an incorporation of oxygen deeply in the tholins structure rather than an incorporation in terminal function such as -OH bonds. This is consistent with the possible detection of formaldehyde in the gaseous phase. However, the joint augmentations of the H and O contents when the initial

amount of CO₂ increases as determined by the elemental analysis is in favor of a formation of -OH bond.

Solid materials present large absorption bands, which limits the analysis of the chemical composition. Another analysis technique would be required to better understand the chemical composition of the tholins and particularly to characterize the influence of the oxygen on the composition. Such a work has been realized with an analysis of the chemical composition of the tholins by high resolution mass spectrometry, particularly to characterize with nitrogen incorporation in tholins produced in N₂-CH₄ plasma (Gautier et al., 2014a; Pernot et al., 2010). Moreover, similar analysis has been done to infer the oxygen incorporation in tholins produced in a plasma made of N₂, CH₄ and labelling C¹⁸O (Hörst et al., 2012). Determined the chemical compositions of the tholins could permit to determine the type of oxygenated molecules formed and conclude about the presence of C=O and -OH functions.

Finally aerosols in the atmosphere of the early Earth could interact with solid water forming PSC or PMC. These interactions could be at the origin at a chemical evolution of the aerosols during their sedimentation to the surface under UV solar flux.

IV.4 Importance of methane for the formation of organic compounds in the atmosphere of the early Earth

In the Chapter III and in the present Chapter, I investigate the formation of organic compounds in two gaseous mixtures mimicking the composition of the early Earth atmosphere. First one is made of N₂, CO₂ and H₂ and the second one is made of N₂, CO₂ and CH₄. The results obtained in these chapters have highlighted a potential organic growth in both gaseous mixtures with a coupling between the C, N, H and O chemistries leading to the formation of heavier gaseous compounds and solid aerosols. However, differences have been founded between the reactivity of the two mixtures.

Firstly, the chemistry is more efficient in the mixture containing CH₄ than one containing H₂. Indeed, heavier volatiles products have been detected in gaseous mixtures containing CH₄ than those containing H₂. Moreover, quantitative production of solid particles growing in volume in the plasma has been collected in experiments realized with CH₄ when only organic thin films deposited on substrate has been observed for experiments with H₂. This reflects the more important reactivity of reduced carbon as in CH₄ comparatively to oxidized carbon as in CO₂.

Methane is favorable for a quantitative production of organic compounds and particularly to produce solid hazes. However, results from Chapter III show that an organic growth was possible without methane with CO₂ as source of reactive carbon with the formations of some organics compounds with principally nitrogenized molecules. Moreover, abiotic production of methane is limited and the methane concentration was limited at a few ppm_v prior the apparition of life (Guzmán-Marmolejo et al., 2013). The reactivity of an early atmosphere made of N₂, CO₂ and H₂ could be a source of small organic molecules and could provide at the surface small organics molecules as HCN implicated in the formation of prebiotic molecules (Patel et al., 2015). After the apparition of methanogen bacteria (Woese, 1987), the concentration of methane could increase in the early Earth atmosphere and reach levels as high as 1000 ppm_v (Pavlov et al., 2000) leading to a more important organic chemistry with potentially the formation of a haze layer providing a UV shield (Pavlov et al., 2001; Wolf and Toon, 2010) or impacting climate (McKay et al., 1999).

IV.5 Conclusion

In this chapter I have presented the first study of the reactivity of the early Earth atmosphere realized with the PAMPRE reactor in a gaseous mixture made of N₂, CO₂ and CH₄.

The study of the formation gaseous and solid products has shown the potential of such oxidized mixtures to form quantitatively organic compounds. Indeed, the reactivity of this gaseous mixture leads to the formation of gaseous compounds with mass up to 65 a.m.u and leads to the formation of a solid aerosols.

The analysis of the composition of the gaseous phase is realized by *in-situ* mass spectrometry and infrared spectroscopy with the help of a cryogenic trapping of the gaseous species. This analysis points out the formation of water vapor. H₂O formed from the oxidation of H₂ or CH₄ can play an important role for the chemistry of the early Earth atmosphere above the troposphere. Indeed, H₂O is a very reactive species, which can notably contribute to the formation of NH radicals by its reaction with N(²D). Moreover, this water formed in the thermosphere could condense in the mesosphere and in the stratosphere and involve the formation of high altitudes clouds comparable to actual PMC and PSC. The formation of such clouds can also impact the chemistry through heterogeneous processes or climate depending of their optical thickness.

In addition of this important water formation different gaseous species have been identified with these techniques. Different small reactive organic species have been identified: HCN,

NH₃ and H₂CO. The identification of these species highlights the reactivity of this gaseous mixture with an effective coupling between the chemistry of C, N, H and O. Moreover, in addition of these gaseous species, the formation of a solid organic particles has been observed highlighting the important complexity that can reached this gaseous mixture reactivity and so the early Earth atmosphere.

Finally, the CO₂ mixing ratio in the initial gaseous mixture mimicking the early Earth atmosphere has been found as important parameters for the observed chemistry. Indeed, the increased of the CO₂ initial mixing ratio inhibits the formation of organic compounds both in the gaseous and in the solid phases. Indeed, the quantity of gaseous trapped and the production rate of tholins decreases when the CO₂ initial amounts increases from 1 % to 10 %. However, the quantity of oxygen incorporated in the tholins increases with the increase of the CO₂ concentration. The analysis of the infrared spectra of these tholins points out an apparition of C=O bonds as a result of this oxygen incorporation. The presence C=O bonds is interesting from the perspective of prebiotic chemistry. Indeed, these functions are presents in many prebiotic molecules such as amino acids or pyrimidine-bases.

The reactivity of a gaseous mixture made of N₂, CO₂ and CH₄ relevant of the early Earth atmosphere has been studied previously (DeWitt et al., 2009; Hasenkopf et al., 2010; Trainer et al., 2004; Trainer et al., 2006). These works were focused on the chemical analysis of the aerosols compositions. In this thesis chapter, I provide new information about the gaseous phase composition as well as quantitative information on the elemental composition of the aerosols. Moreover, this study has highlighted the important impact of the early Earth atmospheric reactivity on the entire environment principally the climate with the formation of aerosols and potentially of clouds.

Chapter V Effect of CO on the Titan's atmospheric reactivity

V.1 Introduction

Titan has been frequently presented as an “icy analogues” of the early Earth. Indeed, the formation of complex organic molecules and possibly the formation of organic aerosols in the early Earth atmosphere has been proposed, in a similar mechanism that the one observed on Titan, which could impact the climate of the Earth at this period (McKay et al., 1999) and be possibly at the origin of prebiotic molecules. However, our knowledge of the atmosphere of the early Earth presents a major difference with the current Titan's atmosphere: a different composition. Indeed, the atmosphere of Titan is particularly reduced with mostly N_2 and CH_4 (Niemann et al., 2005) when the atmosphere of the early Earth was more oxidized with mostly N_2 and CO_2 (Kasting, 1993). Nevertheless, the observation of oxygenated molecules in the atmosphere of Titan with ~ 50 ppm_v of CO (de Kok et al., 2007) and an important debate on the CH_4 content in the early Earth atmosphere (Feulner, 2012) shown few similarities between the both atmospheres with molecules composed by C, N, H and O atoms.

The dissociation and ionization of N_2 and CH_4 by solar UV radiation, cosmic rays and Saturn's magnetospheric electrons bombardment are at the origin of a complex organic chemistry in the Titan's atmosphere leading to the formation of solid organic aerosols (Waite et al., 2007). This makes the organic chemistry of Titan's atmosphere one of the most complex known in the Solar System. Moreover, Titan's atmosphere contains traces of oxygen molecules which can involves a coupling between C, N, H and O chemistry in a similar process than in the early Earth atmosphere. Thus, the comprehension of the nature and formation processes of the organic complex molecules on Titan can be useful to understand the chemistry which could occur in the early Earth atmosphere.

A review of oxygen species detected in Titan's atmosphere is given in (de Kok et al., 2007). CO, CO_2 and H_2O have been detected in the atmosphere. A proposed mechanism includes an O^+ flow from Saturn's magnetosphere and by micrometeorites impacts into Titan's atmosphere to explain their formations (Hörst et al., 2008). The most abundant oxygen bearing molecule is carbon monoxide (CO), detected at 47 ppm_v level in the troposphere. Its molar fraction is considered constant with altitude (de Kok et al., 2007).

Although only three oxygen bearing inorganic compounds have been observed up to day, Titan's atmospheric models predict the formation of small organic species such as H_2CO , CH_3OH , NO , N_2O , HNO or CH_2CO (Dobrijevic et al., 2014; Hébrard et al., 2006; Hörst et al., 2008; Krasnopolsky, 2009; Krasnopolsky, 2012; Wilson and Atreya, 2004). Moreover, the ACP instrument on-board the Huygens probe analyzed *in-situ* aerosols collected at different altitudes in the Titan's atmosphere. These aerosols were thermally decomposed (pyrolysed) into gases which were analyzed by GC-MS experiment (Israel et al., 2005). But no oxides has been detected among the pyrolysis products (Israel et al., 2005), the sensitivity of the ACP-GCMS instrumentation was quite low, and probably not sufficient to detect trace species that could include oxygen bearing species. Therefore, the question of the oxygen incorporation in heavier gaseous compounds and in aerosols of Titan's atmosphere remains open today. Indeed, a review of photochemical models, which include chemistry of oxygen, shows a use of a low number of species and reactions. Particularly, only the model used in (Dobrijevic et al., 2014) considers the coupling between oxygen and nitrogen chemistry. Moreover, chemical schemes implemented in these models are limited to light compounds.

To address the question of the coupling between C, N, H and O chemistries as well as, the question of the formation of large organic species, laboratory simulation can be useful. The production of Titan's aerosols analogues, or tholins, can be achieved by several experimental setups. Previous results, obtained with a direct current plasma discharge in $\text{N}_2\text{-CH}_4\text{-CO}$ mixing, show the formation of oxygen compounds in the gaseous phase such as ethylene oxide ($\text{C}_2\text{H}_4\text{O}$) (Bernard et al., 2003; Coll et al., 2003). Photolysis of $\text{N}_2\text{-CH}_4\text{-H}_2\text{-C}_2\text{H}_2\text{-C}_2\text{H}_4\text{-HC}_3\text{N-CO}$ mixture (Tran et al., 2008) shows the formation of several aldehydes and ketones and the incorporation of oxygen in the tholins produced. A previous study was realized with the PAMPRE experiment to study the influence of CO on the chemical composition of tholins produces with carbon monoxide enriched in ^{18}O (Hörst et al., 2012). Analyses of these samples by high resolution mass spectrometry showed an effective incorporation of oxygen from CO in the tholins.

This chapter presents complementary experimental campaigns, realized with PAMPRE, devoted to estimate the influence of CO on the $\text{N}_2\text{-CH}_4$ reactivity. This chapter presents results from a study of quantitative incorporation of oxygen in Titan's tholins produced with carbon monoxide and addresses the effects of CO on the gas phase reactivity. A first part is focused on the effect of CO on the transient regime and the kinetics of methane consumptions and products formation in the plasma. A second part is focused on the effect of CO on the gas

phase steady-state. The third part of this chapter is interested in the oxygen incorporation in the gas and in the solid products. Results presented in this chapter have been published in (Fleury et al., 2014).

V.2 Experimental method and protocols

In the experiments presented in this chapter a gaseous mixture composed by N₂, CH₄ and CO is used to investigate the influence of carbon monoxide on the Titan's atmospheric reactivity. The methane mixing ratio is kept constant at 5 % for all experiments. The gas flow is adjusted from an experiment to another to introduce carbon monoxide at different mixing ratio ranging from 0 % to 4.5 %. The 5 % mixing ratio of CH₄ is chosen because it was demonstrated that the production of tholins is the most efficient with PAMPRE under this experimental condition (Sciamma-O'Brien et al., 2010). Compositions of the different gaseous mixtures studied here are given in Table 18.

Table 18: Initial composition of the studied gaseous mixtures.

Mixture number	[N ₂] ₀ (%)	[CH ₄] ₀ (%)	[CO] ₀ (%)
1	95	5	0
2	94	5	1
3	92.8	5	2.2
4	90.5	5	4.5

The CO mixing ratio used in the experiments presented in this study are higher than the 47 ppm_v measured in Titan atmosphere (de Kok et al., 2007). These values are chosen with the aim to enhance the reactions with CO, that possibly allow to detect oxides compounds produced in larger amounts in the plasma reactor and to ensure the discrimination between effects due to ambient air contamination on tholins during their collection or *ex-situ* and those obtained from CO (Sciamma-O'Brien et al., 2010).

V.2.1 *In situ* mass spectrometry

In this chapter, we used *in situ* mass spectrometry to monitor the influence of CO on the kinetics of the methane consumption. In order to prevent any overlapping of CH₄ ion signal with O⁺ signal at *m/z* 16, the methane consumption is measured using a time-tracking of CH₃⁺ (*m/z* 15) after a correction of the contribution of ¹⁵N⁺ based on laboratory calibration. HCN and CH₃CN principal gas products found in (Gautier et al., 2011) are also studied (*m/z* 27 and 41 respectively).

V.2.2 *Ex situ* GC-MS analysis: cold trapping principle

As explained in the Chapter 2, a cold trapping process is used to accumulate gaseous product in order to analyze the gaseous phase composition by *ex situ* GC-MS. In this chapter, we include a cold trap at the gas outlet of the reactor. It is a cylindrical glass coil, with a diameter of 1.3 cm, 1 m length and a total volume of 133 cm³, which is immersed in liquid nitrogen. The gases pumped out of the reactor can condense in the trap, depending on the pressure and temperature. Under the working condition selected, N₂, CH₄ and CO do not condense in the cold trap. With the cold trap, due to the increase of pumping pipe length, the reactor pressure increases up to 1.8 mbar for 55 sccm of total gas flow rate. The increase of the pressure in the reactor could induce some modifications on the plasma properties, as for example the electron energy distribution. Nevertheless, for pressures above 1 mbar, these modifications can be neglected (Chabert and Braithwaite., 2011). So we assume that the plasma discharges are similar at 0.9 mbar and 1.8 mbar. Gases are accumulated during 3 h in the cold trap. Then, the cold trap is warmed up to room temperature and the pressure is measured. The gases trapped are then analyzed by GC-MS.

V.3 Results

V.3.1 Effect of CO on the kinetics

The kinetics study is performed for the experiments led at 0.9 mbar, without the cold trap. It is done by monitoring, with the mass spectrometer, the evolution of the concentration of detectable volatile species with time (Sciamma-O'Brien et al., 2010). Experiments have been doubled in order to check the reproducibility.

In a general way, we observed that CH₄ and gaseous products mixing ratio reach a steady-state, after a transient regime as seen in Figure 39.

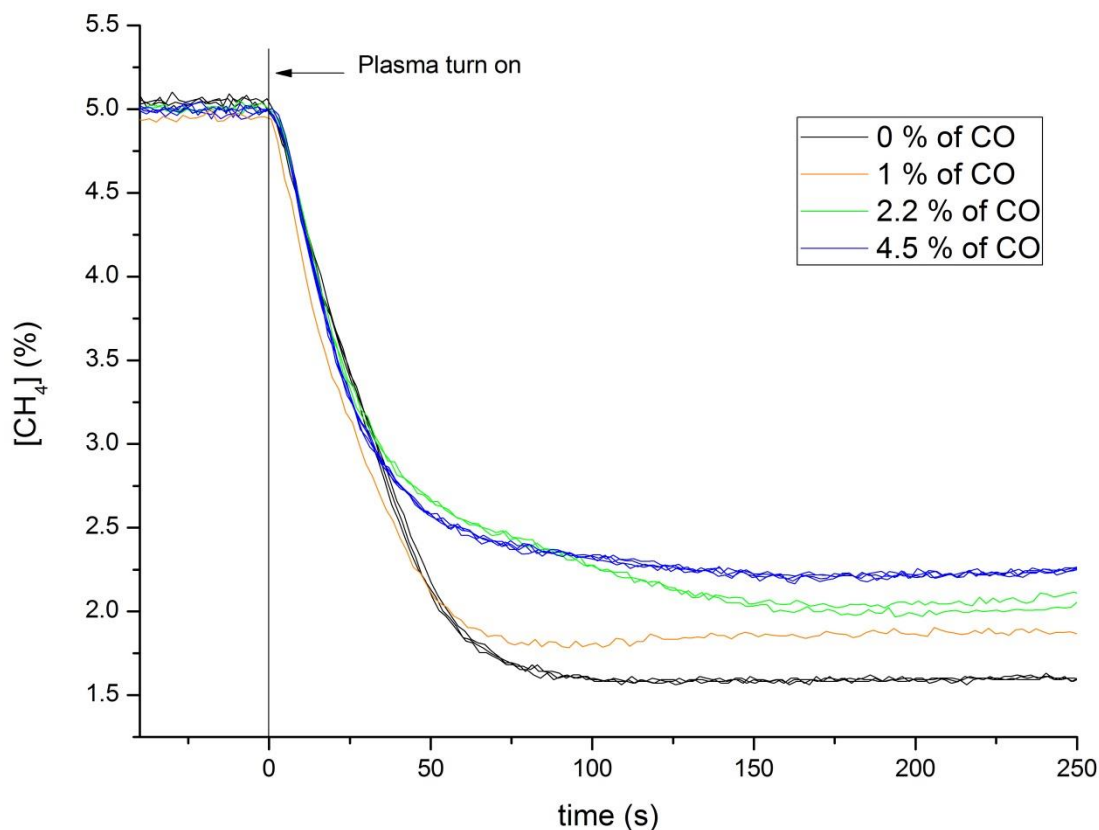


Figure 39: Evolution of CH_4 mixing ratio in the gaseous reactive medium with the plasma duration. Origin is set as the moment when the plasma is turned on.

Figure 39 shows the CH_4 consumption when the plasma is switched on. As explained in (Sciamma-O'Brien et al., 2010), the initial CH_4 concentration injected is known. It is possible to normalize the m/z 15 signal intensity measurement before to turn on the plasma in order to represent the *in situ* CH_4 concentration. The CH_4 decay is quite slow, compared to the residence time of the gas in the reactor (about 1 s): a steady-state is reached after a few tens of seconds. We observed that the methane concentration decreases with time and seems to have an exponential decay. For this reason, we plot the evolution of CH_4 with time with a semi-log scale in Figure 40. The plot is interrupted when the steady-state is reached.

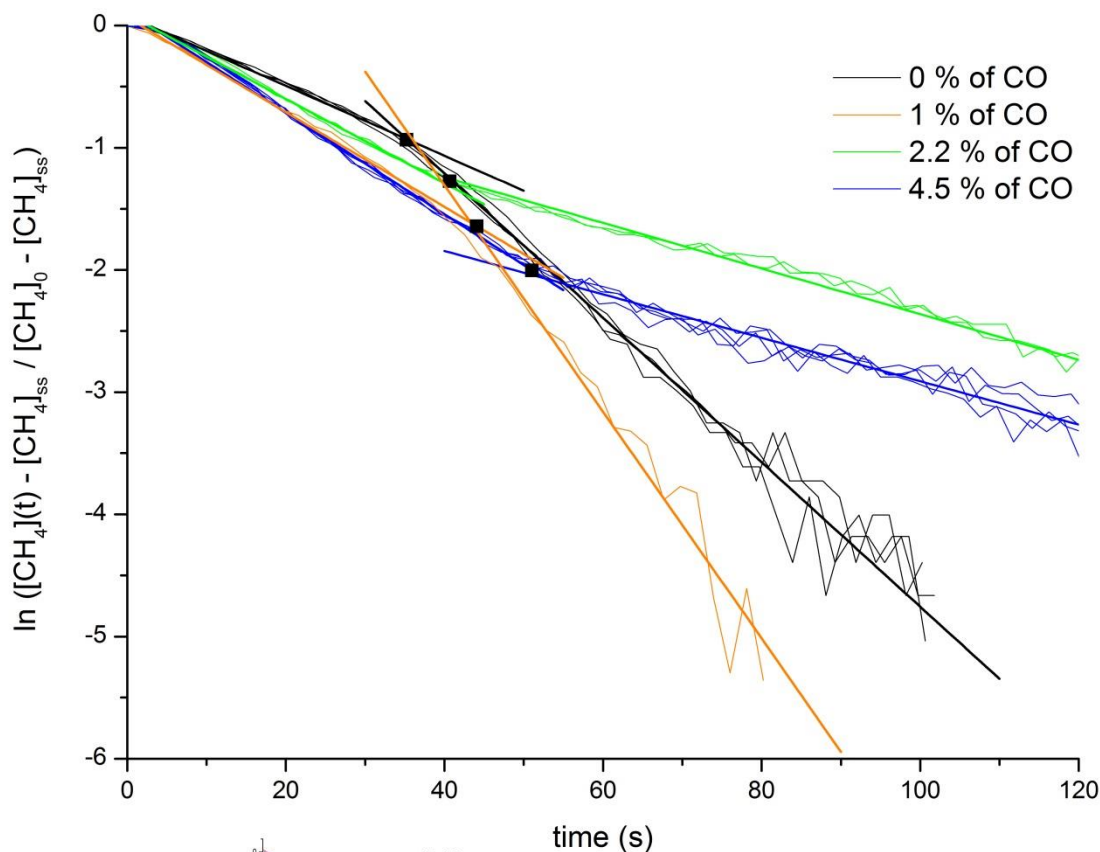


Figure 40: Evolution of CH_4 mixing ratio, in a semi-log scale, in the gaseous reactive medium with the plasma duration. Origin of time is set as the moment when the plasma is turned on. For each percentage of CO, a fit is performed by two straight lines. The two characteristic times τ_1 and τ_2 are determined from the slopes of the lines. The time of the regime change t_i is set at the intersection of the two lines for each initial amount of CO and represented by a black square.

Two regimes in CH_4 consumption are identifiable. The change of slope is identified with a black square in Figure 40 and the corresponding intersection t_i is recorded in Table 19. The regime change occurs later when the CO amount increases: from about 30 to 50 s. The addition of CO in the reaction mixture has an influence on both phases. Two cases can be distinguished. Without and with 1 % of CO, the first decay is slower than the second. When a more important amount of CO is added i.e. 2.2 % and 4.5 % mixing ratio, the second decay is slower than the first one. Both characteristic times τ_1 and τ_2 are given for each percentage of CO Table 19.

Table 19: Kinetics characteristics times for different $[\text{CO}]_0$. τ_1 and τ_2 are characteristic times for the two regimes of methane decay. t_i is the moment of the transition between the two regimes. t_p is the aerosols appearance time detected by V_{dc} .

$[\text{CO}]_0$ (%)	τ_1 (s)	τ_2 (s)	t_i (s)	t_p (s)
0	35 ± 2	16 ± 2	35	21
1	26 ± 2	11 ± 2	45	40
2.2	29 ± 2	50 ± 2	40	~ 80
4.5	24 ± 2	55 ± 2	50	-

For the first period, for all CO amounts, the characteristic time τ_1 remains in the 24-35 s range. Changes on the second characteristic time τ_2 are more drastic, the decay is slowed by a factor of 5 with the addition of CO at concentrations larger than 1 %. Characteristics times are of the order of 10-50 s which cannot be attributed to gas residence time into the plasma (about 1 s). The changes could be due to plasma evolution in the presence of aerosols. In order to test this hypothesis, the time variations of V_{dc} are measured.

V_{dc} is measured as a function of time when the plasma is turned on (Figure 41). For all amounts of CO studied, the initial value is -60 V. For a few seconds, V_{dc} increases rapidly and then reaches a slowly decreasing plateau. The rapid variation of V_{dc} is attributed to the formation of solid particles (Alcouffe et al., 2010). This variation is well pronounced for 0 % and 1 % of CO, less important for 2.2 % of CO and no more visible for 4.5 % of CO. The instant t_p when the solid particles appear is given in Table 19. t_p is set at the beginning of the increase of V_{dc} in Figure 41.

With 1 % of CO, the delay for the V_{dc} increase, from the moment when the plasma is turned on, is longer of about 20 s than without CO. This suggests an increase of the delay for solid particles formation in the plasma in the presence of CO. Such an effect is also visible and even stronger at 2.2 % of CO, but it is difficult to quantify because of slower temporal change of the V_{dc} value. For higher amount of CO, no change in V_{dc} is observed. It could be explained by a too low quantity of solid particles formed in the plasma to induce a sufficient decrease of the electronic density to induce variation of V_{dc} .

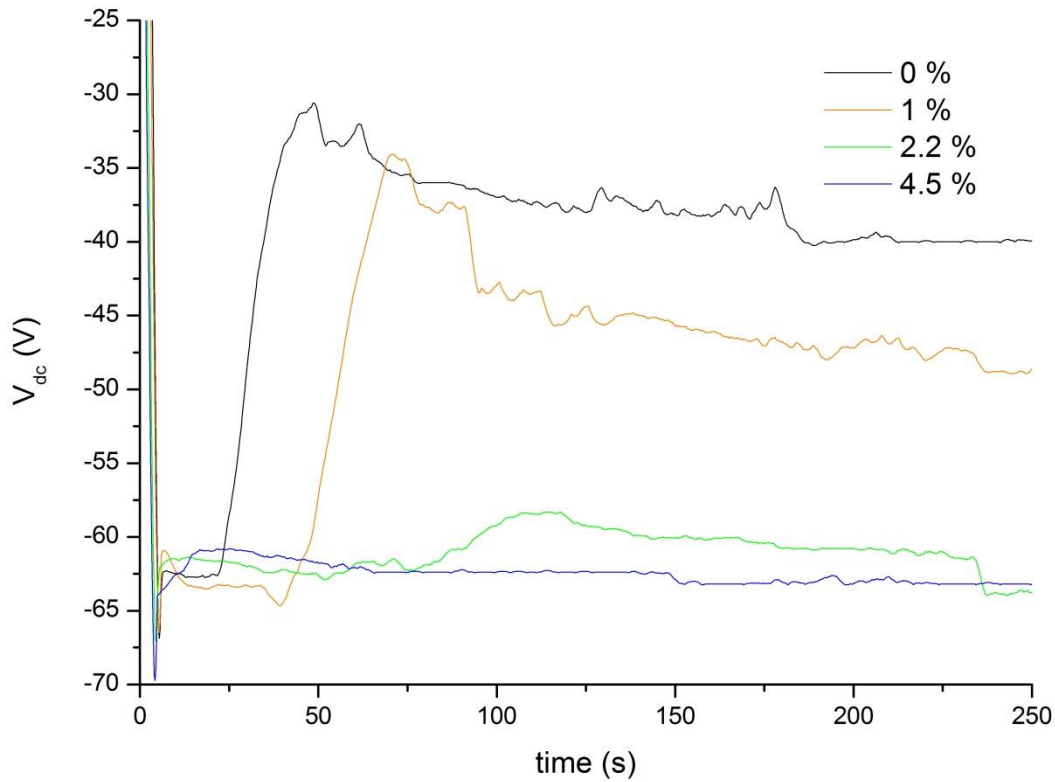


Figure 41: Evolutions of the self-bias voltage V_{dc} as a function of time. The instant t_p when the solid particles appear is set at the beginning of the increase of V_{dc} .

Both the aerosols apparition and the phase change in the consumption of methane are therefore delayed in the presence of CO. Knowing that methane is consumed by electronic impact in the plasma; we have therefore to identify the link between the concentration of CO and the electron density and electron temperature in the plasma. The regime change in the methane consumption seems to be related to the presence of aerosols in the plasma. When aerosols are present in the plasma, electrons are attached; then the electron density decreases. In order to balance this depletion of electrons, the electron temperature usually increases as explained in (Alcouffe et al., 2010). These two parameters have an opposite influence on the methane consumption rate: the decrease of the electron density reduces the kinetic rate when the increase of electron temperature increases drastically the kinetic rate constant.

In the case of no CO and 1 % of CO, the second regime in the methane consumption is accelerated by the presence of aerosols (decrease of τ_2 , compared to τ_1), this acceleration is due to the dominant effect of the increase of the electron temperature.

More surprisingly, for larger amounts of CO, the opposite trend is observed. The methane consumption slows down in the presence of aerosols. It can be noticed that in these cases the

amount of aerosols is strongly reduced considering the V_{dc} measurements. It seems that in the presence of small amounts of aerosols, the change of the electron temperature is not significant compared to the decrease of the electron density.

As aerosols are produced from gas phase products, we have chosen to monitor the most abundant ones, i.e. HCN (at m/z 27) and CH_3CN (at m/z 41) (Gautier et al., 2011), in order to correlate methane consumption rate with the gas phase products. The attribution of these two peaks at HCN and CH_3CN has been performed in a previous study about the analyze of the gaseous phase composition by *in situ* mass spectrometry (Carrasco et al., 2012) with the help of cross comparison with *ex-situ* analysis of gaseous products by GC-MS (Gautier et al., 2011). Figure 42 presents the evolution of the mixing ratio of these molecules with time, for the different initial CO mixing ratio studies. The intensity of each mass are normalized to the intensity of the mass peak at m/z 28 in order to overcome a possible drift of the mass spectrometer (Carrasco et al., 2012).

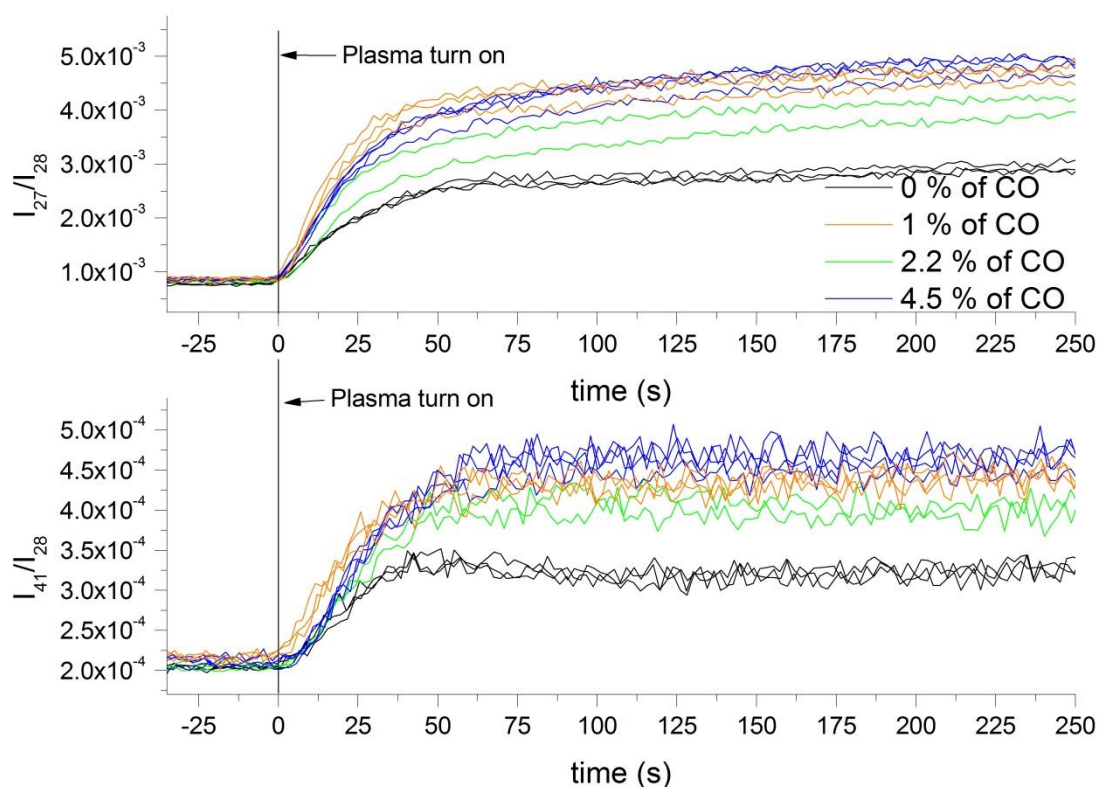


Figure 42: Evolution of HCN mixing ratio (top) and CH_3CN mixing ratio (bottom) in the gaseous reactive medium with the plasma duration. The origin of time is set as the moment when the plasma is turned on.

When the plasma is turned on, we observe an increase of the signal for HCN and CH_3CN . The concentration of these species increases and reaches a steady-state after about 50 s without

CO. For every CO amounts, CH₃CN signal is found to be one order of magnitude lower than HCN, in agreement with a previous quantification by GC-MS analysis (Gautier et al., 2011). This involves a lower signal to noise ratio in the case of CH₃CN. The characteristic times of production for HCN and CH₃CN are obtained from exponential fit according the method described in (Peng et al., 2013). For HCN and CH₃CN, the laws are:

$$I_{27}(t) = I_{27_{ss}} - (I_{27_{ss}} - I_{27_0}) \times e^{-t/\tau} \quad (10)$$

$$I_{41}(t) = I_{41_{ss}} - (I_{41_{ss}} - I_{41_0}) \times e^{-t/\tau} \quad (11)$$

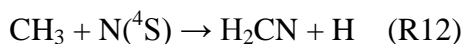
Where I_{27_0} and I_{41_0} represents the initial intensity of HCN and CH₃CN signals. $I_{27_{ss}}$ and $I_{41_{ss}}$ represents the steady-state signals of HCN and CH₃CN.

The fit is made on the first 50 s after the beginning of the plasma discharge (Table 20).

Table 20: Characteristic times of HCN and CH₃CN productions for different [CO]₀.

[CO] ₀ (%)	τ_{HCN} (s)	$\tau_{\text{CH}_3\text{CN}}$ (s)
0	30 ± 2	50 ± 5
1	25 ± 2	60 ± 5
2.2	45 ± 2	60 ± 5
4.5	40 ± 2	70 ± 5

τ_{HCN} is in good agreement with τ_1 , the time of the first phase in the methane consumption (Table 19) but in opposite direction. The kinetic of HCN formation slows down with CO, showing an inhibiting effect of CO on HCN formation. In (Hörst and Tolbert, 2014), CO is suggested to consume H radicals. H is involved in HCN formation according to the following mechanism (Wilson and Atreya, 2004):



An efficient consumption of H by CO could explain the observed limiting process for HCN formation. The characteristic time for CH₃CN production is significantly larger than for HCN, which is consistent with a heavier compound, requiring further steps in its production process.

V.3.2 Effects of CO on the steady-state

By comparison of the amount of CH₄ in the initial and the steady-state conditions, we defined the methane consumption efficient e (Sciamma-O'Brien et al., 2010), which can be deduced from Figure 39 with equation (9):

$$e = \frac{[CH_4]_0 - [CH_4]_{ss}}{[CH_4]_0} \quad (9)$$

Where [CH₄]₀ and [CH₄]_{ss} represent the initial and steady-state percentages of methane respectively. Results are presented in Table 21.

The CH₄ consumption efficient decreases from 68 % to 53 % when the CO initial concentration increases from 0 % to 4.5 %. The presence of CO in the plasma inhibits the consumption of CH₄ and this effect increases with the amount of CO, as well as the aerosols production (see below). If we compare the CH₄ consumption with the production of gaseous species, Figure 42 shows that the amounts of CH₃CN and HCN in steady-state condition increase with the amount of CO. As no absolute calibration of the mass spectrometer is done for these molecules, signals are normalized to 1 without CO, for relative comparison. These relative production yields are given for HCN and CH₃CN for each initial CO percentages in Table 21 assuming a steady-state condition for each molecule after the transient regime. Figure 42 shows that HCN signal does not reached an asymptotic value in the recorded time scale. For this molecule, the relative production yield is then underestimated.

Table 21: Evolution of the consumption efficient of CH₄ and relative production yields of HCN and CH₃CN for different [CO]₀ with the reference being the experiment without CO. The uncertainties are given as 2σ (standard deviation) and are calculated from the standard fluctuations of the mass spectrometry measurements.

[CO] ₀ (%)	e (%)	Relative HCN production yield	Relative CH ₃ CN production yield
0	68 ± 2	1.0 ± 0.1	1.0 ± 0.1
1	62 ± 2	1.6 ± 0.4	1.4 ± 0.2
2.2	59 ± 2	1.4 ± 0.2	1.2 ± 0.2
4.5	53 ± 2	1.7 ± 0.3	1.5 ± 0.2

Table 21 shows an increase of the production yield of two nitriles identified as two important compounds in the reactive gas mixture in the PAMPRE reactor. This result does not seem to be in agreement with the decrease of the CH₄ consumption efficient. The increase of HCN and CH₃CN production yield are the same with the overlapping error bars for the three initial

amounts of CO studies. This fact could be explained by the diminution of the gas to solid conversion presented below. (Gautier et al., 2011) showed in their article that there is an opposite evolution between the gaseous species production and the gas to solid conversion. In our case, the addition of CO decreases drastically the production of tholins. Table 22, which is presented below, shows that the tholins production rate is sensibly the same for each CO percentages. So, we expect an equivalent decrease of the gas to solid conversion for the three CO initial amounts and therefore the same increases of the gaseous production which is particularly visible on HCN and CH₃CN.

In order to determine the total amount of gaseous products, the gases are condensed in the cold trap for 3 h as mentioned in section V.2.2. The pressure measured after warming up the cold trap is presented in Figure 43 as a function of the initial percentage of CO. For 0 % and 4.5 % of CO, two experiments have been done in order to estimate the reproducibility. Figure 43 shows that the pressure increases linearly with the CO percentage. This increase is in agreement with the higher amounts of HCN and CH₃CN detected by mass spectrometry (Figure 42) but also with the formation of CO₂ and N₂O detected by GC-MS as described in V.3.3.b.

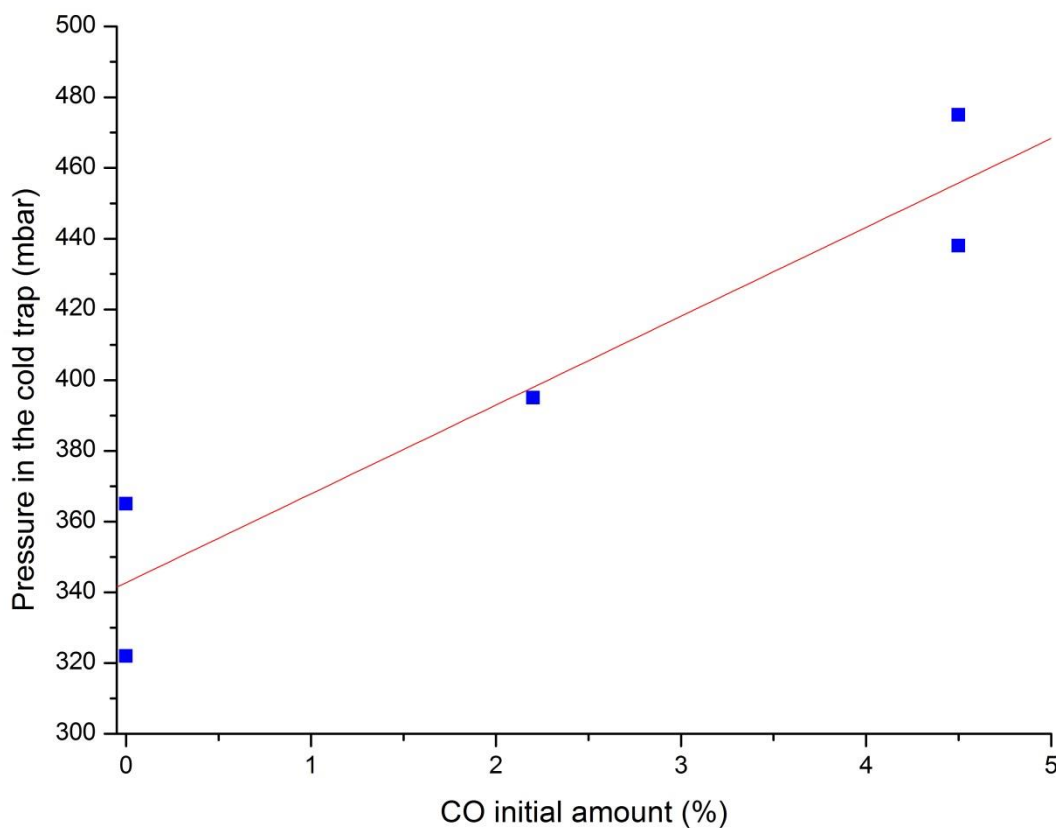


Figure 43: Pressure in the cold trap.

Up to now, only results about the gaseous phase have been presented. In order to study the evolution of the tholins production rate with the amount of CO, the mass production rate is measured following the same protocol described in (Sciamma-O'Brien et al., 2010). Tholins collected are weighted with a 0.1 mg precision scale. As a part of the tholins produced is dragged by the gas flow outside the glass vessel, the production rates are given here are lower limits. Results are presented in Table 22

Table 22: tholins production rate as a function of $[\text{CO}]_0$ at 0.9 mbar.

$[\text{CO}]_0$ (%)	Tholins mass collected (mg)	Production rate ($\text{mg}\cdot\text{h}^{-1}$)
0	96	16
	94	16
2.2	6.0	1
	6.8	1.1
4.5	2.8	0.5
	<0.1	

An important decrease of the tholins production rate with the addition of CO is observed. The injection of few percents of CO in a $\text{N}_2\text{-CH}_4$ mixture leads to a strong inhibition of tholins formation. The very low production rate observed using 4.5 % of CO in the initial gaseous mixture, is in agreement with the absence of V_{dc} variations in Figure 41. This significant effect of CO on the tholins production is in agreement with the increase of the production of gaseous species. Then, when CO is added to the $\text{N}_2\text{-CH}_4$ mixture, the production of solid particles is restrained. The decay of tholins production rate is in agreement with the drastic reduction of V_{dc} variation presented in Figure 41. As a matter of fact, V_{dc} variation is due to the formation of solid particles. We see in section V.3.1 that there is no variation of V_{dc} with a higher percentage of CO.

In order to study the effect of CO on the size of tholins, observations were done with scanning electronic microscopy (SEM). Figure 44 shows images of tholins produces for different initial amount of CO at 1.8 mbar, pressure condition when the cold trap is used. From SEM images, the grains size (diameter) distribution is determined taking into account more than 400 grains following the procedure presented in (Hadamcik et al., 2009).

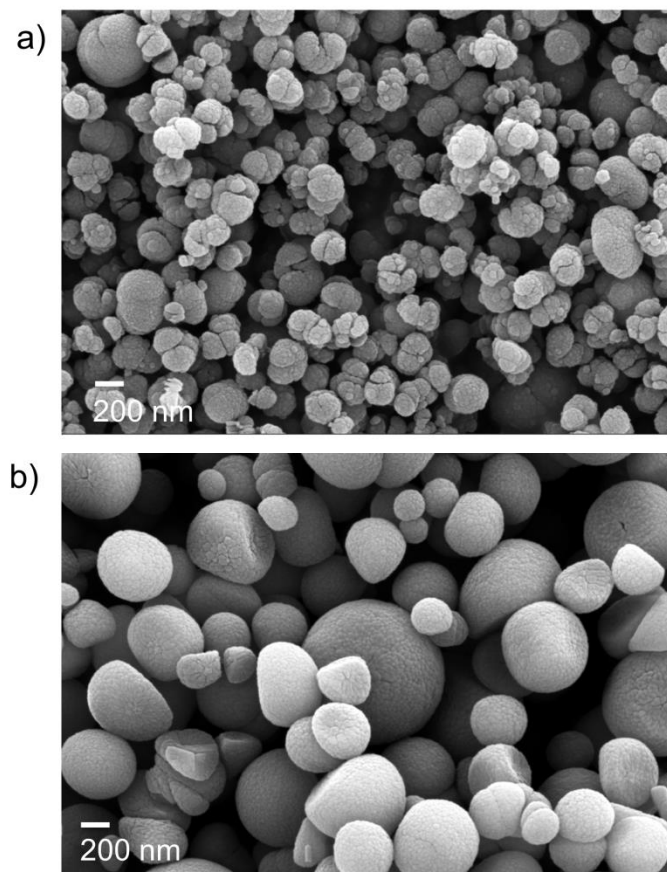


Figure 44: Morphologies of tholins at 1.8 mbar and for different gas mixture: (a) $\text{N}_2\text{-CH}_4$ (95%/5%) and (b) $\text{N}_2\text{-CH}_4\text{-CO}$ (90.5%/5%/4.5%).

Figure 45 presents the so obtained grain size distribution and the deduced Gaussian fit. When CO is present, bigger particles are formed as shown in Figure 44. We observe that for a gas mixture free of CO, a size distribution with a maximum of 460 ± 160 nm is obtained. For a similar amount of CH_4 (Hadamcik et al., 2009) obtained a mean value of 300 nm. In our case, the increase of grain size distribution comparatively to results obtained in (Hadamcik et al., 2009) is due to the reduction of gas speed due to the reduction of pumping efficient through the cold trap. In fact, when the gas speed is reduced, the residence time of the gas in the reactor increases. The gaseous compounds have more time to react which involves the formation of larger particles.

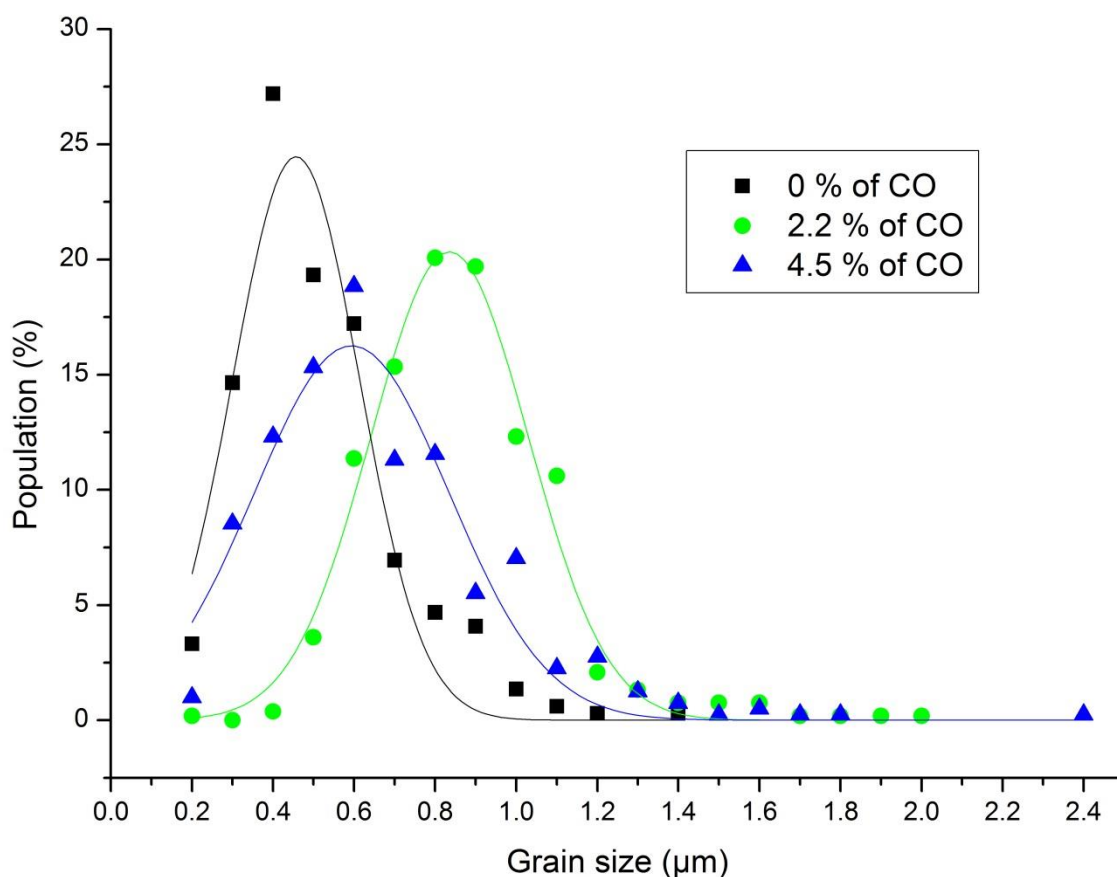


Figure 45: Comparison of the grain size distribution of tholins products at 1.8 mbar for different CO initial percentages.

With the addition of CO, an increase of the main size distribution of tholins is observed. Maxima are observed for diameters measuring 840 ± 194 nm and 600 ± 240 nm for 2.2 % and 4.5 % of CO respectively. The distribution is broader at 4.5 % of CO.

In presence of CO the consumption of methane in the plasma decreases with an increase of the amount of gas products, as seen *in-situ* by mass spectrometry and *ex-situ* by measurement of the gas pressure in the cold trap. In contrast, the mass of tholins collected decreases drastically in presence of CO. It seems that addition of oxygen in the plasma leads to an inhibition of the tholins production and an increase of the gas production, showing a reduction of the gas to solid conversion. The increase of the size of the aerosols products in gaseous mixture with CO is also observed in (Hörst and Tolbert, 2014). However they observed an increase of the quantity of aerosols products when the initial amount of CO increases. This is in opposition with the measurement of the tholins production rate in our experiment and with another study by (Trainer et al., 2004) obtained with carbon dioxide; CO₂. Indeed the study of the N₂-CH₄-CO₂ reactivity in a plasma discharge showed a linear decrease of the tholins

production with the addition of CO₂ in the initial gaseous mixture. With the addition of oxygen bearing molecules in the initial gaseous mixture, there are O atoms produced in the discharge to terminate molecules and to inhibit the growth of long-chains (Trainer et al., 2006). It seems therefore that the aerosol concentration can evolve, with the concentration of CO, in opposite trends according to the experimental conditions as the initial percentage of methane

V.3.3 Oxygen incorporation

V.3.3.a Elemental analysis of tholins

A first study of the addition of CO in a N₂-CH₄ system had been realized with the PAMPRE experimental setup (Hörst et al., 2012). The aim of the study was the analysis of tholins by high resolution mass spectrometry, thus giving access to the exact mass of the molecules present in tholins and then their raw chemical formula. Tholins were dissolved in methanol to be analyzed by LTQ-Orbitrap. C¹⁸O was used to produce tholins in PAMPRE reactor. Few oxygenated molecules had been identified unequivocally by this method (Hörst et al., 2012), but the total amount of oxygen incorporated in the tholins could be quantified with this technique.

It is the aim of the present elemental analysis. Table 23 presents the elemental analysis of tholins produced in the same conditions as the one used for gaseous phase studies.

Table 23: Elemental composition of tholins for different [CO]₀.

[CO] ₀ (%)	Nitrogen (%)	Carbon (%)	Hydrogen (%)	Oxygen (%)
0	20.8	34.5	41.7	3
	20.5	34.9	41.1	3.5
2.2	16.6	33.1	45.6	4.6
	15.6	32.7	47.1	4.6
4.5	16.2	33.1	45.7	5.1

3 % of oxygen is present in tholins product without CO. Similar results have been reported in (Sciamma-O'Brien et al., 2010) which explained that two phenomena could occur and explain this oxygen contamination: oxidation of the tholins or water adsorption. Even if we try to minimize the oxygen contamination during tholins production, plasma polymers are very quickly oxidized when exposed to air for collection and it is difficult to protect samples from oxygen contamination. However, we observe that the oxygen contamination of the sample

remains constant at a level of 3 % which will be considered as a reference for the other samples.

When the CO initial amount increases, we show a quantitative increase of oxygen in tholins up to 2 % and hydrogen up to 3 % balanced with a decrease of nitrogen, but the carbon content remains constant. This significant increase of oxygen incorporation is consistent with the detection of oxygen bearing molecules in tholins produced with labelled CO in (Hörst et al., 2012).

V.3.3.b Analysis of the gaseous phase

The incorporation of few percents of oxygen in tholins produced with CO suggests the formation of oxygenated gaseous intermediates species in the plasma. However, the identification of species separated in GC by their mass spectra gives similar results as in (Gautier et al., 2011) without CO. There is one main exception, the detection of CO₂ which is eluted at 2.9 min retention time (see Figure 46).

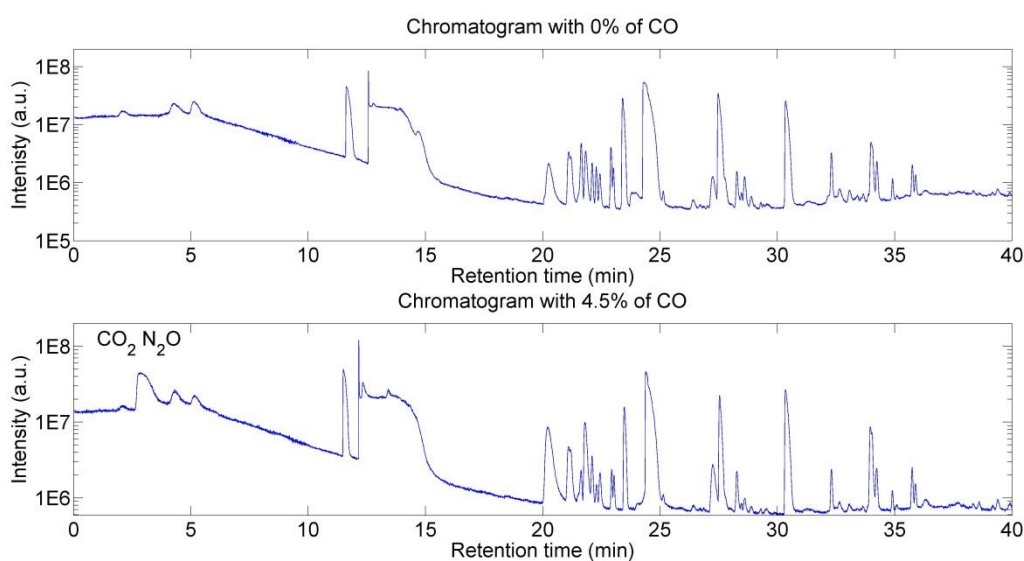
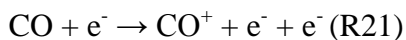
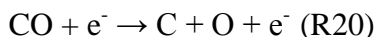


Figure 46: Chromatograms of gas trapped during experiments with 0 % of CO (top) and 4.5 % of CO (bottom). CO₂ and N₂O have been detected in chromatogram of gas trapped during experiment with 4.5 % of CO.

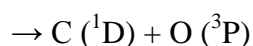
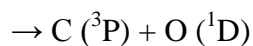
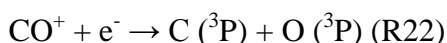
The detection of CO₂ in this experiment is consistent with the observations of Titan atmosphere (de Kok et al., 2007) and also with prediction of photochemical models (Dobrijevic et al., 2014; Hébrard et al., 2006; Hörst et al., 2008; Krasnopolsky, 2009; Krasnopolsky, 2012; Wilson and Atreya, 2004).

Dissociation and ionization in the plasma involve the formation of radicals by the following reaction:

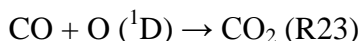


The reactions R20, R21 with energy respectively at 11.09 eV and 14 eV are produced by electrons from the electrons energy distribution tail.

CO^+ ion can also induce the formation of O radicals by dissociative recombination (Mitchell and Hus, 1985):



So, the formation of CO_2 can be explained by the reaction:



To detect minor compounds in the chromatograms, a research is realized for different m/z values specific of oxygen bearing molecules which are selected for their possible presence in mass spectra of organic molecules. One of this m/z gives an interesting result. Two chromatograms obtained at the specific m/z 30 for experiments realized at 0 % and 4.5 % of CO are plotted in Figure 47. Figure 47 shows at a retention time of 3.2 min a peak for m/z 30 present only in the chromatogram for 4.5 % of CO, and not in the chromatogram without CO. This peak, specific of the presence of CO in the gas mixture, can therefore be assigned to an oxygenated species. The retention time of this species is short. We can presume that is a small oxygen volatile molecule.

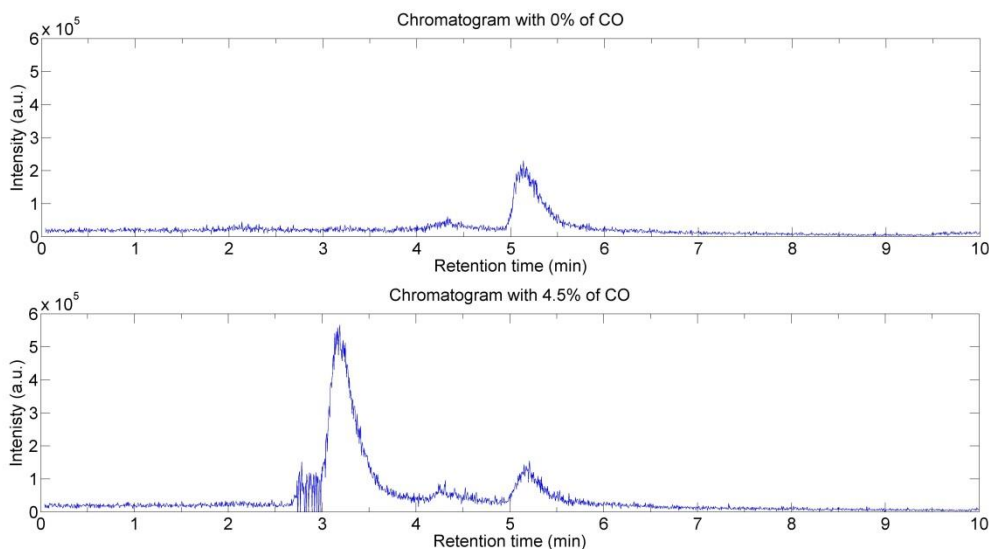


Figure 47: Chromatograms obtained at the specific m/z 30.

To identify this species, several chemical standards were analyzed by GC-MS in the same instrumental conditions. The molecules selected are H_2CO , NO and N_2O . These are three oxygenated molecules with a low molecular weight which are compatible with the low retention time of the unknown compound. Moreover these molecules have an important fragment at m/z 30 in their mass spectrum. This is the major fragment for NO . This fragment has 31 % of m/z 44 intensity for N_2O and 58 % of m/z 29 intensity for H_2CO . To identify, the unknown compound of our chromatogram, we need to compare the reduce retention time t'_R which is:

$$t'_R = t_R - t_M \quad (12)$$

Where t_R is the retention time of one compound and t_M the time measured for a not retained compound to pass through the column.

The comparison of the reduced retention time eliminates NO and H_2CO . The last possible species is N_2O which has a second fragment at m/z 30 and a principal fragment at m/z 44. The m/z 44 signal of N_2O is mixed with the signature of CO_2 .

The identification of N_2O among the gaseous species product by an experimental simulation of the Titan atmospheric reactivity is consistent with model prediction (Dobrijevic et al., 2014). This model studies a coupling between nitrogen chemistry and oxygen chemistry in the atmosphere of Titan and predicts the formation of NO , HNO , HNCO and N_2O (Dobrijevic et al., 2014). Here, we give an experimental confirmation of this model prediction for one of

their molecules. Furthermore, the coupling between oxygen and nitrogen chemistry is interesting for astrobiology with the possible formation in gas phase of molecules containing C, N, H and O atoms.

The non-detection of H₂CO in the gaseous phase has been previously observed in a plasma discharge by (Bernard et al., 2003) where the gaseous phase composition was studied by GC-MS and infrared spectroscopy. This result is surprising in the way that photochemical models predict an important production H₂CO in Titan's upper atmosphere by the reaction of O(³P) and CH₃ (Dobrijevic et al., 2014), with a concentration about two order of magnitude larger than CO₂. The efficient incorporation of oxygen in the aerosols points out that H₂CO in the gaseous phase could react with aerosols through heterogeneous mechanism and be a key molecule for oxygen incorporation in the aerosols.

V.4 Titan's atmospheric reactivity in presence of CO: a natural example of the early Earth atmospheric reactivity?

Titan has been frequently presented as an "icy analogues" of the early Earth. Indeed, the formation of complex organic molecules and possibly the formation of organic aerosols in the early Earth atmosphere has been proposed, in a similar mechanism that one observed on Titan, which could impact the climate of the Earth at this period (McKay et al., 1999) and be possibly at the origin of prebiotic molecules. However, our knowledge of the atmosphere of the early Earth presents a major difference with the current Titan's atmosphere: a different composition. Indeed, the atmosphere of Titan is particularly reduced with mostly N₂ and CH₄ (Niemann et al., 2005) when the atmosphere of the early Earth was more oxidized with mostly N₂ and CO₂ (Kasting, 1993). Nevertheless the observation of oxygenated molecules in the atmosphere of Titan with ~50 ppm_v of CO (de Kok et al., 2007) and an important debate on the CH₄ content in the early Earth atmosphere (Feulner, 2012) shown few similarities between the both atmosphere with molecules compositing of C, N, H and O atoms.

In the Chapters III and IV, I investigated experimentally the reactivity of the early Earth atmosphere. Particularly, in the Chapter IV, I investigated the reactivity of a primitive atmosphere made of N₂, CO₂ and CH₄ when in the current Chapter I investigated the reactivity of the atmosphere of Titan made of N₂, CH₄ and CO. CO and CO₂ have globally similar effects on the reactivity of the N₂-CH₄ system. An addition of one of these two species principally inhibits the formation of tholins. Moreover, the presence of one of these species involves a complexification of the chemistry with a coupling between the C, N, H chemistry

and the O chemistry leading to the formation of oxygenated volatile molecules and to the incorporation of oxygen in the tholins. Several differences are also observed: the incorporation of oxygen is slightly more efficient with CO₂. Indeed, for a same amount of 5 % of CO or CO₂, we observed an incorporation of 4 % of oxygen in tholins produced with CO₂ and only 2 % in tholins produced with CO. Moreover, the inhibiting effect on the organic growth of the addition of CO or CO₂ is different. When CO is added to a N₂-CH₄ gaseous mixture, it inhibits the formation of tholins through a decrease of the conversion gas-particles resulting in an increase of the quantity of gaseous species product. In contrary, for CO₂ the decrease of the tholins formation is coming from a global decrease of the organic growth in the reactive medium, with a decrease of the quantity of gaseous products at the same time.

The similarity observed in these experimental simulations realized with CO and CO₂ highlighted a possible similarity between the Titan and the early Earth atmospheric reactivity. In the two cases we observed the formation of complex organic molecules with an efficient coupling between the C, N, H chemistry and the O chemistry. Despite a low amount of CO observed on Titan, it could involve the formation of other oxygenated gaseous species and an oxygen incorporation in the aerosols surrounding Titan. A new analysis of the chemical composition of the aerosols of Titan with a more sensitive instrument than the one onboard the Cassini-Huygens mission could confirm this hypothesis and give new information about the type of molecules, which could have been formed in the atmosphere of the early Earth 4 Ga ago.

V.5 Conclusion

In this chapter, I have presented several results concerning the influence of CO on the reactivity of the N₂-CH₄ gas mixture with the PAMPRE reactor.

The study of the kinetics in our experiments shows a correlation between the consumption of methane and the formation of tholins. The addition of CO in the plasma involves a delay in the apparition of tholins, which modifies the kinetics of the methane consumption.

Moreover, this chapter points out an effect of the addition of CO on the quantity of gases and tholins produced. There is an anti-correlation between the quantity of gas products and the quantity of tholins produced. Indeed, the addition of CO involves a drastic diminution of the tholins production when the gas production increases. It is the result of a diminution of the gas-particles conversion. The inhibiting process could come from the concentration of O

atoms in the reactive medium which terminate the organic chains and reduce the organic growth (Trainer et al., 2006).

The analysis of the gas phase by GC-MS has made it possible to demonstrate the formation of two new oxygenated products in the gas phase: CO₂ and N₂O. Furthermore, we have quantified the O incorporation in the tholins. Elemental analysis of tholins gives a maximum ~2 % of O incorporated in the aerosols for an initial amount of CO of 4.5 %. It seems to be that the addition of CO in the initial gas mixture allows a more complex organic chemistry than for N₂-CH₄ mixture used to simulate the reactivity of Titan's atmosphere. Such effects could be observed in the atmosphere of Titan. The formation of complex organic molecules incorporating oxygen in both gaseous and solid phases could occur in the ionosphere of Titan where the dissociations of N₂ and CO by VUV solar photons and magnetospheric electrons are possible.

In a more general way, the study presented in this chapter on the Titan's atmospheric reactivity is important to understand the chemistry which could have occurred in the early Earth atmosphere. Comparison of these results with observations of Titan is an important tool to validate experimental simulation performed with the PAMPRE experience.

One question does not find answer in this chapter. If incorporation of oxygen in tholins is found to be efficient, the pathway for its incorporation remains unknown. This question is directly related to a more general question about the comprehension of the aerosols formation mechanism in Titan's atmosphere.

Chapter VI Chemical evolution of Titan's tholins

VI.1 Introduction

Aerosols were observed up to 500-600 km in the atmosphere of Titan by the ISS optical imager onboard Cassini (Porco et al., 2005) and above up to about 1000 km in the upper atmosphere by the UVIS Cassini-spectrometer (Liang et al., 2007). The detection of nanometer-size molecules by the Cassini-Huygens space mission (Dinelli et al., 2013; Liang et al., 2007; López-Puertas et al., 2013; Waite et al., 2007) suggest that the Titan's aerosols formation is initiated in the ionosphere at about 1000 km where the atmospheric layer is partially ionized by the Vacuum-Ultraviolet (VUV, wavelengths below 200 nm) solar flux and the energetic particles from the Saturn's magnetosphere. Positive and negative ions have been found to promote an active organic chemistry in the upper atmosphere, with the detection of large nanometer-size charged species (Lavvas et al., 2013; Tomasko and West, 2010). These molecules then aggregate during sedimentation at lower altitudes (Lavvas et al., 2011b; Lavvas et al., 2009) and form larger haze particles detected below 600 km by the ISS imager (Porco et al., 2005) and close to the surface by the DIS-Radiometer of the Huygens probe (Tomasko et al., 2005; Tomasko et al., 2008).

During their descent between 1000 and 600 km in the thermosphere, aerosols continue to evolve through further physical and chemical processes. Benchmark modelling studies were provide on the microphysical evolution of the particles in this altitude range (Lavvas et al., 2011b; Lavvas et al., 2013; Lavvas et al., 2009; Lavvas et al., 2008), but no study has been focused on their possible photochemical evolution. An active photochemistry is however expected considering the significant VUV solar radiation flux encountered at these altitudes. Such chemical modifications will further affect the aerosols in their physical, chemical and optical properties, impacting the radiative budget calculated for Titan's atmosphere.

Moreover, the chemical evolution of the aerosols could continue lower in the atmosphere (troposphere and stratosphere). Indeed, the measurement of the temperature profile in the Titan's atmosphere by the HASI instrument onboard the Huygens probe showed a drop of temperature in the lower atmosphere with a minimum about 70 K at 44 km of altitude

(Fulchignoni et al., 2005). These low temperatures allow a possible condensation of photochemical products. Different emission bands have been observed in the far infrared by the IRIS instrument onboard the Voyager spacecraft. Several bands cannot be attributed to gaseous species present in Titan's atmosphere and have been attributed to stratospheric clouds composed by condensed species (Coustenis et al., 1999). The band observed at 478 cm^{-1} has been attributed to C_4N_2 ice (Samuelson et al., 1997). HC_3N in solid phase emission bands have been observed at 505 cm^{-1} and 753 cm^{-1} and the presence of condensed C_2H_2 mixed with solid HC_3N is proposed to interpret the emission band in the $700\text{-}800\text{ cm}^{-1}$ range (Khanna, 2005b). Condensed $\text{C}_2\text{H}_5\text{CN}$ has been attributed to the band observed at 221 cm^{-1} (Khanna, 2005a). More recently, similar observations have been realized in the far infrared by the CIRS instrument of the Cassini-Huygens mission. The more important band observed is at 220 cm^{-1} and has been previously attributed to propionitrile ice (Khanna, 2005a). However, a recent modeling study has showed that the concentration of $\text{C}_2\text{H}_5\text{CN}$ was too low to explain this important band (de Kok et al., 2008). Another important band observed by CIRS is located at 160 cm^{-1} and is potentially attributed to nitrile ices, HCN or HC_3N notably, which have important features in this part of the spectrum (Anderson and Samuelson, 2011). This is consistent with the presence of HCN ice in the atmosphere confirmed by its observation in a high altitude southern polar cloud with the VIMS instrument onboard Cassini (de Kok et al., 2014). The condensation of such ices could occur on the aerosols surface during their sedimentation through the atmosphere where they could play a role of condensation core. Such a phenomenon has been modeled using a 1-D model (Lavvas et al., 2011a). Authors of this article proposed the formation of different clouds in the lower atmosphere constituted by aerosols coated with condensed species.

If high energy solar photons initiating the organic chemistry in the ionosphere of Titan's have been significantly absorbed at the altitude where species can condense, photons with longer wavelengths are still present at altitude as low as 100 km. A chemical evolution of aerosols can then be initiated by the reactivity of aerosols coated with condensed species and irradiated by solar photons in the UV-visible range.

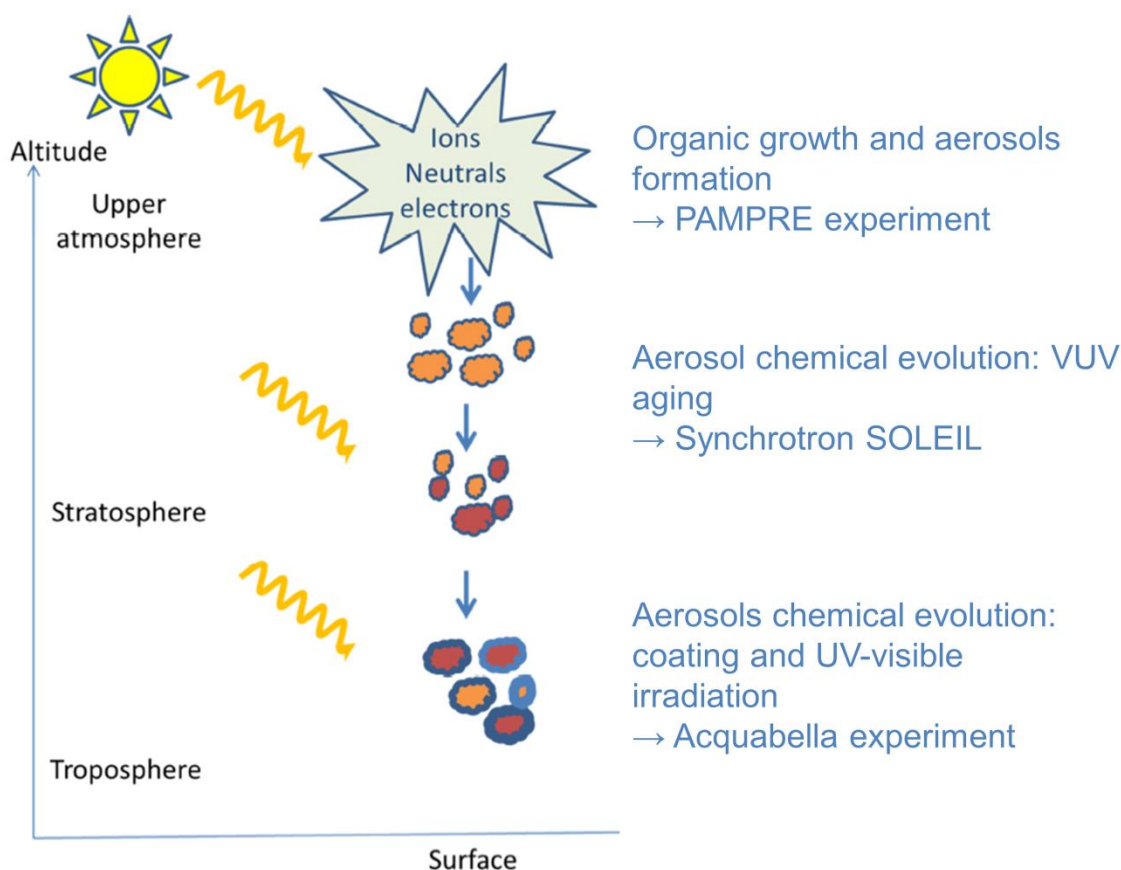


Figure 48: Different processes occurring in the atmosphere of Titan with the experimental setup associated as a function of the altitude.

In this chapter, I studied the potential chemical evolution of aerosols formed in Titan's thermosphere during their sedimentation to the surface. The different step of the aerosols formation and evolution simulated in this chapter is presented with the experimental setup associated depending on the altitude in Figure 48. Firstly I present experimental results of the aerosol 'aging' in the thermosphere of Titan during their exposition to VUV solar photons. For that, I exposed analogues of aerosols named tholins produced with the PAMPRE reactor to the monochromatic VUV flux of synchrotron facility. Secondly, I present another experimental study of the potential chemical evolution of the Titan's aerosols when coated by condense species in the stratosphere and troposphere of Titan; they are exposed to longer wavelength solar photons. For that, I exposed PAMPRE tholins sample coated with selected condense species to a laser flux in the Acquabella experimental device to reproduce such phenomenon.

VI.2 Simulation of aging processes in the thermosphere

VI.2.1 Experimental methods and protocols

To simulate aging processes due to aerosols exposition to VUV solar flux in the higher atmospheric layers of Titan, I exposed aerosols analogues produced with PAMPRE to synchrotron generated VUV radiations.

Titan's aerosol analogues have been produced by plasma deposition in the PAMPRE reactor. They are deposited as thin films onto SiO₂ windows (0.5 mm thickness and 11 mm² surface) disposed in the plasma box. Films are produced during 2 hours of plasma duration in an initial gaseous mixture composed by 5 % of methane in nitrogen. The energy provided by the electric discharge is comparable to the charged particles from Saturn's magnetosphere (Cable et al., 2011) and the VUV photon energy in the upper atmosphere of Titan enabling to partially dissociate and ionize molecular nitrogen and methane (Szopa et al., 2006). Such a cold plasma technique has been shown to be the best known laboratory experiment to reproduce the relative amounts of NH₃ and HCN released by the core of Titan's aerosols during their *in-situ* analysis with the ACP-GCMS instrument onboard the Huygens probe (Coll et al., 2012; Israel et al., 2005), in spite of the limited information provided by this Huygens instrument (Biemann, 2006; Israel et al., 2006).

Four equivalent samples (S_x x=1-4) have been prepared. A blank SiO₂ substrate (S₀) is also used as a reference in the experiment. The thickness of films produced in PAMPRE have been measured by spectroscopic ellipsometry technique in the 370-1000 nm wavelength range (Mahjoub et al., 2012), using a M-2000V spectroscopic ellipsometer from J.A. Woollam CO. A film thickness of 600 ± 20 nm is found for all the films synthesized in the study.

The 11 mm² sample surface matches the beam spot of the DESIRS-synchrotron beam line (Nahon et al., 2012) with the sample located at 107 cm downstream of the focal point, using a high precision XYZ positioning sample holder ensuring the translation from one sample to another. Samples produced under the same conditions are positioned on the sample holder for irradiation along with a blank SiO₂ window. High harmonics of the undulator spectrum were filtered off by using a gas filter filled with Xe or Ar depending on the irradiation wavelength (Mercier et al., 2000).

The aerosols when produced in the ionosphere are exposed to the full VUV solar spectrum. The effect on the aerosols may vary according to the wavelength considered. We have

therefore chosen three typical wavelengths for the synchrotron irradiation experiments, representative of irradiation effects on the aerosols according to the altitude:

- 1) 95 nm to probe possible harsh ionizing effects (and dissociation of N₂ molecules);
- 2) 121.6 nm, Lyman- α , as an important solar contribution in the VUV wavelength range;
- 3) 190 nm to probe softer irradiation effects, a wavelength that represents the effects of the less energetic radiations of the VUV range.

The total of 2 days duration of synchrotron irradiation has been practically distributed among the three wavelengths in order to expect detectable evolutions at all wavelengths: shorter 3 h irradiation duration for the highest 95 nm photon energy, longer 6 h duration at 190 nm to compensate for the lower energy, and longest 28 h duration at 121.6 nm considering the prominent role of this wavelength in the solar distribution.

To simulate the irradiation conditions, the aerosol analogues are exposed to the light from the 0th order grating position of the DESIRS beamline's monochromator. In such conditions, the grating acts a simple mirror and the beamline transmits the intense pseudo-Gaussian broadband spectrum of the undulator feeding the beamline, with an energy bandwidth of $\Delta E/E = 7\%$ at half height at the chosen photon energy. A high photon flux density of 10^{16} photons.cm⁻².s⁻¹ (integrated over the 7% bandwidth) is applied to the total surface of the samples. The solar photons reaching the top of Titan's atmosphere are characterized by a total VUV-UV flux density about 10^{14} photons.cm⁻².s⁻¹, and 3×10^9 photons.cm⁻².s⁻¹ at the Lyman- α wavelength (Gans et al., 2013). As illustrated in Table 24, each synchrotron irradiation experiment corresponds to a monochromatic exposure of the aerosols analogues to a photon flux density hundred times higher than the total VUV-UV solar one.

According to microphysical models, Titan's aerosols produced at 1000 km spend about 10^6 s, in the thermosphere between 1000 and 600 km, the latter altitude being the threshold below which fractal aggregation occurs (Lavvas et al., 2011b). This residence time is the same order of magnitude as a Titanian day ($\sim 1.4 \times 10^6$ s). As a consequence a significant number of the aerosols are continuously irradiated during their journey in the 1000-600 km thermospheric layer. The two order of magnitude higher flux density of the synchrotron beam compared to the integrated solar flux on Titan is counterbalanced by shorter irradiation time of a few hours, enabling the total irradiation dose to be comparable between our laboratory simulations and Titan's atmosphere between 1000 and 600 km.

Table 24: Photon fluxes in our monochromatic synchrotron experiments and on the top of Titan's atmosphere.

Wavelength (nm)	Photons flux (photons.cm ⁻² .s ⁻¹)	
	This work (monochromatic synchrotron irradiations)	Top of Titan's atmosphere
95	10 ¹⁶	1×10 ⁶
121.6	10 ¹⁶	3×10 ⁹
190	10 ¹⁶	4×10 ⁹
Spectrally integrated flux (photons.cm ⁻² .s ⁻¹)	-	10 ¹⁴

The chemical and optical modifications of the organic films induced by the VUV irradiation are probed subsequently by infrared absorption spectroscopy using Attenuated Total Reflectance (ATR) technique as described in the Chapter II.

VI.2.2 Results

VI.2.2.a General observations of the infrared signature evolution of Titan's aerosols analogues

The absorbance of the initial non-irradiated tholins film is shown in Figure 49 in the 1200-4000 cm⁻¹ wavenumber range, normalized at the highest absorption value found about 1560 cm⁻¹. The film homogeneity is validated by the very similar spectra obtained from measurements at five locations on the non-irradiated film S₁. The dispersion represents about 20 % of the absorbance value.

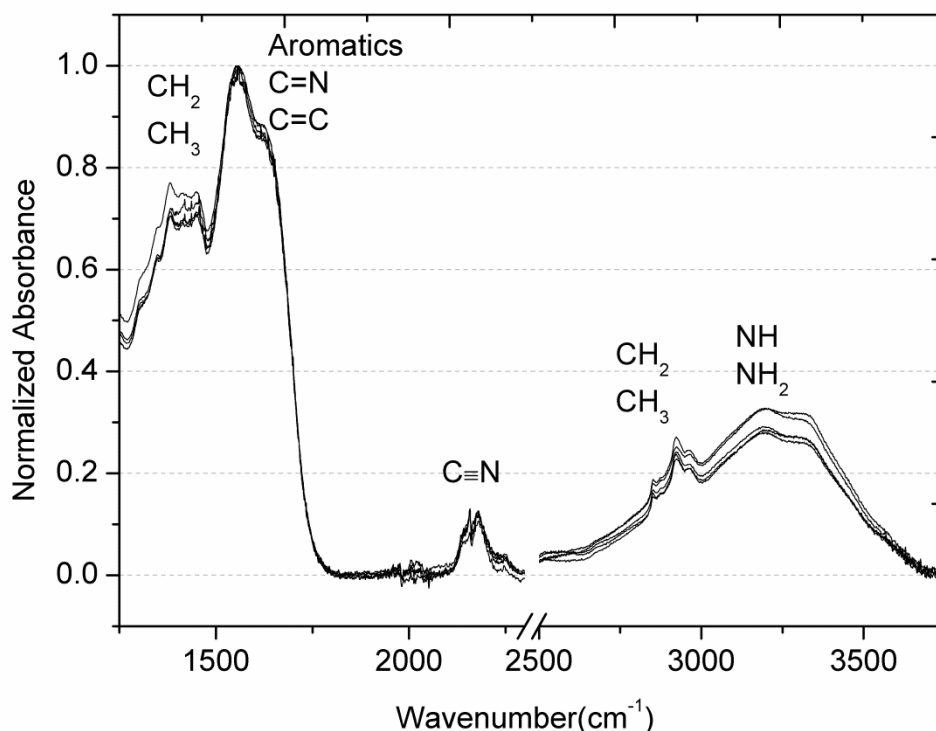


Figure 49: Functional homogeneity of the films is demonstrated by the five spectra measured at different locations on the non-irradiated sample. Spectra are normalized at their maximum absorption (1560 cm^{-1})

The assignment of the absorption bands to vibrational modes has been described in details in (Gautier et al., 2012). The $1500\text{-}1600\text{ cm}^{-1}$ spectra region involves C=C and C=N bonds contributions within carbon chains. The band centered at about 2200 cm^{-1} is assigned to the presence of terminal -CN or possibly -NC units. The large $2700\text{-}3700\text{ cm}^{-1}$ signature corresponds to the presence of -NH₂ and possibly -NH functional groups, primary and secondary amine functions respectively. The sharper bands in the $2700\text{-}3000\text{ cm}^{-1}$ region, are consistent with the alkyl signatures, containing -CH₃- symmetric, asymmetric stretching mode and -CH₂- asymmetric stretching mode. The bending modes of these chemical groups are found at 1450 cm^{-1} .

The absorbance spectra of irradiated samples at 95 nm, 121.6 nm and 190 nm respectively are compared to the reference one in Figure 50, normalized at the highest absorption value at $\sim 1560\text{ cm}^{-1}$.

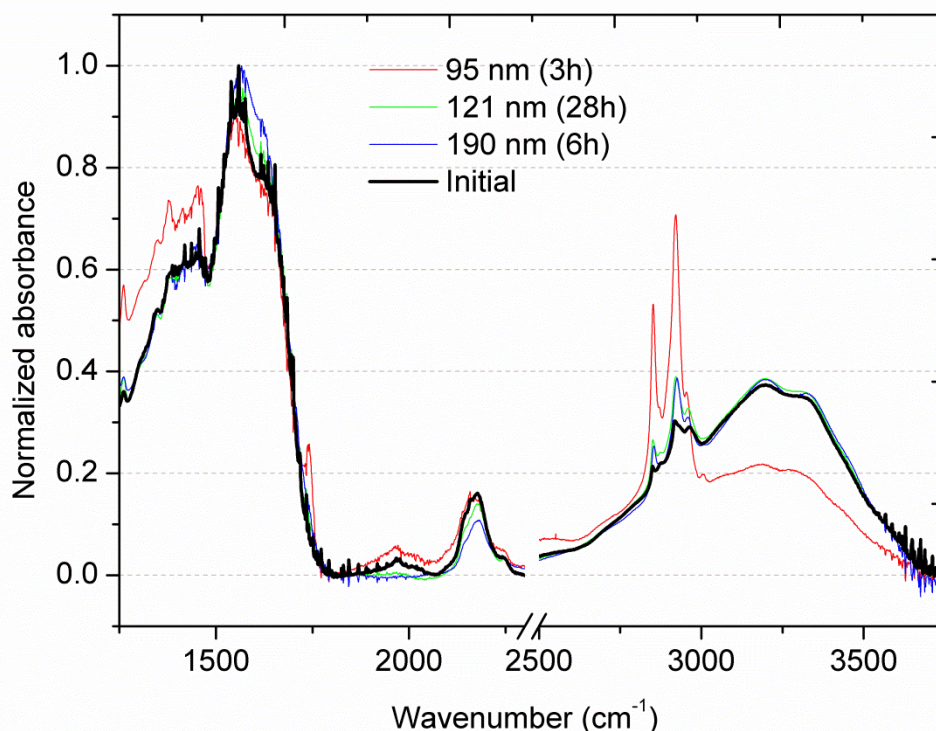


Figure 50: Infrared absorption spectra recorded from samples irradiated by photons for 3 h (95 nm), 28 h (121.6 nm) and 6 h (190nm). The thick black spectrum is the mean of the non-irradiated spectra shown in Figure 49.

In a general way for all wavelengths of irradiation used in these experiments, I observe an increase of the alkyl signatures in the 2700-3000 cm^{-1} region. However, the most significant changes are observed for the sample irradiated at 95 nm.

Indeed, for 95 nm irradiation, we observed that the amine signature (NH and NH_2), centered at 3250 cm^{-1} , decrease by nearly 50 % as compared to the reference sample. On the other hand, CH_2 and CH_3 alkyl bands increase dramatically. When looking more closely in the 2700-3000 cm^{-1} region, two absorption maxima become prominent at 2850 cm^{-1} and 2920 cm^{-1} . These features correspond to the symmetrical and asymmetrical stretching modes of CH_2 (Gautier et al., 2012; Gautier et al., 2014b), inferring an increase of the ratio CH_2/CH_3 in the sample after irradiation. This observation is confirmed by the correlated increase of the CH_2 and CH_3 bending modes at about 1400 cm^{-1} . The key chemical transformations are thus a transfer of H from N to C resulting in a decrease of amines and increase of saturated hydrocarbon. Nitrile ($-\text{CN}$) absorption bands at $\sim 2220 \text{ cm}^{-1}$ are less altered by irradiation.

For Lyman- α and 190 nm irradiations, the effect observed on Figure 50 is qualitatively similar. Mainly, we observed an increase of the aliphatic stretching mode in the 2700-3000 cm^{-1} wavenumber range. We can note that at both wavelengths, this increase is not coupled to an amine decrease as for 95 nm irradiation. To better emphasize this result, a focus is given on the aliphatic/amine ratio evolution. This evolution is presented on Figure 51. The relative aliphatic absorption intensity is obtained after subtraction of the normalized amine contribution. A significant increase of the aliphatic contribution is actually observed on the 121.6 nm and 190 nm irradiation cases.

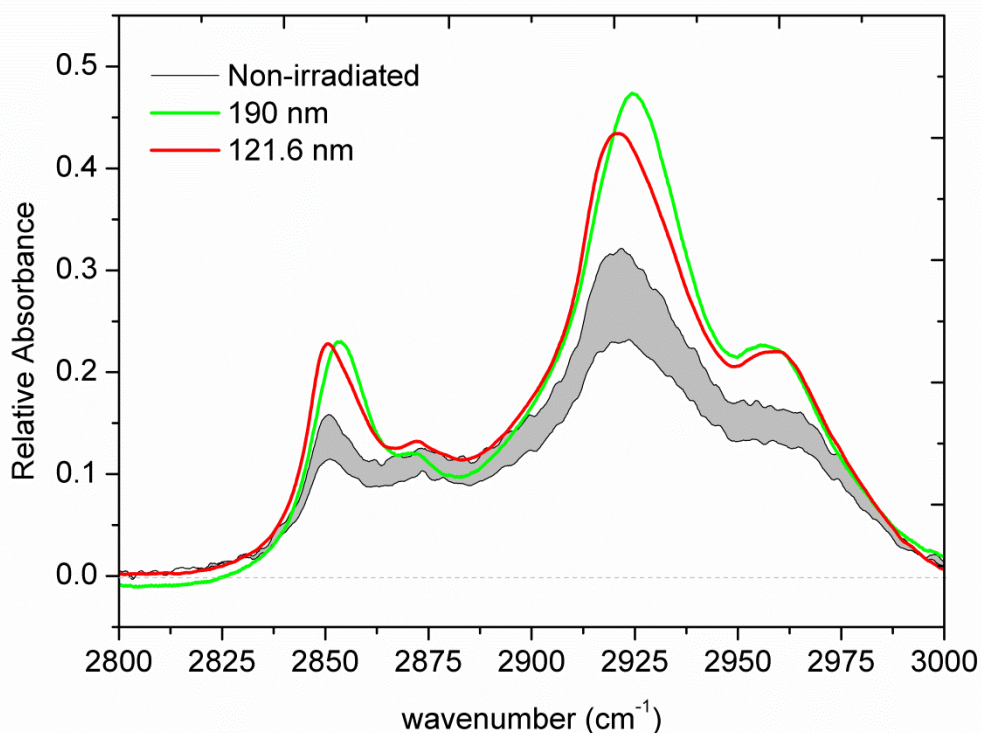


Figure 51: Absorption of the aliphatic bands relative to the amine one: absorbance spectra between 2800 cm^{-1} and 3000 cm^{-1} after subtraction of the normalized amine contribution. The grey envelop is the reference spectrum before irradiation, with the 20 % homogeneity uncertainty. The green curve is the spectrum obtained after 6 h of synchrotron irradiation at 190 nm, and the red one is the spectrum obtained after 28 h of irradiation at 121.6 nm.

VI.2.2.b Wavelength dependence of the irradiation effect on the tholins

If a difference is observed between irradiation at 95 nm and irradiations at 121.6 nm and 190 nm, the global effect of the Lyman- α radiation is similar to the one obtained at 190 nm in spite of the higher energy carried by photons of shorter wavelength. It seems that there is not linearity between the evolution of the wavelength and the evolution of the irradiated samples. Indeed, the larger dose deposited in the Lyman- α experiment does not result in a significant

increase of the aliphatic IR bands and the effect observed in Figure 51 is similar at 190 nm despite the shorter irradiation duration. The non-linearity observed between Lyman- α and 190 nm could be explained by the lower penetration depth, $D(\lambda)$, of the radiations at 121.6 nm than at 190 nm. $D(\lambda)$, the penetration depth is defined as the layer thickness below which the radiation intensity has been reduced by an order of magnitude compared to the initial incident intensity at a given wavelength. The VUV absorption cross sections of such complex organic materials are unknown preventing any calculation of the penetration depth in our sample in function of the wavelength. However, these cross sections are expected to be large considering the VUV cross sections of organic molecules typical of our samples signature: alkane, amine and nitrile. We can assume that 190 nm radiations penetrate deeply in the sample and induce photochemical transformation (aging) on a thicker layer of the tholins samples offsetting the lower energy and irradiation time for 190 nm than for 121.6.

The 95 nm wavelength is nevertheless much more efficient than the two other wavelengths resulting in a notable increase of the aliphatic content of our samples. The amine functional groups are as well evicted from the material, which is not observed in the case of 121.6 nm and 190 nm irradiations. This is a significant photochemical process that transforms the functional groups and the polymer itself and deserves further discussion. One major difference between 95 nm (13.1 eV) and 121.6 nm (10.2 eV) or 190 nm (6.5 eV) is that 95 nm photons can cause significant ionization of organic molecules inside the polymer whereas the two other wavelengths do not carry enough energy to do the same, resulting in an ionization-mediated more efficient photochemistry at 95 nm. Moreover, Rydberg excitations of primary and secondary amines are known to initiate photodissociation processes whereas tertiary amines are more stable. Therefore with the increase in the photons energy at 95 nm, all the primary and secondary amines are depleted (hence the absorption at 3250 cm^{-1}) building up tertiary amines or imines (C=N) functions. In this process, the hydrogens atoms are transferred to the adjacent alkanes, increasing their band intensities. The lack of increase in -CN (nitrile) absorption at $\sim 2250\text{ cm}^{-1}$ is in agreement with this mechanism that primary and secondary amines are transformed into tertiary amines or imines, not towards the nitrile group (Kassab and Evleth, 1999). Tertiary amines are known to undergo efficient fluorescent decay making them less photolabile. The hydrogen atoms during the photodissociation of primary and secondary amines would react with adjacent olefinic carbon generating CH or CH₂ groups, in agreement with our observation that CH₂/CH₃ ratio increases in the infrared spectra after photolysis. Based on this analysis we propose a mechanism that involves photochemical

transformation of primary and secondary amines to tertiary amines and imine on one side and unsaturated olefinic carbon to saturated hydrocarbon on the other side - essentially transferring hydrogen from "N" centers to "C" centers. The mechanisms proposed are:

- the formation of tertiary amines by addition of N-H on a C=C double bond
 $\text{-C=C-} + \text{H-N-} \rightarrow \text{-CH-C(N)-}$
- the formation of imines by tautomerization
 $\text{-CH=C(NH}_2\text{)-} \rightarrow \text{-CH}_2\text{-C(=NH)-}$

The absorption of a 95 nm photons (13.1 eV) gives enough energy to ionize the majority of the organic molecules constituting the tholins film. This induces a hydrogen transfer process from the nitrogen to carbon in the so formed ion. The absorption of a 190 nm photon (6.5 eV) is not enough to ionize molecules in the polymer. This energy can be enough for a photo-induced H transfer in the neutral molecule, but this process is much less efficient in the non-charged molecules compared to ionic species.

The consequence of the VUV photochemistry is that only the N-H amine functions are actually consumed, which results in a transfer of H from N to C centers, with no net loss of nitrogen from the analogues.

VI.2.2.c Expected effect on aerosols in Titan's atmosphere

During the sedimentation process in the thermosphere, the solar spectrum is progressively and wavelength-dependently extinguished because of absorption by atmospheric components. In order to comprehend how the wavelengths selected in our study can selectively affect the aerosols according to the altitude, we estimate the penetration depth of the solar irradiation in Titan's atmosphere as a function of wavelength. At a given wavelength, the penetration depth is the altitude corresponding to the maximum absorption of the solar radiance, which occurs at an optical thickness of unity $\tau(\lambda) = 1$ ($I/I_0 = e^{-\tau}$; at $\tau = 1$, $I/I_0 = 1/e$ or 0.3678). It is calculated using representative density profiles of only the main absorbing neutral species in Titan's atmosphere (Hébrard et al., 2009), their absorption cross-sections (Huebner et al., 1992), and the solar flux (Floyd et al., 1998). The $\tau(\lambda) = 1$ profile is shown in Figure 52 displaying several successive dominant wavelength-range levels according to the altitude 1) 50-100 nm down to 1000 km of altitude, 2) 100-140 nm down to 800 km, 3) 140-200 nm progressively absorbed below 800 km.

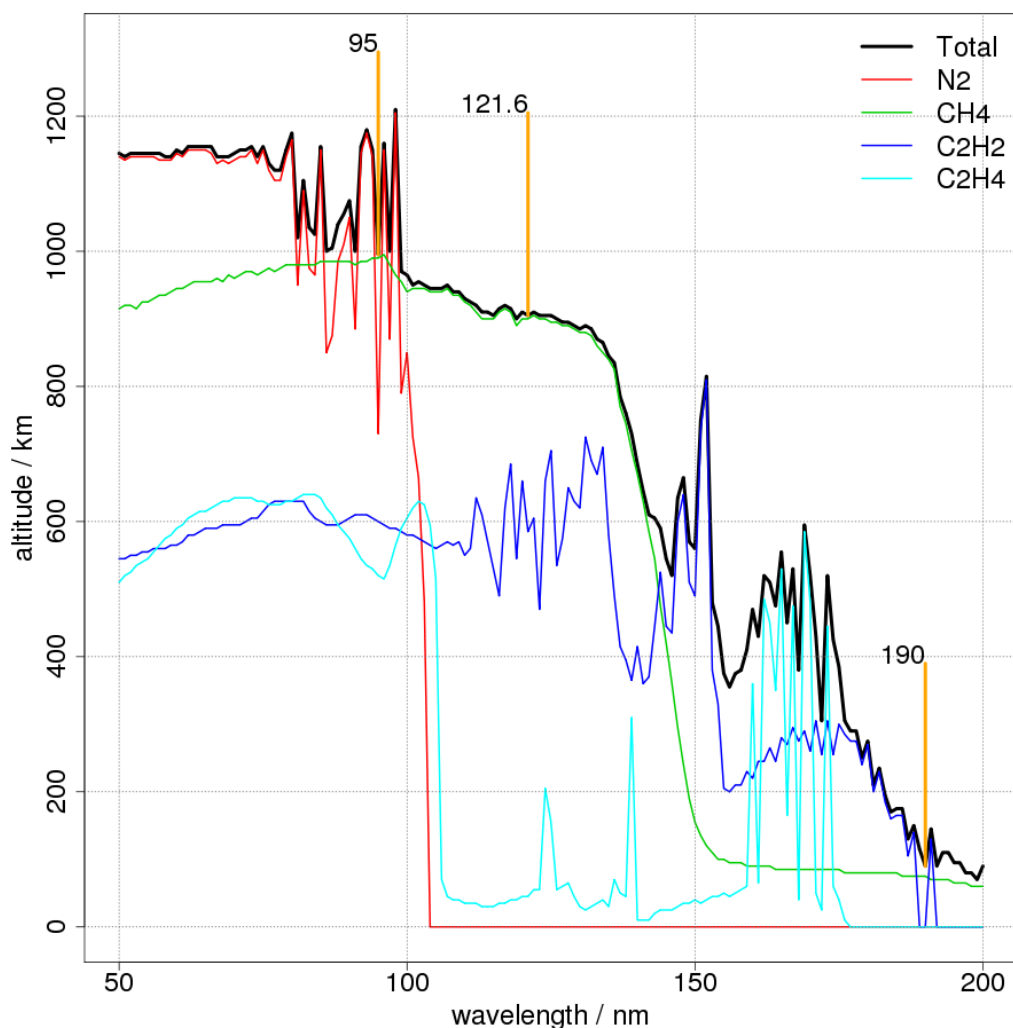


Figure 52: Unity optical thickness profiles: total $\tau=1$ curve (black), optical depth=1 for individual molecules (colored curves). Altitude optical depths of 95 nm (~1000 km), 121.6 nm (~900 km) and 190 nm (~100 km) wavelengths penetration of the solar radiation in Titan's atmosphere are indicated as orange vertical lines.

In Titan atmosphere, the 95 nm wavelength is representative of radiations occurring above 1000 km of altitude where the aerosols formation is initiated and they reach nanometric dimensions (Lavvas et al., 2011b; López-Puertas et al., 2013). If analogues of aerosols used in these experiments have a more important size than nanometric particles formed in the ionosphere of Titan, the effect observed experimentally with analogues irradiated at 95 nm will therefore involve an aging and a chemical evolution of aerosols as soon as they appear in the thermosphere through harsh VUV radiations below 100 nm.

Below 1000 km, this is Lyman- α radiation which have a predominant effect and then progressively radiations with more important wavelengths when altitude of aerosols decreases. According to experimental results obtained for 121.6 nm and 190 nm, the aging

process of the aerosols of Titan and their chemical evolution is expected to continue during all their sedimentation through the thermosphere.

These processes, initiated by VUV radiation with wavelength lower than 100 nm around 1000 km and continue by higher wavelength radiations during the sedimentation of the aerosols through the Titan's atmosphere, are expected to involve a modification of the infrared signature of the aerosols with a diminution of the amines signature and an increase of the alkyl group signature.

These experimental results also shed a new light on the apparent contradiction unsolved to date between measurements by various instruments of the Cassini-Huygens mission and also between measurement of Cassini-Huygens instruments and laboratory experiments to synthesize analogues of aerosols.

Indeed, the ACP-GCMS instrument onboard the Huygens probe has analyzed the composition of aerosols. Aerosols have been collected at two altitudes ranges (130-35 km and 25-20 km), vaporized by pyrolysis and the gas release have been analyzed by GC-MS. These analysis reveal the presence in the aerosols of a nucleus rich in nitrogen (Israel et al., 2005). This refractory nucleus formation is supposed to be initiate in the thermosphere of Titan, where *in-situ* mass spectrometry measurement actually depict an efficient ion-mediated organic growth (Waite et al., 2007). Titan's positive and negative ions chemistries with masses lower than 100 a.m.u detected by Cassini-INMS and Cassini-CAPS/ELS (Carrasco et al., 2013; Vuitton et al., 2009; Vuitton et al., 2007) are strongly supported by nitrogen containing molecules. Moreover NH₃ is a molecule found in abundance in Titan's ionosphere (Yelle et al., 2010), which is expected to participate as a precursor for the aerosol chemical formation and would provide amine N-H bonds in the aerosols structure (He and Smith, 2014). These different observations are in favor of amine-rich aerosols when their building-up initiated in the ionosphere. This is moreover consistent with the significant N-H signatures found by mid-infrared spectroscopy in our laboratory analogues of Titan's ionospheric aerosols (Gautier et al., 2012), in spite of the low amount of specific primary amine molecules extracted from similar analogues in (Cable et al., 2014).

However, this aerosol nitrogen rich seems in disagreement with the infrared spectral signature of the aerosols when observed in the stratosphere by the VIMS and CIRS Cassini instrument which only display clear signatures of aliphatic structure (Kim et al., 2011; Vinatier et al., 2012). Indeed, in the 2750-3250 cm⁻¹ wavenumber range observed by VIMS, only C-H bonds

signatures are observed, where N-H bonds could have also been expected for N-containing aerosols as observed in laboratory analogues (Gautier et al., 2012). A comparison of the infrared signatures of our analogues of aerosols product in our experiment before and after irradiation at 95 nm with the VIMS and CIRS observations is presented in Figure 53.

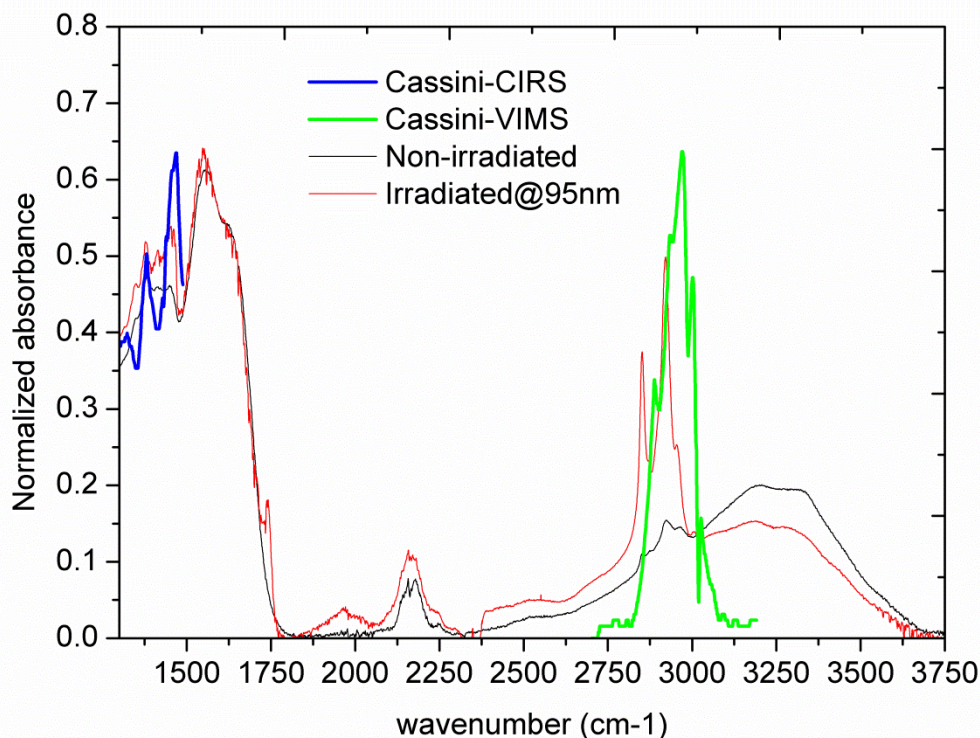


Figure 53: Comparison of the 95 nm irradiated film with the non-irradiated film (Gautier et al., 2012) and with normalized data from Cassini-VIMS (Kim et al., 2011) and Cassini-CIRS (Vinatier et al., 2012) mid-IR instruments at altitude ~200 km. VIMS and CIRS spectra were normalized to the maximum of our spectra (i.e. the CIRS spectrum was normalized at the 1450 cm^{-1} band, and the VIMS spectrum at the 2930 cm^{-1} band).

The experimental results obtained from the aging of analogues of nitrogen rich aerosols point out a mechanism which could participate to explain this contradiction. Indeed, chemical growth processes in the upper atmosphere as simulated with PAMPRE lead to nitrogen-rich aerosols, involving all kind of nitrogen-bearing groups: nitriles, imines and amines (primary, secondary and tertiary). The strong VUV photochemistry, with wavelength below 100 nm possibly affecting aerosols in the thermosphere, can selectively deplete them in primary and secondary amine functions in favor of aliphatic functions in agreement with the VIMS and CIRS observations in the stratosphere. This irradiation effect preserves nitrogen bearing function more deeply buried in the aerosols structure such as nitriles, imines and tertiary

amines in agreement with remaining nitrogen content in the aerosols as detected by ACP at lower altitude. The interpretation of our laboratory results for the aerosols of Titan is limited by the knowledge about the composition of the aerosols of Titan and particularly their nitrogen content. Indeed, the presence of nitrile functions in the Titan's aerosols has not been observed by VIMS at 4.6 μm but this results cannot be confirmed because of the overlapping on the nitrile band with the CO atmospheric absorption at 4.7 μm (Bellucci et al., 2009). Another analysis of the aerosols composition would be necessary to conclude about the contradiction between laboratory works and ACP-GCMS on the one hand and VIMS and CIRS observation on the other hand. Indeed, the confirmation of the presence of nitrile bands in the infrared signature of the aerosols could be given by the VIMS instrument onboard the Cassini spacecraft. Information for the nitrogen content of the aerosols could be given by a new *in-situ* analysis of the aerosols composition in the way of the first one realized by the Huygens probe. However, such analysis required a new mission dedicated to the study of Titan.

VI.3 Simulation of tropospheric/stratospheric aging processes

VI.3.1 Experimental methods and protocols

To simulate aging processes due to exposition of aerosols coated with condensed species to UV-visible solar flux in the lower atmospheric layers of Titan, I exposed analogues of aerosols produced with PAMPRE coated with condensed species to a laser flux with the Acquabella device.

Titan's aerosol analogues have been produced by plasma deposition in the PAMPRE reactor. They are deposited as thin films onto sapphire windows (2 mm thickness and 25 mm diameter) disposed in the plasma box. Samples have been produced during 2 hours of plasma duration. In order to evaluate the effect of the tholins composition on the reactivity of the condensed species, three different types of samples have been produced using three different $\text{N}_2\text{-CH}_4$ initial gaseous mixtures containing: 1 % of CH_4 , 5 % of CH_4 and 10 % of CH_4 . A blank sapphire window without any tholins is also used as a reference to control the reactivity of the condensed species alone.

A tholins sample or a blank sapphire window is mounted in the Acquabella experiment. The condense species is deposited at low temperature (Table 25) to form an ice film on the top of the tholins sample. The reactivity of C_2H_2 and CH_3CN coated on tholins has been studied in this thesis. They have been chosen because of their relative abundances in Titan's atmosphere

and their possible condensation in Titan's lower atmosphere. Indeed, C_2H_2 is one of the most abundant species in the atmosphere of Titan's with a mixing ratio about 2 ppm_v as measured by the CIRS instrument at 120 km (Vinatier et al., 2007). CH_3CN is also an abundant species. If its mixing ratio has not been measured in the stratosphere by the CIRS instrument (Coustenis et al., 2007), CH_3CN has been detected in the thermosphere of Titan with a mixing ratio of 1 ppm_v as measured by Cassini-INMS below 1050 km (Cui et al., 2009).

The selected species are deposited at low pressure on the cooled sample. The different conditions of deposition are summarized for each species in Table 25.

Table 25: Conditions of temperature, pressure and duration for the deposition of the different species studied (C_2H_2 , C_2D_2 and CH_3CN) on the sample.

Species	Temperature (K)	Pressure (mbar)	Duration (s)
C_2H_2	50	1.10^{-6}	20
C_2D_2	50	1.10^{-7}	5
CH_3CN	100	1.10^{-6}	20

The deposition is controlled using the monitoring of the infrared absorption band of each species.

Finally the sample (tholins or blank sapphire window) is irradiated at different wavelengths in order to determine the influence of the wavelength on the photo-reactivity of the system. The wavelengths used are 266 nm, 355 nm, 410 nm and 450 nm. The sample is irradiated for a total duration of 3 to 7 hours by step of 30 min, 1 hour or 2 hours. This protocol is used to evaluate the kinetics of condensed species consumption. The absorbance of the species and the tholins samples in the range of wavelengths used for the irradiation is measured by UV-VIS absorption spectroscopy. The decay of the condensed species during its irradiation is monitored by infrared spectroscopy on an infrared absorption band of the species. The evolution of the tholins absorbance spectra is monitored, after the sublimation of the remaining ices using IR spectroscopy.

VI.3.2 Results

VI.3.2.a C₂H₂ reactivity

Acetylene reactivity at 355 nm

Firstly, I investigated the reactivity of solid acetylene alone in order to be able to compare and to later distinguish the effect of the aerosols on the reactivity of C₂H₂. Following the protocol described in VI.3.1, C₂H₂ is deposited on a blank sapphire window. An infrared spectrum is recorded after the deposition to control the absorbance of solid acetylene. A spectrum of the blank sapphire window before the deposition is used as reference. The spectrum is presented in Figure 54.

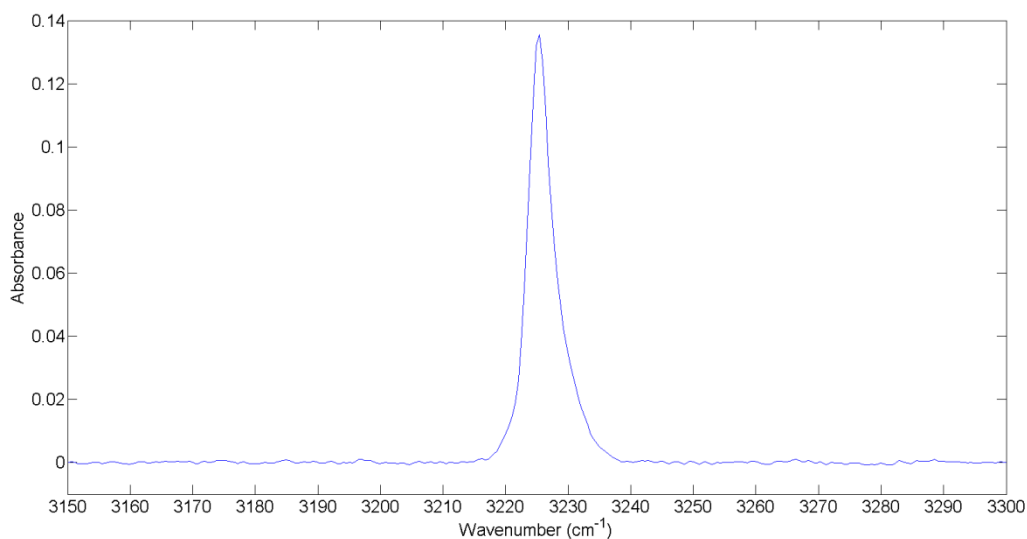


Figure 54: Absorbance spectrum of solid C₂H₂ after deposition at 50 K on a blank sapphire spectrum. The spectrum is center on the C-H stretching band of solid acetylene at 3225 cm⁻¹.

C₂H₂ presents a broad absorption band centered at 3225 cm⁻¹ corresponding to a C-H stretching mode (Hudson et al., 2014). This band is monitored after each irradiation to study the reactivity of the species. C₂H₂ is then irradiated during 3 hours by step of 30 min. An infrared spectrum is recorded after each irradiation. The differential evolution of the C₂H₂ absorption band in function of the irradiation duration is presented in the panel a) of Figure 55. A low consumption of C₂H₂ is shown on this figure. Indeed after 3 hours of irradiation at 355 nm, the absorbance has decreased by $\sim 2 \cdot 10^{-3}$ for an initial absorbance of ~ 0.14 (see Figure 54). A progressive increase of the base line is also visible on this spectrum. This increase corresponds to the absorption of water ice. Indeed, during the experiment, residual water vapor in the vacuum chamber can condense and deposit on the sample surface.

Knowing the low reactivity of only acetylene measured at this wavelength, I repeated the same experiment with acetylene deposited on a tholins sample. For this second experiment, C_2H_2 is coated (following the same protocol) on a PAMPRE tholins sample produced with 1 % of CH_4 . Then, C_2H_2 is irradiated by step of 30 min for a total irradiation time of 3 hours. The differential evolution of the C_2H_2 absorption band as a function of the irradiation duration is presented in the panel b) of the Figure 55. A higher consumption of C_2H_2 is measured compared to the irradiation of acetylene alone. Indeed, a decrease of the absorbance about ~ 0.05 is measured for an initial absorbance of ~ 0.14 . The band intensity decrease after 3 hours of irradiation at 355 nm is a factor of 25 higher when C_2H_2 is coated on a tholins sample ($\sim 5 \cdot 10^{-2}$) than coated on a sapphire window ($\sim 2 \cdot 10^{-3}$).

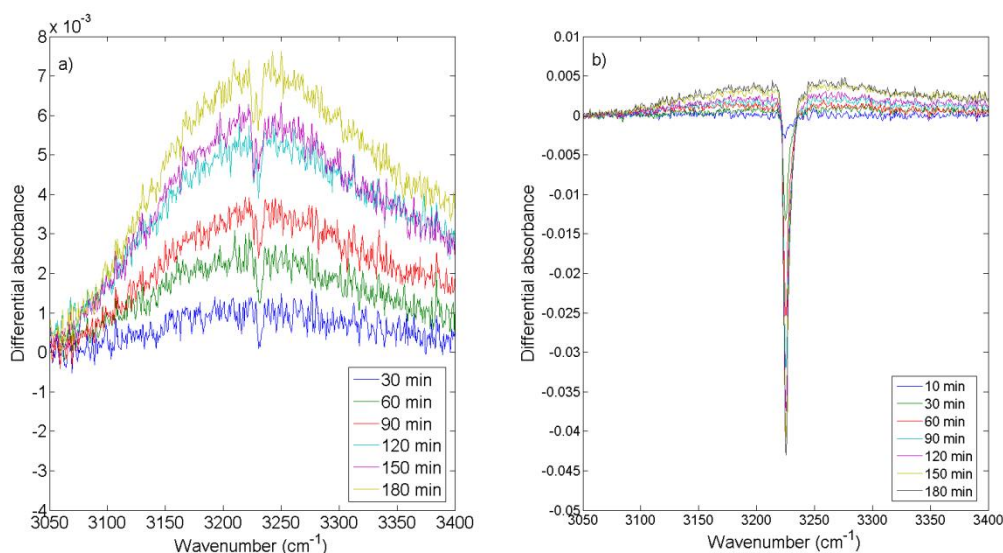


Figure 55: Evolution of the differential absorbance of C_2H_2 as a function of the irradiation duration at 355 nm. The reference is taken as the initial absorbance before irradiation. The panel a) presents this evolution for solid acetylene coated on blank sapphire window. The panel b) presents this evolution for solid acetylene coated on a PAMPRE tholins sample produced in a gaseous mixture composed by N_2 - CH_4 with 1 % of CH_4 .

To better represent the evolution of C_2H_2 with the duration of the irradiation, I represent the evolution of the area of the absorption band as a function of the irradiation time. This area is normalized by the initial area of the band before the irradiation. Figure 56 shows the evolution of this relative area of the absorption band of C_2H_2 as a function of the irradiation time for the two cases: the first one is the experiment where C_2H_2 is coated on a blank sapphire window and the second one is the experiment where C_2H_2 is coated on a tholins sample. Trend lines (without physical signification) have been added to highlight the very different evolution of

the area for the two studied cases. Indeed, for the experiment with a blank sapphire window, the area of the absorption band decreases linearly when C_2H_2 is irradiated at 355 nm, with a maximum of 5 % of depletion after three hours of irradiation. For the second experiment with a tholins sample, the depletion of the C_2H_2 absorbance is more important. The area decrease exponentially and reaches a plateau after 3 hours of irradiation with a diminution of about 45 % comparatively to the initial area.

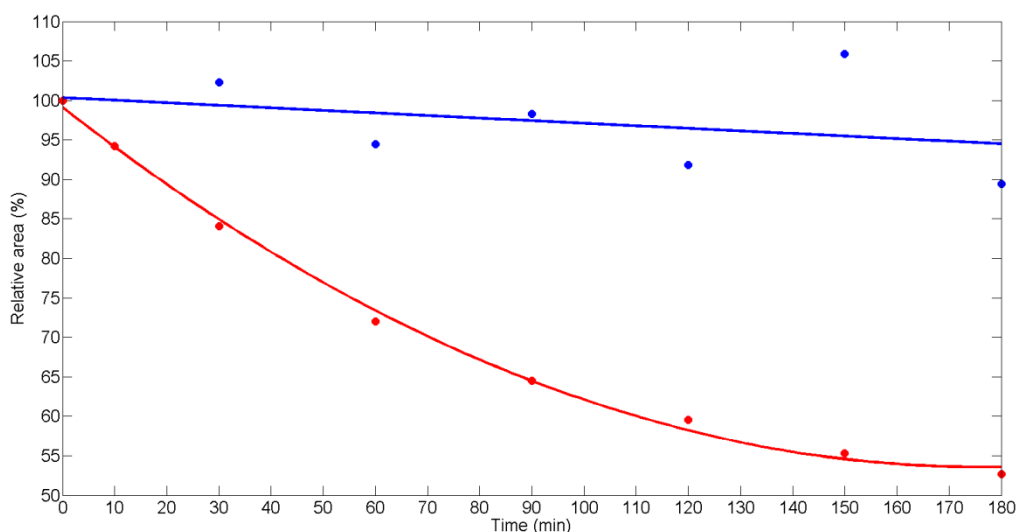


Figure 56: Evolution of the area of the absorption band of C_2H_2 relatively to the initial absorbance of C_2H_2 before the irradiation at 355 nm. The blue points correspond to an experiment with C_2H_2 coated on a blank sapphire window. The red points correspond to an experiment with C_2H_2 coated on a tholins sample. Trend lines have been added to highlight the evolution of the band area.

According to Figure 55 and Figure 56, the irradiation of solid acetylene with a laser at 355 nm involves a consumption of acetylene. However, this consumption is drastically increased when C_2H_2 is deposited on a tholins sample. It seems that acetylene reactivity is promoted by the presence of the organic substrate. To understand the reactivity of C_2H_2 pointed out here, a first step is to measure the absorbance of C_2H_2 and tholins in the range of wavelength studied in this thesis. The absorption spectrum of solid C_2H_2 at 50 K is presented in the 200-850 nm range in the Figure 57.

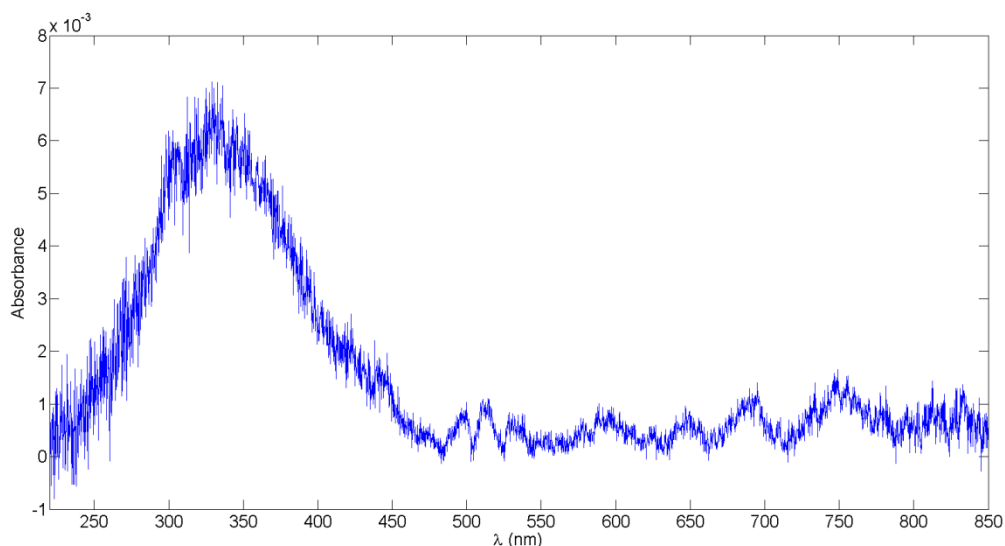


Figure 57: UV-visible absorbance spectrum of solid acetylene deposited at 50 K.

As visible on Figure 57, solid C_2H_2 presents only a broad absorption band centered at 346 nm. This corresponds to a singlet-triplet absorption predicted in (Malsch et al., 2001). Oscillations of the base line observed in this spectrum are caused by scattering. This low absorption of C_2H_2 at this wavelength can explain the limited reactivity when deposited on a blank sapphire window.

The low UV absorption of acetylene points out the importance of tholins for the reactivity of acetylene observed here. Figure 58 presents the absorption spectrum of the tholins sample recorded in the 220-850 nm range. Tholins are transparent in the visible range with an absorbance close to 0 between 520 nm and 850 nm. However, tholins presents an important absorption in the UV range. Indeed, absorbance increases from the visible ($A \sim 0$ at $\lambda = 520$ nm) to UV and reaches a maximum of absorbance about 0.97 for a wavelength of 295 nm. The decrease of the absorbance for shorter wavelengths than 290 nm is due to the decrease of the lamp emission at these wavelengths.

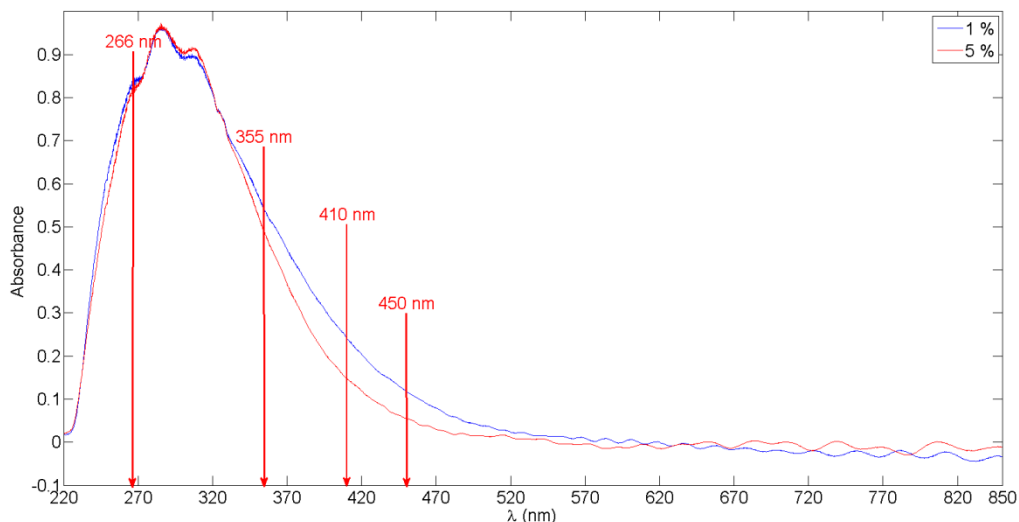


Figure 58: UV-visible absorption spectra of the tholins samples produced with 1 % of CH_4 (blue) and 5 % of CH_4 (red) in the 220-850 nm range. The arrows are placed at the used wavelengths for the study of the reactivity of C_2H_2 and CH_3CN .

If C_2H_2 does not absorb significantly photons at the wavelength of 355 nm used for the irradiation, tholins samples present a strong absorption at this wavelength. These results highlight the fact that the absorption of tholins is necessary for, in interaction with C_2H_2 , activating the reactivity of solid acetylene.

Wavelengths dependence of the C_2H_2 photo-reactivity

If the absorbance of the tholins sample plays a role in the reactivity of acetylene coated on the tholins, the reactivity of acetylene should decrease when the laser wavelength decreases. Indeed, a decrease of the reactivity of C_2H_2 is expected in agreement with the decrease of the tholins absorption.

To evaluate this effect, we perform the irradiation of C_2H_2 coated on tholins following the same protocol than the one at 355 nm but using a higher wavelength. Here we use 410 nm and 450 nm to probe the effect of the wavelength on the acetylene chemistry. The consumption of acetylene during the irradiation is always controlled through the monitoring of its absorption band at 3325 cm^{-1} . As explained in chapter II, for the irradiation at 410 nm and 450 nm, the laser is not defocused and irradiated only a part of the sample contrary to the irradiation at 355 nm where the laser is defocused involving a beam size of the laser equal to the sample size. However, the infrared beam used to monitor the acetylene consumption has approximatively the size of the sample. So all the acetylene deposited on the sample contributes to the

absorption measured. This induces a bias for comparison of the C_2H_2 consumption. Indeed, for irradiation at 410 nm and 450 nm, only part of the acetylene ice contributing to the absorption has been irradiated. This underestimates the percentage of C_2H_2 consumed when compared to irradiation at 355 nm. In order to prevent this problem and obtain a quantitative comparison of the three experiments, the depletion measured at 355 nm is corrected using a correction factor taking account the difference of the areas irradiated. The evolution of the normalized relative area of C_2H_2 is shown in Figure 59. Initial band areas have been taken as references at each wavelength.

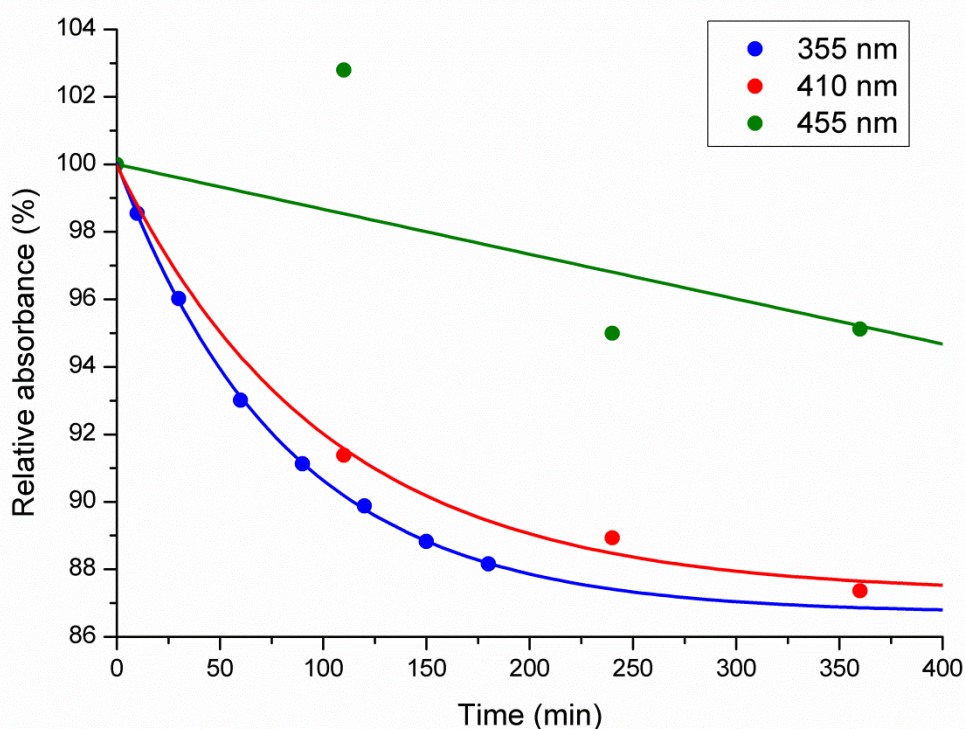


Figure 59: Evolution of the relative area as a percentage of the absorption band of C_2H_2 as a function of the irradiation duration for the three studied wavelengths: 355 nm (red points), 410 nm (purple points) and 450 nm (blue points). The initial area of the band before irradiation has been taken as reference for each wavelength. The measured values at 355 nm have been normalized to take into account the difference of sample area irradiated at 355 nm comparatively to 410 nm and 450 nm.

The Figure 59 shows a comparable exponential consumption of C_2H_2 for the experiments realized at 355 nm and 410 nm. For these two experiments, the relative absorbance decreases and reaches a plateau after ~250 min with a relative area about 88 %. These relatively low 12 % of C_2H_2 depletion are caused by the irradiation, which covers only a part of the sample. For the irradiation at 450 nm, a linear decrease is observed with a maximum of depletion about 4 % after 360 min of irradiation. There is a good correlation between the reactivity of acetylene

coated on tholins and the absorbance of the tholins sample at the laser wavelength used. At 355 nm and 410 nm, the absorbance is about 0.5 and 0.25 respectively. At 450 nm, the absorbance decreases below 0.1 which seems to be a limit to observe a reactivity of acetylene.

C₂D₂ reactivity at 355 nm

The consumption of acetylene coated on a tholins sample has been highlighted by the monitoring of the C-H stretching bond at 3225 cm⁻¹. If C₂H₂ is consumed, the apparition of new products and/or the modification of the tholins composition are expected. However, we do not observe the apparition of new absorption bands during the irradiation. Moreover, the comparison of the absorption spectrum of tholins in the infrared before and after the irradiation does not easily highlight any changes.

In order to investigate the fate of the acetylene which has reacted, I have chosen to perform new experiments with acetylene labelled with deuterium (D) (isotope of hydrogen): C₂D₂. The modification of masses of the molecule induced by the use of another isotope involves a modification of the frequencies of the absorption bands. For example, the C-H stretching band of solid C₂H₂ is observed at 3225 cm⁻¹ when the C-D stretching absorption band of C₂D₂ is observed at 2393 cm⁻¹ in our experiments. The absorption spectrum of C₂D₂ after its deposition on a tholins sample at 50 K is presented in Figure 60.

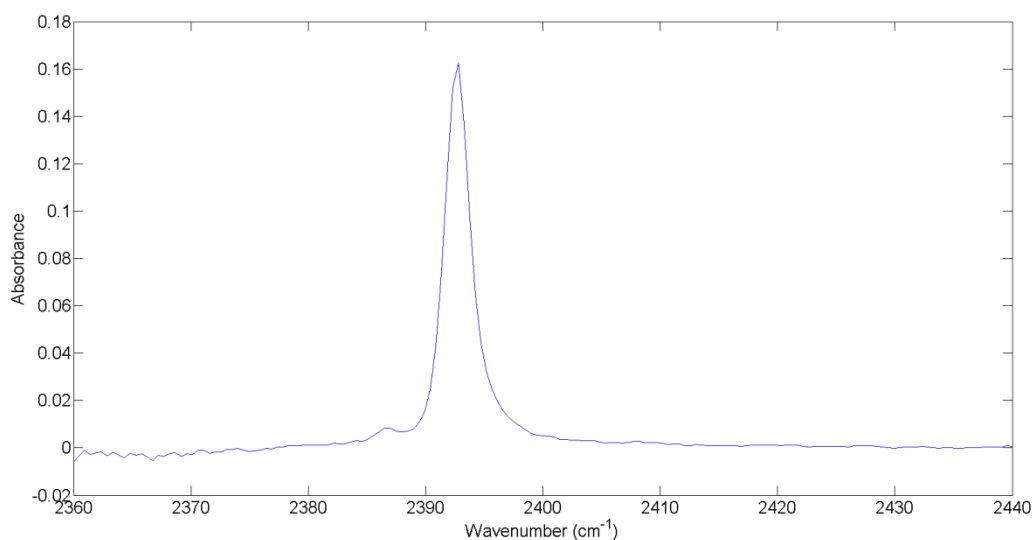


Figure 60: Absorption spectrum of solid C₂D₂ after deposition at 50 K on a tholins sample (99/1). The spectrum is center on the C-D stretching band at 2393 cm⁻¹.

After the deposition, the absorbance of C_2D_2 is 0.16. Following the same protocol that for C_2H_2 , I irradiated solid C_2D_2 at 355 nm during 3 hours: by step of 30 min for the 2 first hours of irradiation and then by step of one hour.

The reactivity of C_2D_2 is firstly controlled with the monitoring of its absorption band. Figure 61 presents the evolution of the differential absorbance of C_2D_2 as a function of the irradiation duration. The initial absorbance before the irradiation is used as a reference.

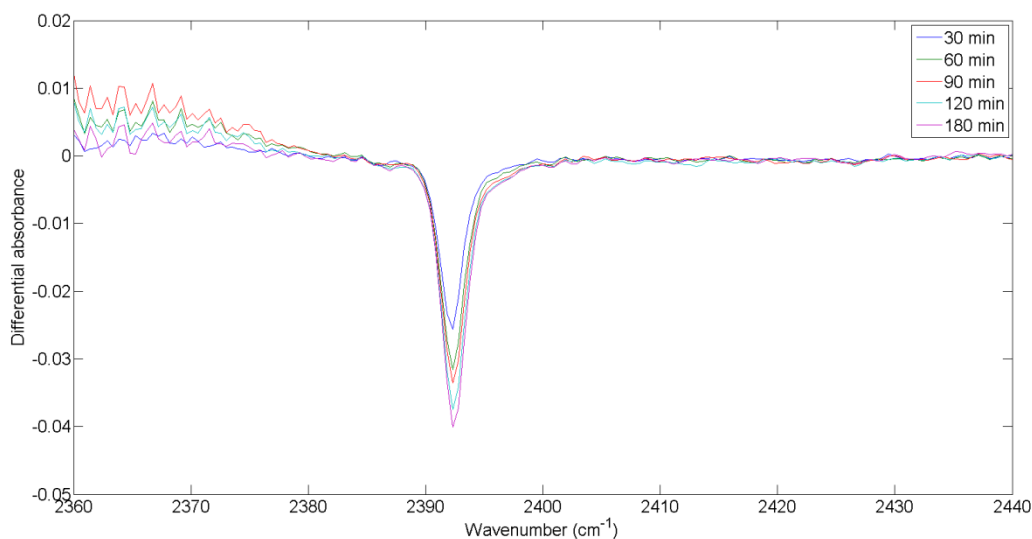


Figure 61: Evolution of the C-D stretching band at 2393 cm^{-1} of C_2D_2 coated on tholins during the irradiation at 355 nm.

We observed, as for C_2H_2 , a depletion of the C_2D_2 absorption band. The maximum of the band absorbance decreases by 0.04 after 3 hours of irradiation at 355 nm. The C_2D_2 reactivity is comparable to the reactivity of C_2H_2 in the same condition.

The experiment with C_2D_2 is reproduced four times on the same tholins sample. After each deposition and irradiation at 355 nm of C_2D_2 , the tholins sample is warmed up to room temperature and the infrared spectrum of the sample is recorded. The evolution of the differential absorbance in the mid-IR range after each experiment is presented in Figure 62. The infrared spectrum at room temperature of the tholins sample before the experiments is used as a reference. The spectrum is centered on the $2000\text{-}2700\text{ cm}^{-1}$ range. Two evolutions in the infrared spectrum are visible on the Figure 62. A first large absorption band appears in the spectrum after the irradiation of C_2D_2 . This band is centered at 2152 cm^{-1} . The intensity of the band is low and does not change between the first three experiments.

However an increase can be observed in the fourth experiment. A second large band appears in the spectrum. This band is centered at 2385 cm^{-1} . The evolution of this band between the experiments is difficult to quantify due to its convolution with the absorption band of atmospheric gaseous carbon dioxide.

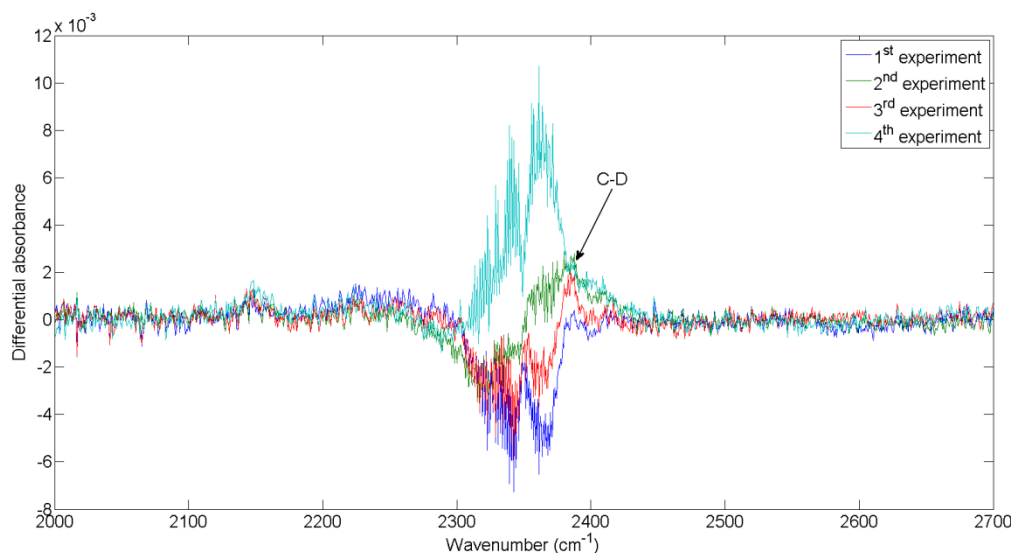


Figure 62: Evolution of the differential absorbance of the tholins sample in the $2000\text{-}2700\text{ cm}^{-1}$ range. Each spectrum has been recorded at room temperature after an experiment of C_2D_2 photolysis. Fourth successive experiments have been realized on the same tholins sample. The absorbance spectrum of the tholins sample before the experiments is used as reference.

The broad band at 2385 cm^{-1} corresponds to a C-D stretching band. The apparition of this new absorption band in the tholins infrared signature gives indication on the mechanism explaining the reactivity of solid acetylene coated on tholins. Indeed, different mechanisms could explain the decay of acetylene and especially the increase of the acetylene consumption when it is coated on a tholins sample.

The first process to be considered is photodesorption process. Indeed, the absorption of UV photon by molecules composing the ice thin film can involve Desorption Induced by Electronic Transition (DIET) (Fayolle et al., 2011). Photodesorption of ice film can also occur at wavelengths where the ice molecules do not absorb if they are deposited on a substrate, which absorbs this wavelength and transmit the energy to an ice molecule involving its desorption (Bertin et al., 2012).

The second process, which can be considered to explain the acetylene decay, is photochemical process.

Because of the very low absorption of solid acetylene at 355 nm (Malsch et al., 2001), the photodesorption of acetylene by direct DIET mechanism is not expected in our experiment. Moreover, this mechanism does not explain the increase of the acetylene decay when it is deposited on a tholins sample. Indirect photodesorption triggered by the tholins absorption remains possible. Indeed, the important tholins absorption at 355 nm can involve desorption of acetylene molecules coated on tholins through an energy transfer. However, this mechanism can explain the higher decay of acetylene coated on tholins than acetylene alone but this mechanism does not explain the apparition of a new band in the infrared tholins signature after the release of the remaining ices. The apparition of new band is in favor of an acetylene consumption caused by a photochemical process. Indeed photochemistry can explain the consumption of acetylene, which can react with the tholins. The apparition of an infrared absorption band attributed to a C-D stretching mode shows that acetylene is partially integrated in the polymer structure. The activation of the chemistry is driven by the tholins absorption at the wavelength used for the irradiation. If these results demonstrate the reaction of acetylene with the tholins, the mechanism and the exact integration of acetylene in the tholins structure remains unknown.

Effect of the tholins composition on the acetylene reactivity

For these experiments, tholins samples were produced in various gaseous mixture composed by N_2 and CH_4 . Coating acetylene on a tholins sample instead of a sapphire window has clearly increased the reactivity of C_2H_2 .

Different studies have been previously realized to understand the effect of the initial composition of the gaseous mixture used in PAMPRE to produces analogues of aerosols. Particularly, these studies highlight the importance of the initial amount of CH_4 on the composition of tholins (Gautier et al., 2014a; Sciamma-O'Brien et al., 2010) and on their optical properties (Gautier et al., 2012; Mahjoub et al., 2012). The analysis of the composition of the aerosols showed an increase of the nitrogen content in the aerosols when the initial amount of CH_4 decreases (Gautier et al., 2014a; Sciamma-O'Brien et al., 2010). This more important nitrogen content leads to a more important absorption of the aerosols in the UV-visible range (Mahjoub et al., 2012) in correlation with an increase of the amine signature in the mid-IR range (Gautier et al., 2012).

Starting from this, I studied the influence of the composition of the tholins sample on the reactivity of solid acetylene. The experiments presented before on the reactivity of C_2H_2 are

reproduced using two other tholins samples produced in gaseous mixtures containing 5 % and 10 % of CH₄ respectively. Solid acetylene is irradiated during three hours at 355 nm and the reactivity of C₂H₂ is monitored with the evolution of its C-H stretching band. The evolution of the differential absorbance of C₂H₂ after three hours of irradiation is presented on Figure 63. The reference is the initial absorbance of acetylene before irradiation. Figure 63 presents this evolution for C₂H₂ coated on a blank sapphire windows and coated on three different tholins samples produced in a gaseous mixture containing 1 %, 5 % and 10 % of methane respectively.

For all the experiments, an increase of the baseline between 3000 cm⁻¹ and 3500 cm⁻¹ is visible on the spectra. This increase corresponds to the absorption of solid water. This water signature results from the deposition of the residual water vapors in the reactor on the surface of the sample. Moreover, a depletion of the infrared acetylene signature is observed after three hours of irradiation for the experiments presented.

In spite of these artifacts, the consumption of C₂H₂ changes drastically as a function of the sample used. As explained previously, the reactivity of C₂H₂ is very low when it is coated on a blank sapphire window. The interaction with an aerosol sample is necessary to activate the chemistry at 355 nm. We observe here an important evolution of the C₂H₂ consumption as a function of the tholins sample used. Indeed, if for a tholins sample produced with 1 % of CH₄ the reactivity observed is important with about 45 % of acetylene consumed, this is not the case for the two other samples produced in a gaseous mixture containing 5 % and 10 % of CH₄.

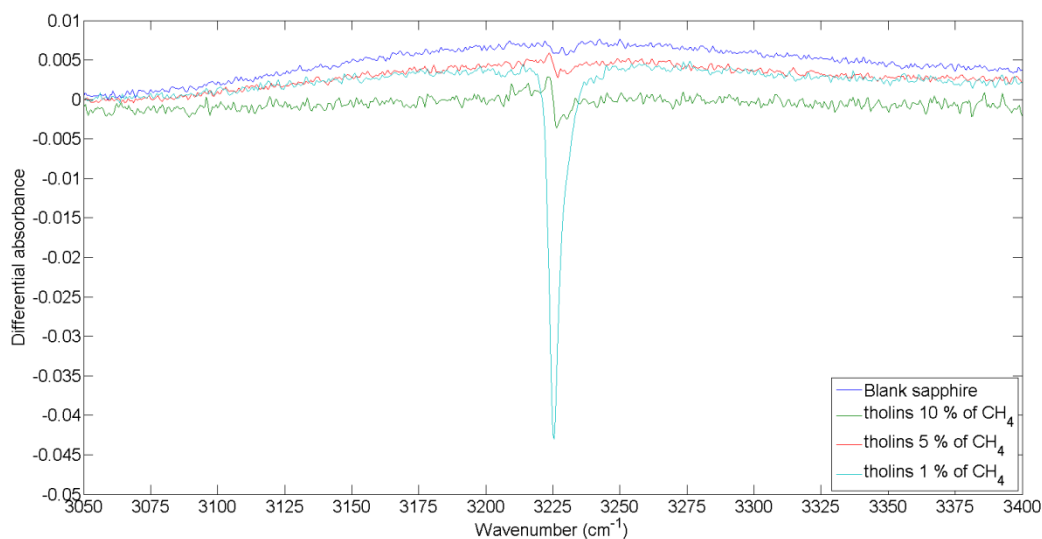


Figure 63: Differential absorbance of the C_2H_2 infrared absorption band at 3225 cm^{-1} after 3 hours of laser irradiation at 355 nm for different substrates. The reference is the initial absorbance spectrum of C_2H_2 before irradiation. The substrates are a blank sapphire window and three tholins samples produced with three different initial amounts of CH_4 : 1 %, 5 % and 10 %.

The reactivity of acetylene deposited on tholins produced at 5 % and 10 % of CH_4 is close to the reactivity of acetylene deposited on a blank sapphire window. Contrary to tholins sample produced with 1 % of CH_4 , the two other samples do not promote the reactivity of C_2H_2 . These experiments point out the evolution of the tholins ability to promote acetylene reactivity as a function of the amount of methane used for their production. The reactivity of C_2H_2 is strongly increased for tholins produced with 1 % of CH_4 . Two hypotheses can be made to explain this result.

Firstly, the comparison of the absorption spectra of the tholins samples in the UV-visible range presented in the Figure 58 shows a higher absorbance for the sample produced with 1 % of CH_4 than for the sample produced with 5 % of CH_4 between 320 nm and 450 nm. This is in agreement with the optical indices measured by (Mahjoub et al., 2012) even if we cannot conclude for the absolute evolution of the absorbance because of the difference of thickness between the samples produced with different CH_4 amounts (Mahjoub et al., 2012). However, if this difference of absorbance can involve a little decrease of the reactivity, the absorbance for the 5 % sample is always about 0.5 i.e. higher than the absorbance of the 1 % sample at 410 nm where an important reactivity is always observed.

A second reason can be the difference of composition of the tholins as a function of the CH_4 initial amount. Indeed, the elemental analysis of these tholins has shown an increase of the nitrogen content in the tholins produced with a low amount of CH_4 (Sciamma-O'Brien et al.,

2010). This modification of the composition results in an increase of the nitrile and amine content and a decrease of the aliphatic content of the tholins produced with 1 % of methane comparatively to the tholins produced at 5 % and 10 % of methane (Gautier et al., 2012). The acetylene reactivity seems to be related to the composition and the chemical functions of the tholins substrate susceptible to react with C_2H_2 . The higher effect observed in the case of tholins produced with 1 % of methane suggests that acetylene reactivity could be triggered by the interaction with the ammine or nitrile functions of the tholins sample, which are themselves activated by the efficient absorption of the laser UV radiation. Moreover, VUV irradiation of tholins samples has been presented in section VI.2.2.a. The modification of the infrared signature of the tholins after the irradiation presented in Figure 50 showed that amine functions are very reactive when irradiated comparatively to nitrile functions, which are not affected. This result is in favor of an acetylene reactivity triggered by amine function more than nitrile function. The two last subsections suggest an interaction between the amine N-H functions of tholins and the $C\equiv C$ bonds of acetylene.

VI.3.2.b CH_3CN reactivity

Acetonitrile reactivity at 355 nm

After the study of the reactivity of an abundant small hydrocarbons (C_2H_2) present in Titan atmosphere, I conducted the study of the reactivity of another family of compounds present in the atmosphere of Titan: the nitrile family. For that, I apply the same protocol as for C_2H_2 to study the reactivity of acetonitrile (CH_3CN) coated on tholins. Firstly, CH_3CN is deposited on a blank sapphire window. The deposition is controlled with the monitoring of the absorption of CH_3CN in the infrared range. The infrared absorption spectrum of CH_3CN in the 2200-3100 cm^{-1} range is presented in Figure 64.

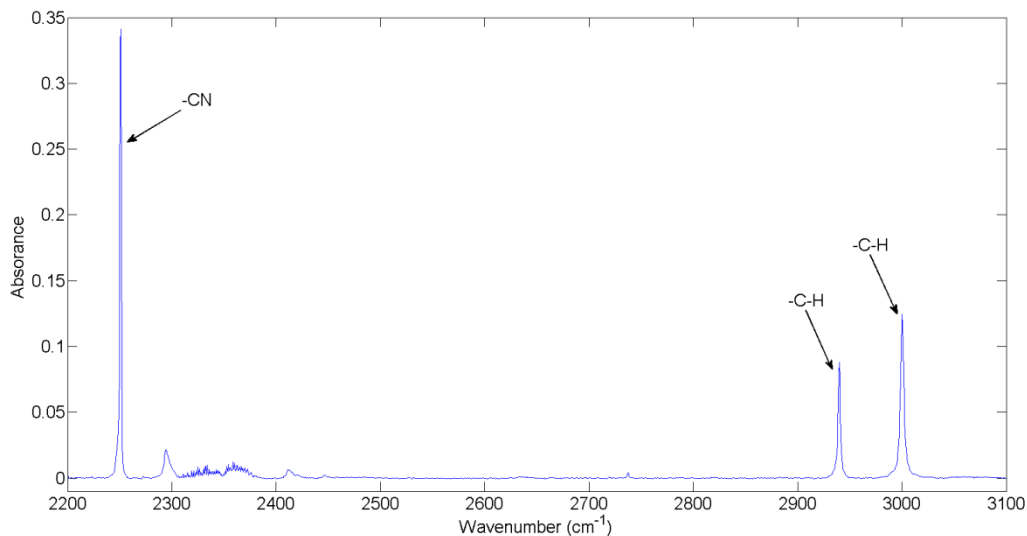


Figure 64: Infrared absorption spectrum of solid CH_3CN coated at 100 K on a blank sapphire window.

Acetonitrile presents several absorption bands in this domain of wavenumber. The assignment of the stronger absorption bands to vibrational mode have been realized for crystalline CH_3CN at 95 K in (Russo and Khanna, 1996). CH_3CN presents three strong bands: -C-H asymmetric stretching at 3000 cm^{-1} , -C-H symmetric stretching at 2940 cm^{-1} and -CN symmetric stretching at 2251 cm^{-1} . To evaluate the photo-reactivity of solid acetonitrile, the evolution of the absorbance of these three bands is monitored after each irradiation. Firstly, solid acetonitrile is irradiated during four hours after deposition on a blank sapphire window. The evolution of the differential absorbance of CH_3CN as a function of the duration of the irradiation at 355 nm is presented in panel a) of the Figure 65. The reference is the initial absorbance of CH_3CN before irradiation.

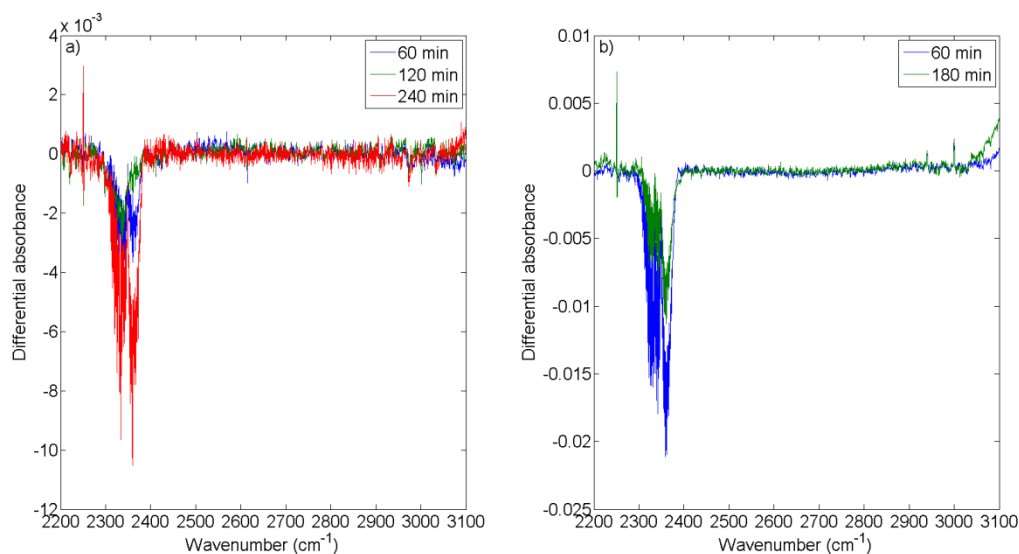


Figure 65: Evolution of the differential absorbance of CH_3CN in function of the irradiation duration at 355 nm. The reference is taken as the initial absorbance before irradiation. Panel a) presents this evolution for solid acetonitrile coated on blank sapphire window. The Panel b) presents this evolution for solid acetonitrile coated on a PAMPRE tholins sample produced in a gaseous mixture composed by N_2 - CH_4 with 1 % of CH_4 .

The infrared spectrum does not evolve during irradiation. Acetonitrile ice on the sapphire window is not consumed and there is no new absorption band. It seems that solid CH_3CN does not react when it is irradiated at 355 nm after a deposition on a blank sapphire window.

Then solid acetonitrile is deposited on a PAMPRE tholins sample produced in a gaseous mixture containing 1 % of methane. The evolution of the differential absorbance of CH_3CN as a function of the irradiation duration is presented in the panel b) of Figure 65. The reference is the initial absorbance of CH_3CN before the irradiation. As for the irradiation of CH_3CN coated on a blank sapphire window, we do not observed any change in the infrared spectrum during irradiation. When deposited on a tholins sample, CH_3CN does not react. This is a different evolution from the reactivity observed for C_2H_2 . Indeed, if the organic material composing tholins promotes the reactivity of acetylene, this is not the case for acetonitrile. At these low energy wavelengths, the nature of the species in interaction with the tholins is critical for the potential reactivity and so the possible evolution of tholins.

If solid acetonitrile does not react when irradiated a 355 nm, the study of the reactivity of solid acetylene has highlighted the wavelength dependence of the species reactivity. For this reason, a last experiment of CH_3CN irradiation is realized at a wavelength of 266 nm. Indeed when the wavelength decreases, the energy of the photons increases. Acetonitrile coated on a tholins sample has been irradiated during 2 hours at 266 nm. An infrared spectrum has been

recorded after 30 min and 60 min of irradiation to measure the consumption of CH_3CN as a function of the irradiation time. The evolution of the differential absorbance of acetonitrile as a function of the duration of irradiation at 266 nm is presented in Figure 66. The initial absorption spectrum before irradiation is used as a reference.

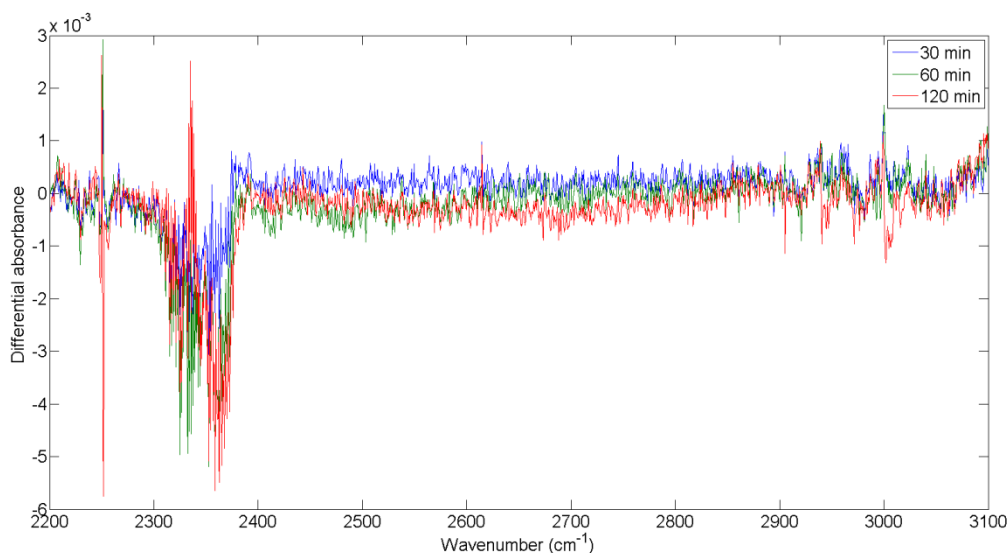


Figure 66: Evolution of the differential absorbance of CH_3CN in function of the irradiation duration at 266 nm. The reference is the initial absorbance before the irradiation. The figure presents this evolution for solid acetonitrile coated on a PAMPRE tholins sample produced in a gaseous mixture composed by N_2 - CH_4 with 1 % of CH_4 .

Contrary to the experiment realized at 355 nm, a small depletion in the infrared signature of CH_3CN is visible after 2 hours of irradiation at 266 nm. This is particularly visible on the two strong absorption bands of acetonitrile located at 2940 cm^{-1} and 3000 cm^{-1} . However, even at this wavelength the reactivity is limited with a depletion of CH_3CN of about 1 % of the initial signal. Indeed, even if the energy of the photons has increased between 355 nm (3.5 eV) to 266 nm (4.7 eV) it does not change drastically the reactivity of CH_3CN .

The chemistry of solid species coated on aerosols analogues is highly sensitive to the nature of the species but also to wavelengths used to irradiate. This study has shown before that the C_2H_2 reactivity was also dependent on the composition of the tholins, and was probably driven by the amine content in tholins. My study has highlighted the specificity of the chemical interaction between the coating molecules and the supporting aerosols, whose composition will selectively allow the promotion of the reactivity of the solid species coated when the solid system is irradiated with low energy photons. It seems that small highly unsaturated molecules such as acetylene adsorb, diffuse, or dock into pores of the tholins. Upon photoexcitation of the tholins, the excitation energy is either transferred to a location

where an acetylene molecule is present. In either situation, a covalent bond between the tholins and acetylene occurs. The resulting radicals further react with the tholins. The difference of reactivity between C_2H_2 and CH_3CN highlights the more important reactivity of $C\equiv C$ unsaturated bond comparatively to $C\equiv N$ unsaturated bond.

VI.3.3 Importance for the atmosphere of Titan

We have found in this study that laboratory analogues of Titan's aerosols can efficiently promote the chemistry of solid species coated on them. The interaction between the aerosols and the coated species is able to activate the chemistry of the species at wavelengths longer than wavelengths directly absorbed by the species. Indeed, we have highlighted that a small unsaturated hydrocarbon as C_2H_2 can react when it is irradiated at wavelengths as high as 355 nm or 410 nm.

This result is in favor of a continuous chemistry on the aerosols from the ionosphere of Titan where they are initiated, to the ground where they are deposited after sedimentation through the atmosphere. The low temperatures measured in the stratosphere and the troposphere of Titan are susceptible to enable the condensation of photochemical product as C_2H_2 on the aerosols surfaces which play the role of nucleation cores. The reactivity observed in the laboratory is interesting for the chemistry of these atmospheric layers because if the more energetic UV photons are absorbed higher in the Titan's atmosphere, near-UV/visible photons reach these low altitudes. This study has highlighted the dependence of the reactivity with the composition of the aerosols and with the nature of the solid species. More observations are necessary about the composition of the Titan aerosols which remains largely unknown. Moreover the observation of condensed species in the atmosphere remains also uncertain with a difficult attribution of the bands observed in the far infrared as developed in section VI.1 even if a clear observation of HCN has been made recently (de Kok et al., 2014).

VI.4 Conclusion

If the comprehension of the aerosols formation processes in the atmosphere of Titan is an important topic, their potential physical and chemical evolutions during their sedimentation in the atmosphere is another one. Indeed, different processes could modify the optical properties and the chemical evolutions of the aerosols after their formation. The comprehension of these processes can help to interpret the data from Cassini-Huygens.

Several laboratory studies produced tholins (*i.e.* laboratory analogues of aerosols) in order to understand their composition and their formation processes. Here, I have chosen to use these analogues to study in the laboratory the potential evolution of the aerosols in the atmosphere of Titan with the simulation of two different possible aging processes.

The first part of the chapter presented a study of the potential evolution of the aerosols in the thermosphere of Titan where they are exposed to the harsh VUV solar flux. Irradiation of tholins samples with the VUV synchrotron flux has highlighted the sensitivity of the aerosols composition at such irradiation. The strong VUV photons, with wavelengths below 100 nm as affecting aerosols in the thermosphere, can selectively deplete them in primary and secondary amine functions in favor of aliphatic functions. This irradiation effect preserves nitrogen bearing function more deeply buried in the aerosols structure such as nitriles, imines and tertiary amines. These results can participate to interpret the apparent contradiction between the nitrogen rich aerosols analyzed by the ACP-GCMS instrument of the Huygens probe and the absence of amine function observed in the infrared by the VIMS instrument of the Cassini spacecraft.

The second part of this chapter presented the potential evolution of the aerosols in the stratosphere and troposphere of Titan where they are exposed to near-UV/visible solar photons and where they are in interaction with solid species which can condense because of the lower temperature and the higher pressure in these atmospheric layers. The results of this part showed that the presence of aerosols in interaction with solid species can promote the photo-reactivity of these species at longer wavelengths where they are generally inert. These results showed an important dependence of the reactivity with the chemical nature of the species. Indeed, the experiments highlight (that small unsaturated hydrocarbons as) acetylene can react at wavelengths as high as 355 nm when nitrile compounds as acetonitrile remain inert. The apparition of new absorption band in the IR signature of the tholins sample for the experiment using D-labelled acetylene has shown that the aerosols composition can also be modified by the reactivity of the coated ice.

General conclusion

The first part of my thesis was dedicated to investigate experimentally with the reactor PAMPRE the formation of organic compounds in the atmosphere of the early Earth. For that, the reactivity of two gaseous mixtures chosen as representative of the primitive atmosphere has been studied: one composed by N_2 , CO_2 and H_2 and one composed by N_2 , CO_2 and CH_4 . In a general way, results have highlighted the formation of organic compounds both in gaseous and solid phases for the two mixtures despite the relative important oxidation state. The formation of organic compounds in gaseous mixture with H_2 points out that CO_2 can be an efficient source of carbon, promoting an important organic growth in the atmosphere of the early Earth, even without the presence of CH_4 .

Water has been detected as the major volatile product in both cases. The important production of water is explained by the production of $\text{O}(^1\text{D})$ radicals by both neutral and ionic pathways, which involve a water formation through an oxidation process of H_2 or CH_4 . This production highlighted experimentally breaches our knowledge of the primitive atmosphere of the Earth where the atmosphere above the troposphere was generally considered as dry. This important production of H_2O would involve a modification of the water mixing ratio profile with an increase of the water content down to the troposphere. The increase of the water content in the stratosphere and mesosphere would notably result in the formation of high-altitude clouds similar to actual PSC and PMC, whose major impact would be the development of heterogeneous processes and chemistry as well as a possible climate impact depending of the optical thickness of these clouds.

Hydrogen cyanide and ammonia have also been detected in the two cases as well as ethanedinitrile and nitrous oxide for the mixture containing H_2 and formaldehyde for the mixture containing CH_4 . These compounds are very reactive species, which are involved in the formation of heavier compounds as complex as tholins. Nitrogen is present in many molecules confirming the activation of nitrogen chemistry in our experiment as expected in the ionosphere of the early Earth. More generally the presence of C, N, H and O in the molecules detected highlighted the coupling between the chemistry of these four elements necessary for the formation of prebiotic compounds. Unfortunately the chemistry of nitrogenized and oxygenated compounds is still unknown and notably the chemistry coupling

General conclusion

these different elements. This limits the identification of the compounds formed and their formation pathways.

In addition of these gaseous species, tholins growing in the reactive medium have been observed for both mixtures. They are composed by C, N, H and O atoms according to elemental analysis and their infrared signatures present amines, aliphatic, nitriles signatures and possibly -OH and C=O signatures. This is in agreement with the diversity of molecules detected in the gaseous phase and the complex chemistry observed.

The comparison between the two simulated atmospheric compositions emphasizes several differences. First, gaseous mixtures containing methane produce a larger quantity of compounds in gaseous and solid phase than one containing hydrogen. This is notably important for tholins, which are formed only as thin films on a substrate with H₂, but in the volume of the plasma in gaseous mixture with CH₄. Second, the increase of the CO₂ amount causes opposite effects on the two simulated atmospheres. As CO₂ is the only source of carbon for the organic growth in mixture containing H₂, the increase of its initial amount involves an increase of the quantity of products. On the contrary, it involves a decrease of the quantity of products in mixture containing CH₄. A high level of CO₂ during the Hadean and the Archean would have been more favorable to a quantitative production of organic matter in the primitive atmosphere if it was made of H₂ than if it was made of CH₄ even if CH₄ is more favorable for a quantitative production of organic molecules. Even if the production of organic products and particularly tholins in mixtures with CH₄ decreases drastically when the amount of CO₂ increases, the O content in tholins increases and could contain a more important variety of molecules and notably prebiotic molecules.

In the second part of my thesis I have investigated the influence of CO on the reactivity of the atmosphere of Titan. Titan has an important atmospheric reactivity leading to the formation of a large amount of organic species and even if this atmosphere is more reduced than the primitive atmosphere of the Earth, studying this atmosphere could help to understand chemical processes, which have taken place on the early Earth atmosphere. The major impact of CO on the reactivity is a drastic decrease of the gas to solid conversion resulting in an important decrease of the tholins production rate. CO involves a complexification of the chemistry including the formation of oxygenated species in the gaseous phase as N₂O and CO₂ and an incorporation of oxygen in tholins. A comparison of these results obtained with

General conclusion

mixtures containing CO₂ and CH₄ showed that CO₂ promotes more efficiently than CO the incorporation of oxygen in tholins.

The last part of my thesis was dedicated to the study of closest analogue of the early Earth: Titan and particularly the chemical evolution of the aerosols of Titan during their sedimentation to the surface. A first study has consisted to an exposition of film of tholins to a synchrotron VUV flux in order to reproduce phenomenon, which could occurs in the thermosphere of Titan. The strong VUV photons, with wavelengths below 100 nm as affecting aerosols in the thermosphere, can selectively deplete them in primary and secondary amine functions in favor of aliphatic functions. This irradiation effect preserves nitrogen bearing function more deeply buried in the aerosols structure such as nitriles, imines and tertiary amines. These results can participate to interpret the apparent contradiction between the nitrogen rich aerosols analyzed by the ACP-GCMS instrument of the Huygens probe and the absence of amine function observed in the infrared by the VIMS instrument of the Cassini spacecraft.

A second study consisted to exposed tholins samples coated by condensed species at a UV-Visible irradiation simulating a potential stratospheric and/or tropospheric chemical evolution of Titan's aerosols. The presence of aerosols in interaction with solid species can promote the photo-reactivity of these species at longer wavelengths where they are usually inert. These results showed an important dependence of the reactivity with the chemical nature of the species. The apparition of new absorption band in the IR signature of the tholins sample for the experiment used D-labelled acetylene has shown that aerosols composition is modified by the reactivity of the coated ice.

Several perspectives for this thesis can be suggested.

The first two are focused on the gaseous mixture made of N₂-CH₄-CO₂. Reactivity of this simulated atmosphere has shown a significant coupling of the O chemistry with the C, N, H chemistry, highlighted by the detection of one oxygenated species in gaseous phase, N₂O, H₂O, and an incorporation of oxygen in tholins. However, the nature of oxygenated molecules composing the tholins and the pathway for the oxygen incorporation remains largely unknown. A first way to better constraint this question would be to analyze more precisely the composition of the gaseous phase. GC-MS, which have been used in other chapters, would allow identifying the smallest volatile species (C1 to C5). The second way would be to analyze the chemical composition of the tholins by high resolution mass spectrometry. Such a

General conclusion

work has been realized previously and allows characterizing nitrogen or oxygen incorporation in tholins produced in various gaseous mixtures. This would allow characterizing the nature of molecules present in the tholins and identifying key molecules for the oxygen incorporation.

I showed in the Chapters III and IV that the reactivity of the gaseous mixture studies in the case of the early Earth atmosphere was highly dependent on the initial composition of the gaseous mixture and so on the hypothesis made on the composition of the early Earth atmosphere. If our knowledge of the primitive atmosphere of the Earth has greatly improved these past 50 years, the lack of constraint on the composition of this atmosphere and especially on the amount of the different species present in the atmosphere remains important. A better knowledge of the Earth's atmospheric composition and its evolution since the start of the Hadean to the end and the Archean would be necessary to better emphasize the chemistry, which could have taken place in the early Earth atmosphere. It would improve our knowledge on the origin of the organic matter on Earth as well as its impact on the climate of the early Earth and finally be able to understand the evolution of this chemistry during these two eons.

Other perspectives of this thesis work concerns the chemical evolution of aerosols during their sedimentation to the surface addressed in the Chapter VI. Firstly for the thermospheric processes drive by VUV photons, experiments have been carried out on tholins thin films with a thickness of a few hundred of nanometers, more important than the few nanometers of aerosols in Titan's thermosphere. The effect of the thickness must be investigated to know if the effect highlighted in this thesis affecting the sample only on the surface or globally. Moreover, the interpretation of the effect highlighted in laboratory for the aerosols of Titan is limited by our knowledge of the composition of Titan's aerosols. ACP-GCMS is the only instrument, which has provided a qualitative analysis of the aerosols composition and new analysis would be useful to answer questions about the nitrogen content of these aerosols.

The second studies of the Chapter VI has highlighted that aerosols could interact with condensed species present in Titan's atmosphere and that their irradiation by UV photons involve a chemical evolution of aerosols. This effect has been studied in the case of the atmosphere of Titan. But one important point in the Chapter III and IV concerning the atmosphere of the early Earth was the important formation of water. This water formation above the troposphere could lead to the formation of high altitude clouds composed by water ice. An interaction between aerosols and water ice is possible and could affect their chemical

General conclusion

composition. This could be investigated experimentally following the protocol used for Titan and microphysical modeling could provide more information for the formation of these clouds and their interactions with the aerosols.

Table of figures and tables

Figure 1: Spectres de masse des produits gazeux formés dans des mélanges N ₂ -CO ₂ -H ₂ pour différentes concentrations initiales de CO ₂ : 1 % de CO ₂ (courbe bleue), 5 % de CO ₂ (courbe verte) et 10 % de CO ₂ (courbe rouge).	3
Table 1: Analyse élémentaire des tholins produits dans des mélanges N ₂ -CO ₂ -CH ₄ pour différentes concentrations initiales de CO ₂	4
Figure 2: Spectres infrarouge de tholins produits dans des mélanges N ₂ -CO ₂ -CH ₄ pour différentes concentrations initiales de CO ₂	4
Table 2: Evolution du taux de production des tholins en fonction de [CO ₂] ₀ . a Tholins produits à 0.9 mbar. b Tholins produits à 2.2 mbar.	5
Figure 3: Spectres d'absorption infrarouge enregistrés pour des échantillons irradiés 3 heures à 95 nm, 28 heures à 121.6 nm et 6 heures à 190 nm. La courbe noire épaisse correspond à la moyenne des spectres de tholins non irradiés présenté dans la Figure 49.	7
Figure 4: Geological time scale.....	11
Figure 5: a) Comet 67P/Churyumov-Gerasimenko image recorded by Rosetta's OSIRIS narrow-angle camera from a distance of 285 km. © ESA/Rosetta/MPS for OSIRIS Team MPS/UPD/LAM/IAA/SSO/INTA/UPM/DASP/IDA b) Murchison meteorite © Smithsonian Institution National Museum of Natural History.	13
Figure 6: A schematic representation of the Miller-Urey experiment (from (Gargaud et al., 2012c)).	17
Table 3: Principal organic synthesis realized with laboratory experiment to simulate the early Earth reactivity. Tholins are solid organic material product in experimental simulations as named by C. Sagan and B. Khare (Sagan and Khare, 1979).....	18
Figure 7: Evolution of the tholins production in experiments of UV irradiation of gaseous mixture made of N ₂ /CO ₂ /CH ₄ as a function of the C/O ratio. (from (Trainer et al., 2006)). ...	19
Figure 8: Schematic representation of the various episodes in the evolution of the atmosphere and the hydrosphere before 4.4 Ga (from (Gargaud et al., 2012a))	20
Figure 9: Modeling of the evolution of the solar luminosity over the geological time (from (Feulner, 2012)).....	22
Figure 10: Comparison of the geochemical estimation of the atmospheric CO ₂ partial pressure (P _{CO2}) at different epochs and the calculation in a 1D model of the P _{CO2} necessary to reach a surface temperature of 273 K and 288 K (from (Feulner, 2012)).	25

Table of figures and tables

Figure 11: Comparison of the calculated young Sun spectrum in the 10-250 nm range (from (Hébrard and Marty, 2014)) and the calculated EEDF in a pure N ₂ plasma for the PAMPRE experiment (adapted from (Alves et al., 2012)).....	32
Figure 12: The PAMPRE experimental setup.....	33
Figure 13: Glass vessel recovered by tholins produced in the PAMPRE experiment.	34
Figure 14: Blank mass spectrum of the isolated mass spectrometer.....	35
Figure 15: Schematic of the FTIR setup on the PAMPRE reactor.	37
Figure 16: Vertical temperature profile retrieval by HASI (black line) and saturation temperature profiles (color lines) for different gas species (from (Lavvas et al., 2011a)).....	40
Figure 17: Schema of the Acquabella experimental setup.....	41
Figure 18: Tholins thin film deposited on a sapphire window produced with the PAMPRE experiment.....	42
Table 4: Photons flux reaches the sample in function of the laser wavelength.....	42
Table 5: Initial composition of the studied gaseous mixtures.....	46
Figure 19: Evolution of the CO ₂ mixing ratio in the gaseous reactive medium with the plasma duration. Origin of the time is set as the moment when the plasma is turn on. CO ₂ mixing ratio has been multiply by a factor 10 and a factor 2 for an initial amount of 1 % and 5% respectively.....	48
Table 6: Evolution of the absolute consumption Δ_{CO_2} and the consumption efficient e_{CO_2} of carbon dioxide in the plasma as a function of the initial amount of CO ₂ . Evolution of the absolute consumption Δ_{H_2} and the consumption efficient e_{H_2} of hydrogen in the plasma as a function of the initial amount of CO ₂ . Evolution of the C/H and C/O ratios in the fraction of gases consumed as a function of the initial amount of CO ₂ . The uncertainties are given as 2σ (standard deviation) and are calculated from the standard fluctuations of the mass spectrometry measurements.	48
Figure 20: Evolution of the H ₂ mixing ratio in the gaseous reactive medium with the plasma duration for the different CO ₂ initial amounts. Origin of the time is set as the moment when the plasma is turn on.....	49
Figure 21: Mass spectra obtained for a N ₂ :CO ₂ :H ₂ 91:5:4 % gas mixture plasma off (blue) and plasma on (red) at room temperature.	51
Figure 22: Evolution of the pressure in the reactor during the warm up of the plasma box to room temperature.	52
Figure 23: Mass spectra recorded at 173 K (blue) and 294 K (red) after 4 hours of gaseous products trapping in N ₂ -CO ₂ -H ₂ (91/5/4) plasma.	53

Table of figures and tables

Figure 24: Infrared spectra recorded at 173 K (blue) and 294 K (red) after the trapping of the gaseous product during 4 hours of plasma duration in an initial gaseous mixture made of N ₂ /CO ₂ /H ₂ (91/5/4).....	54
Table 7: Evolution as a function of the CO ₂ initial amount of the mean of H ₂ O molecules formed in a 4 hours of plasma duration N _{H₂O} and the number of NH ₃ molecules formed in 4 hours of plasma duration. The uncertainties are given as 2σ (standard deviation) and are calculated from the standard fluctuations of the infrared spectroscopy measurements.....	56
Figure 25: : Infrared spectra in the 700-1200 cm ⁻¹ range recorded at 300 K after 4 hours of gaseous products trapping in a N ₂ -CO ₂ -H ₂ (91/5/4) plasma.	57
Table 8: List of the peaks detected in the mass spectrum of the gases released and their possible attribution to molecules (black) or their major fragments (red).....	59
Figure 26: Chromatograms of gas trapped during an experiment with 5 % of CO ₂	62
Table 9: List of gaseous compounds detected in our experiment.	63
Figure 27: ATR spectra of tholins samples produced in a gaseous mixture made of N ₂ /CO ₂ /H ₂ (86/10/4).....	65
Figure 28: Mass spectra of the gases trapped realized at room temperature for different initial CO ₂ amounts: 1 % of CO ₂ (blue), 5 % of CO ₂ (green) and 10 % of CO ₂ (red).....	66
Table 10: Pressure in PAMPRE after the release of the gases trapped during 4 hours of plasma duration at 173 K for different CO ₂ initial amounts: 1 %, 5 % and 10 %.....	67
Table 11: Initial compositions of the studied gaseous mixtures.	76
Figure 29: Evolution of the CO ₂ mixing ratio in the gaseous reactive medium with the plasma duration. Origin of the time is set as the moment when the plasma is turn on. CO ₂ mixing ratio has been multiply by a factor 10 and a factor 2 for an initial amount of 1 %	77
Table 12: Evolution of the consumption efficiencies of carbon dioxide e_{CO_2} and methane e_{CH_4} in the plasma as a function of the initial amount of CO ₂ . The uncertainties are given as 2σ (standard deviation) and are calculated from the standard fluctuations of the mass spectrometry measurements.	78
Figure 30: Evolution of the CH ₄ mixing ratio in the gaseous reactive medium with the plasma duration for the different CO ₂ initial amounts. Origin of the time is set as the moment when the plasma is turn on.....	78
Figure 31: Mass spectra obtained for a N ₂ :CO ₂ :CH ₄ 94:5:1 % gas mixture plasma off (blue) and plasma on (red) at room temperature.....	79

Table of figures and tables

Figure 32: Evolution of the m/z 27 signal (panel a) and m/z 41 signal (panel b) in the gaseous reactive medium with the plasma duration. The origin of time is set as the moment when the plasma is turn on.	80
Figure 33; Mass spectra recorded at 173 K (blue) and 294 K (red) after 4 hours of gaseous products trapping in N_2 - CO_2 - H_2 (94/5/1) plasma.	82
Figure 34: Infrared spectra recorded at 173 K (blue) and 294 K (red) after the trapping of the gaseous product during 4 hours of plasma duration in an initial gaseous mixture made of $N_2/CO_2/CH_4$ (94/5/1).....	83
Figure 35: Infrared spectra in the 700-1200 cm^{-1} range recorded at 300 K after 4 hours of gaseous products trapping in a N_2 - CO_2 - CH_4 (94/5/1) plasma.	85
Table 13: Number of NH_3 molecules N_{NH_3} and number of HCN molecules N_{HCN} formed during for hours of plasma duration in a gaseous mixture made of $N_2/CO_2/CH_4$ (94/5/1).....	86
Figure 36: Infrared spectra in the 2750-3400 cm^{-1} range recorded at 300 K after 4 hours of gaseous products trapping in a N_2 - CO_2 - CH_4 (94/5/1) plasma.	87
Table 14: List of the peaks detected in the mass spectrum of the gases released and their possible attribution to molecules (black) or their major fragments (red).....	89
Table 15: Pressure in PAMPRE after the release of the gases trapped during 2 hours of plasma duration at 173 K for different CO_2 initial amounts: 1 %, 5 % and 10 %.....	90
Figure 37: Mass spectra of the gases trapped realized at room temperature for different initial CO_2 amounts: 1 % of CO_2 (blue), 5 % of CO_2 (green) and 10 % of CO_2 (red).	91
Table 16: Tholins production rate as a function of $[CO_2]_0$. ^a Tholins produced at 0.9 mbar. ^b Tholins produced at 2.2 mbar.....	93
Table 17: Elemental composition of tholins for different $[CO_2]_0$. ^a Tholins produced at 0.9 mbar. ^b Tholins produced at 2.2 mbar.	94
Figure 38: Comparative IR spectra of tholins produced in PAMPRE in gaseous mixture containing 1 % of CH_4 and different amounts of CO_2 : 0 %, 1 %, 5 % and 10 %. The spectra were normalized on the amine band at 3200 cm^{-1}	94
Table 18: Initial composition of the studied gaseous mixtures.	103
Figure 39: Evolution of CH_4 mixing ratio in the gaseous reactive medium with the plasma duration. Origin is set as the moment when the plasma is turned on.	105
Figure 40: Evolution of CH_4 mixing ratio, in a semi-log scale, in the gaseous reactive medium with the plasma duration. Origin of time is set as the moment when the plasma is turn on. For each percentage of CO, a fit is performed by two straight lines. The two characteristics times τ_1 and τ_2 are determined from the slopes of the lines. The time of the regime change t_i is set at	

Table of figures and tables

the intersection of the two lines for each initial amount of CO and represent by a black square.	106
Table 19: Kinetics characteristics times for different $[\text{CO}]_0$. τ_1 and τ_2 are characteristic times for the two regimes of methane decay. t_i is the moment of the transition between the two regimes. t_p is the aerosols appearance time detected by V_{dc}	107
Figure 41: Evolutions of the self-bias voltage V_{dc} as a function of time. The instant t_p when the solid particles appear is set at the beginning of the increase of V_{dc}	108
Figure 42: Evolution of HCN mixing ratio (top) and CH_3CN mixing ratio (bottom) in the gaseous reactive medium with the plasma duration. The origin of time is set as the moment when the plasma is turn on.	109
Table 20: Characteristic times of HCN and CH_3CN productions for different $[\text{CO}]_0$	110
Table 21: Evolution of the consumption efficient of CH_4 and relative production yields of HCN and CH_3CN for different $[\text{CO}]_0$ with the reference being the experiment without CO. The uncertainties are given as 2σ (standard deviation) and are calculated from the standard fluctuations of the mass spectrometry measurements.	111
Figure 43: Pressure in the cold trap.	112
Table 22: tholins production rate as a function of $[\text{CO}]_0$ at 0.9 mbar.	113
Figure 44: Morphologies of tholins at 1.8 mbar and for different gas mixture: (a) $\text{N}_2\text{-CH}_4$ (95%/5%) and (b) $\text{N}_2\text{-CH}_4\text{-CO}$ (90.5%/5%/4.5%).	114
Figure 45: Comparison of the grain size distribution of tholins products at 1.8 mbar for different CO initial percentages.	115
Table 23: Elemental composition of tholins for different $[\text{CO}]_0$	116
Figure 46: Chromatograms of gas trapped during experiments with 0 % of CO (top) and 4.5 % of CO (bottom). CO_2 and N_2O have been detected in chromatogram of gas trapped during experiemnt with 4.5 % of CO.	117
Figure 47: Chromatograms obtained at the specific m/z 30.	119
Figure 48: Different processes occurring in the atmosphere of Titan with the experimental setup associated as a function of the altitude.	125
Table 24: Photon fluxes in our monochromatic synchrotron experiments and on the top of Titan's atmosphere.	128
Figure 49: Functional homogeneity of the films is demonstrated by the five spectra measured at different locations on the non-irradiated sample. Spectra are normalized at their maximum absorption (1560 cm^{-1})	129

Table of figures and tables

Figure 50: Infrared absorption spectra recorded from samples irradiated by photons for 3 h (95 nm), 28 h (121.6 nm) and 6 h (190nm). The thick black spectrum is the mean of the non-irradiated spectra shown in Figure 49.	130
Figure 51: Absorption of the aliphatic bands relative to the amine one: absorbance spectra between 2800 cm ⁻¹ and 3000 cm ⁻¹ after subtraction of the normalized amine contribution. The grey envelop is the reference spectrum before irradiation, with the 20 % homogeneity uncertainty. The green curve is the spectrum obtained after 6 h of synchrotron irradiation at 190 nm, and the red one is the spectrum obtained after 28 h of irradiation at 121.6 nm.	131
Figure 52: Unity optical thickness profiles: total $\tau=1$ curve (black), optical depth=1 for individual molecules (colored curves). Altitude optical depths of 95 nm (~1000 km), 121.6 nm (~900 km) and 190 nm (~100 km) wavelengths penetration of the solar radiation in Titan's atmosphere are indicated as orange vertical lines.	134
Figure 53: Comparison of the 95 nm irradiated film with the non-irradiated film (Gautier et al., 2012) and with normalized data from Cassini-VIMS (Kim et al., 2011) and Cassini-CIRS (Vinatier et al., 2012) mid-IR instruments at altitude ~200 km. VIMS and CIRS spectra were normalized to the maximum of our spectra (i.e. the CIRS spectrum was normalized at the 1450 cm ⁻¹ band, and the VIMS spectrum at the 2930 cm ⁻¹ band).	136
Table 25: Conditions of temperature, pressure and duration for the deposition of the different species studied (C ₂ H ₂ , C ₂ D ₂ and CH ₃ CN) on the sample.	138
Figure 54: Absorbance spectrum of solid C ₂ H ₂ after deposition at 50 K on a blank sapphire spectrum. The spectrum is center on the C-H stretching band of solid acetylene at 3225 cm ⁻¹	139
Figure 55: Evolution of the differential absorbance of C ₂ H ₂ as a function of the irradiation duration at 355 nm. The reference is taken as the initial absorbance before irradiation. The panel a) presents this evolution for solid acetylene coated on blank sapphire window. The panel b) presents this evolution for solid acetylene coated on a PAMPRE tholins sample produced in a gaseous mixture composes by N ₂ -CH ₄ with 1 % of CH ₄	140
Figure 56: Evolution of the area of the absorption band of C ₂ H ₂ relatively to the initial absorbance of C ₂ H ₂ before the irradiation at 355 nm. The blue points correspond to an experiment with C ₂ H ₂ coated on a blank sapphire window. The red points correspond to an experiment with C ₂ H ₂ coated on a tholins sample. Trend lines have been added to highlight the evolution of the band area.	141
Figure 57: UV-visible absorbance spectrum of solid acetylene deposited at 50 K.	142

Table of figures and tables

Figure 58: UV-visible absorption spectra of the tholins samples produced with 1 % of CH ₄ (blue) and 5 % of CH ₄ (red) in the 220-850 nm range. The arrows are placed at the used wavelengths for the study of the reactivity of C ₂ H ₂ and CH ₃ CN.....	143
Figure 59: Evolution of the relative area as a percentage of the absorption band of C ₂ H ₂ as a function of the irradiation duration for the three studied wavelengths: 355 nm (red points), 410 nm (purple points) and 450 nm (blue points). The initial area of the band before irradiation has been taken as reference for each wavelength. The measured values at 355 nm have been normalized to take into account the difference of sample area irradiated at 355 nm comparatively to 410 nm and 450 nm.	144
Figure 60: Absorption spectrum of solid C ₂ D ₂ after deposition at 50 K on a tholins sample (99/1). The spectrum is center on the C-D stretching band at 2393 cm ⁻¹	145
Figure 61: Evolution of the C-D stretching band at 2393 cm ⁻¹ of C ₂ D ₂ coated on tholins during the irradiation at 355 nm.	146
Figure 62: Evolution of the differential absorbance of the tholins sample in the 2000-2700 cm ⁻¹ range. Each spectrum has been recorded at room temperature after an experiment of C ₂ D ₂ photolysis. Fourth successive experiments have been realized on the same tholins sample. The absorbance spectrum of the tholins sample before the experiments is used as reference.	147
Figure 63: Differential absorbance of the C ₂ H ₂ infrared absorption band at 3225 cm ⁻¹ after 3 hours of laser irradiation at 355 nm for different substrates. The reference is the initial absorbance spectrum of C ₂ H ₂ before irradiation. The substrates are a blank sapphire window and three tholins samples produced with three different initial amounts of CH ₄ : 1 %, 5 % and 10 %.....	150
Figure 64: Infrared absorption spectrum of solid CH ₃ CN coated at 100 K on a blank sapphire window.	152
Figure 65: Evolution of the differential absorbance of CH ₃ CN in function of the irradiation duration at 355 nm. The reference is taken as the initial absorbance before irradiation. Panel a) presents this evolution for solid acetonitrile coated on blank sapphire window. The Panel b) presents this evolution for solid acetonitrile coated on a PAMPRE tholins sample produced in a gaseous mixture composed by N ₂ -CH ₄ with 1 % of CH ₄	153
Figure 66: Evolution of the differential absorbance of CH ₃ CN in function of the irradiation duration at 266 nm. The reference is the initial absorbance before the irradiation. The figure presents this evolution for solid acetonitrile coated on a PAMPRE tholins sample produced in a gaseous mixture composes by N ₂ -CH ₄ with 1 % of CH ₄	154

Table of figures and tables

References

- Abramov, O., Mojzsis, S. J., 2009. Microbial habitability of the Hadean Earth during the late heavy bombardment. *Nature*. 459, 419-422.
- Albarede, F., 2009. Volatile accretion history of the terrestrial planets and dynamic implications. *Nature*. 461, 1227-1233.
- Albarede, F., et al., 2013. Asteroidal impacts and the origin of terrestrial and lunar volatiles. *Icarus*. 222, 44-52.
- Alcouffe, G., et al., 2010. Capacitively coupled plasma used to simulate Titan's atmospheric chemistry. *Plasma Sources Science and Technology*. 19, 015008.
- Alexander, C. M. O. D., Fogel, M., Yabuta, H., Cody, G. D., 2007. The origin and evolution of chondrites recorded in the elemental and isotopic compositions of their macromolecular organic matter. *Geochimica et Cosmochimica Acta*. 71, 4380-4403.
- Alves, L. L., et al., 2012. Capacitively coupled radio-frequency discharges in nitrogen at low pressures. *Plasma Sources Science and Technology*. 21, 045008.
- Anderson, C. M., Samuelson, R. E., 2011. Titan's aerosol and stratospheric ice opacities between 18 and 500 μm : Vertical and spectral characteristics from Cassini CIRS. *Icarus*. 212, 762-778.
- Bar-Nun, A., Chang, S., 1983. Photochemical reactions of water and carbon monoxide in Earth's primitive atmosphere. *Journal of Geophysical Research: Oceans*. 88, 6662-6672.
- Bar-Nun, A., Hartman, H., 1978. Synthesis of organic compounds from carbon monoxide and water by UV photolysis. *Origins of life*. 9, 93-101.
- Bar-nun, A., Herman, G., Laufer, D., Rappaport, M. L., 1985. Trapping and release of gases by water ice and implications for icy bodies. *Icarus*. 63, 317-332.
- Bartik, K., Bruylants, G., Locci, E., Reisse, J., et al., 2011. Liquid water: a necessary condition for all forms of life? , *Origins and Evolution of Life*. Cambridge University Press.
- Bellucci, A., et al., 2009. Titan solar occultation observed by Cassini/VIMS: Gas absorption and constraints on aerosol composition. *Icarus*. 201, 198-216.
- Bernard, J. M., Coll, P., Coustenis, A., Raulin, F., 2003. Experimental simulation of Titan's atmosphere: Detection of ammonia and ethylene oxide. *Planetary and Space Science*. 51, 1003-1011.
- Bertin, M., et al., 2012. UV photodesorption of interstellar CO ice analogues: from subsurface excitation to surface desorption. *Physical Chemistry Chemical Physics*. 14, 9929-9935.
- Biemann, K., 2006. Astrochemistry: Complex organic matter in Titan's aerosols? *Nature*. 444, E6-E6.
- Bockelée-Morvan, D., Crovisier, J., Mumma, M. J., Weaver, H. A., 2004. The Composition of Cometary Volatiles. In: U. o. A. Press, (Ed.), *COMETS II*, pp. 391-423.
- Bogaerts, A., Neyts, E., Gijbels, R., van der Mullen, J., 2002. Gas discharge plasmas and their applications. *Spectrochimica Acta Part B: Atomic Spectroscopy*. 57, 609-658.
- Botta, O., Bada, J., 2002. Extraterrestrial Organic Compounds in Meteorites. *Surveys in Geophysics*. 23, 411-467.
- Bowring, S. A., Williams, I. S., 1999. Priscoan (4.00–4.03 Ga) orthogneisses from northwestern Canada. *Contributions to Mineralogy and Petrology*. 134, 3-16.
- Brocks, J. J. L. G. A. B. R. R. E., 1999. Archean Molecular Fossils and the Early Rise of Eukaryotes. *Science*. 285, 1033-1036.
- Brownlee, D. E., 1985. Cosmic Dust: Collection and Research. *Annual Review of Earth and Planetary Sciences*. 13, 147-173.

References

- Brunetto, R., et al., 2011. Mid-IR, Far-IR, Raman micro-spectroscopy, and FESEM–EDX study of IDP L2021C5: Clues to its origin. *Icarus*. 212, 896-910.
- Burgisser, A., Scaillet, B., 2007. Redox evolution of a degassing magma rising to the surface. *Nature*. 445, 194-197.
- Cable, M. L., et al., 2014. Identification of primary amines in Titan tholins using microchip nonaqueous capillary electrophoresis. *Earth and Planetary Science Letters*. 403, 99-107.
- Cable, M. L., Hörst, S. M., Hodyss, R., Beauchamp, P. M., Smith, M. A., Willis, P. A., 2011. Titan Tholins: Simulating Titan Organic Chemistry in the Cassini-Huygens Era. *Chemical Reviews*. 112, 1882-1909.
- Carrasco, N., Gautier, T., Es-sebbar, E.-t., Pernot, P., Cernogora, G., 2012. Volatile products controlling Titan's tholins production. *Icarus*. 219, 230-240.
- Carrasco, N., Westlake, J., Pernot, P., Waite, H., Jr., 2013 Nitrogen in Titan's Atmospheric Aerosol Factory. In: J. M. Trigo-Rodriguez, F. Raulin, C. Muller, C. Nixon, (Eds.), *The Early Evolution of the Atmospheres of Terrestrial Planets*. Springer New York, pp. 145-154.
- Catling, D. C., 2006. Comment on "A Hydrogen-Rich Early Earth Atmosphere". *Science*. 311, 38.
- Cavarroc, M., Mikikian, M., Perrier, G., Boufendi, L., 2006. Single-crystal silicon nanoparticles: An instability to check their synthesis. *Applied Physics Letters*. 89, 013107-3.
- Chabert, P., Braithwaite., N., 2011. *Physics of Radio-Frequency Plasmas*. Cambridge University Press.
- Charnay, B., et al., 2013. Exploring the faint young Sun problem and the possible climates of the Archean Earth with a 3-D GCM. *Journal of Geophysical Research: Atmospheres*. 118, 10,414-10,431.
- Chyba, C., Sagan, C., 1992. Endogenous production, exogenous delivery and impact-shock synthesis of organic molecules: an inventory for the origins of life. *Nature*. 355, 125-132.
- Chyba, C., Thomas, P., Brookshaw, L., Sagan, C., 1990. Cometary delivery of organic molecules to the early Earth. *Science*. 249, 366-373.
- Claire, M. W., Sheets, J., Cohen, M., Ribas, I., Meadows, V. S., Catling, D. C., 2012. The Evolution of Solar Flux from 0.1 nm to 160 μm : Quantitative Estimates for Planetary Studies. *The Astrophysical Journal*. 757, 95.
- Coll, P., Bernard, J.-M., Navarro-González, R., Raulin, F., 2003. Oxirane: An Exotic Oxygenated Organic Compound on Titan? *The Astrophysical Journal*. 598, 700.
- Coll, P., et al., 2012. Can laboratory tholins mimic the chemistry producing Titan's aerosols? A review in light of ACP experimental results. *Planetary and Space Science*.
- Coustenis, A., et al., 2007. The composition of Titan's stratosphere from Cassini/CIRS mid-infrared spectra. *Icarus*. 189, 35-62.
- Coustenis, A., Schmitt, B., Khanna, R. K., Trotta, F., 1999. Plausible condensates in Titan's stratosphere from Voyager infrared spectra. *Planetary and Space Science*. 47, 1305-1329.
- Couturier-Tamburelli, I., Gudipati, M. S., Lignell, A., Jacovi, R., Piétri, N., 2014. Spectroscopic studies of non-volatile residue formed by photochemistry of solid C₄N₂: A model of condensed aerosol formation on Titan. *Icarus*. 234, 81-90.
- Cui, J., et al., 2009. Analysis of Titan's neutral upper atmosphere from Cassini Ion Neutral Mass Spectrometer measurements. *Icarus*. 200, 581-615.
- de Kok, R., Irwin, P. G. J., Teanby, N. A., 2008. Condensation in Titan's stratosphere during polar winter. *Icarus*. 197, 572-578.

References

- de Kok, R., et al., 2007. Oxygen compounds in Titan's stratosphere as observed by Cassini CIRS. *Icarus*. 186, 354-363.
- de Kok, R. J., Teanby, N. A., Maltagliati, L., Irwin, P. G. J., Vinatier, S., 2014. HCN ice in Titan's high-altitude southern polar cloud. *Nature*. 514, 65-67.
- DeLand, M. T., Shettle, E. P., Thomas, G. E., Olivero, J. J., 2006. A quarter-century of satellite polar mesospheric cloud observations. *Journal of Atmospheric and Solar-Terrestrial Physics*. 68, 9-29.
- Delano, J., 2001. Redox History of the Earth's Interior since ~3900 Ma: Implications for Prebiotic Molecules. *Origins of life and evolution of the biosphere*. 31, 311-341.
- Denman, K. L., et al., 2007. Couplings Between Changes in the Climate System and Biogeochemistry. In: S. Solomon, et al., (Eds.), *Climate Change 2007: The Physical Science Basis. Contribution of Working Group I to the Fourth Assessment Report of the Intergovernmental Panel on Climate Change*. Cambridge University Press.
- DeWitt, H. L., et al., 2009. Reduction in Haze Formation Rate on Prebiotic Earth in the Presence of Hydrogen. *Astrobiology*. 9, 447-453.
- Dinelli, B. M., et al., 2013. An unidentified emission in Titan's upper atmosphere. *Geophysical Research Letters*. 40, 1489-1493.
- Dobrijevic, M., Dutour, I., 2006. A random graphs model for the study of chemical complexity in planetary atmospheres. *Planetary and Space Science*. 54, 287-295.
- Dobrijevic, M., Hébrard, E., Loison, J. C., Hickson, K. M., 2014. Coupling of oxygen, nitrogen, and hydrocarbon species in the photochemistry of Titan's atmosphere. *Icarus*. 228, 324-346.
- Elsila, J. E., Glavin, D. P., Dworkin, J. P., 2009. Cometary glycine detected in samples returned by Stardust. *Meteoritics & Planetary Science*. 44, 1323-1330.
- Emmanuel, S., Ague, J. J., 2007. Implications of present-day abiogenic methane fluxes for the early Archean atmosphere. *Geophysical Research Letters*. 34, L15810.
- Fayolle, E. C., et al., 2011. CO Ice Photodesorption: A Wavelength-dependent Study. *The Astrophysical Journal Letters*. 739, L36.
- Ferris, J. P., Chen, C. T., 1975. Chemical evolution. XXVI. Photochemistry of methane, nitrogen, and water mixtures as a model for the atmosphere of the primitive earth. *Journal of the American Chemical Society*. 97, 2962-2967.
- Feulner, G., 2012. The faint young Sun problem. *Reviews of Geophysics*. 50, RG2006.
- Fleury, B., et al., 2014. Influence of CO on Titan atmospheric reactivity. *Icarus*. 238, 221-229.
- Floyd, L. E., Reiser, P. A., Crane, P. C., Herring, L. C., Prinz, D. K., Brueckner, G. E., 1998. Solar Cycle 22 UV Spectral Irradiance Variability: Current Measurements by SUSIM UARS. In: J. M. Pap, C. Fröhlich, R. K. Ulrich, (Eds.), *Solar Electromagnetic Radiation Study for Solar Cycle 22*. Springer Netherlands, pp. 79-87.
- Fulchignoni, M., et al., 2005. In situ measurements of the physical characteristics of Titan's environment. *Nature*. 438, 785-791.
- Gans, B., Peng, Z., Carrasco, N., Gauyacq, D., Lebonnois, S., Pernot, P., 2013. Impact of a new wavelength-dependent representation of methane photolysis branching ratios on the modeling of Titan's atmospheric photochemistry. *Icarus*. 223, 330-343.
- Gargaud, M., Martin, H., López-García, P., Montmerle, T., Pascal, R., 2012a. Formation and Early Infancy of the Earth. *Young Sun, Early Earth and the Origins of Life*. Springer Berlin Heidelberg, pp. 37-59.
- Gargaud, M., Martin, H., López-García, P., Montmerle, T., Pascal, R., 2012b. Intermezzo: The Gestation of Life and its First Steps. *Young Sun, Early Earth and the Origins of Life*. Springer Berlin Heidelberg, pp. 93-154.

References

- Gargaud, M., Martin, H., López-García, P., Montmerle, T., Pascal, R., 2012c Water, Continents, and Organic Matter. Young Sun, Early Earth and the Origins of Life. Springer Berlin Heidelberg, pp. 61-91.
- Gautier, T., Carrasco, N., Buch, A., Szopa, C., Sciamma-O'Brien, E., Cernogora, G., 2011. Nitrile gas chemistry in Titan's atmosphere. *Icarus*. 213, 625-635.
- Gautier, T., et al., 2012. Mid- and far-infrared absorption spectroscopy of Titan's aerosols analogues. *Icarus*. 221, 320-327.
- Gautier, T., et al., 2014a. Nitrogen incorporation in Titan's tholins inferred by high resolution orbitrap mass spectrometry and gas chromatography–mass spectrometry. *Earth and Planetary Science Letters*. 404, 33-42.
- Gautier, T., Carrasco, N., Stefanovic, I., Sikimic, B., Cernogora, G., Winter, J., 2014b. Methane Conversion in a N₂ - CH₄ Radiofrequency Discharge. *Plasma Processes and Polymers*. 11, 472-481.
- Geppert, W. D., Larsson, M., 2008. Dissociative recombination in the interstellar medium and planetary ionospheres. *Molecular Physics*. 106, 2199-2226.
- Gomes, R., Levison, H. F., Tsiganis, K., Morbidelli, A., 2005. Origin of the cataclysmic Late Heavy Bombardment period of the terrestrial planets. *Nature*. 435, 466-469.
- Green, B. D., Caledonia, G. E., 1982. Observations of NH infrared chemiluminescence. *The Journal of Chemical Physics*. 77, 3821-3823.
- Greenberg, J. M., 1982. In: L. L. Wilkening, (Ed.), *Comets*. University of Arizona Press, pp. 131-163.
- Gudipati, M. S., Jacovi, R., Couturier-Tamburelli, I., Lignell, A., Allen, M., 2013. Photochemical activity of Titan's low-altitude condensed haze. *Nat Commun*. 4, 1648.
- Guzmán-Marmolejo, A., Segura, A., Escobar-Briones, E., 2013. Abiotic Production of Methane in Terrestrial Planets. *Astrobiology*. 13, 550-559.
- Hadamcik, E., Renard, J. B., Alcouffe, G., Cernogora, G., Lvasseur-Regourd, A. C., Szopa, C., 2009. Laboratory light-scattering measurements with Titan's aerosols analogues produced by a dusty plasma. *Planetary and Space Science*. 57, 1631-1641.
- Haldane, J. B. S., 1929. The origin of life. *Rationalist Annual*. 148, 3-10.
- Haqq-Misra, J. D., Domagal-Goldman, S. D., Kasting, P. J., Kasting, J. F., 2008. A Revised, Hazy Methane Greenhouse for the Archean Earth. *Astrobiology*. 8, 1127-1137.
- Hasenkopf, C. A., et al., 2010. Optical properties of Titan and early Earth haze laboratory analogs in the mid-visible. *Icarus*. 207, 903-913.
- Hasenkopf, C. A., Freedman, M. A., Beaver, M. R., Toon, O. B., Tolbert, M. A., 2011. Potential Climatic Impact of Organic Haze on Early Earth. *Astrobiology*. 11, 135-149.
- He, C., Smith, M. A., 2014. A comprehensive NMR structural study of Titan aerosol analogs: Implications for Titan's atmospheric chemistry. *Icarus*. 243, 31-38.
- Hébrard, E., Dobrijevic, M., Bénilan, Y., Raulin, F., 2006. Photochemical kinetics uncertainties in modeling Titan's atmosphere: A review. *Journal of Photochemistry and Photobiology C: Photochemistry Reviews*. 7, 211-230.
- Hébrard, E., Dobrijevic, M., Loison, J. C., Bergeat, A., Hickson, K. M., 2012. Neutral production of hydrogen isocyanide (HNC) and hydrogen cyanide (HCN) in Titan's upper atmosphere. *A&A*. 541, A21.
- Hébrard, E., et al., 2009. How Measurements of Rate Coefficients at Low Temperature Increase the Predictivity of Photochemical Models of Titan's Atmosphere†. *The Journal of Physical Chemistry A*. 113, 11227-11237.
- Hébrard, E., Marty, B., 2014. Coupled noble gas–hydrocarbon evolution of the early Earth atmosphere upon solar UV irradiation. *Earth and Planetary Science Letters*. 385, 40-48.

References

- Heinrich, M. N., Khare, B. N., McKay, C. P., 2007. Prebiotic organic synthesis in early Earth and Mars atmospheres: Laboratory experiments with quantitative determination of products formed in a cold plasma flow reactor. *Icarus*. 191, 765-778.
- Hessler, A. M., Lowe, D. R., Jones, R. L., Bird, D. K., 2004. A lower limit for atmospheric carbon dioxide levels 3.2 billion years ago. *Nature*. 428, 736-738.
- Hirschmann, M. M., 2012. Magma ocean influence on early atmosphere mass and composition. *Earth and Planetary Science Letters*. 341–344, 48-57.
- Holland, H. D., 1962 Model of the evolution of the Earth's atmosphere. In: G. S. o. America, (Ed.), *Petrologic Studies: A Volume to Honor A. F. Buddington*, pp. 447-477.
- Hörst, S. M., Tolbert, M. A., 2014. The Effect of Carbon Monoxide on Planetary Haze Formation. *The Astrophysical Journal*. 781, 53.
- Hörst, S. M., Vuitton, V., Yelle, R. V., 2008. Origin of oxygen species in Titan's atmosphere. *Journal of Geophysical Research: Planets*. 113, E10006.
- Hörst, S. M., et al., 2012. Formation of Amino Acids and Nucleotide Bases in a Titan Atmosphere Simulation Experiment. *Astrobiology*. 12, 809-817.
- Hudson, R. L., Ferrante, R. F., Moore, M. H., 2014. Infrared spectra and optical constants of astronomical ices: I. Amorphous and crystalline acetylene. *Icarus*. 228, 276-287.
- Huebner, W. F., Keady, J. J., Lyon, S. P., 1992 Solar Photo Rates for Planetary Atmospheres and Atmospheric Pollutants. In: W. F. Huebner, J. J. Keady, S. P. Lyon, (Eds.), *Solar Photo Rates for Planetary Atmospheres and Atmospheric Pollutants*. Springer Netherlands, pp. 1-289.
- Israel, G., et al., 2005. Complex organic matter in Titan's atmospheric aerosols from in situ pyrolysis and analysis. *Nature*. 438, 796-799.
- Israel, G., et al., 2006. Astrochemistry: Complex organic matter in Titan's aerosols? (Reply). *Nature*. 444, E6-E7.
- Jacquinet-Husson, N., et al., 2011. The 2009 edition of the GEISA spectroscopic database. *Journal of Quantitative Spectroscopy and Radiative Transfer*. 112, 2395-2445.
- Johnson, A. P., Cleaves, H. J., Dworkin, J. P., Glavin, D. P., Lazcano, A., Bada, J. L., 2008. The Miller Volcanic Spark Discharge Experiment. *Science*. 322, 404.
- Kassab, E., Evleth, E. M., 1999 The Rydberg Photophysics and Photochemistry of Amines. In: C. Sándorfy, (Ed.), *The Role of Rydberg States in Spectroscopy and Photochemistry*. Springer Netherlands, pp. 231-246.
- Kasting, J., 1993. Earth's early atmosphere. *Science*. 259, 920-926.
- Kasting, J. F., 1988. Runaway and moist greenhouse atmospheres and the evolution of Earth and Venus. *Icarus*. 74, 472-494.
- Kasting, J. F., 2005. Methane and climate during the Precambrian era. *Precambrian Research*. 137, 119-129.
- Kasting, J. F., Zahnle, K. J., Walker, J. C. G., 1983. Photochemistry of methane in the Earth's early atmosphere. *Precambrian Research*. 20, 121-148.
- Kerridge, J. F., 1985. Carbon, hydrogen and nitrogen in carbonaceous chondrites: Abundances and isotopic compositions in bulk samples. *Geochimica et Cosmochimica Acta*. 49, 1707-1714.
- Khanna, R. K., 2005a. Condensed species in Titan's atmosphere: Identification of crystalline propionitrile (C₂H₅CN, CH₃CH₂CN) based on laboratory infrared data. *Icarus*. 177, 116-121.
- Khanna, R. K., 2005b. Condensed species in Titan's stratosphere: Confirmation of crystalline cyanoacetylene (HC₃N) and evidence for crystalline acetylene (C₂H₂) on Titan. *Icarus*. 178, 165-170.
- Kharecha, P., Kasting, J., Siefert, J., 2005. A coupled atmosphere–ecosystem model of the early Archean Earth. *Geobiology*. 3, 53-76.

References

- Kim, S. J., et al., 2011. Retrieval and tentative identification of the 3 μm spectral feature in Titan's haze. *Planetary and Space Science*. 59, 699-704.
- Kissel, J., Krueger, F. R., 1987. The organic component in dust from comet Halley as measured by the PUMA mass spectrometer on board Vega 1. *Nature*. 326, 755-760.
- Körner, U., Sonnemann, G. R., 2001. Global three-dimensional modeling of the water vapor concentration of the mesosphere-mesopause region and implications with respect to the noctilucent cloud region. *Journal of Geophysical Research: Atmospheres*. 106, 9639-9651.
- Köroğlu, B., Loparo, Z., Nath, J., Peale, R. E., Vasu, S. S., 2015. Propionaldehyde infrared cross-sections and band strengths. *Journal of Quantitative Spectroscopy and Radiative Transfer*. 152, 107-113.
- Krasnopolsky, V. A., 2009. A photochemical model of Titan's atmosphere and ionosphere. *Icarus*. 201, 226-256.
- Krasnopolsky, V. A., 2012. Titan's photochemical model: Further update, oxygen species, and comparison with Triton and Pluto. *Planetary and Space Science*. 73, 318-326.
- Kulikov, Y., et al., 2007. A Comparative Study of the Influence of the Active Young Sun on the Early Atmospheres of Earth, Venus, and Mars. *Space Science Reviews*. 129, 207-243.
- Kunze, M., Godolt, M., Langematz, U., Grenfell, J. L., Hamann-Reinus, A., Rauer, H., 2014. Investigating the early Earth faint young Sun problem with a general circulation model. *Planetary and Space Science*. 98, 77-92.
- Kuramoto, K., Umemoto, T., Ishiwatari, M., 2013. Effective hydrodynamic hydrogen escape from an early Earth atmosphere inferred from high-accuracy numerical simulation. *Earth and Planetary Science Letters*. 375, 312-318.
- Kvenvolden, K., et al., 1970. Evidence for Extraterrestrial Amino-acids and Hydrocarbons in the Murchison Meteorite. *Nature*. 228, 923-926.
- Lammer, H., Kasting, J., Chassefière, E., Johnson, R., Kulikov, Y., Tian, F., 2008. Atmospheric Escape and Evolution of Terrestrial Planets and Satellites. *Space Science Reviews*. 139, 399-436.
- Lavvas, P., Griffith, C. A., Yelle, R. V., 2011a. Condensation in Titan's atmosphere at the Huygens landing site. *Icarus*. 215, 732-750.
- Lavvas, P., Sander, M., Kraft, M., Imanaka, H., 2011b. Surface Chemistry and Particle Shape: Processes for the Evolution of Aerosols in Titan's Atmosphere. *The Astrophysical Journal*. 728, 80.
- Lavvas, P., et al., 2013. Aerosol growth in Titan's ionosphere. *Proceedings of the National Academy of Sciences*. 110, 2729-2734.
- Lavvas, P., Yelle, R. V., Vuitton, V., 2009. The detached haze layer in Titan's mesosphere. *Icarus*. 201, 626-633.
- Lavvas, P. P., Coustenis, A., Vardavas, I. M., 2008. Coupling photochemistry with haze formation in Titan's atmosphere, Part II: Results and validation with Cassini/Huygens data. *Planetary and Space Science*. 56, 67-99.
- Lefevre, F., et al., 2008. Heterogeneous chemistry in the atmosphere of Mars. *Nature*. 454, 971-975.
- Liang, M.-C., Yung, Y. L., Shemansky, D. E., 2007. Photolytically Generated Aerosols in the Mesosphere and Thermosphere of Titan. *The Astrophysical Journal Letters*. 661, L199.
- Loison, J. C., et al., 2015. The neutral photochemistry of nitriles, amines and imines in the atmosphere of Titan. *Icarus*. 247, 218-247.
- López-Puertas, M., et al., 2013. Large Abundances of Polycyclic Aromatic Hydrocarbons in Titan's Upper Atmosphere. *The Astrophysical Journal*. 770, 132.

References

- Lowe, D., MacKenzie, A. R., 2008. Polar stratospheric cloud microphysics and chemistry. *Journal of Atmospheric and Solar-Terrestrial Physics*. 70, 13-40.
- Määttänen, A., Pérot, K., Montmessin, F., Hauchecorne, A., 2013. Mesospheric clouds on Mars and on the Earth. In: S. J. Mackwell, A. A. Simon-Miller, J. W. Harder, M. A. Bullock, (Eds.), *Comparative Climatology of Terrestrial Planets*. University of Arizona Press.
- Mahjoub, A., Carrasco, N., Dahoo, P. R., Gautier, T., Szopa, C., Cernogora, G., 2012. Influence of methane concentration on the optical indices of Titan's aerosols analogues. *Icarus*. 221, 670-677.
- Malsch, K., Hohlneicher, G., Schork, R., Koppel, H., 2001. A quantum dynamical examination of the vibronic structure of singlet and triplet spectra of acetylene. *Physical Chemistry Chemical Physics*. 3, 5393-5407.
- Marshall, W. L., 1994. Hydrothermal synthesis of amino acids. *Geochimica et Cosmochimica Acta*. 58, 2099-2106.
- Martin, H., Claeys, P., Gargaud, M., Pinti, D., Selsis, F., 2006. 6. Environmental Context. *Earth, Moon, and Planets*. 98, 205-245.
- Marty, B., 2012. The origins and concentrations of water, carbon, nitrogen and noble gases on Earth. *Earth and Planetary Science Letters*. 313-314, 56-66.
- Marty, B. L. M. R. P., 2013. Nitrogen Isotopic Composition and Density of the Archean Atmosphere. *Science*. 342, 101-104.
- McKay, C. P., Lorenz, R. D., Lunine, J. I., 1999. Analytic Solutions for the Antigreenhouse Effect: Titan and the Early Earth. *Icarus*. 137, 56-61.
- Mercier, B., et al., 2000. Experimental and theoretical study of a differentially pumped absorption gas cell used as a low energy-pass filter in the vacuum ultraviolet photon energy range. *Journal of Vacuum Science & Technology A*. 18, 2533-2541.
- Mikikian, M., Boufendi, L., 2004. Experimental investigations of void dynamics in a dusty discharge. *Physics of Plasmas*. 11, 3733-3737.
- Miller, S. L., 1953. A Production of Amino Acids Under Possible Primitive Earth Conditions. *Science*. 117, 528-529.
- Miller, S. L., 1957. The mechanism of synthesis of amino acids by electric discharges. *Biochimica et Biophysica Acta*. 23, 480-489.
- Miller, S. L., Bada, J. L., 1988. Submarine hot springs and the origin of life. *Nature*. 334, 609-611.
- Mitchell, J. B. A., Hus, H., 1985. The dissociative recombination and excitation of CO⁺. *Journal of Physics B: Atomic and Molecular Physics (1968-1987)*. 18, 547-555.
- Mojzsis, S. J., Arrhenius, G., McKeegan, K. D., Harrison, T. M., Nutman, A. P., Friend, C. R. L., 1996. Evidence for life on Earth before 3,800 million years ago. *Nature*. 384, 55-59.
- Mojzsis, S. J., Harrison, T. M., Pidgeon, R. T., 2001. Oxygen-isotope evidence from ancient zircons for liquid water at the Earth's surface 4,300 Myr ago. *Nature*. 409, 178-181.
- Morbidelli, A., 2008. *Comets and Their Reservoirs: Current Dynamics and Primordial Evolution*. *Trans-Neptunian Objects and Comets*. Springer Berlin Heidelberg, pp. 79-163.
- Mutsukura, N., 2001. Deposition of Diamondlike Carbon Film and Mass Spectrometry Measurement in CH₄/N₂ RF Plasma. *Plasma Chemistry and Plasma Processing*. 21, 265-277.
- Nahon, L., et al., 2012. DESIRS: a state-of-the-art VUV beamline featuring high resolution and variable polarization for spectroscopy and dichroism at SOLEIL. *Journal of Synchrotron Radiation*. 19, 508-520.

References

- Nakamura, K., Kato, Y., 2004. Carbonatization of oceanic crust by the seafloor hydrothermal activity and its significance as a CO₂ sink in the Early Archean. *Geochimica et Cosmochimica Acta*. 68, 4595-4618.
- Newman, M. J., Rood, R. T., 1977. Implications of Solar Evolution for the Earth's Early Atmosphere. *Science*. 198, 1035-1037.
- Niemann, H. B., et al., 2005. The abundances of constituents of Titan's atmosphere from the GCMS instrument on the Huygens probe. *Nature*. 438, 779-784.
- Nisbet, E. G., Sleep, N. H., 2001. The habitat and nature of early life. *Nature*. 409, 1083-1091.
- Notesco, G., Bar-Nun, A., 1997. Trapping of Methanol, Hydrogen Cyanide, and Hexane in Water Ice, above Its Transformation Temperature to the Crystalline Form. *Icarus*. 126, 336-341.
- Oparin, A. I., 1938. *The Origin of Life*.
- Oro, J., 1961. Comets and the Formation of Biochemical Compounds on the Primitive Earth. *Nature*. 190, 389-390.
- Owen, T., Bar-Nun, A., 1995. Comets, Impacts, and Atmospheres. *Icarus*. 116, 215-226.
- Papineau, D., et al., 2011. Young poorly crystalline graphite in the >3.8-Gyr-old Nuvvuagittuq banded iron formation. *Nature Geosci.* 4, 376-379.
- Parker, E. T., et al., 2011. Primordial synthesis of amines and amino acids in a 1958 Miller H₂S-rich spark discharge experiment. *Proceedings of the National Academy of Sciences*. 108, 5526-5531.
- Patel, B. H., Percivalle, C., Ritson, D. J., Duffy-Colm, D., Sutherland, J. D., 2015. Common origins of RNA, protein and lipid precursors in a cyanosulfidic protometabolism. *Nat Chem*. 7, 301-307.
- Pavlov, A. A., Brown, L. L., Kasting, J. F., 2001. UV shielding of NH₃ and O₂ by organic hazes in the Archean atmosphere. *Journal of Geophysical Research: Planets*. 106, 23267-23287.
- Pavlov, A. A., Kasting, J. F., Brown, L. L., Rages, K. A., Freedman, R., 2000. Greenhouse warming by CH₄ in the atmosphere of early Earth. *Journal of Geophysical Research: Planets*. 105, 11981-11990.
- Peng, Z., et al., 2013. Titan's atmosphere simulation experiment using continuum UV-VUV synchrotron radiation. *Journal of Geophysical Research: Planets*. 118, 778-788.
- Pernot, P., Carrasco, N., Thissen, R., Schmitz-Afonso, I., 2010. Tholinomics—Chemical Analysis of Nitrogen-Rich Polymers. *Analytical Chemistry*. 82, 1371-1380.
- Pérot, K., et al., 2010. First climatology of polar mesospheric clouds from GOMOS/ENVISAT stellar occultation instrument. *Atmos. Chem. Phys.* 10, 2723-2735.
- Pizzarello, S., Cooper, G. W., Flynn, G. J., 2006 The Nature and Distribution of the Organic Material in Carbonaceous Chondrites and Interplanetary Dust Particles. In: U. o. A. Press, (Ed.), *Meteorites and the Early Solar System II*, pp. 625-651.
- Porco, C. C., et al., 2005. Imaging of Titan from the Cassini spacecraft. *Nature*. 434, 159-168.
- Praburam, G., Goree, J., 1996. Experimental observation of very low-frequency macroscopic modes in a dusty plasma. *Physics of Plasmas*. 3, 1212-1219.
- Proskurowski, G. M. D. S. J. S. F.-G. G. L. O. E. J. L. J. E. S. S. P. K. D. S., 2008. Abiogenic Hydrocarbon Production at Lost City Hydrothermal Field. *Science*. 319, 604-607.
- Ribas, I., Guinan, E. F., Güdel, M., Audard, M., 2005. Evolution of the Solar Activity over Time and Effects on Planetary Atmospheres. I. High-Energy Irradiances (1-1700 Å). *The Astrophysical Journal*. 622, 680.
- Ribas, I., et al., 2010. Evolution of the Solar Activity Over Time and Effects on Planetary Atmospheres. II. κ 1 Ceti, an Analog of the Sun when Life Arose on Earth. *The Astrophysical Journal*. 714, 384.

References

- Ring, D., Wolman, Y., Friedmann, N., Miller, S. L., 1972. Prebiotic Synthesis of Hydrophobic and Protein Amino Acids. *Proceedings of the National Academy of Sciences*. 69, 765-768.
- Rosing, M. T., 1999. ^{13}C -Depleted Carbon Microparticles in >3700-Ma Sea-Floor Sedimentary Rocks from West Greenland. *Science*. 283, 674-676.
- Rosing, M. T., Bird, D. K., Sleep, N. H., Bjerrum, C. J., 2010. No climate paradox under the faint early Sun. *Nature*. 464, 744-747.
- Rothman, L. S., et al., 2009. The HITRAN 2008 molecular spectroscopic database. *Journal of Quantitative Spectroscopy and Radiative Transfer*. 110, 533-572.
- Russo, N. D., Khanna, R. K., 1996. Laboratory Infrared Spectroscopic Studies of Crystalline Nitriles with Relevance to Outer Planetary Systems. *Icarus*. 123, 366-395.
- Sagan, C., Chyba, C., 1997. The Early Faint Sun Paradox: Organic Shielding of Ultraviolet-Labile Greenhouse Gases. *Science*. 276, 1217-1221.
- Sagan, C., Khare, B. N., 1979. Tholins: organic chemistry of interstellar grains and gas. *Nature*. 277, 102-107.
- Sagan, C., Mullen, G., 1972. Earth and Mars: Evolution of Atmospheres and Surface Temperatures. *Science*. 177, 52-56.
- Samsonov, D., Goree, J., 1999. Instabilities in a dusty plasma with ion drag and ionization. *Physical Review E*. 59, 1047-1058.
- Samuelson, R. E., Mayo, L. A., Knuckles, M. A., Khanna, R. J., 1997. C_4N_2 ice in Titan's north polar stratosphere. *Planetary and Space Science*. 45, 941-948.
- Sandford, S. A., et al., 2006. Organics Captured from Comet 81P/Wild 2 by the Stardust Spacecraft. *Science*. 314, 1720-1724.
- Sandford, S. A., et al., 2010. Assessment and control of organic and other contaminants associated with the Stardust sample return from comet 81P/Wild 2. *Meteoritics & Planetary Science*. 45, 406-433.
- Schlesinger, G., Miller, S., 1983a. Prebiotic synthesis in atmospheres containing CH_4 , CO , and CO_2 . *Journal of Molecular Evolution*. 19, 376-382.
- Schlesinger, G., Miller, S., 1983b. Prebiotic synthesis in atmospheres containing CH_4 , CO , and CO_2 . *Journal of Molecular Evolution*. 19, 383-390.
- Schmitt-Kopplin, P., et al., 2010. High molecular diversity of extraterrestrial organic matter in Murchison meteorite revealed 40 years after its fall. *Proceedings of the National Academy of Sciences*. 107, 2763-2768.
- Schopf, J. W., 2006. Fossil evidence of Archaean life. *Philosophical Transactions of the Royal Society B: Biological Sciences*. 361, 869-885.
- Schwarzschild, M., 1958. *Structure and evolution of the stars*. Princeton University Press.
- Sciamma-O'Brien, E., Carrasco, N., Szopa, C., Buch, A., Cernogora, G., 2010. Titan's atmosphere: An optimal gas mixture for aerosol production? *Icarus*. 209, 704-714.
- Sharpe, S. W., Johnson, T. G., Sams, R. L., Chu, P. M., Rhoderick, G. C., Johnson, P. A., 2004. Gas-phase databases for quantitative infrared spectroscopy. *Applied Spectroscopy*. 58, 1452-1461.
- Shipp, J., Gould, I. R., Herckes, P., Shock, E. L., Williams, L. B., Hartnett, H. E., 2013. Organic functional group transformations in water at elevated temperature and pressure: Reversibility, reactivity, and mechanisms. *Geochimica et Cosmochimica Acta*. 104, 194-209.
- Shock, E. L., 1992. Stability of peptides in high-temperature aqueous solutions. *Geochimica et Cosmochimica Acta*. 56, 3481-3491.
- Shock, E. L., Schulte, M. D., 1998. Organic synthesis during fluid mixing in hydrothermal systems. *Journal of Geophysical Research: Planets*. 103, 28513-28527.

References

- Siskind, D. E., Stevens, M. H., Hervig, M. E., Randall, C. E., 2013. Recent observations of high mass density polar mesospheric clouds: A link to space traffic? *Geophysical Research Letters*. 40, 2813-2817.
- Skrzypkowski, M. P., Gougousi, T., Johnsen, R., Golde, M. F., 1998. Measurement of the absolute yield of CO(a 3Π)+O products in the dissociative recombination of CO₂⁺ ions with electrons. *The Journal of Chemical Physics*. 108, 8400-8407.
- Sleep, N. H., Zahnle, K., 2001. Carbon dioxide cycling and implications for climate on ancient Earth. *Journal of Geophysical Research: Planets*. 106, 1373-1399.
- Som, S. M., Catling, D. C., Harnmeijer, J. P., Polivka, P. M., Buick, R., 2012. Air density 2.7 billion years ago limited to less than twice modern levels by fossil raindrop imprints. *Nature*. 484, 359-362.
- Strazzulla, G., Baratta, G. A., Johnson, R. E., Donn, B., 1991. Primordial comet mantle: Irradiation production of a stable organic crust. *Icarus*. 91, 101-104.
- Szopa, C., Cernogora, G., Boufendi, L., Correia, J. J., Coll, P., 2006. PAMPRE: A dusty plasma experiment for Titan's tholins production and study. *Planetary and Space Science*. 54, 394-404.
- Thissen, R., et al., 2009. Laboratory Studies of Molecular Growth in the Titan Ionosphere†. *The Journal of Physical Chemistry A*. 113, 11211-11220.
- Thomas, G. E., Olivero, J. J., Jensen, E. J., Schroeder, W., Toon, O. B., 1989. Relation between increasing methane and the presence of ice clouds at the mesopause. *Nature*. 338, 490-492.
- Tian, F., Kasting, J. F., Zahnle, K., 2011. Revisiting HCN formation in Earth's early atmosphere. *Earth and Planetary Science Letters*. 308, 417-423.
- Tian, F., Toon, O. B., Pavlov, A. A., 2006. Response to Comment on "A Hydrogen-Rich Early Earth Atmosphere". *Science*. 311, 38.
- Tian, F., Toon, O. B., Pavlov, A. A., De Sterck, H., 2005. A Hydrogen-Rich Early Earth Atmosphere. *Science*. 308, 1014-1017.
- Tomasko, M., West, R., 2010 Aerosols in Titan's Atmosphere. In: R. Brown, J.-P. Lebreton, J. H. Waite, (Eds.), *Titan from Cassini-Huygens*. Springer Netherlands, pp. 297-321.
- Tomasko, M. G., et al., 2005. Rain, winds and haze during the Huygens probe's descent to Titan's surface. *Nature*. 438, 765-778.
- Tomasko, M. G., et al., 2008. A model of Titan's aerosols based on measurements made inside the atmosphere. *Planetary and Space Science*. 56, 669-707.
- Trail, D. E. B. N. D., 2011. The oxidation state of Hadean magmas and implications for early Earth's atmosphere. *Nature*. 480, 79-82.
- Trainer, M. G., Jimenez, J. L., Yung, Y. L., Toon, O. B., Tolbert, M. A., 2012. Nitrogen Incorporation in CH₄-N₂ Photochemical Aerosol Produced by Far Ultraviolet Irradiation. *Astrobiology*. 12, 315-326.
- Trainer, M. G., et al., 2004. Haze Aerosols in the Atmosphere of Early Earth: Manna from Heaven. *Astrobiology*. 4, 409-419.
- Trainer, M. G., et al., 2006. Organic haze on Titan and the early Earth. *Proceedings of the National Academy of Sciences*. 103, 18035-18042.
- Tran, B. N., Force, M., Briggs, R. G., Ferris, J. P., Persans, P., Chera, J. J., 2008. Titan's atmospheric chemistry: Photolysis of gas mixtures containing hydrogen cyanide and carbon monoxide at 185 and 254 nm. *Icarus*. 193, 224-232.
- Urey, H. C., 1952. On the early chemical history of the Earth and the origin of life. *Proceedings of the National Academy of Sciences*. 138, 378-382.
- Vinatier, S., et al., 2007. Vertical abundance profiles of hydrocarbons in Titan's atmosphere at 15° S and 80° N retrieved from Cassini/CIRS spectra. *Icarus*. 188, 120-138.

References

- Vinatier, S., Rannou, P., Anderson, C. M., Bézard, B., de Kok, R., Samuelson, R. E., 2012. Optical constants of Titan's stratospheric aerosols in the 70–1500 cm⁻¹ spectral range constrained by Cassini/CIRS observations. *Icarus*. 219, 5-12.
- von Paris, P., et al., 2008. Warming the early earth—CO₂ reconsidered. *Planetary and Space Science*. 56, 1244-1259.
- Vuitton, V., et al., 2009. Negative ion chemistry in Titan's upper atmosphere. *Planetary and Space Science*. 57, 1558-1572.
- Vuitton, V., Yelle, R. V., McEwan, M. J., 2007. Ion chemistry and N-containing molecules in Titan's upper atmosphere. *Icarus*. 191, 722-742.
- Waite, J. H., et al., 2007. The Process of Tholin Formation in Titan's Upper Atmosphere. *Science*. 316, 870-875.
- Wattiaux, G., Carrasco, N., Henault, M., Boufendi, L., Cernogora, G., 2015. Transient phenomena during dust formation in a N₂–CH₄ capacitively coupled plasma. *Plasma Sources Science and Technology*. 24, 015028.
- Whitehouse, M. J., Myers, J. S., Fedo, C. M., 2009. The Akilia Controversy: field, structural and geochronological evidence questions interpretations of >3.8 Ga life in SW Greenland. *Journal of the Geological Society*. 166, 335-348.
- Wilson, E. H., Atreya, S. K., 2004. Current state of modeling the photochemistry of Titan's mutually dependent atmosphere and ionosphere. *Journal of Geophysical Research: Planets*. 109, E06002.
- Woese, C. R., 1987. Bacterial evolution. *Microbiological Reviews*. 51, 221-271.
- Wolf, E. T., Toon, O. B., 2010. Fractal Organic Hazes Provided an Ultraviolet Shield for Early Earth. *Science*. 328, 1266-1268.
- Wolf, E. T., Toon, O. B., 2014. Controls on the Archean Climate System Investigated with a Global Climate Model. *Astrobiology*. 14, 241-253.
- Wordsworth, R., Pierrehumbert, R., 2013. Hydrogen-Nitrogen Greenhouse Warming in Earth's Early Atmosphere. *Science*. 339, 64-67.
- Yelle, R. V., et al., 2010. Formation of NH₃ and CH₂NH in Titan's upper atmosphere. *Faraday Discussions*. 147, 31-49.
- Yoon, Y. H., Hörst, S. M., Hicks, R. K., Li, R., de Gouw, J. A., Tolbert, M. A., 2014. The role of benzene photolysis in Titan haze formation. *Icarus*. 233, 233-241.
- Zahnle, K., Schaefer, L., Fegley, B., 2010. Earth's Earliest Atmospheres. *Cold Spring Harbor Perspectives in Biology*. 2.
- Zahnle, K., Sleep, N., 2006 Impacts and the Early Evolution of Life. In: P. Thomas, R. Hicks, C. Chyba, C. McKay, (Eds.), *Comets and the Origin and Evolution of Life*. Springer Berlin Heidelberg, pp. 207-251.
- Zahnle, K. J., 1986. Photochemistry of methane and the formation of hydrocyanic acid (HCN) in the Earth's early atmosphere. *Journal of Geophysical Research: Atmospheres*. 91, 2819-2834.
- Zook, H., 2001 Spacecraft Measurements of the Cosmic Dust Flux. In: B. Peucker-Ehrenbrink, B. Schmitz, (Eds.), *Accretion of Extraterrestrial Matter Throughout Earth's History*. Springer US, pp. 75-92.

Titre : La haute atmosphère de la Terre primitive, une source de composés organiques prébiotiques

Mots clés : Terre primitive, Titan, Planétologie, Astrochimie, Aérosols

Résumé : L'origine de la matière de la Terre primitive est un important sujet de recherche en planétologie. Cette thèse présente une étude expérimentale de la formation de composés organiques dans l'atmosphère de la Terre primitive en étudiant la réactivité de mélanges gazeux majoritairement composé de N_2 et CO_2 . Ils présentent une importante réactivité se traduisant par la formation de produits gazeux et solides, appelés tholins. La formation de ces produits met en avant l'efficacité de CO_2 comme source de carbone pour la croissance organique atmosphérique. L'identification des produits gazeux et l'analyse élémentaire des tholins ont montré qu'ils étaient constitués de C, N, H et O, soulignant un couplage efficace entre la chimie de ces éléments nécessaire à la formation de composés d'intérêts prébiotiques. Ce type d'étude a été appliqué ensuite à Titan qui a une atmosphère plus réduite,

faite de N_2 et CH_4 , mais contient des traces d'espèces oxygénées, majoritairement CO. L'ajout de CO au mélange réactif induit également un couplage entre la chimie de l'O et la chimie C, N, H considérée habituellement pour Titan. Enfin je propose et étudie expérimentalement deux phénomènes susceptibles de modifier la composition des aérosols de Titan durant leur sédimentation vers la surface. Premièrement une exposition de tholins aux photons VUV caractéristique de la thermosphère de Titan et qui induit une diminution sélective des fonctions amines en faveur des fonctions aliphatiques. Deuxièmement une irradiation par des photons UV d'espèces condensées à la surface de tholins et qui induit une réactivité de l'espèce en interaction avec les tholins, modifiant sa composition chimique.

Title : The upper atmosphere of the early Earth, a source of prebiotic organic compounds

Keywords : early Earth, Titan, Planetology, Astrochemistry, Aerosols

Abstract : The origin of the organic matter on the early Earth is an important subject of research in planetology. This thesis presents an experimental study of the formation of organic compounds in the atmosphere of the early Earth investigating the reactivity of gaseous mixtures majority made of N_2 and CO_2 . They present an important reactivity highlighted by the formation of gaseous products and solid products called tholins. The formation of these products points out CO_2 as an efficiency source of carbon for the organic atmospheric growth. The identification of the gaseous products and the elemental analysis of the tholins showed a composition by C, N, H and O highlighting an efficiency coupling between the chemistry of these elements necessary for the formation of prebiotic compounds. This type of study have been applied then to

Titan, which have a more reduced atmosphere, made of N_2 and CH_4 , but, which contained also oxygenated trace species: principally CO. The addition of CO in the reactive medium involves also a coupling between the chemistry of O and the C, N, H chemistry currently considered for Titan. Finally I propose and investigate experimentally two phenomena, which may involve a chemical evolution of the aerosols of Titan during their sedimentation to the surface. First, an exposition of tholins to VUV photons, characteristic of the thermosphere of Titan, involves a selective depletion of amines function in favor of aliphatic functions. Second, an irradiation by UV photons of condensed species at the surface of tholins involves a reactivity of the solid species in interaction with the tholins, changing their chemical composition.

